IRE Transactions on ANTENNAS and PROPAGATION

Volume AP-5 **JULY, 1957** **Number 3**

Published Quarterly

TABLE OF CONTENTS

PUBLISHED BY THE

ofessional Group on Antennas and Propagation

IRE TRANSACTIONS® PGAP IS A QUARTERLY PUBLICATION DEVOTED TO EXPERIMENTAL AND THEORETICAL PAPERS ON ANTENNAS AND WIRELESS PROPAGATION OF ELECTROMAGNETIC WAVES

MANUSCRIPTS should be submitted to John B. Smyth, Editor, SRA, 3930 4th Avenue, San Diego 3, California. Manuscripts should be original typewritten copy, double spaced, plus one carbon copy. References should appear as footnotes and include author's name, title, journal, volume, initial and final page numbers, and date. Each paper must have an abstract of not more than 200 words. News items concerning PGAP members and group activities should be sent to the News Editor, Mr. Arthur Dorne, Dorne and Margolin, Inc., 30 Sylvester Street, Westbury, L.I., N.Y.

ILLUSTRATIONS should be submitted as follows: All line drawings (graphs, charts, block diagrams, cutaways, etc.) should be inked uniformly and ready for reproduction. If commercially printed grids are used in graph drawings, author should be sure printer's ink is of a color that will reproduce. All half-tone illustrations (photographs, wash, airbrush, or pencil renderings, etc.) should be clean and ready to reproduce. Photographs should be glossy prints. Call-outs or labels should be marked on a registered tissue overlay, not on the illustration itself. No illustration should be larger than 8 x 10 inches.

Copies can be purchased from
THE INSTITUTE OF RADIO ENGINEERS
1 East 79 St., New York 21, N.Y.

PRICE PER COPY: members of the Professional Group on Antennas and Propagation, $2.00; members of the IRE, $3.00; nonmembers, $6.00.

ANNUAL SUBSCRIPTION PRICE: PGAP members, included in PGAP assessment of $4.00; IRE members, $8.50; Colleges and public libraries, $10.00; nonmembers, $17.00.

IRE TRANSACTIONS ON ANTENNAS AND PROPAGATION

Entered as second-class matter, at the post office at Menasha, Wisconsin, under the act of August 24, 1912. Acceptance for mailing at a special rate of postage is provided for in the act of February 28, 1925, embodied in Paragraph 4, Section 412, P. L. & R., authorized October 26, 1927.

news and views

Administrative Committee Meetings

Meeting of March 20, 1957, New York, N. Y. Present were H. G. Booker, Chairman, J. I. Bohnert, P. S. Carter, Arthur Dorne, R. A. Heising, J. W. Herbstreit, D. D. King, R. L. Mattingly, Philip Newman, D. C. Ports, V. H. Rumsey, R. C. Spencer, L. G. Trolese (for J. B. Smyth), A. H. Waynick.

1) Affiliate membership: It was announced that IRE headquarters has approved four societies for PGAP affiliate membership. These are: The American Astronomical Society, The Royal Astronomical Society, The Optical Society of America, and The American Meteorological Society. After discussion it was decided that a list of additional societies would be prepared and submitted to IRE headquarters for approval.

2) Finances and the Transactions: There was an extended discussion of the group financial situation and the prospects of increased income from advertising and other sources. It was brought out that no definite commitments for advertising have yet been received (although several tentative expressions of interest have been obtained), and that extra financial assistance from IRE is not to be expected at this time. Accordingly, the only income to be counted on for the immediate future is that from membership dues and institutional listings. This is not sufficient to publish all the papers our editor finds acceptable and would like to publish. In particular, it is not sufficient to permit publication of papers which have already been accepted while still accepting a reasonable proportion of the new papers submitted. It is also to be noted that the editor has had no way of knowing when publication of papers that he had accepted would be possible. In order to provide the editor with some instructions from this committee and in particular with regard to the July and October issues, a motion was made by D. D. King and modified by J. W. Herbstreit to instruct the editor to restrict the July issue to approximately sixty-seven pages, a length consistent with the funds currently on hand. Later instructions, taking into account the latest financial figures, will be furnished Editor Smyth in regard to the October issue. This motion was seconded and passed unanimously.

3) Four vacancies will occur on the Administrative Committee on June 1. The Chairman appointed a committee consisting of D. C. Ports, P. S. Carter, and George Sinclair to nominate a slate of officers for the coming year, as well as four candidates to fill these vacancies.

4) There was discussion of the following: a) means of encouraging the formation of new Local Chapters; b) suitable topics for future meetings and symposia; c) means of increasing liaison between astronomers and radio people.

Meeting of May 24, 1957, Washington, D. C. Present were: H. G. Booker, Outgoing Chairman, J. I. Bohnert, Incoming Chairman, W. W. Balwanz, J. T. Bolljahn, P. S. Carter, J. T. de Bettencourt, Arthur Dorne, F. T. Haddock, R. A. Helliwell, J. W. Herbstreit, R. L. Mattingly, D. C. Ports, George Sinclair, E. K. Smith, J. B. Smyth, R. C. Spencer, A. W. Straiton, A. H. Waynick, G. H. Welch.

1) Elections: The Nominating Committee nominated John I. Bohnert and Robert L. Mattingly for Chairman and Vice-Chairman, respectively. They were then elected by unanimous vote of the committee. John Bohnert then assumed the chair. The following were then recommended as the nominees for the four committee vacancies which will occur June 1, 1957: John W. Findlay, Richard K. Moore, William H. Radford, Oswald G. Villard. The recommendations of the Nominating Committee were unanimously accepted and the secretary was instructed to prepare a ballot for distribution to the membership.

2) Affiliate membership: It was reported that the following societies have been approved for affiliate membership status with the PGAP: Acoustical Society of America, American Astronomical Society, American Institute of Electrical Engineers, American Geophysical Union, American Mathematical Society, American Meteorological Society, Institute of the Aeronautical Sciences, Mathematical Association of America, Optical Society of America, The Institution of Electrical Engineers (London), The Physical Society (London), Royal Astronomical Society (London), Royal Astronomical Society of Canada, Institute of Radio Engineers, Australia, Federation Française des Societes de Physique (France), Nippon Butsuri Gakkai (Physical Society of Japan), and Verband Deutcher Elektrotechnika e.v. (Germany). The American Physical Society will be added within the next few weeks.

3) Finances and TRANSACTIONS: This matter was again the subject of an extended discussion. It was brought out that there is still a backlog of approximately 35 accepted but unpublished reports and that approximately $6000 will be required to publish them. In addition, to publish in an orderly fashion new papers as they are accepted will require about $15,000 per year. The present balance is less than $1000 and definite future income is approximately $11,000 to $12,000 per year, no advertising income as yet being definitely assured. All agreed upon the importance of publishing the back papers promptly. There was a widespread feeling that IRE should offer more assistance than they have in the past. Finally, it was decided that a subcommittee comprising Chairman John Bohnert, Arthur Dorne, and Delmer Ports will present the problem to IRE, and take such other steps to relieve the problem as may prove feasible.

R. L. MATTINGLY
Vice-Chairman, Secretary-Treasurer, pro tem.

CHAPTER NEWS

Chicago

The program for the last meeting of the season of the Chicago IRE Section was sponsored by PGAP and was held May 17, 1957. It was devoted to the DEW Line and included a film, "Arctic Mission" by Western Electric, and a paper by Warren Morgan of Federal Electric Company. A PGAP meeting followed the section meeting with a paper by Charles Camillo of Amphenol entitled "Practical Applications of Radio Frequency Coaxial Cables."

The following officers were elected for the year beginning July 1, 1957: Chairman, N. J. Sladek, Amphenol Electronics Company; Vice-Chairman, F. A. Beaver, Sears Roebuck and Company; Secretary, H. L. Woodbury, Andrew Corporation.

Boulder

The following meetings have been held recently. On May 1, 1957, E. T. Pierce, Director of Atmospheric Physics Group at Cavendish Laboratory, Cambridge spoke on "Lightning Discharge Phenomena." This meeting was cosponsored by N.B.S. Radio Propagation Seminar. On May 23, 1957, K. G. Budden, guest worker at National Bureau of Standards, from the Cavendish Laboratory, Cambridge, England spoke on "Ionospheric Reflexion of Radio Waves." This was the tenth and last of a series of lectures on ionospheric wave propagation given by Dr. Budden while he was a guest worker at Boulder.

On June 12, 1957, Dr. B. Yost, Research Director, Ohio Oil Company, Denver, Colo., spoke on "Modelling in Electromagnetic Methods of Geophysical Prospecting."

On June 3, 1957, Jack W. Herbstreit spoke on "The Present Status and Future Prospects of PGAP." Mr. Herbstreit explained the financial problem facing PGAP and possible solutions were suggested. The local chapter agreed to donate $100 to the National Committee. The unanimous opinion of the members was that the IRE should provide direct assistance. The Boulder Chapter elected new officers: Herman V. Cottony, Chairman; Don Watt, Vice-Chairman; Al Barsis, Secretary-Treasurer.

Los Angeles

The January meeting of the Los Angeles Chapter of the PGAP was held jointly with PGMTT and featured speakers from both groups. Robert E. Plummer of Hughes Aircraft spoke on "Microwave Aspects of a Circularly Polarized Feed for Beacon Antennas," and G. Fonda-Bonardi of DeMornay-Bonardi, Inc., spoke on "A Microwave System for the Accurate Measurement of Frequency in the 10–50 KMC Region." At the March meeting of the PGAP, Georges G. Weill of California Institute of Technology presented a paper on "The Cigar Antenna," an extremely long modulated end-fire array developed when the author was in Paris. Meetings are held every other month at the IAS Building, 7660 Beverly Boulevard at 8 P.M., and are preceded by a dinner at the Encore Restaurant, 806 N. LaCienega, at 6 P.M.

FUTURE MEETINGS

An International Conference on "Ultra High Frequency Circuits and Antennas," will be held in Paris from October 21 to 26, 1957. Correspondence should be directed to the Conference Central Office, Congres "Circuits et Antennas Hyper-Frequences," Societe des Radioelectriciens, 10 avenue Pierre-Larousse, Malakoff (Seine).

contributions

An Interferometer for Radio Astronomy with a Single-Lobed Radiation Pattern*

A. E. COVINGTON† AND N. W. BROTEN†

Summary—**The 150-foot slotted waveguide antenna for operation on a wavelength of 10 centimeters at the National Research Council, Ottawa, Canada, is now in operation as one element of an interferometer. The other element is itself a simple interferometer with element separation equal to that of the long array and is placed to the west on the common E-W axis. A rotary phase shifter in the arm between the array and simple interferometer is used, after Ryle, with a phase-sensitive detector. The resultant pattern consists of the product of three terms: 1) The single-lobe pattern of the long array; 2) the interference pattern of the simple interferometer, and 3) the interference pattern between the simple interferometer and array. This configuration gives a twofold increase in E-W resolving power over a uniformly collecting aperture of equal dimension. The presence of two interference patterns suggests the name, "compound interferometer," and the new antenna produces a fan-shaped beam 2′ E-W×2° N-S. The instrument has been used to obtain daily drift curves of the sun.**

ASTRONOMICAL investigations made in the optical and radio regions of the electromagnetic spectrum require telescopes for the purpose of collecting radiant energy from distant sources with negligible contributions from adjacent sources. The parabolic reflector, for example, is extremely useful as a telescope where the power is collected at the focus by suitable methods in either the radio or the optical regions. This power is proportional to the area of the reflector, while the ability to separate one radiating source from another is proportional to the linear dimension of the aperture expressed in number of wavelengths. The construction of successively larger and larger reflectors has been principally for the purpose of detecting fainter sources. In the optical region, it has been found that the resolution of larger apertures is seldom fully effective because the earth's atmosphere presents localized regions of varying refraction. This effect becomes severe for apertures greater than 10 or 20 inches. The resolution of large radio telescopes operating in the middle of the radio spectrum appears to be fully effective, but still falls far short of that of even a modest optical telescope. In the radio spectrum, the present limitation of achieving high resolution lies in the difficulties of construction and in high cost. Resolution will be a problem of prime importance and already several telescopes have been made with one dimension considerably lengthened so that much greater resolving power is attained in one plane. The resultant reception pattern is analogous to the diffraction pattern of a slit aperture. Further increase in the resolution is most readily obtained by interferometry methods. These principles were applied to optical astronomy by Michelson,[1] and in radio astronomy were applied by McCready, Pawsey, and Payne-Scott,[2] Ryle,[3] Bolton,[4] and others, as soon as it was ap-

* Manuscript received by the PGAP, September 17, 1956.
† Natl. Res. Council of Canada, Ottawa, Can.

[1] A. A. Michelson, "On the application of interference methods to astronomical measurements," *Phil. Mag.*, vol. 30, pp. 1–21; July, 1890.

[2] L. L. McCready, J. L. Pawsey, and R. Payne-Scott, "Solar radiation at radio frequencies and its relation to sunspots," *Proc. Roy. Soc. A*, vol. 190, pp. 357–375; August, 1947.

[3] M. Ryle and D. D. Vonberg, "Solar radiation on 175 mc/s," *Nature*, vol. 158, pp. 339–340; September, 1946.

[4] J. G. Bolton and G. J. Stanley, "Variable source of radio frequency radiation in the constellation of Cygnus," *Nature*, vol. 161, pp. 312–313; February, 1948.

parent that point-like sources of emission existed on the solar disk and in the sky.

Radio techniques for the transmission and amplification of radio waves have a flexibility that as yet has not been found for the handling of light emissions. This difference has led to the development of several new types of radio interferometers. One form employs a radio transmitter link[5] between two elements of an interferometer. Another entirely new development employs cross correlation of the low-frequency energy fluctuations[6] from the two antennas. In the system of phase switching introduced by Ryle,[7] a half wavelength of feeder to one antenna is alternately introduced and removed, and has the effect of combining the voltages from the two antennas alternately in phase and then out of phase. A phase-sensitive detector is required to separate the steady and the fluctuating components and enables the continuous background emission to be separated from point-like sources of emission. The above systems have multiple lobes or fringes and thus lead to ambiguity when two or more discrete sources are contained within the angular lobe structure. Ryle[7] also showed that shaping of the resultant antenna patterns was possible by using different antennas for the two elements of an interferometer. A system suggested by Ryle and adapted by Mills[8] consists of two linear arrays mutually perpendicular to each other to form a cross. Phase switching between the two linear arrays gives a signal only for those sources which lie in the common part of the crossed fan-shaped antenna patterns, and the result is a pencil beam antenna pattern having a resolving power equivalent to the rectangle enclosing the cross but with greatly reduced gain. Vitkevich[9,10] has suggested that the interference fringes formed by path differences of several wavelengths will be minimized by receiving a large portion of the intrinsically wide spectrum of the radio sources and will thus lead to the formation of a single central lobe.

Interferometry has recently been brought into use at the solar noise observatory of the National Research Council at Ottawa, to study the surface brightness of the sun at a wavelength of 10 cm (3000 mc). Two small antennas are so arranged in conjunction with the 150-foot nonresonant slotted waveguide array that the overall aperture in the E-W direction is 300 feet, or 900 wavelengths. The combination of the array and the twin-element interferometer antenna patterns by a phase-switching system results in a single-lobed receiving pattern with a half-power width of 2.4 minutes of arc in the E-W direction.

Description of Apparatus

The slotted waveguide array was built in 1951 and has a fan-shaped antenna pattern whose beamwidth to the half-power points is 8 minutes of arc in the E-W direction, and 22° in the N-S direction. A more detailed description has been made elsewhere.[11] Fig. 1 shows the physical arrangement of the array and the two antennas which form a simple interferometer. The additional antennas are parabolic cylinders, 10 feet wide and 8 feet long, with short lengths of slotted waveguide at the focus having characteristics similar to the slotted waveguide in the long array. One unit is set close to the west end of the long array, while the other is set further away on the same common E-W axis, so that the separation between the two is approximately equal to the length of the array. The narrow section of the array pattern may be placed at any hour angle from about 3° to 9° east of the meridian by proper choice of the receiver frequency in a band ranging from 2770 mc to 3000 mc. The individual elements of the simple interferometer have primary patterns of 3° E-W by 2° N-S, and likewise will be automatically placed at the same hour angle as the array. However, all three units must be adjusted mechanically in order to have the same elevation. The feature of shifting the resultant beam in hour angle has proven very valuable, and instrumentation has been made to take four drift curves each day. This involves the successive use of two local oscillators in the superheterodyne receiver, with reception occurring separately, first on the higher frequency sideband and then on the lower frequency sideband of the respective oscillator. The long array aperture is 148.2 feet, the separation of the two parabolic elements is 144.6 feet, and separation of the phase centers of the array and interferometer is 154.4 feet.

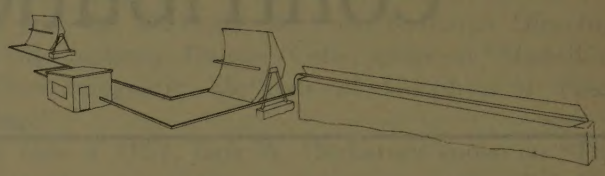

Fig. 1—Schematic of 10-cm compound interferometer for radio astronomy. Left-hand antennas—twin element interferometer, and right-hand antenna—slotted waveguide array.

The two small antennas operate as a simple interferometer, while the array and this unit operate as a

[5] B. Y. Mills, "Apparent angular sizes of discrete radio sources," *Nature*, vol. 170, p. 1063; December, 1952.

[6] R. H. Brown and R. Q. Twiss, "A new type of interferometer for use in radio astronomy," *Phil. Mag.*, vol. 45, pp. 663–682; July, 1954.

[7] M. Ryle, "A new radio interferometer and its application to the observations of weak radio stars," *Proc. Roy. Soc. A*, vol. 211, pp. 351–365; March, 1952.

[8] B. Y. Mills and A. G. Little, "A high-resolution aerial system of a new type," *Austral. J. Phys.*, vol. 6, pp. 272–278; September, 1953.

[9] V. V. Vitkevich, "Wide band radio interferometer," *Doklady Akad. Nauk S.S.S.R.*, vol. 91, no. 6, pp. 1301–1303; 1953.

[10] V. V. Vitkevich, "A new system of modulation radio reception of weak signals and its application to the creation of a high resolving power radio telescope," *Doklady Akad. Nauk S.S.S.R.*, vol. 102, no. 3, pp. 469–472; 1955.

[11] A. E. Covington and N. W. Broten, "Brightness of the solar disk at a wave-length of 10.3 centimeters," *Astrophys. J.*, vol. 119 pp. 569–589; May, 1954.

second interferometer. A rotary phase shifter[12] in the waveguide transmission line between the array and the interferometer introduces a linear change of phase with respect to time, as needed in a phase-switching system. The radio-frequency voltage at the receiver input is a vector sum of the voltages from the interferometer and the array, and since the phase shifter rotates one vector with respect to the other at 15 cps, the rectified power output contains a steady term as well as an alternating term. The resultant antenna pattern is obtained by combining the alternating receiver voltage, after appropriate amplification, with a reference voltage of the same frequency in a phase-sensitive detector, and appears as the product of three antenna patterns: the simple interferometer pattern, a second interference pattern due to the displacement of the two component antenna systems, and the single-lobe fan-shaped pattern of the long array. The new antenna configuration involves an E-W length twice that of the array, but produces a single-lobed antenna pattern whose E-W width, as measured by the angular distance from maximum to first zero (2 minutes of arc), is one quarter that of the long array. The presence of the two interference terms suggests the name "compound interferometer," although this same principle whereby three radiation patterns are multiplied together may be applied to other configurations. In the present arrangement, the resultant pattern contains both positive and negative side lobes, and has an angular power distribution approximated by $\sin \chi/\chi$. Although the side lobes are larger than customary, this particular pattern has considerable advantage in the resolution of a source brightness function.

General Theory

The advantage of the particular pattern approximated by the compound interferometer is perhaps best revealed by considering the general formula in the one-dimensional case which relates the power received by an antenna to the power emitted from a distant distribution of sources emitting thermal or thermal-like radiation. This is given by the convolution of the source brightness distribution with the antenna pattern, and written as (1):

$$R(\theta) = \int A(\theta - \chi) S(\chi) d\chi \qquad (1)$$

where

$R(\theta)$ is the power output when the maximum of the antenna pattern is directed towards θ,

$A(\chi)$ is the power pattern of the antenna at an angular distance χ from the antenna maximum, and

$S(\theta)$ is the temperature brightness of the source as a function of the angle θ.

[12] A. G. Fox, "An adjustable wave-guide phase changer," Proc. IRE, vol. 35, pp. 1489–1498; December, 1947.

As the antenna scans the object, the observed response, $R(\theta)$, will be the source brightness blurred by the antenna power pattern. In order to obtain a true knowledge of the source distribution, it is necessary to remove the averaging effect of the antenna pattern by solving (1) for $S(\theta)$ in one of several ways. Another representation of this averaging process involves the Fourier integral theorem, which transforms the convolution in the angular variable θ into a corresponding relationship in the spatial-frequency variable s. This relationship is given by

$$\overline{R(s)} = \overline{A(s)} \cdot \overline{S(s)} \qquad (2)$$

where $\overline{R(s)}$, $\overline{A(s)}$, and $\overline{S(s)}$ are the Fourier spectra for the three functions defined for (1). As in the previous equation, the source function, now $\overline{S(s)}$, is unknown, and is to be found by solving (2). A much simplified geometrical representation of the two equations is shown in Fig. 2. The spectrum representation of the

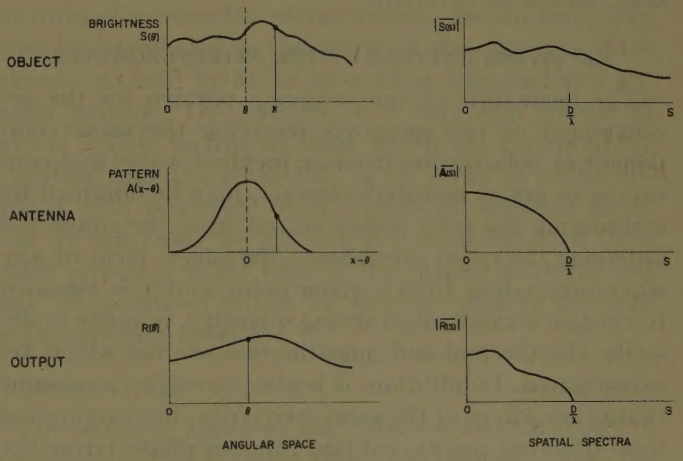

Fig. 2—Modification of object structure by antenna pattern. Left-hand side—in angular space, and right-hand side—in spatial frequency.

antenna pattern is known from other experiments and has the property of being zero for all values greater than some limiting frequency s_e given by the relationship $s_e = D/\lambda$, where D is the aperture of the antenna. This method of analysis suggests that the action of the antenna may be regarded as a filter, and the spectrum of the antenna pattern may be spoken of as the antenna band-pass.[13,14] The spectrum of the observed response $\overline{R(s)}$ is, according to (2), the original spectrum of the source multiplied by the band-pass of the antenna. The process of observing through any telescope thus distorts the image of the distant object, corresponding to the irretrievable loss of all frequencies from the source

[13] R. N. Bracewell and J. A. Roberts, "Aerial smoothing in radio astronomy," *Austral. J. Phys.*, vol. 7, pp. 615–640; December, 1954.

[14] J. Arsac, "Transmissions des fréquences spatiales dans les systèmes récepteurs d'ondes courtes," *Optica Acta*, vol. 2, pp. 112–118; October, 1955.

distribution greater than the cut-off frequency, and to a modification of the lower frequencies passed by the telescope. This modification is related to the relative shape of the antenna pattern, and may be removed from the observed results by solving (2). This solution, known as the principal solution,[13] gives the original spectrum with, however, the higher frequencies still missing. Although it may not be a good approximation to the source function, it is the best that can be obtained without other knowledge of the source. If this additional knowledge about the source exists, then the principal solution with its maximum of initial information represents the best starting point for further approximations. The principal solution may also be obtained with an antenna having the pattern represented by the function $\sin \chi/\chi$ since the corresponding frequency band-pass is constant from zero to the cut-off frequency, and no distortion is introduced in the portion of the source spectrum accepted by the antenna. It is in this sense that this particular antenna pattern with its relatively large side lobes is an optimum.

Receiving Pattern of the Interferometer

The derivation of the receiving pattern for the arrangement of two antennas receiving the same component of polarization from an incident wave, and connected to act as an interferometer, may be obtained by considering the total power output from the connected antennas. In radio astronomy, the phase term of any wave originating from a given point source is assumed to contain a randomly varying quantity, in order to describe the thermal and quasithermal sources which are investigated. In addition, it is also necessary to assume that other waves of the same frequency, but originating from different points, contain random phase terms not related to the first. The origin of a particular system of co-ordinates is taken at the central point of the line joining the two antennas. The angular variable θ lies in the plane containing the normal to the apertures and the joining line, while the variable ϕ is in a plane at right angles; both variables are measured from the normal to the aperture planes. The line joining the two antennas is usually placed in an E-W direction and, in this case, the θ variable describes the drifting motion of the sun or other celestial source through the antenna pattern. A schematic representation of the interferometer system and system of co-ordinates for the plane $\phi =$ constant is shown in Fig. 3.

A passing plane wavefront from a single point source induces voltages in the two antennas. Since the origin is taken at the central point of the two antenna systems, then at a given instant of time, the voltage from antenna A is given by

$$v_a = A(\theta, \phi) \exp [j(\omega t + k\theta + \beta)] \quad (3)$$

and from antenna B is given by

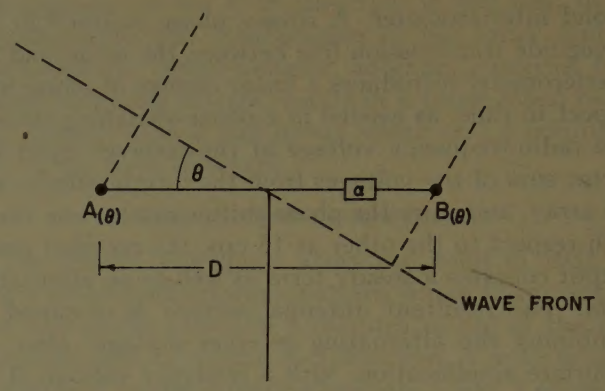

Fig. 3—Representation of system of co-ordinates for interferometer for plane $\phi =$ constant.

$$v_b = B(\theta, \phi) \exp [j(\omega t - k\theta + \beta + \alpha t)] \quad (4)$$

where

- ω is the angular frequency of the incident wave,
- k is π times the distance between the phase centers of the antenna, expressed in terms of wavelength,
- β is a random phase variable with values from 0 to 2π, and
- α is the time rate of phase change introduced by the rotary phase shifter.

The voltage output from the junction is

$$v = \frac{v_a + v_b}{\sqrt{2}}$$

$$= \frac{1}{\sqrt{2}} [A(\theta, \phi)e^{jk\theta} + B(\theta, \phi)e^{-j(k\theta - \alpha t)}]e^{j\omega t + \beta}. \quad (5)$$

The power output is

$$p = \frac{v \cdot \bar{v}}{2} = \frac{1}{2}\left[\frac{A^2(\theta, \phi) + B^2(\theta, \phi)}{2} + A(\theta, \phi)B(\theta, \phi) \cos (2k\theta - \alpha t)\right]. \quad (6)$$

The right-hand side of (6) is the power pattern of the interferometer; the first term is one half the sum of the power from each of the two antennas, and is present on the dc output of the receiver; the last term is a cross product output from the two antennas, and is present as a low-frequency fluctuating power corresponding in frequency to the electrical rotation of the phase shifter. The effective power gain of the fluctuating component is equal to the square root on the product of the power gains of each antenna. Two phases of fluctuating power are present which represent two antenna patterns and correspond to the trigonometrical expansion of the cosine term. This power output may be written

$$A(\theta, \phi)B(\theta, \phi) \cos 2k\theta \cos \alpha t + A(\theta, \phi)B(\theta, \phi) \sin 2k\theta \sin \alpha t. \quad (7)$$

In further discussions, the coefficients of cos αt and sin αt will be designated respectively as antenna patterns A_1 and A_2. The first pattern A_1 with suitable values for A and B gives a maximum in the direction of the point source; while the second pattern A_2 gives a minimum in the direction of the source, and as yet has not found much use in radio astronomy.

When several sources are present, both antenna patterns must be used in the convolution in order to obtain the total power received by the system. The magnitude of the fluctuating power as measured by the envelope of the low-frequency voltage is given by

$$v = \sqrt{\left[\int A_1(\theta - \chi)S(\chi)d\chi\right]^2 + \left[\int A_2(\theta - \chi)S(\chi)d\chi\right]^2} \tag{8}$$

and so is independent of the reference point of the phase term αt. On the other hand, the phase-sensitive channel, when adjusted to zero or quadrature phase, records only the power gathered by one of the antenna patterns. This separation of the two phases is accomplished electrically by means of a phase-sensitive detector driven by a reference voltage from the rotary phase shifter. The recorded output is a direct voltage proportional to the amplitude of the applied voltage times the cosine of the angle between the input and reference voltages. Corresponding to the in-phase and the quadrature-phase adjustments, either antenna pattern A_1 or antenna pattern A_2 is effective. The operation of two channels properly adjusted permits the simultaneous reception of A_1 and A_2. For the present application, simplification of the desired antenna pattern occurs if cylindrical antenna patterns are used such that $A(\theta, \phi) = A(\theta) \cdot A(\phi)$ and $B(\theta, \phi) = B(\theta) \cdot B(\phi)$; and in this case the pattern A_1 becomes the well-known result of the phase-switching system as used by Ryle,[7] and is given by (9):

$$A_1 = A(\phi) \cdot B(\phi) \cdot A(\theta) \cdot B(\theta) \cos 2k\theta. \tag{9}$$

The design of an antenna receiving pattern based upon the multiplication of two different patterns, together with an interference cosine pattern, has many possibilities. These possibilities may be discussed conveniently in classes, depending upon the relative values assigned to each of the factors: pattern A, pattern B, and phase term $k\theta$. Three classes of antenna pattern are suggested and will be discussed with reference to certain configurations of antennas.

1) $k\theta \neq 0$, $A = B$

The antenna elements are identical and if their angular pattern is broad with respect to one of the lobes of the interference pattern, the original interferometer system introduced by Ryle[3] is obtained. The receiver output gives the appropriate Fourier component of the source distribution.

2) $k\theta = 0$, $A \neq B$

If the separation between the phase centers of each antenna is zero, the interference term will be a constant equal to one, and the resultant power pattern is the product of the two voltage patterns. When one of these patterns is very broad with respect to the other, the resultant power pattern approximates the narrower voltage pattern of the other antenna. The antenna patterns of A and B may be those associated with two slit apertures, and if the antenna elements are arranged in the form of a cross, the phase centers overlap and a gap must be introduced in the center of the elements. This system was used by Mills[8] to produce a single-lobed antenna pattern. The pattern of A may also consist of several widely separated lobes which are produced by a grating antenna consisting of an array of small antennas with relatively large separation between members. In this case, the pattern of B must have the form which selects a single lobe of the grating pattern, and may be produced either by another grating or large single-aperture antenna.

3) $k\theta \neq 0$, $A \neq B$

The antenna elements are different and arranged to have a separation between their phase centers. Since the interference term is effective, the antenna systems in this class may be called asymmetrical interferometers. The separation can be chosen, for the antennas discussed in 2), so that the cosine term of the interference sharpens the resultant single-lobe patterns.

Compound Interferometer

The arrangement of simple interferometer and long array previously outlined, form an asymmetrical interferometer. The asymmetrical antenna configuration in the form of a T was also investigated at the same time as the compound interferometer, since this involved using only the parabolic reflector adjacent to the long array. Its operation was satisfactory, and the resultant antenna pattern and adjustment may be inferred readily from the discussion of the compound interferometer. In order to calculate the resultant antenna pattern of this antenna, it will be assumed that the adjustments have been made so that the three components of the antenna pattern lie with coincident maxima. The array pattern

is formed by collecting energy uniformly along the length of the waveguide, and its voltage pattern in the θ direction is given by

$$B(\theta) = B\frac{\sin k_2\theta}{k_2\theta};$$

the voltage pattern of the simple interferometer is given by the expression

$$A(\theta) = A\cos k_1\theta;$$

and the resultant power pattern is given by

$$A_1' = A\cos(k_1\theta)B\frac{\sin k_2\theta}{k_2\theta}\cos 2k_3\theta \qquad (10)$$

where

k_1 is equal to π times the effective distance between the two elements of the simple interferometer expressed in number of wavelengths,

k_2 is equal to π times the aperture of the long array expressed in number of wavelengths,

k_3 is equal to π times the effective distance between the phase centers of the array and the interferometer.

The resultant antenna pattern is an optimum when the component antennas are spaced such that $k_1 = k_2 = k_3 = k$; since with $k\theta = \chi$, (10) becomes

$$A\cdot B\cdot\frac{\sin\chi}{\chi}\cdot\cos\chi\cdot\cos 2\chi = AB\frac{\sin 4\chi}{4\chi}. \qquad (11)$$

It was not considered mechanically feasible to incorporate the dimensions for the production of the optimum pattern in the θ plane, into an experiment designed to test the feasibility of the system, but rather to work with the convenient distances which give a slightly different proportionality of phase terms, namely $k_1:k_2:k_3 :: 1.025:1.000:1.07$. The resultant pattern for a narrow band of frequencies is shown in Fig. 4, and is similar to the optimum pattern. The feature of great interest arising from the nonintegral ratio of phase terms is the predominence of negative side lobes extending over a considerable range of angle. In the ϕ direction (N-S), the resultant power pattern is essentially the 2° voltage pattern of the simple interferometer element, since the long array pattern in this direction is 22° broad. In the θ direction the corresponding 3° pattern of this antenna has been neglected since it is very broad with respect to the interference pattern.

Broadening of Antenna Pattern

The shape and positioning of an antenna pattern formed by interferometry are very dependent upon the frequency of observation. The shape of the antenna pattern that has been calculated holds for a small band of frequencies, and must be summed over a much larger range to find the effect of the actual receiver bandwidth used. The maximum of the array pattern shifts 1.5 minutes of arc per megacycle, and the broadening effect upon its resultant pattern has been calculated for various receiver bandwidths, and may be found in another report.[15] When the array was put into operation originally, a band-pass for the IF amplifier of about 1.5 mc was chosen, with only a 10 per cent increase in the half-power points. This was later changed to 0.5 mc band-pass, and when the compound interferometer was put into operation, this smaller band-pass was used.

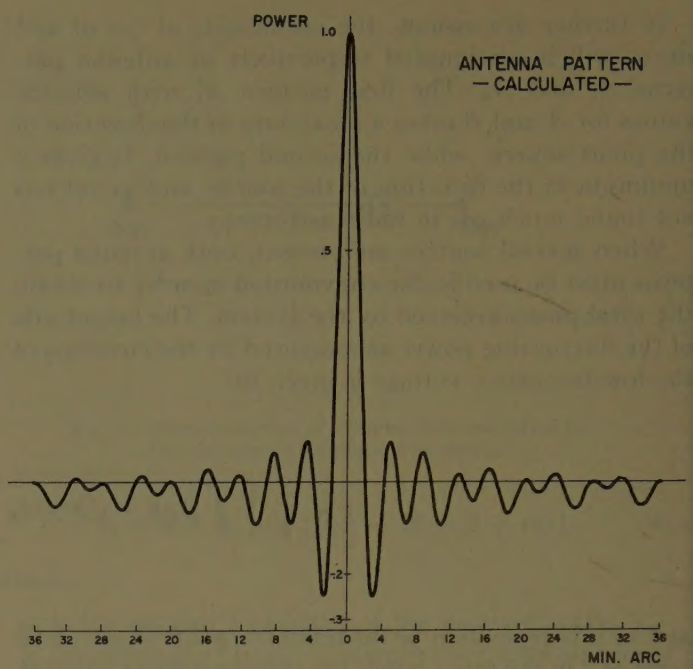

Fig. 4—Calculated power pattern of compound interferometer.

In the operation of this antenna, the angular shift with frequency of the array pattern is used to advantage in selecting the appropriate lobe given by the multiplication of the two cosine terms which form component parts of the over-all antenna pattern, and which are responsible for the sharpness of the resultant pattern. The broadening of this pattern will thus be introduced mainly by the frequency sensitivity of these two terms. When the frequency of observation is 2831 mc the antenna pattern is formed at an angle 4°28′ east of the meridian, and is the third in the series that is possible with the present instrumentation. At this angle from the central zero order fringe of the interferometer, the 32nd and 65th interference fringes are used in the formation of the lobe, and the shift with frequency amounts to 0.2 minute of arc per megacycle. Thus the broadening introduced into the main lobe of 2.4 minutes of arc is small, and has been neglected.

Alignment of Component Patterns

The linear dimension of an antenna such as the compound interferometer is so great that the antenna pattern cannot be tested by the conventional method of

[15] H. Gruenberg, "A waveguide array for solar noise studies," IRE Trans., vol. AP-3, pp. 147–152; October, 1954.

transmitting to the antenna from a distant point at various angles. Instead, reliance must be placed upon the calculated pattern based upon measured parameters. However, certain natural sources produce drift curves which are only slightly broader than the antenna pattern, and if these sources are assumed to be point-like, the drift curves provide an upper limit to the half-power width of the antenna pattern. Although the position of the long array single lobe, for various operating frequencies, was known from previous work, it was not known with sufficient accuracy to permit its alignment with one of the lobes of the simple interferometer. Further, the phase of the reference voltage generated by the rotary phase shifter cannot be set by calculation to give the desired pattern, and recourse must be made to experiment. The alignment of the three component antenna patterns has been by a series of approximations made on successive days, the necessary correction for the next day being deduced from certain features observed in the drift curves of the sun. These features were found in the drift curves through the use of a set of antenna patterns constructed with various errors in two of the three terms which make up the resultant pattern. This series of antenna patterns is based upon the optimum pattern, as given by $\sin 4\chi/4\chi$ of (11), and are shown in Fig. 5. The simple interferometer pattern was regarded as fixed, while phase shifts of 45° were placed in various combinations in the second interference term and in the long array pattern. Physically, the phase shift in the interference term is controlled by a dielectric phase shifter in the waveguide transmission line (alternatively, it may be adjusted by changing the phase of the reference voltage) while the phase of the array pattern is adjusted by a frequency change. Before making any adjustments, the arms of the simple interferometer were equalized.

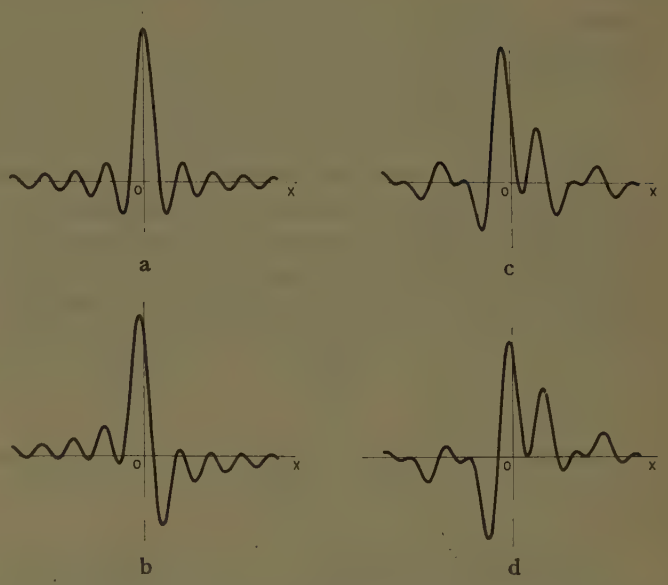

Fig. 5—Resultant patterns of compound interferometer produced by phase shifts in component parts. (a) Optimum pattern $\sin \chi/\chi \cdot \cos \chi \cdot \cos 2\chi = \sin 4\chi/4\chi$, (b) 45° phase shift in $\cos 2\chi$ term, (c) 45° phase shift in $\sin \chi/\chi$ term, and (d) 45° phase shift in both $\cos 2\chi$ and $\sin \chi/\chi$ terms.

In the drift curve of the sun, the easiest error to detect is in the second interference term, since in this case the side lobes on one side of the central lobe are predominantly negative, and on the other side are predominantly positive. This pattern has the effect of causing the base line of the scan, representing the sky background, to have a tilt with respect to zero level. A shift of about 10° in this term has been detected readily. A shift in the position of the long array pattern has the effect of introducing a ripple on the base of the scan with a period corresponding to that of the simple interferometer as recorded in the total power channel (dc) and is not so readily detected. The alignment of the simple interferometer and the array has also been studied by recording the envelope of the fluctuating power given by (8).

The adjustment of the antenna patterns should remain unchanged, provided all factors relating to the phase terms remain the same. However, the antenna and the feeder system are outdoors, and subject to the temperature changes which occur from day to day. Changes in waveguide dimensions occur with corresponding phase changes in the component antenna patterns. The interferometer feeder systems have been designed with equal arm lengths so that only temperature differences are significant. A temperature difference of 1°C between the two 75-foot lengths of waveguide used in the simple interferometer cause a shift of about 2.25° in phase angle, with a corresponding shift of the reception pattern of about 0.04 minute of arc. Since the feeder arms between the interferometer and the array (antennas A and B) are about twice as long, a similar differential would produce twice as large an angular phase shift. The temperature difference between interferometer arms may be minimized by placing the waveguide in a housing, but this has not been done. On occasion, effects attributed to a phase difference in the arms of the interferometer were discernible in the drift curves, and have been related in a qualitative manner to phase changes measured by means of a standing wave pattern.

The squint angle of the array pattern with respect to the normal of the array is a function of the frequency, the spacing of the slot radiators, and the dimensions of the waveguide. A temperature change of +10°C will cause the squint angle to increase by approximately 1 minute of arc, while a frequency change of −0.75 mc causes a decrease in squint by the same amount. These calculated rates of change have been successfully used with the observed temperature changes of the array to maintain the antenna pattern over a wide range of temperature variation. Other residual second-order effects remain, and have not yet been explained.

In order to keep the frequency of observation constant, the oscillator frequency is monitored by a cavity wavemeter with a Q of 20,000, and the frequency is set manually to the desired value. The short-term fre-

quency stability of the local oscillator is generally considerably better than required.

Observations of the Sun on January 19 and 21, 1956

The compound interferometer was put into operation temporarily during the summer of 1955, and toward the end of the year nearly continuous observations were started. Two of the four drift curves taken near noon on January 19, 1956, are shown in Fig. 6. The upper (first)

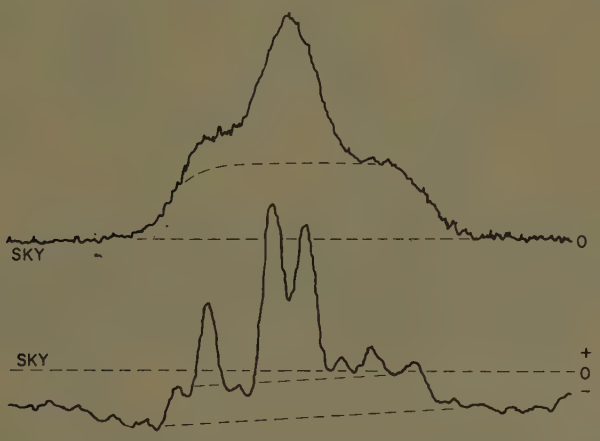

Fig. 6—Upper curve—solar drift curve taken by 150-foot array with pattern 8 minutes of arc E-W, and lower curve—solar drift-curve of 300-foot compound interferometer with pattern of 2 minutes of arc E-W, January 19, 1956.

drift curve was taken with the long array operating alone, while the lower (third) curve was taken with the compound interferometer. The fourfold increase in resolution obtained with the compound interferometer, with its single lobe, is very evident in its drift curve, since the unresolved structure of the upper drift curve appears as three intense point-like sources with possibly several fainter sources. The lower envelope, representing the emission from the solar background, is shown by the curved dashed lines joining the shoulders of both drift curves, and serves as a reference for the excess radiation from the regions of sunspot activity. The interferometer drift curve of the intense source on the eastern limb (left-hand side) has a half-power width which agrees with the calculated main lobe of the antenna within the error of observation, estimated to be ± 5 per cent; the first of the side lobes—taken as the small enhancements on either side of the central lobe—show an amplitude much smaller than expected, and are also displaced further from the main lobe than expected. These measured features of the drift curve are not consistent with a point source, and it is believed that the width of the main lobe and one of the side lobes has been modified by the side lobes of the intense double source whose center is 11 minutes of arc to the west. The other side lobe of the point-like source is modified by falling upon the edge of the solar disk. The components of the double source are apparently separated by 5 minutes of arc, and are about twice the limit of resolution of the antenna. The small single enhancement to the west of the double source is regarded as a side lobe of that spot, while the next larger enhancement is regarded as a combination of side lobe and possible weak radio-emissive region. The small source on the western limb was just about to disappear and was distinguished from a side lobe because it was seen several days before the intense source became visible.

The drift curve taken with the compound interferometer two days later, on January 21, is shown in Fig. 7.

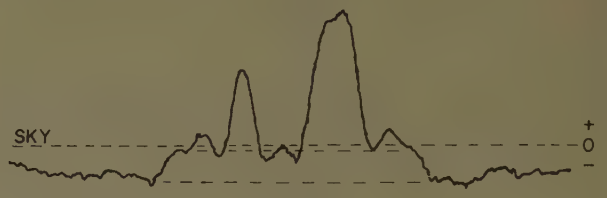

Fig. 7—Drift curve taken by 300-foot compound interferometer on January 21, 1956.

This reveals the effect of solar rotation of the spots with respect to the disk, as well as small but definite changes in their structure. The most noticeable change is that the double spot has become a single large region of E W extent comparable to that of January 19, and indicates either a broadening of the spots or a growth of emission between them. The single spot on the eastern limb is now slightly further away from the broad double region, 12 minutes of arc instead of 11 minutes of arc, and the principal lobe has increased from a half-power width of 2.4 to 3.0 minutes of arc. The side lobes are more pronounced than before, but still probably modified by other features such as the limb and nearby broadened double source. If it is assumed that the radio source is a point, the measured lobe width represents only a 25 per cent increase in beamwidth from the computed value of 2.4 minutes of arc. However, on the basis of various models of spots, the combination of broadened main lobe and side lobe reduction could be taken as an indication of the finite E-W width of the spot, and an upper limit of about 1 minute of arc may be assigned to this diameter. In this region of confusion, however, the exact width will be best revealed only through the use of an antenna with greater resolution. This point-like source is significant in that it shows that the antenna system operates essentially in the manner described, and that increased resolution by a factor of two or four may be sufficient to isolate one spot from another, as well as providing some indication of the spot structure. During the six months of observations, this source was the only one sufficiently isolated to serve as a test object. The absence of resolution in the N-S direction may introduce a fictitious doubling or broadening of spots, but fortunately for this period of observations, the intense solar activity, as revealed photographically, was so distributed that the indicated E-W extents of the radio-emissive regions must be real.

Other features of these drift curves may be related to the unusual nature of the antenna pattern. The sky background shows as a negative signal, and is produced by the extensive, predominantly negative, side lobes collecting energy when the main lobe is off the sun. The tilt of the sky base line on January 19 indicates a phase error of about 10° in the phase term of the second interference pattern (cos 2χ). The two drift curves have been copied from the curved Esterline-Angus paper, and have not been normalized with respect to the total disk emission as measured by the 4-foot reflector. If this is done the average intensity of the double peak on January 19 equals the intensity of the same region which appears broadened on January 21.

ACKNOWLEDGMENT

The authors wish to express their sincere thanks to Dr. G. A. Miller for his encouragement of the work, to W. J. Medd for designing the rotary phase shifter, to W. A. G. Kennedy for supervising construction of the interferometer, and to others who have given assistance in various ways.

Statistical Data for Microwave Propagation Measurements on Two Oversea Paths in Denmark*

P. GUDMANDSEN† AND B. F. LARSEN‡

Summary—**Measurements were carried out on 6.4-cm. and 17-cm wavelength on two optical paths, 54-km and 82-km long, stretching over sea nearly East-West and starting at the same point. For the greater part of the measurements, height-spaced receivers were used. The bulk of the statistical data comprises distributions of field strengths for every day of measurement. Curves for single receivers and diversity combinations of two receivers have been worked out. Distributions for every hour of a day as well as distributions of fade durations for a few days with special propagation conditions were obtained. A study of special fading phenomena with almost coinciding fades on the receivers in operation has been made.**

The data reveal that the field strength distribution for single receivers on days with a great number of fades generally approximates the Rayleigh distribution irrespective of wavelength, path, and antenna height within the range of height considered. The field strength distributions for diversity systems approximate the diversity Rayleigh distribution, which is derived from two uncorrelated Rayleigh distributed signals. Deviations from appropriate Rayleigh distribution towards more serious fading conditions seem to be more frequent and more pronounced for diversity systems than for single receivers. Distributions of fade durations are found to be log-normal. Measurements on three-height-spaced receivers on 17-cm wavelength indicate that the simple two-ray theory is insufficient to describe the fadings on a path over sea.

INTRODUCTION

THE PRESENT paper gives a summary of statistical analyses of recordings from propagation measurements carried out on two optical oversea paths in Denmark. These measurements were made in order to gather information concerning certain of the parameters of importance to a microwave link over sea.

The problems to be considered were: 1) choice of link distance, 2) choice of wavelength, 3) determination of the improvement obtainable by means of diversity reception, and 4) the necessary clearance of the direct ray of the paths. These items were mainly considered from a reliability point of view.

The first item was taken into consideration because, in a preliminary planning of a given link between two points on each side of the sea, it was found necessary—from a reliability point of view—to set up a relay station in an intervening island. In this way the link was divided into two paths, 54-km and 40-km long, both stretching over sea. However, it would be of great interest to avoid the relay station by using the direct path between the two points, 82 km over sea. Accordingly, simultaneous measurements were carried out on the 54-km path and the 82-km path, in order that a comparison of the propagation conditions could be made.

For the choice of equipment for the final communication link, it was important to ascertain if there were any essential difference between the reliability of the communication on different wavelengths. For this purpose, measurements were carried out on two wavelengths, 6.4 cm and 17 cm.

Diversity reception was investigated by the employment of height-spaced receivers on both paths and wavelengths. In the statistical analyses the recordings from single receivers were treated so as to simulate dual diversity switch systems (selector type).

In order to investigate the problem of clearance, a receiver was placed rather low so as to enable the detection of diffraction loss under unfavorable meteorological conditions.

The measurements were carried out in the autumn of 1953 and in the spring of 1954 on the 54-km path, while

* Original manuscript received by the PGAP, November 5, 1956; revised manuscript received, January 27, 1957. Presented at the International Symposium on Wave Propagation, Paris, France; September 21, 1956.

† SHAPE Air Def. Tech. Ctr., The Hague, Holland. Formerly with Microwave Lab., Danish Academy of Tech. Sciences, Copenhagen, Denmark.

‡ Microwave Lab., Danish Academy of Tech. Sciences, Copenhagen, Denmark.

the simultaneous measurements on the 54-km and the 82-km path were performed in the summer and autumn of 1954. A total of 14,000 hours of recording was obtained.

Test Circuits

The position of the antennas in the test circuit was determined on the basis of the simple two-ray theory.[1] This theory assumes that the refractive index of the atmosphere varies linearly with the height above the surface of the earth so that the direct and the sea-reflected rays on a sea path may become straight lines, a suitable correction factor, k, for the radius of the earth being employed. In general, this assumption oversimplifies the meteorological state of the atmosphere by taking only the major course into account. Accordingly, the two-ray theory should be regarded more as a convenient mathematical model than as a detailed physical description.

Fig. 1 shows the field strength variations which may be expected, according to this theory, when k varies between 0.7 and infinity. The field strengths are given relative to the calculated free space field strength, dBF. The curves have been labeled by a code stating the receiver antenna height above normal sea level in meters. The path length, d, the wavelength, λ, and the transmitter antenna height, h_T, are indicated in the diagrams. In the calculations the divergence of the reflected ray caused by the curvature of the earth has been allowed for. In the range of small k values the calculations have been based on the classical diffraction theory.

The position of the receivers has been chosen in such a way that no simultaneous fades will occur on the two receivers of a diversity system within the range of k values where interference fades occur. This diversity principle is fulfilled by all receivers except the lower 17-cm receiver on the 54-km path. This receiver, however, is the receiver for the detection of diffraction loss associated with small k values. The marks on the curves indicate the values of k for which grazing incidence occurs. It is seen that grazing may be expected for relatively great values of k on the lower 17-cm receiver on the 54-km path and especially on the receivers on the 82-km path.

The 17-cm measurements were carried out by means of equipment described by Grønlund and Lund.[2] A square-wave modulated magnetron was used as transmitter, while the receivers were of the crystal rectifier type with selective amplification of the repetition frequency. The 6.4-cm equipment was a commercial portable television equipment with superheterodyne receivers.

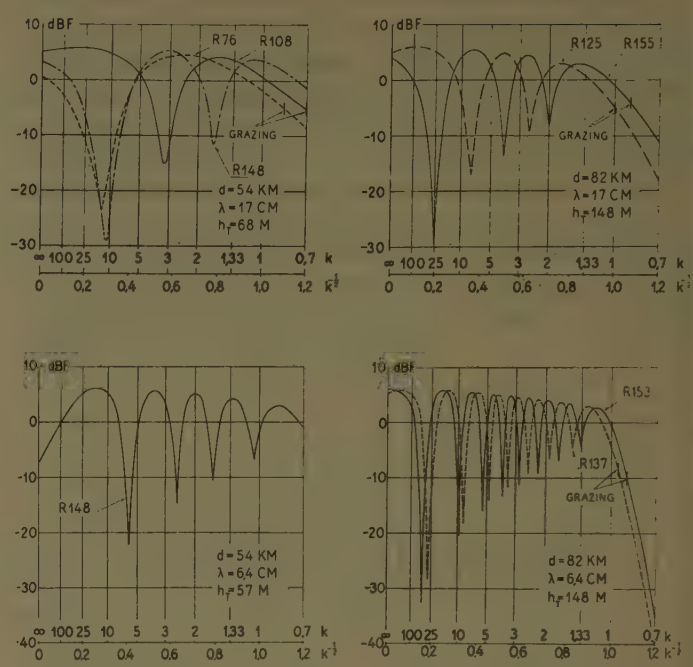

Fig. 1—Field strength variations calculated by the two-ray theory.

Results

The greater part of the statistical analysis has been performed by means of statistical equipment described by Lund and Grønlund.[3] The subsequent diagrams give a number of examples of the results obtained.

Fig. 2 gives distributions of field strengths for a day of a spring period, May 23, 1954. This day is considered representative of days with a great number of fades. The diagrams comprise curves for the three 17-cm receivers and the single 6.4-cm receiver in operation on that day, together with distributions for the three diversity combinations of the 17-cm receivers. In the diagrams, the field strengths are given by the ordinate in dbf. The abscissa gives the relative total fading time of a day in a logarithmic scale.

It is seen that all the curves for single receivers approximate the so-called Rayleigh distribution in the range of low field strengths. This theoretical distribution has a slope of 10 db per decade in a coordinate system like the one presented. The diversity curves approximate straight lines with a slope half that of the Rayleigh distribution. This distribution is called the diversity Rayleigh distribution, because it may be obtained by selecting the greater of two Rayleigh-distributed signals which fade independently.

It is obvious that a rather great improvement in reliability is obtained by employment of diversity in comparison with that obtained by means of a single receiver. Thus, it is seen, when taking as an example the

[1] D. E. Kerr, "Propagation of Short Radio Waves," M.I.T. Rad. Lab. Ser., McGraw-Hill Book Co., Inc., New York, N. Y., vol. 13, ch. 2; 1951.

[2] M. Grønlund and C. O. Lund, "Equipment for propagation measurements in the microwave range," presented at the URSI Meeting, Paris, France; September, 1956.

[3] C. O. Lund and M. Grønlund, "Electronic Equipment for Statistical Analysis," presented at the URSI Meeting, Paris, France; September, 1956. Published as Microwave Lab. Rep., The Danish Academy of Tech. Sciences, Copenhagen, Denmark; September, 1956.

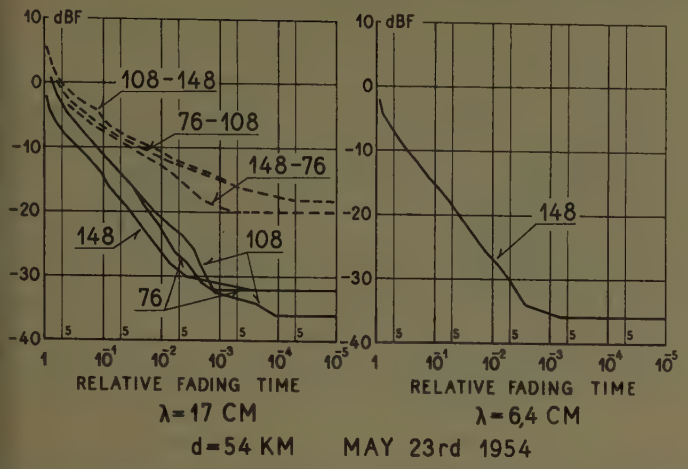

Fig. 2—Distribution of field strengths, May 23, 1954, 0–24 hours' 54-km path, 17-cm and 6.4-cm wavelengths. Numbers on curves indicate the receiver antenna height.

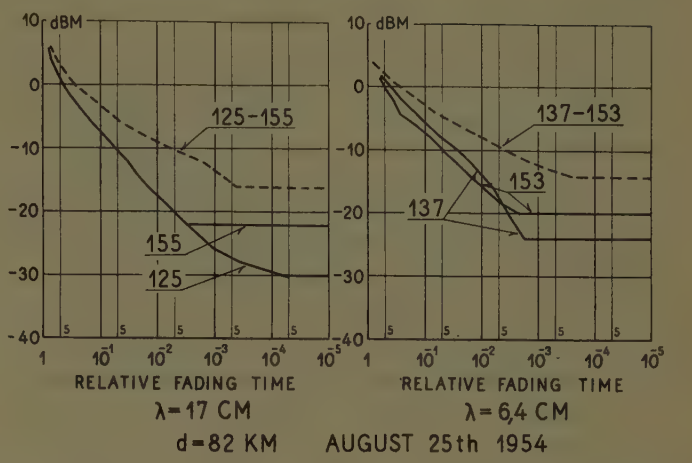

Fig. 3—Distributions of field strengths, August 25, 1954, 0–24 hours, 82-km path, 17-cm and 6.4-cm wavelengths. Numbers on curves indicate the receiver antenna height.

level of −16 dbf, that an improvement of about 13 times results from the use of the diversity combination of the upper and lower receivers, R148–R76. For the other two diversity combinations, improvements of about 100 times have been found.

The amelioration attained by means of height-diversity may be expressed in a different way, as it is seen that even if the field strength of the single receivers becomes very low, no simultaneous fades were below −20 dbf on that day. Thus, the amelioration may be given as a gain in db at a certain reliability. In the case considered here, a gain of 12 db has been found for the diversity combination of the lower and the upper receivers. In this connection, it should be mentioned that the largest gain encountered during the measurements was 19 db, while the smallest gain was only 4 db, the average value being 13.5 db. These figures are referred to 99.9 per cent reliability (10^{-3} relative fading time) and a field strength of −30 dbf.

An example of a day, August 25, of an autumn period with measurements on the 82-km path is given in Fig. 3. On that day very adverse fading conditions were found. The diagrams present distributions of field strengths for the two 17-cm and the two 6.4-cm receivers then in operation. The coordinate systems are similar to those used in Fig. 2, but the field strengths are given relative to the daily median field strength, dbm.

It is seen that also in these cases the distributions approximate the appropriate Rayleigh distributions. It is found that the diversity gain on that day is a little smaller on the 6.4-cm wavelength than on the 17-cm wavelength. However, the entire material of the tests on the 82-km path shows that the average value of gain is 12.5 db on the 6.4-cm wavelength against 10.5 db on the 17-cm wavelength. These figures have been obtained at 99.9 per cent reliability and with a field strength of −20 dbm.

From these examples and a great number of similar results, it may be concluded that on days with a great many fades the distributions of field strengths, both for single receivers and for diversity reception, approximate the appropriate Rayleigh distributions. This is the case irrespective of season, path, wavelength, and antenna height.

The ascertainment of the diversity distribution approximating the diversity Rayleigh distribution implies that the signal on the two receivers in question is non-correlated rather than that the fades are in phase-opposition, as might be foreseen from the simple two-ray theory, Fig. 1.

The rule, that the approximation to the Rayleigh distribution is independent of the parameters of the path, is a rather useful one, since no material limitations as to the choice of values for the parameters to be considered are imposed upon the designer of a communication link on an oversea path. However, a number of deviations from the Rayleigh distributions that reflect more serious propagation conditions have been found.

The schematic diagrams, Fig. 4, give an idea of the magnitude of the deviations met with; the examples are taken from the 17-cm measurements on the 54-km path. The left diagram concerns a single receiver, R108, and the right diagram the diversity combination formed by the receivers R108 and R148. The theoretical Rayleigh distributions have been drawn in the diagrams, together with dotted curves illustrating the distributions during 111 days, the entire period of measurement on this path. The other curves deviating from the Rayleigh distributions are envelopes of all distributions obtained. Envelopes are given for 24-hour periods as well as for single hours.

The distribution for the single receiver representing the entire period coincides with the theoretical curve, except on the lower field strength levels where the empirical curve reflects a smaller occurrence of fadings. The corresponding distribution for the diversity combination is approximately parallel to the theoretical Rayleigh distribution, but shows a smaller reliability. The

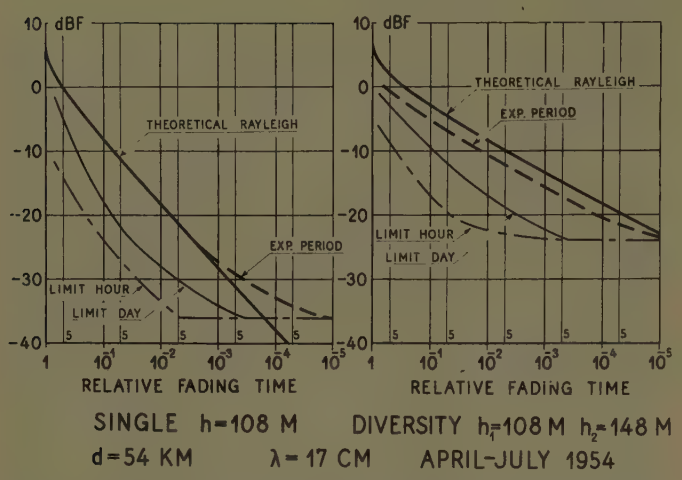

Fig. 4—Distributions of field strengths, April–July, 1954 (111 days), 54-km path, 17-cm wavelength. Limits of deviations from the Rayleigh distributions.

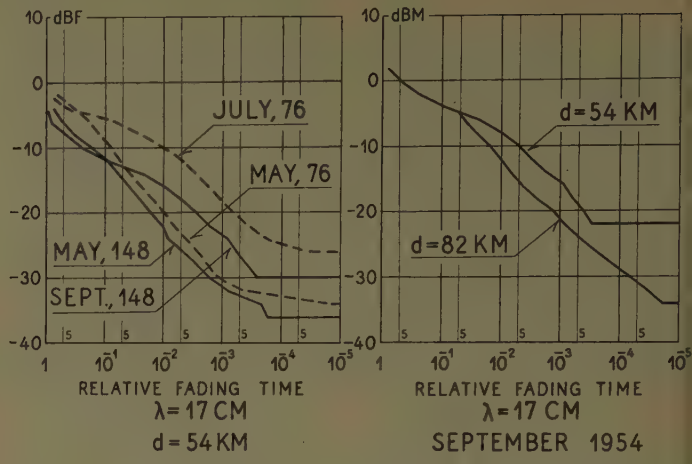

Fig. 5—Distributions of field strengths, monthly for May, July, and September, 1954, 54-km and 82-km paths, 17-cm wavelength.

displacement of the distribution is due to the fact that the median field strengths of the two receivers are different.

Deviations from the Rayleigh distribution within the limit given in this diagram have been found for a single receiver on 2.6 per cent of the days of the period of measurement. Deviations from the diversity Rayleigh distribution are exhibited 4.6 per cent of the days with diversity reception. These figures concern the measurements on the 17-cm wavelength; it should be added that the 6.4-cm wavelength exhibits no deviations on any day.

For the two days previously dealt with, May 23 and August 25, it was found that about 20 per cent of the hours of these days showed deviations from the Rayleigh distribution, and that the 6.4-cm wavelength had a slightly larger percentage of deviations than the 17-cm wavelength.

It has been found that the propagation is subject to a seasonal variation observable during the months from April to September in which measurements were carried out on the 54-km path. This will appear from Fig. 5, which shows distributions of field strengths for single receivers for certain months of the period. Curves are given for the upper and the lower 17-cm receivers, from which it may be seen that the seasonal variation is different at different antenna heights. The distribution for July, receiver 148, happens to coincide with the May curve for receiver 76. The lower receiver shows a much greater variation than the upper one. This observation should be given further consideration before it can be fully explained.

In the other diagram in Fig. 5 the propagation on the 54-km and the 82-km paths can be compared. The curves are derived from the measurements carried out simultaneously on the two paths in September. It is obvious that the shorter path has a greater reliability than the longer, but it must be admitted that the difference is a slight one. It should be added that a comparison between individual days of the month reveals that the longer path exhibits a larger number of days with Rayleigh distribution, and that deviations due to fading conditions severer than those of the Rayleigh distribution are far more frequent on the longer path than on the shorter.

A detailed investigation of various phenomena of simultaneous fades on at least the two lower receivers on the 54-km path has been carried out. This investigation was made as an attempt to detect whether the field strength variations could be ascribed to small values of k (see Fig. 1). An example of such an investigation is given in Fig. 6. Such diagrams are called correlation diagrams, as the simultaneous field strength variations on two receivers are plotted, one against the other.

The two correlation diagrams illustrate the same fading phenomena on the three height-spaced receivers in operation. The course of field strength variations is given by the letters added to the curves, the letters in the two diagrams corresponding to the same moment. In order to enable a reproduction of the diagrams, the actual variations have to some extent been simplified, the more important characteristics of the observed fadings being maintained. In the diagrams, the field strength variations calculated by means of the two-ray theory are also given for comparison with those arrived at experimentally. The parameters of the calculated curves are k values.

The most conspicuous characteristic of the experimental curves is that the field strengths generally are depressed during a fading period. This depression is superposed by other comparatively fast fades. Considering each diagram separately, it will appear that the fast fades, to a certain extent, may be described by means of the calculated course of field strengths, the depression

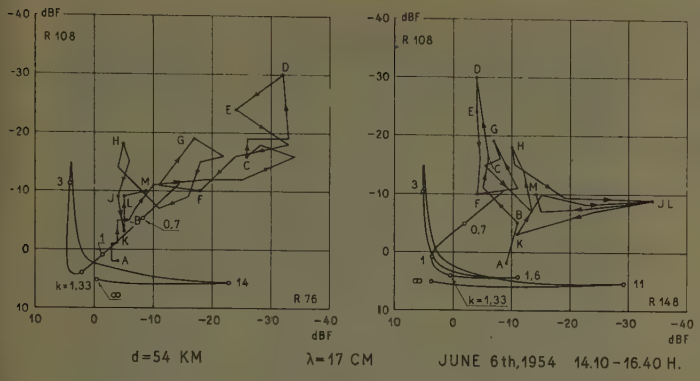

Fig. 6—Correlation diagram, June 6, 1956, 14.10–16.40 hours, 54-km path, 17-cm wavelength.

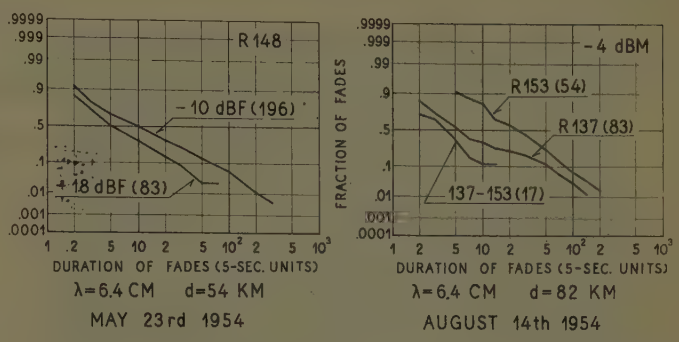

Fig. 7—Distributions of fade durations, May 23, 1954, 0–24 hours, 54-km path, 6.4-cm wavelength, and August 14, 1954, 0–24 hours, 82-km path, 6.4-cm wavelength. Numbers in parentheses indicate number of contributing fades.

mentioned being ignored, and the observations can be related to values of k. But, when the simultaneous diagrams are referred to each other, a difference in k-values will be found. The variations on the lower receiver can best be explained by meteorological effects corresponding to small values of k—diffraction—while the upper receivers exemplify interference fades associated with great values of k.

Similar fading phenomena have been studied and the same result arrived at. On this basis it may be concluded that small k values occur rather seldom, and that in rare cases only the propagation during deep fades can be described by means of the simple two-ray theory. However, it must be admitted, and this is confirmed by the diagrams in Fig. 6, that fades occurring simultaneously on two receivers are due to other meteorological effects, and that such fades are just as important as those expected in connection with diffraction effects. As the available meteorological data (synoptic data only) are rather coarse, no reliable information on the nature of the above mentioned meteorological effects has been obtained. It should be mentioned that no simultaneous deep fades on all three receivers were encountered during the measurements.

Finally, two examples of distributions of fade durations are given in Fig. 7.

The left diagram presents distributions for two field strength levels of a single receiver (148 m above normal sea level) on a day of the spring period. The figures added to the curves indicate the number of fades observed on that day. The durations are given in 5-second units in a logarithmic scale; the ordinate is a Gaussian scale. From this diagram it may be seen, for instance, that 0.05 or 5 per cent of the fades below −10 dbf on that day had a duration greater than 100 5-second units or about 8 minutes. Moreover, it is seen that the curves approximate straight lines, and thus, the distributions may approximate log-normal distributions.

The right diagram gives the distribution for a single field strength level but for two receivers and their diversity distribution. Again the distributions approximate log-normal distributions. The number of distributions of fade durations worked out is considered too small to give any reliable information as to the fit to the log-normal distribution and the parameters of distributions, but it has been found that the standard deviation of the approximating log-normal distributions tend to decrease with decreasing field strength level.

Acknowledgment

This paper rests on a more detailed report by the Microwave Laboratory, the Danish Academy of Technical Sciences, Copenhagen.[4] Copies of this report can be obtained from the Laboratory on request.

[4] P. Gudmandsen and B. F. Larsen, "Statistical data for microwave propagation measurements on two oversea paths in Denmark," Acta Polytechnica 213, Elec. Eng. Ser., vol. 7.

Some Observations of Antenna-Beam Distortion in Trans-Horizon Propagation*

A. T. WATERMAN, JR.†, N. H. BRYANT‡, AND R. E. MILLER†

Summary—3000-mc signals from a rotating narrow-beam transmitting antenna have been observed at distances from 92 to 177 miles. The manner in which the received power builds up and falls off as the transmitting beam sweeps past the receiver shows a variety of shapes instead of merely reflecting the transmitting-antenna pattern, as would be expected on a line-of-sight path. From a series of these received-power patterns, mean received power as a function of transmitting-antenna azimuth is obtained and, from this, an angular scattering function is derived. This angular scattering function, which is a characteristic of the path only, is used to predict the optimum antenna size for this path. These observations are also used to predict the improvement provided by a diversity system employing two identical receiving beams separated in azimuth only.

I. Introduction

IN RECENT YEARS considerable attention ha been given the propagation of microwaves to distances well beyond the horizon. Of the various characteristics of the received signal which have been the subject of measurement, those pertaining to the receiver response when a narrow beam is directed off-bearing from the great-circle path are of concern here. Interest in off-path contributions to the received signal has been stimulated by the turbulent-scattering hypothesis[1] which has important consequences[2] in regard to realizable antenna gain and usable bandwidths. Inasmuch as this type of scattering would be incoherent, net power reaching the receiver would not be expected to come entirely from the precise direction of the transmitter. Thus, the plane-wave gain of a narrow-beam antenna would not be fully realized, and the associated range of delay times would cause signal distortion.

The observations discussed below, which deal with transmissions at about 3000 mc over paths ranging from 92 to 177 statute miles, have a direct bearing on this problem. They illustrate the distortions that are introduced in an antenna pattern owing to inhomogeneities in the atmosphere through which the wave propagates.[3] Section II of this report outlines the methods by which these observations were made and indicates qualitatively the type of distortions in individual beam patterns that are likely to be encountered. In Section III, the mean received power vs transmitting-antenna bearing is reduced for a series of observations, to illustrate the apparent beam broadening that results when a trans-horizon transmission path is used. In Section IV, an analysis is made and an angular scattering function is developed, which is used in Section V to obtain an expression for the useful antenna width in transhorizon propagation. In Section VI, the usefulness of angular diversity as a result of the apparent beam broadening is discussed.

II. Qualitative Observations of Antenna-Pattern Distortions

Chisolm and co-workers[4] and Trolese[5] have performed beam-swinging experiments, results of which indicate that a significant amount of the received power arrives from angles a degree or so off the great-circle path. Measurements reported here differ from Chisolm's in that a movable narrow beam was used at only one end of the transmission path, the other end having a fixed broad beam. They differ from those of both Chisolm and Trolese in that the narrow beam was swung in azimuth through the great-circle bearing in a time interval which was short compared with the fading cycle of the received signal. Instead of averaging the received power associated with a given antenna orientation, this technique effectively provides an instantaneous snapshot of the apparent horizontal antenna pattern as viewed from a location well below the earth's bulge.

Fig. 1 provides some examples of these instantaneous antenna-pattern snap-shots.[3] To obtain the records shown, the signal from a high-power pulsed transmitter, as its narrow-beam (0.9°) was swung rapidly and uniformly in azimuth, was received using a relatively broad-beam (9°) stationary antenna. Both antennas were ground-based at elevations less than 40 feet above surrounding terrain. The rectified receiver output was displayed as the vertical deflection on an an oscilloscope whose beam was swept horizontally slowly enough to include the complete signal. Thus, the envelope of the received pulses portrays literally the effective horizontal transmitting-antenna pattern as seen from the receiving site. The pictures in the top row, Fig. 1(a)–1(c), were obtained in October, 1952, at a transmission distance of 92 miles. In Fig. 1(a) there is a double-peaked pattern, the left peak alone being roughly the shape of the free-space antenna pattern. Fig. 1(b) shows a very

* Manuscript received by the PGAP, January 24, 1957. Prepared under Signal Corps Contract DA 36-039-SC-63189.

† Stanford Electronics Labs., Stanford Univ., Stanford, Calif.
‡ Cornell Univ., Ithaca, N. Y. Formerly with Stanford Electronics Labs., Stanford Univ., Stanford, Calif.

[1] H. G. Booker and W. E. Gordon, "A theory of radio scattering in the scattering in the troposphere," PROC. IRE, vol. 38, pp. 401–412; April, 1950.

[2] H. G. Booker and J. T. deBettencourt, "Theory of radio transmission by tropospheric scattering," PROC. IRE, vol. 43, pp. 281–290; March, 1955.

[3] A. T. Waterman, Jr., "A Note on Microwave Reception Well Beyond the Horizon," Tech. Rep. No. 8, Nonr 225(10), Electronic Res. Labs., Stanford University, Stanford Calif.; October 15, 1953.

[4] J. H. Chisolm, *et al.*, "Multipath properties of tropospheric propagation," PROC. IRE, vol. 43, pp. 1317–1335; October, 1955.

[5] L. G. Trolese, "Characteristics of tropospheric scattered fields," PROC. IRE, vol. 43, pp. 1300–1305; October, 1955.

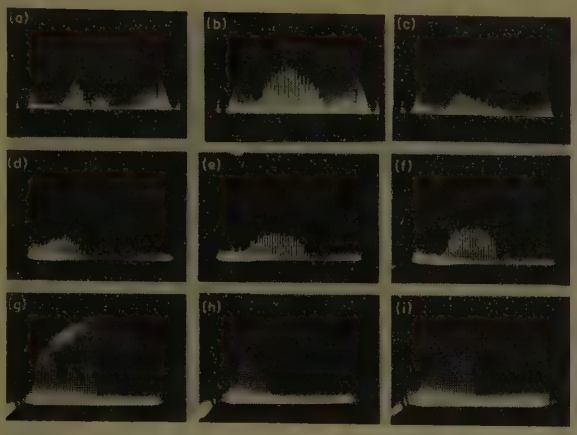

Fig. 1—Received patterns from a rotating transmitting antenna well beyond the horizon.

much broadened pattern, while in Fig. 1(c) there is a marked skewing. The remaining pictures in Fig. 1 were made in March, 1953, over greater distances in which the terrain was exceedingly flat. Receiver gain setting was readjusted but other equipment factors were the same as before. In Fig. 1(d)–1(f), the transmission distance was 129 miles. The prominent feature here is the pronounced "flattening" of the main lobe (definitely not caused by logarithmic response or saturation of the receiver) and the increased strength of the apparent side lobes to within 4 or 5 db of the main lobe, as distinct from the more-than-13-db difference measured at line-of-sight. After the distance was extended to 177 miles, the last three pictures, Fig. 1(g)–1(i), were obtained. Similar characteristics of skewing, multiple peaks, and broadening are in evidence here.

It is highly unlikely that these variations in apparent antenna pattern were caused by rapid fading of the signal during the brief interval in which the transmitted beam was sweeping past. In each case, the single sweep of the oscilloscope occupied $\frac{1}{5}$ second. Observations made with the transmitting beam stationary indicated no such rapid time fluctuations as could account for the above phenomena. Consequently, it seems reasonable to assume that the observed patterns were caused by spatial distortions. Time variations take place from one picture to another (at least several seconds), but not within one passage of the transmitted beam.

In order to provide a qualitative measure, of the extent of broadening, the horizontal antenna pattern as viewed within line-of-sight was measured. It is shown as a smooth curve superimposed on the two received patterns of Fig. 2. In each of these pictures it is the relative shape of the distant pattern as compared with the line-of-sight pattern that is of significance, not the relative position either horizontally or vertically. There was no synchronization between antenna rotation and oscilloscope sweep, so the precise instant at which the transmitting beam was aimed in the direction of the receiver was not known; and, of course, the line-of-sight signal level was many decibels above that measured beyond the horizon.

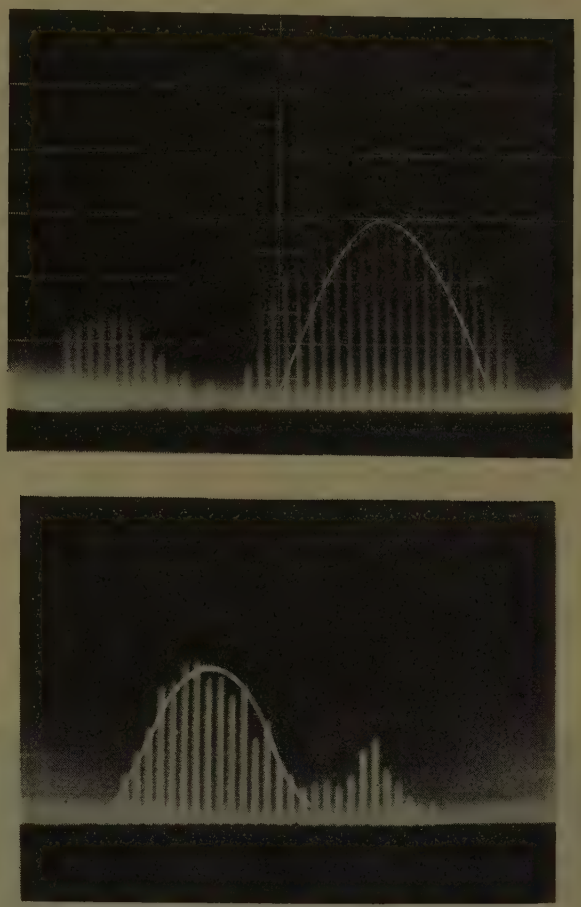

Fig. 2—Examples of received patterns with antenna pattern superimposed.

III. Mean Power vs Azimuth

For the 92-mile path, it was possible to make use of the reflection from a mountain that was within line-of-sight of both the transmitter and the receiver to obtain a time reference for the comparison of different signal patterns. The terminals of this path are each approximately 200 feet above sea level; the path is crossed by a range of hills 2000 feet in elevation at about one third of the distance from the receiver to the transmitter. This profile results in a minimum scattering angle of 1.7°.

Fig. 3 is a plan view of the path to illustrate how the rotating transmitting beam is reflected from the mountain 5.5° before reaching the great-circle bearing. This reflection provides a signal at the receiver that is a duplication of the transmitting-antenna pattern and one that is consistent from sweep to sweep.

Because of a lack of knowledge of the exact location of the reflecting area, no great accuracy can be attached to the instantaneous antenna bearing as determined from this signal; however, the relative positions of the antenna for different sweeps could be determined to within 0.1°.

Some typical pictures that include this reference signal are shown in Fig. 4. Each set of three pictures represents three consecutive passes of the transmitting beam at the rate of one pass every 12 seconds. The portion of

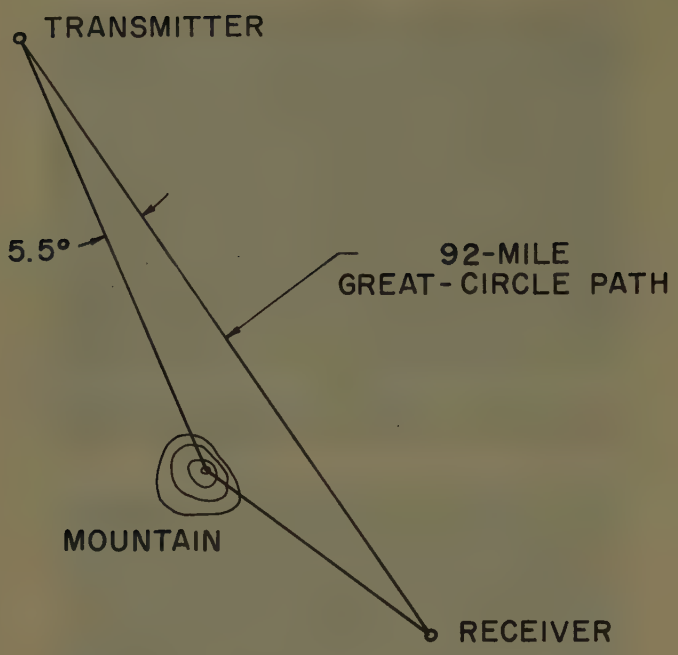

Fig. 3—Plan view of propagation path.

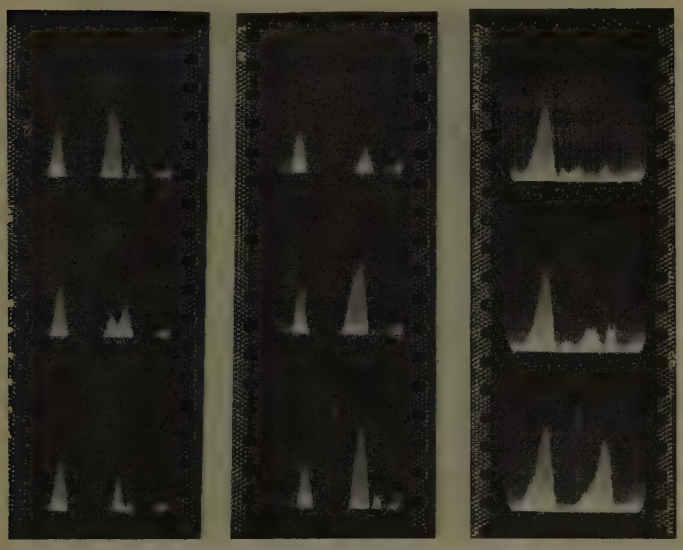

Fig. 4—Examples of received patterns with reference signal included.

the signal shown at the left of the picture is that received from the direction of the mountain—a separate narrow-beam antenna directed at the mountain was used to receive this signal. This reference signal remains unchanged in shape for a set of pictures, while the signal at the right, received on a 9° antenna beam directed along the great-circle path, shows the same variability that was discussed in connection with Figs. 1 and 2.

For Fig. 5, the data from two sets of consecutive pictures have been converted to power and plotted with their reference signals aligned. Thus, all the pictures of one set are plotted to a common antenna-azimuth scale. This plot clearly illustrates that the signal received along the great-circle path not only fades in amplitude,

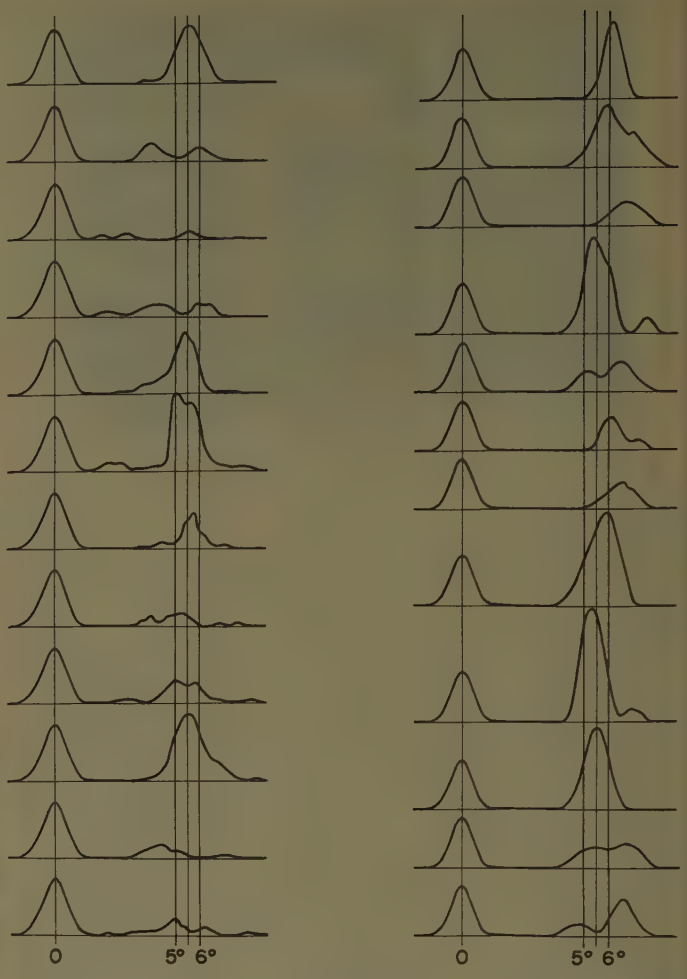

Fig. 5—Received power vs transmitting-antenna azimuth for two sets of consecutive passes of the transmitting antenna. Azimuth relative to that of the reflecting mountain.

but also changes shape, and that the direction for maximum signal shifts, relative to a fixed bearing.

Using the reference signals to align the pictures of a set, the received power can be averaged for each bearing to obtain a resultant curve of mean received power vs transmitting-antenna bearing. Examples of these curves of mean power are plotted in Fig. 6 along with the actual free-space transmitted pattern (dashed curve) to illustrate the apparent beam broadening.

If the width of the mean-power curve for 25 consecutive passes requiring 5 minutes is compared with that for 25 taken during the following 5 minutes, little difference is detected. However, from day-to-day, or at different times of the day, no such consistency is observed. The observed half-power widths varied from 1.0 to 1.8° with a 0.9° transmitting beam, and from 1.6 to 2.5° with a 1.3° transmitting beam. Attempts to correlate these variations with meteorological conditions have not been successful thus far. At this point, about the only general comment that can be made is that there appears to be an upper limit to the broadening and that, about half the time, the broadening exhibited is almost equal this

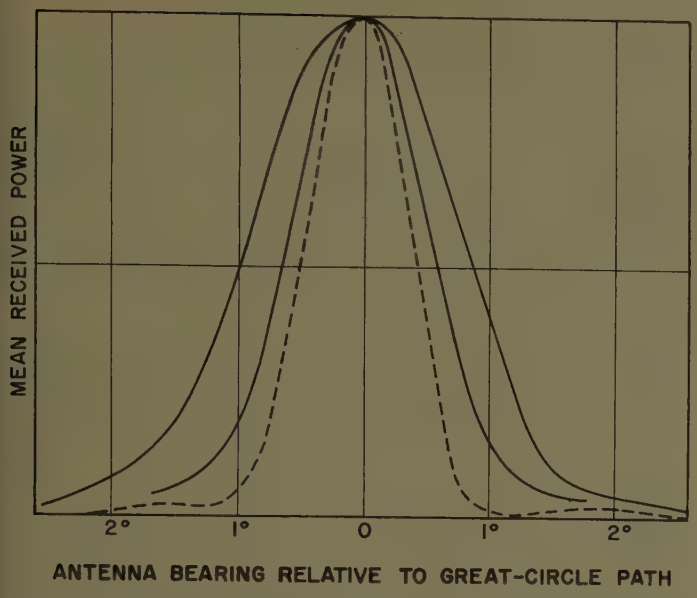

Fig. 6—Examples of mean received power vs transmitting antenna bearing. Free-space pattern of transmitting antenna shown with dashed curve.

maximum value. The broader of the two curves of Fig. 6 is typical of this half of the data.

IV. Angular Scattering Function

Curves of mean received power vs azimuth are dependent not only on the path geometry and the scattering properties of the atmosphere, but also upon the beam pattern of the rotating antenna. Only for an infinitely narrow beam can the received pattern be interpreted directly in terms of the scattering. If the pattern of the rotating antenna is known, however, the desired information is available from the application of a Fourier analysis.

In order to make the desired Fourier analysis, we introduce a scattering function $\rho_{(\alpha)}$ equal to the received power for an infinitely narrow transmitting antenna beam of unity gain. Thus, $\rho_{(\alpha)}$ is the response of this system to a unit impulse of antenna gain. If it is assumed that energy coming from different parts of the scattering volumes is uncorrelated, then the contributions to power will add and the net received power may be written in the same form as the superposition integral where the output of an electric circuit is written in terms of response of the circuit to a unit impulse. Thus, in terms of the bearing angles defined by Fig. 7, the received power as a function of transmitting antenna position is

$$P_{(\alpha_1)} = \int_{-\pi}^{+\pi} G_{(\alpha-\alpha_1)}\rho_{(\alpha)}d\alpha \qquad (1)$$

where

$G_{(\alpha-\alpha_1)}$ = gain of transmitting antenna in the α direction when the antenna itself is directed at α_1.

$\rho_{(\alpha)}$ = received power per unit azimuth angle for unity transmitting antenna gain.

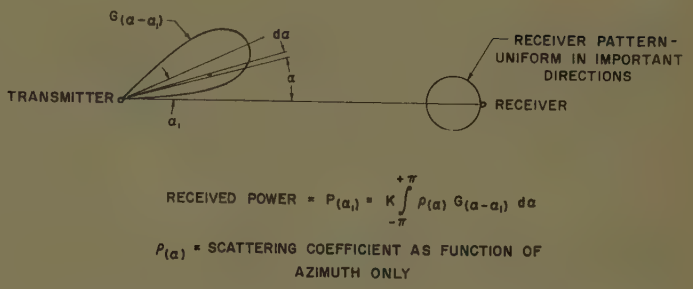

Fig. 7—Plan view illustrating relationships among received power, rotating beam pattern, and rotating beam position.

The analogy between (1) and the superposition integral of electric-circuit analysis can be carried further. Fourier transforms can be applied to this situation precisely as they are to electric circuits. Thus

$$\mathfrak{F}[P_{(\alpha)}] = \mathfrak{F}[G_{(\alpha)}]\cdot\mathfrak{F}[\rho_{(\alpha)}] \qquad (2)$$

where $\mathfrak{F}$ indicates the Fourier transform of the bracketed function. If (2) is solved for $\rho_{(\alpha)}$, we obtain

$$\rho_{(\alpha)} = \mathfrak{F}^{-1}\left\{\frac{\mathfrak{F}[P_{(\alpha)}]}{\mathfrak{F}[G_{(\alpha)}]}\right\} \qquad (3)$$

where $\mathfrak{F}^{-1}$ indicates the inverse Fourier transform. Eq. (3) gives a method of determining $\rho_{(\alpha)}$ from a knowledge of received power vs azimuth and the rotating-antenna gain pattern.

The operation just described (except that the Fourier series form was used) was performed on the two $P_{(\alpha)}$ curves of Fig. 6, and the resultant $\rho_{(\alpha)}$ curves plotted in Fig. 8 (solid lines). Although the data for Figs. 6 and 8 were obtained using a 0.9° transmitting beam, similar results were obtained with a 1.3° beam; that is, the broadest $\rho_{(\alpha)}$ curves were essentially the same width for both beams.

In order to make a comparison between the broadening so observed and that to be inferred from various theoretical models, some computations were carried out under the assumption of a noncoherent volume scattering. The received power, in such circumstances, can be expressed as a volume integral involving antenna gain functions and the scattering cross section σ (power scattered per unit solid-angle per unit incident power-density per unit volume). If one of the volume coordinates is the azimuth angle α, then integration over the other two yields the above scattering function $\rho_{(\alpha)}$. Such integrations were performed numerically for an approximation to the experimental radio path which involved the following simplifications: 1) receiver-antenna gain independent of azimuth and elevation; 2) transmitter-antenna gain dependent on azimuth only; 3) same minimum scatter angle of 1.7° as on actual path; 4) a horizontal intersection of the two radio horizons; and 5) same location of radio-horizon intersection with respect to the two terminals as on actual path. The resulting

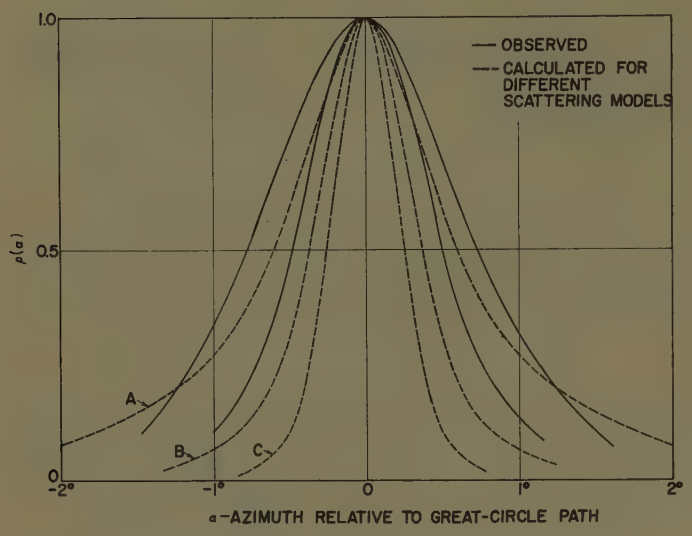

Plot of Angular Scattering Function

Experimental curves for 92-mile path with 1.7° between radio horizons. Calculated curves for smooth earth path with 1.7° between horizons.

A) Inverse fourth power with scatter angle and uniform with height.

B) Inverse fourth power with scatter angle, but limited to intersection of two horizontal planes.

C) Same as B, except inverse eighth power.

Fig. 8—Scattering as a function of azimuth for omnidirectional receiving antenna and no elevation dependence at transmitting antenna. 92-mile experimental path with minimum scattering angle of 1.7°.

curves, shown as dashed lines in Fig. 8, correspond to the following three scattering dependencies (of the cross section σ):

Case A) Inverse fourth-power dependence on scatter angle and uniform scattering with height.

Case B) Inverse fourth-power dependence but scattering limited to the intersection of the two radio horizons—as with scattering from a low layer.

Case C) Same as B but with inverse eighth-power dependence on the scatter angle.

The half-power widths of the empirical and theoretical curves of the scattering function $\rho_{(\alpha)}$ are listed in Table I (for the same data as employed in Fig. 8).

TABLE I

Half-Power Width of Scattering-Function Curves $\rho_{(\alpha)}$

Observed experimentally		Computed theoretically	
1) Typical of half the data:	1.5°	Case A:	1.20°
		Case B:	0.75°
2) An example from other half of data	1.0°	Case C:	0.49°

It is to be noted that only one of these theoretical models (Case A) yields a pattern of a breadth comparable with the cases observed; and even it is not as wide as the broader of the two empirical curves (solid lines). The implication is that if the propagation mechanism involves a noncoherent volume scattering characterized by an inverse power dependence on scattering angle ($\sigma \propto 1/\theta^m$), then this power must be less than fourth ($m<4$), to account for the amount of beam broadening observed in about half the sets of observations. If the scattering decreases with height, then this power would have to be smaller still. Application of more realistic assumptions than 1) and 2) above would merely accentuate these conclusions.

As an alternative to a turbulent volume scattering, various researchers[6] have suggested a mechanism involving reflections, or partial reflections, from layers, or portions of layers, which are observed to be present a large part of the time in many geographical locations. Each individual reflection would contribute a received power pattern indicative of the moving transmitted beam pattern. Contributions from the various reflecting patches would differ in amplitude, phase, and location, and these contributions would add vectorially to produce the resultant observed power pattern. Referring back to Fig. 5, it is apparent that there are cases in which the observed pattern can be constructed from the vectorial addition of a limited number of such contributions. However, in attempting to explain all the observed patterns in this fashion, one soon finds that the number of contributing reflections required becomes large. Consequently, the degrees of freedom for fitting the experimental data go up, and confirmation becomes meaningless unless the postulated model is made specific as to the interrelation between the contributing reflections.

V. Useful Antenna Size

The curves of Fig. 8 contain information that is applicable to the determination of the useful width of antenna aperture. If an antenna size is so chosen that its beam is just filled by the important scattering volume, the antenna beamwidth must equal the width of the appropriate $\rho_{(\alpha)}$ curve, and the aperture width is

$$D = \frac{\lambda}{W_\rho} \tag{4}$$

where:

D = horizontal dimension of the aperture

λ = wavelength

W_ρ = half-power width of $\rho_{(\alpha)}$.

On this basis, the useful antenna width for a frequency of 3000 mc and the experimental conditions that gave the broadest $\rho_{(\alpha)}$ curves is approximately 12.5 feet.

"Useful width," as used here, refers to an aperture size which forms a not-too-sharply defined boundary

[6] H. T. Friis, A. B. Crawford, and D. C. Hogg, Bell Telephone Labs., Holmdel, N. J.; J. B. Smyth, Smyth Res. Assoc., San Diego, Calif.; W. S. Ament, Naval Res. Lab., Washington, D. C.; J. R. Bauer, Lincoln Labs., M.I.T., Lexington, Mass.

between "small" antennas, whose beams are wide enough to illuminate the entire portion of the atmosphere which contributes to the received signal, and "large" antennas whose beams are so narrow as to illuminate only part of the significant portion of the atmosphere. It is closely akin to Gordon's concept of horizontal diversity-distance,[7] and represents the region in which realization of the full plane-wave gain of the antenna begins to deteriorate.

It is possible to generalize (4) so as to apply to propagation over a smooth spherical earth if one makes two simplifying but fairly plausible assumptions: 1) that the experimentally observed width W_p of the received power pattern can be adjusted (on theoretical grounds) to apply to a symmetrical path having the same minimum scattering angle—this adjustment amounts to increasing the width by a factor of 1.3—and 2) that the width so adjusted (W_p') is porportional to minimum scattering angle θ_0 for any particular path. For smooth terrain unobstructed by hills, $\theta_0 = d/a$, in which d is the great-circle path length and a is the effective earth radius. Taking the empirical value for the broader of the two curves above (Fig. 8 and Table I), one has $W_p = 1.5°$, so that $W_p' = 1.3 \times 1.5° = 1.95°$; and for the path in question, $\theta_0 = 1.7°$. Then the expression for useful antenna aperture becomes

$$D = \frac{\lambda}{W_p'} = \frac{\lambda}{\left(\frac{W_p'}{\theta_0}\right)\left(\frac{d}{a}\right)} = \frac{\lambda}{\left(\frac{1.3 \times 1.5}{1.7}\right)\left(\frac{d}{a}\right)} = \frac{\lambda a}{1.1 d}. \quad (5)$$

This generalization of an empirical result is about half the magnitude of Gordon's theoretically derived result,[7] which when rearranged to have a form corresponding to (5) is

$$D = \frac{\lambda a}{0.67\, d}. \quad (6)$$

VI. Angular Diversity

Since the propagation mechanism under consideration is a linear phenomenon, the curves of Fig. 5 may quite properly be interpreted as curves of received power vs receiver-antenna bearing to provide information as to the improvement that might be expected from the application of angular diversity to this path. For example, the intersections of the individual curves of Fig. 5 with the two vertical lines marked 5° and 6° indicate the powers that would be received on two beams identical in shape to the test antenna and directed one-half degree either side of the great-circle path (5° and 6° from the reflecting mountain). With a large enough sample of consecutive pictures, one could then determine the probability that a certain power level was exceeded by one or both beams and compare it with the probability when using a single antenna directed along the great-circle path.

Figs. 9 and 10 show angular-diversity information taken from two sets of received-power patterns, one with a 0.9° beam and the other with a 1.3° beam. (To obtain this data, it was assumed that the two antennas would be symmetrically placed with respect to the transmitter bearing that resulted in maximum average power.) Both of these diagrams indicate that the optimum angular separation between the two beams of an angular-diversity system is approximately equal to the half-power width of the beams employed. The width of each of the two beams used for these experiments was smaller than W_p, the angle subtended by the important scattering volume; no attempt should be made to generalize this equality to include antenna beams larger than W_p.

There are two ways in which varying the angular separation between the two beams of an angular-diversity system can affect the probability that a given level is exceeded on at least one of the beams: 1) The mean power available on each beam must decrease as the separation increases as shown in Fig. 6 and the probability of reaching a certain level decreases as the mean decreases. 2) As the beam separation is increased the scattering volume common to both beams decreases thereby decreasing the correlation between the two signals and increasing the probability. That is, at zero separation the correlation is unity and the probability is equal to p, the probability with a single beam; as the correlation decreases to zero the probability increases to $2p - p^2$. At separations greater than the beam width, the correlation is essentially zero so that only the first factor, mean power, affects the probability; the probability decreases continuously as the separation is increased beyond the beam width. At small separations the mean power does not change greatly so 2) should be the predominant influence. Thus, the probability should increase as the separation is increased from zero, reach a maximum in the neighborhood of the beam width, then decrease to zero at large separations.

The curves of Figs. 9 and 10, which were derived from data obtained with a sweeping antenna beam, agree qualitatively with what one would expect actually using two separate beams. They indicate that the application of angular diversity to a scatter link can in fact effect some improvement in the time that a given signal level is exceeded.

VII. Conclusion

In propagation to distances appreciably beyond the radio horizon, narrow-beam 3000-mc transmissions ex-

[7] W. E. Gordon, "Radio scattering in the troposphere," Proc. IRE, vol. 43, pp. 23–28; January, 1955.

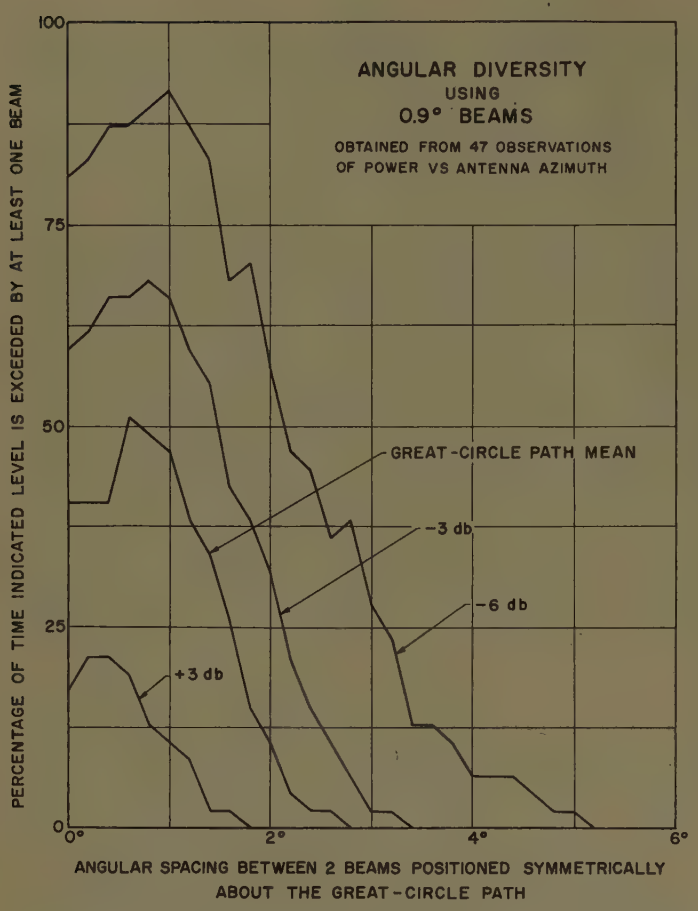

Fig. 9—Probability of exceeding each of four different power levels by at least one of two antennas as a function of the spacing between them.

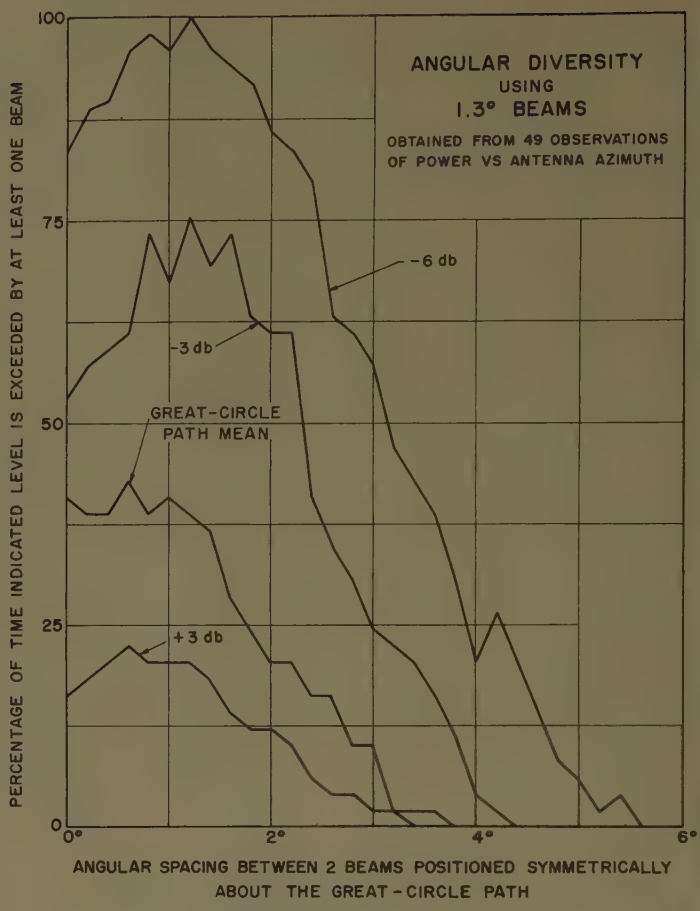

Fig. 10—Probability of exceeding each of four different power levels by at least one of two antennas as a function of the spacing between them.

hibit spatial distortions introduced by the atmosphere. These distortions in the apparent received antenna pattern at times indicate a displacement in angle of arrival from the great-circle bearing and at other times a general smearing in effective angle of arrival. The average received power pattern is appreciably broader than the antenna pattern alone.

The net received signal can be considered as consisting of several components bearing no systematic phase relationship to one another. On the basis of these results it is possible to define an atmospheric scattering function characteristic of the transmission path only. This function, together with its half-power width, has been calculated for the received power patterns measured.

If the propagation mechanism involves a turbulent volume scattering characterized by some inverse power dependence of cross section on scattering angle, then the amount of beam broadening typical of about half the observations requires this power dependence to be less than fourth (*i.e.*, if $\sigma \propto \theta^{-m}$, then $m < 4$).

The useful antenna aperture size, indicative of the transition between full and partial realization of plane-wave gain, has been calculated for the experimental path and generalized so as to apply to others.

The measurements have been interpreted quantitatively in terms of the statistical improvement realizable through the use of angular diversity.

Back-Scattering Cross Section of a Thin, Dielectric, Spherical Shell*

MOGENS G. ANDREASEN†

Summary—**The back-scattering cross section of a thin, dielectric, spherical shell is calculated on the basis of simplified boundary conditions at the shell. These conditions approximate the correct conditions at the shell better, the higher the dielectric constant of the shell, and the less the variation of the normal component of the electric field along the surface of the shell. Numerical results are added for a shell, whose electrical radius $kr_1<5$, and whose thickness d and dielectric constant κ_e obey the relation $(\kappa_e-1)kd=0.4$. A comparison is made, with the results obtained, by applying Rayleigh's scattering law to objects that are small as compared to the wavelength.**

Introduction

IN THE RADAR technique, the capacity of an object for reflecting power back to the radar is expressed by the back-scattering cross section of the object. This usually is defined as the scattering area of the object, as seen from a distant transmitter, the object being to scatter isotropically. If one denotes the distance between the transmitter and the object by R, the electrical component of the incident field at the object by E_0, and that of the scattered field at the transmitter by E_s, the back-scattering cross section may be written

$$\sigma = 4\pi R^2 \frac{|E_s|^2}{|E_0|^2}. \tag{1}$$

It is the aim of this paper to determine the back-scattering cross section of a thin, dielectric, spherical shell. This problem was solved previously by Aden[1] for a shell of arbitrary thickness. However, the results obtained by Aden are rather complicated for numerical treatment. The investigation of the present paper is confined to the practically important case of a shell being thin geometrically as well as electrically. For this case, numerical computations are relatively easy to make, as simplified boundary conditions of the electromagnetic field at such a shell may be used for the determination of the field scattered from the shell.

Formulation of the Problem

The back-scattering cross section of a thin, dielectric, spherical shell, is expressed by the field scattered from the shell, back towards the transmitter. For the purposes of the following calculations, the transmitter is assumed to be placed at the point $(x, y, z)=(0, 0, R)$ of the coordinate system in Fig. 1. Further, the field radiated by this transmitter in the negative z direction towards the spherical shell, the center of which coincides with the origin of the coordinate system, is assumed to be linearly polarized in the direction of the x axis.

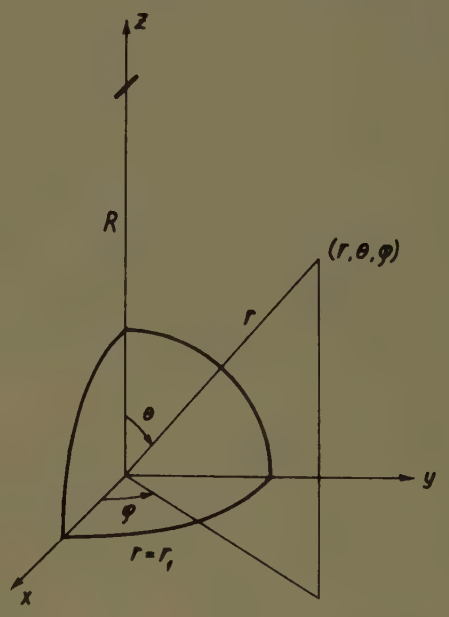

Fig. 1—Coordinate system used for the calculations.

The field scattered from the shell will be found by expanding the primary and certain secondary fields in spherical TE and TM waves and then satisfying the boundary conditions of the electromagnetic field at the shell. For a shell being thin geometrically as well as electrically, simplified boundary conditions previously used by the author[2] may be used with advantage. The actual shell is replaced by a shell of infinitesimal thickness δ and dielectric constant ϵ', chosen so that $\lim_{\delta\to 0}(\delta\epsilon')=(\kappa_e-1)\epsilon_0 d$, where κ_e and d denote the relative dielectric constant and the thickness, respectively, of the actual shell, while ϵ_0 is the dielectric constant of the free space outside the region occupied by the shell. According to the paper referred to above,[2] the boundary conditions of the tangential component of the electric field at the infinitesimally thin shell are, using the time factor $e^{j\omega t}$,

$$\hat{n}\times(\overline{H}_2-\overline{H}_1)=j\frac{(\kappa_e-1)kd}{\zeta}(\hat{n}\times\overline{E}_1)\times\hat{n}$$
$$=j\frac{(\kappa_e-1)kd}{\zeta}(\hat{n}\times\overline{E}_2)\times\hat{n}. \tag{2}$$

* Manuscript received by the PGAP, March 21, 1956.
† Siemens & Halske, Munich, Germany.

[1] A. L. Aden, and M. Kerker, "Scattering of electromagnetic waves from two concentric spheres," *J. Appl. Phys.*, vol. 22, pp. 1242–1246; October, 1951.

[2] M. G. Andreasen, "Radiation from a radial dipole through a thin dielectric spherical shell," submitted for publication to IRE TRANS. ON ANTENNAS AND PROPAGATION.

Here $\hat{n}$ is a unit vector normal to the shell and oriented from medium 1 to medium 2 at either side of the shell, while ζ and k are the specific impedance and the propagation constant, respectively, of free space. This set of boundary conditions is approximate, however, assuming that $kd \ll 1$, $(\kappa_e - 1)kd \ll 1$, and $\kappa_e \gg 1$, or that the gradient of the normal component of the electric field along the surface of the shell is small as compared with the tangential component of the electric field at the shell. For a shell being small, as compared to the wavelength, the latter condition cannot be fulfilled; thus, for small shells the boundary conditions stated are valid only for $\kappa_e \gg 1$. On the other hand, for a shell of the same order of size as, or greater than, the wavelength, the latter condition is fulfilled to a good approximation. In such a case, it is not necessary to assume the dielectric constant of the shell to be great in order to use the simplified boundary conditions (2).

By replacing the actual thin shell by a shell of infinitesimal thickness, only one set of equations evidently is required for determining the field scattered from the shell. This fact greatly simplifies the following analysis in contrast to the case of a shell of arbitrary thickness, where two sets of equations are necessary for determining the scattered field.

Primary Field

As the spherical shell is assumed to be placed in the far zone of the antenna (see Fig. 1), the primary field at a point $\bar{r}$ in the neighborhood of the shell represents a plane wave, the only nonzero field components of which are

$$E_x = E_0 e^{-jk\hat{R}\cdot(\bar{R}-\bar{r})}, \tag{3}$$

$$H_y = -\frac{E_x}{\zeta}, \tag{4}$$

E_0 being a constant. This field is expanded in spherical TM and TE modes by introducing the magnetic and electric vector potentials $\overline{A}$ and $\overline{F}$ given by

$$\overline{B} = \mu_0 \overline{H} = \nabla \times \overline{A} = \nabla \times (rA\hat{r}), \tag{5}$$

$$\overline{D} = \epsilon_0 \overline{E} = \nabla \times \overline{F} = \nabla \times (rF\hat{r}). \tag{6}$$

The scalar potentials A and F satisfy the homogeneous wave equation and determine the electromagnetic field vectors through the following spherical field components

$$\left.\begin{aligned} E_r &= \frac{1}{j\omega\mu_0\epsilon_0}\left[\frac{\partial^2(rA)}{\partial r^2} + k^2 rA\right] \\ E_\theta &= \frac{1}{j\omega\mu_0\epsilon_0}\,\frac{1}{r}\,\frac{\partial^2(rA)}{\partial r\partial\theta} + \frac{1}{\epsilon_0}\,\frac{1}{\sin\theta}\,\frac{\partial F}{\partial\phi} \\ E_\phi &= \frac{1}{j\omega\mu_0\epsilon_0}\,\frac{1}{r\sin\theta}\,\frac{\partial^2(rA)}{\partial r\partial\phi} - \frac{1}{\epsilon_0}\,\frac{\partial F}{\partial\theta} \end{aligned}\right\}, \tag{7}$$

$$\left.\begin{aligned} H_r &= -\frac{1}{j\omega\mu_0\epsilon_0}\left[\frac{\partial^2(rF)}{\partial r^2} + k^2 rF\right] \\ H_\theta &= -\frac{1}{j\omega\mu_0\epsilon_0}\,\frac{1}{r}\,\frac{\partial^2(rF)}{\partial r\partial\theta} + \frac{1}{\mu_0}\,\frac{1}{\sin\theta}\,\frac{\partial A}{\partial\phi} \\ H_\phi &= -\frac{1}{j\omega\mu_0\epsilon_0}\,\frac{1}{r\sin\theta}\,\frac{\partial^2(rF)}{\partial r\partial\phi} - \frac{1}{\mu_0}\,\frac{\partial A}{\partial\theta} \end{aligned}\right\}. \tag{8}$$

From this set of relations and from the radial components of the primary field (3), (4)

$$E_r = E_0 \sin\theta\cos\phi\, e^{-jk(R - r\cos\theta)}, \tag{9}$$

$$H_r = -\frac{E_0}{\zeta}\sin\theta\sin\phi\, e^{-jk(R - r\cos\theta)}, \tag{10}$$

the expansion of the potentials of the primary field in characteristic spherical wave functions may be shown to be

$$A_{pr} = \cos\phi \sum_{n=1}^{\infty} M_n j_n(kr)\,\frac{dP_n(\cos\theta)}{d\theta}, \tag{11}$$

$$F_{pr} = \sin\phi \sum_{n=1}^{\infty} N_n j_n(kr)\,\frac{dP_n(\cos\theta)}{d\theta}, \tag{12}$$

j_n and P_n being the spherical Bessel function and the Legendre polynomial, respectively, and the constants M_n and N_n being given by

$$M_n = -\sqrt{\mu_0\epsilon_0}E_0 e^{-jkR j^n}\,\frac{2n+1}{n(n+1)}, \tag{13}$$

$$N_n = \frac{M_n}{\zeta}. \tag{14}$$

Scattered Field

The field outside the shell (region 2) may be expressed by the sum of the primary field and the scattered field. The latter represents diverging waves, whereas the field inside the shell (region 1) represents standing waves. Thus, considering (11) and (12) we may express the potentials inside and outside the shell by

$$A_1 = \cos\phi \sum_{n=1}^{\infty} C_n j_n(kr)\,\frac{dP_n(\cos\theta)}{d\theta}, \tag{15}$$

$$F_1 = \sin\phi \sum_{n=1}^{\infty} D_n j_n(kr)\,\frac{dP_n(\cos\theta)}{d\theta}, \tag{16}$$

$$A_2 = A_{pr} + A_s = \cos\phi \sum_{n=1}^{\infty} \left[M_n j_n(kr) + A_n h_n^{(2)}(kr)\right] \cdot \frac{dP_n(\cos\theta)}{d\theta}, \tag{17}$$

$$F_2 = F_{pr} + F_s = \sin\phi \sum_{n=1}^{\infty} \left[N_n j_n(kr) + B_n h_n^{(2)}(kr)\right] \cdot \frac{dP_n(\cos\theta)}{d\theta}, \tag{18}$$

where $h_n^{(2)}$ is a spherical Hankel function of the second kind. The constants A_n, B_n, C_n, and D_n may be determined by satisfaction of the simplified boundary conditions (2) at an equivalent, infinitesimally thin shell of radius r_1. According to (7) and (8) these ocnditions of the field are reduced to the following conditions of the potentials

$$A_1 + kr\frac{\partial A_1}{\partial(kr)} = A_2 + kr\frac{\partial A_2}{\partial(kr)} = \frac{1}{(\kappa_e - 1)kd} kr_1(A_2 - A_1) \quad (19)$$

and

$$F_1 = F_2 = -\frac{1}{(\kappa_e - 1)kd}\left[\frac{\partial F_2}{\partial(kr)} - \frac{\partial F_1}{\partial(kr)}\right] \quad (20)$$

for $r = r_1$. To find the field scattered from the shell, the interest attaches only to the constants A_n and B_n which, when inserting the potentials (15)–(18) into the above boundary conditions and making use of the following relation between spherical Bessel functions

$$j_n(\rho)\frac{d[\rho h_n^{(2)}(\rho)]}{d\rho} - h_n^{(2)}(\rho)\frac{d[\rho j_n(\rho)]}{d\rho} = \frac{1}{j\rho}, \quad (21)$$

are found to be given by

$$A_n = -j(\kappa_e - 1)kd\left[\frac{d[kr_1 j_n(kr_1)]}{d(kr_1)}\right]^2 R_n M_n, \quad (22)$$

$$B_n = -j(\kappa_e - 1)kd[kr_1 j_n(kr_1)]^2 S_n N_n, \quad (23)$$

where for simplicity the constants R_n and S_n below have been inserted.

$$R_n = \left[1 + j(\kappa_e - 1)kd\frac{d[kr_1 j_n(kr_1)]}{d(kr_1)} \cdot \frac{d[kr_1 h_n^{(2)}(kr_1)]}{d(kr_1)}\right]^{-1} \quad (24)$$

$$S_n = [1 + j(\kappa_e - 1)kd\, kr_1 j_n(kr_1) kr_1 h_n^{(2)}(kr_1)]^{-1}. \quad (25)$$

Now, as the field scattered from the spherical shell is polarized in the x direction at the position of the antenna, the electric component of the scattered field at this point follows from the θ component of (7) by inserting the potentials A_s and F_s from (17) and (18) and then setting $\theta = \phi = 0$ and $r = R$. The contributions given by the scattered TM waves thus are

$$E_{s\mathrm{TM}} = \frac{1}{j\omega\mu_0\epsilon_0}\frac{1}{R} \cdot \cos\phi \sum_{n=1}^{\infty} A_n \frac{d[kRh_n^{(2)}(kR)]}{d(kR)} \frac{d^2P_n(\cos\theta)}{d\theta^2}\bigg|_{\theta=\phi=0} \quad (26)$$

and similarly the contributions given by the scattered TE waves are

$$E_{s\mathrm{TE}} = \frac{1}{\epsilon_0}\frac{\cos\phi}{\sin\theta}\sum_{n=1}^{\infty} B_n h_n^{(2)}(kR)\frac{dP_n(\cos\theta)}{d\theta}\bigg|_{\theta=\phi=0} \quad (27)$$

As it has been assumed that the shell is placed in the far zone of the antenna, $kR \gg 1$, these expressions may be reduced by inserting the asymptotic expression of the spherical Hankel function of the second kind

$$h_n^{(2)}(\rho) = j^{n+1}\frac{e^{-j\rho}}{\rho} \qquad \text{for } \rho \gg n. \quad (28)$$

Further, using the relations below applying to the Legendre polynomials

$$\frac{d^2P_n(\cos\theta)}{d\theta^2}\bigg|_{\theta=0} = \frac{1}{\sin\theta}\frac{dP_n(\cos\theta)}{d\theta}\bigg|_{\theta=0} = -\frac{n(n+1)}{2}, \quad (29)$$

the electrical components (26, 27) of the scattered field may be transformed into

$$E_{s\mathrm{TM}} = -\frac{1}{j\omega\mu_0\epsilon_0}\frac{e^{-jkR}}{R}\sum_{n=1}^{\infty} A_n j^n \frac{n(n+1)}{2}, \quad (30)$$

$$E_{s\mathrm{TE}} = -\frac{1}{\epsilon_0 k}\frac{e^{-jkR}}{R}\sum_{n=1}^{\infty} B_n j^{n+1}\frac{n(n+1)}{2}, \quad (31)$$

where the constants A_n and B_n were found previously (22, 23).

Back-Scattering Cross Section

The electrical component of the field scattered from the spherical shell, at the position of the antenna, is equal to the sum of the contributions (30), (31) found above from the scattered TM and TE waves, $E_s = E_{s\mathrm{TM}} + E_{s\mathrm{TE}}$. By inserting this into (1) for the back-scattering cross section and then reintroducing the secondary constants A_n and B_n (22), (23) and the primary constants M_n and N_n (13), (14), the back-scattering cross section of a thin, dielectric, spherical shell of radius r_1 is found, normalizing it with respect to the geometrical cross section πr_1^2 of the shell, to be given by

$$\frac{b}{\pi r_1^2} = \left[\frac{(\kappa_e - 1)kd}{kr_1}\right]^2 \left|\sum_{n=1}^{\infty}(-1)^n(2n+1) \cdot \left[\left(\frac{d[kr_1 j_n(kr_1)]}{d(kr_1)}\right)^2 R_n - [kr_1 j_n(kr_1)]^2 S_n\right]\right|^2. \quad (32)$$

This expression has been treated numerically, $b/\pi r_1^2$ being represented in Fig. 2 as a function of kr_1 of a shell for which $(\kappa_e - 1)kd = 0.4$. The strongest resonance of the shell is seen to be had for $kr_1 \cong 2$, the circumference of the shell thus being two wavelengths.

When the radius of the spherical shell is small as compared with the wavelength, $kr_1 \ll 1$, the back-scattering

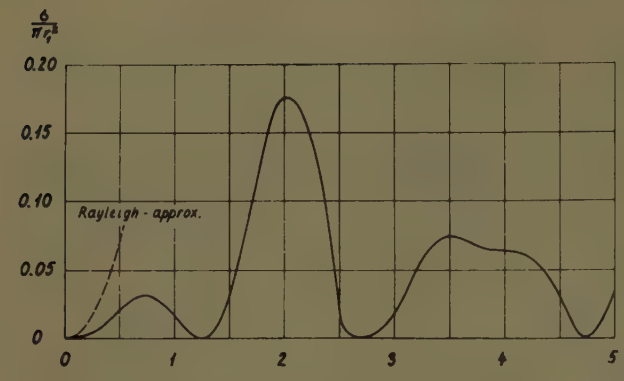

Fig. 2—Back-scattering cross section δ of a thin, dielectric, spherical shell of radius r_1, $(\kappa_e-1)kd$ being equal to 0.4.

cross section of the shell must be proportional to k^4, according to Rayleigh.[3] This is in fact found to be the case; letting $kr_1 \ll 1$, all terms $n \neq 1$ of the infinite sum of (32) are negligible as compared with the term $n=1$, and furthermore

$$\frac{d[kr_1 j_1(kr_1)]}{d(kr_1)} \cong \frac{2}{3} kr_1 \quad \text{for } kr_1 \ll 1, \tag{33}$$

$$kr_1 j_1(kr_1) \cong 0 \quad \text{for } kr_1 \ll 1, \tag{34}$$

$$R_1 \cong 1 \quad \text{for } kr_1 \cong 1, \tag{35}$$

so that the back-scattering cross section (32) of the spherical shell may be reduced to

$$\frac{\delta}{\pi r_1^2} = \frac{16}{9} [(\kappa_e - 1)kd]^2 (kr_1)^2. \tag{36}$$

The scattered field (30), (31) may in this case be identified with the field produced by a distribution of dipole moment which per unit volume of the region occupied by the shell is

$$p = \frac{2}{3} (\kappa_e - 1)\epsilon_0 E_0. \tag{37}$$

This result might have been found also by considering the problem from an electrostatic point of view. As has already been pointed out in this paper, (37) derived above is only valid for large values of κ_e. For small values of $\kappa_e - 1$ an electrostatic treatment gives for the polarization $p = (\kappa_e - 1)\epsilon_0 E_0$.

The back-scattering cross section (36) applying to a small shell with a great dielectric constant has been compared in Fig. 2 with the results obtained by using (32). The single-term approximation is seen to be very poor unless the radius of the shell is extremely small compared with the wavelength.

Acknowledgment

This investigation was carried out in the Institute of Electromagnetic Theory at the Technical University of Denmark by means of a grant from Civilingeniør A. R. Angelos Legat. I wish to express my thanks to Professor H. Lottrup Knudsen for having suggested this investigation. The English translation of the paper was revised by Oskar Kasch, sworn translator and interpreter.

[3] Lord Rayleigh, "On the scattering of light by small particles," *Phil. Mag.*, vol. 41, pp. 447–454; 1871.

Serrated Waveguide—Part I: Theory*

ROBERT S. ELLIOTT†

Summary—**A corrugated waveguide in which the corrugations pierce the broad wall, permitting leakage, is called a serrated waveguide. Controlling the size and spacing of the serrations will permit the design of a practical traveling-wave antenna.**

In this paper, an analysis is presented for the case of serrations which have a transverse dimension equal to the width of the broad wall, and longitudinal dimension and spacing that are small compared to a wavelength.

The analysis yields an expression for the complex propagation constant of the leaky hybrid mode in the serrated guide, and computations reveal an adequate range of leakage.

* Manuscript received by the PGAP, April 7, 1956; revised manuscript received, January 15, 1957. The research reported in this paper was supported in part by the Air Force Cambridge Res. Ctr. under contract with the Hughes Res. Labs.

† Rantec Corp., Calabasas, Calif.

Introduction

In 1954, Stegen and Reed[1] reported the development of a novel antenna which was basically an array of leaky coaxial transmission lines. The outer coaxial conductor was rectangular in cross section and one of its broad walls contained a family of transverse, closely-spaced, nonresonant slots. The inner conductor was capacity-loaded to achieve a phase velocity greater than that of light. The result was a traveling-wave antenna yielding a main beam close to endfire and a pattern, between the main beam and broadside, approximating

[1] R. J. Stegen and R. H. Reed, "Arrays of closely spaced nonresonant slots, *IRE Trans.*, vol. AP-2, pp. 109–112; July, 1954.

cosecant squared. The longitudinal aperture distribution was controllable through the slot dimensions. Two or more such leaky coaxial lines could be placed side by side with negligible interaction through mutual coupling, and thus a transverse aperture distribution could be built up by conventional techniques.

It was recognized that the same type of operation could be obtained if the inner conductor were removed and the outer conductor were fed with the dominant rectangular waveguide mode. It was further recognized that such a leaky waveguide was much akin to a corrugated waveguide, the principal difference being whether or not the corrugations extended all the way through the broad wall. The ensuing study revealed that the aperture distribution, in amplitude and phase, was governed by the slot dimensions and wall thickness, whereas in the Stegen and Reed antenna the control parameters were slot dimensions and capacity-loading.

For convenience, it was decided to call a rectangular waveguide containing closely-spaced, nonresonant, transverse slots in one of its broad walls a serrated waveguide. A photograph of typical serrated guides is shown in Fig. 1 and an artist's sketch in Fig. 2. The following sections of this paper are devoted to an analysis of the serrated waveguide for the limiting case $L=a, G+T \ll \lambda_0$, and $\frac{G}{T} \gg 1$.

Theory

The procedure for obtaining field solutions which satisfy the boundary conditions for a serrated rectangular waveguide follows that previously used for a corrugated guide.[2] Floquet's theorem applies, and it is assumed that the exciting source is a TE_{01} mode incident from a tandem section of regular guide. Referring to Fig. 2, if $L=a$, the allowable modes in the interior of the waveguide are then hybrid, characterized by the absence of an E_z component, and given by

$$E_x = \sum_{n=-\infty}^{\infty} A_n \sinh \Upsilon_n(y-b) \cdot \cos \frac{\pi z}{a} \cdot \exp\left[-\Gamma_n x\right]$$

$$E_y = \sum_{n=-\infty}^{\infty} \frac{\Gamma_n A_n}{\Upsilon_n} \cosh \Upsilon_n(y-b) \cdot \cos \frac{\pi z}{a} \cdot \exp\left[-\Gamma_n x\right]$$

$$H_x = \sum_{n=-\infty}^{\infty} \frac{-\Gamma_n \pi A_n}{j\omega\mu \Upsilon_n a} \cosh \Upsilon_n(y-b) \cdot \sin \frac{\pi z}{a} \cdot \exp\left[-\Gamma_n x\right]$$

$$H_y = \sum_{n=-\infty}^{\infty} \frac{\pi A_n}{j\omega\mu a} \sinh \Upsilon_n(y-b) \cdot \sin \frac{\pi z}{a} \cdot \exp\left[-\Gamma_n x\right]$$

$$H_z = \sum_{n=-\infty}^{\infty} \frac{-K^2 A_n}{j\omega\mu \Upsilon_n} \cosh \Upsilon_n(y-b) \cdot \cos \frac{\pi z}{a} \cdot \exp\left[-\Gamma_n x\right] \quad (1)$$

where

$$\Upsilon_n = j\sqrt{\Gamma_n^2 + K^2}, \qquad K = \sqrt{k^2 - \left(\frac{\pi}{a}\right)^2}. \quad (2)$$

[2] R. S. Elliott, "On the theory of corrugated plane surfaces," IRE Trans., vol. AP-2, pp. 71–81; April, 1954.

Fig. 1—A family of serrated waveguides.

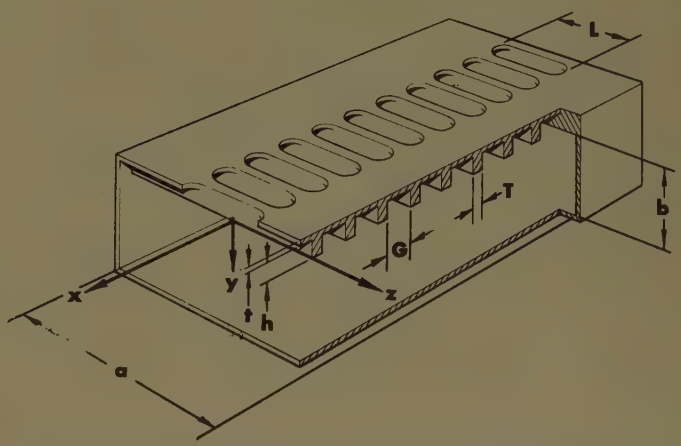

Fig. 2—Geometry of the serrated waveguide.

The complex constants Γ_n are related to each other (through Floquet's theorem) by the expression

$$\Gamma_n = \Gamma_0 + j\frac{2\pi n}{T+G} \quad (3)$$

in which T is the width of a tooth and G is the width of a gap. The goal of this analysis is to determine Γ_0 as a function of the waveguide dimensions and the frequency of operation. Time variations of the form $\exp[j\omega t]$ have been suppressed.

With the origin of coordinates chosen as shown in Fig. 2, and with $L=a$ and $t=0$, the field distribution in the gap adjacent to the origin may be written

$$E_x = -j\omega\mu B_0 \cos\frac{\pi z}{a}\left\{(KZ+\omega\mu)\exp\left[jK(y+h)\right] + (KZ-\omega\mu)\exp\left[-jK(y+h)\right]\right\} + \sum_{m=1}^{\infty} B_m \cos\frac{m\pi x}{G}\cdot\cos\frac{\pi z}{a}\cdot\exp\left[+\gamma_m y\right]$$

$$E_y = \sum_{m=1}^{\infty} \frac{m\pi}{\gamma_m G} B_m \sin\frac{m\pi x}{G}\cos\frac{\pi z}{a}\exp\left[+\gamma_m y\right]$$

$$H_x = -\sum_{m=1}^{\infty} \frac{\pi}{j\omega\mu\gamma_m a} \frac{m\pi}{G} \cdot B_m \cdot \sin \frac{m\pi x}{G} \cdot \sin \frac{\pi z}{a} \cdot \exp\left[+\gamma_m y\right]$$

$$H_y = -\frac{\pi}{a} B_0 \sin \frac{\pi z}{a} \left\{(KZ + \omega\mu) \exp\left[jK(y+h)\right] + (KZ - \omega\mu) \exp\left[-jK(y+h)\right]\right\} + \sum_{m=1}^{\infty} \frac{1}{j\omega\mu} \cdot \frac{\pi}{a} \cdot B_m \cdot \cos \frac{m\pi x}{G} \cdot \sin \frac{\pi z}{a} \cdot \exp\left[+\gamma_m y\right]$$

$$H_z = -jKB_0 \cos \frac{\pi z}{a} \left\{(KZ + \omega\mu) \exp\left[jK(y+h)\right] - (KZ - \omega\mu) \exp\left[-jK(y+h)\right]\right\} - \sum_{m=1}^{\infty} \frac{K^2}{j\omega\mu\gamma_m} B_m \cos \frac{m\pi x}{G} \cdot \cos \frac{\pi z}{a} \cdot \exp\left[+\gamma_m y\right] \quad (4)$$

in which

$$\gamma_m = \sqrt{\left(\frac{m\pi}{G}\right)^2 - K^2} \quad (5)$$

and

$$Z = \frac{E_x\left(\frac{G}{2}, -h, 0\right)}{H_z\left(\frac{G}{2}, -h, 0\right)} \quad (6)$$

is the ratio of the transverse electric and magnetic field components for the fundamental mode, measured at the boundary between the gap and the external environment. Implicit in (4) is the concept that each slot is an open-ended waveguide of length h. The m series represents that combination of TM and TE modes, all beyond cutoff, which together satisfy the requirement that $E_z \equiv 0$. It is assumed that the slot width G is so small, compared to the free space wavelength λ_0, that all of these modes are attenuated to a negligible amplitude before they reach the bottom of the slot and hence have no reflected component. The one propagating mode is represented separately in (4). Thus, K and γ_m, given by (2) and (5) are positive real quantities determined solely by the geometry.

Since the tangential fields must be continuous across the boundary between the two regions, that is, across the plane $y=0$, one may write

$$\int_{-a/2}^{a/2} \int_0^{G+T} \vec{E}_1 \times \vec{H}_1^* \cdot \vec{u}_y dx dz = \int_{-a/2}^{a/2} \int_0^{G} \vec{E}_1 \times \vec{H}_1^* \cdot \vec{u}_y dx dz \quad (7)$$

in which $\vec{E}_1$, $\vec{H}_1$ are unknown fields expressed in terms of (1), and $\vec{E}_1$, $\vec{H}_1$ are the unknown fields expressed in terms of (4). All terms of the integrands of (7) contain z only in the factor $\cos \pi z/a$. Hence, (7) reduces to

$$\int_0^{G+T} EH^* dx = \int_0^{G} \boldsymbol{E}\boldsymbol{H}^* dx \quad (8)$$

where

$$E = -\sum_{n=-\infty}^{\infty} A_n \sinh \Upsilon_n b \cdot \exp\left[-\Gamma_n x\right] \quad (9a)$$

$$H = -\sum_{n=-\infty}^{\infty} \frac{K^2 A_n}{j\omega\mu\Upsilon_n} \cosh \Upsilon_n b \cdot \exp\left[-\Gamma_n x\right] \quad (9b)$$

$$\boldsymbol{E} = -j\omega\mu B_0 \left\{(KZ + \omega\mu) \exp\left[jKh\right] + (KZ - \omega\mu) \exp\left[-jKh\right]\right\} + \sum_{m=1}^{\infty} B_m \cos \frac{m\pi x}{G} \quad (9c)$$

$$\boldsymbol{H} = -jKB_0 \left\{(KZ + \omega\mu) \exp\left[jKh\right] - (KZ - \omega\mu) \exp\left[-jKh\right]\right\} - \sum_{m=1}^{\infty} \frac{K^2}{j\omega\mu\gamma_m} B_m \cos \frac{m\pi x}{G} \quad (9d)$$

and

$$E \equiv \boldsymbol{E}, \qquad H \equiv \boldsymbol{H} \qquad \text{for } 0 \leq x \leq G. \quad (10)$$

The Fourier coefficients, A_n and B_m, may be expressed in terms of integrals of the unknown electric field, that is,

$$A_n^* = -\frac{1}{(G+T) \sinh \Upsilon_n^* b} \int_0^{G+T} E^* \exp\left[+\Gamma_n^* x\right] \quad (11)$$

$$B_0^* = -\frac{\int_0^{G+T} \boldsymbol{E}^* dx}{j\omega\mu G\left\{(KZ^* + \omega\mu) \exp\left[-jKh\right] + (KZ^* - \omega\mu) \exp\left[+jKh\right]\right\}} \quad (12)$$

$$B_m^* = \frac{2}{G} \int_0^{G} \boldsymbol{E}^* \cos \frac{m\pi x}{G} dx \quad (13)$$

and when these relations are substituted in (9b) and (9d), the magnetic field is given in terms of the electric field. Upon inserting the resulting expressions for the magnetic field in (8), making use of (10) and rearranging terms, (14) is obtained:

$$\frac{j\omega\mu\cos Kh + KZ^*\sin Kh}{j\omega\mu\sin Kh - KZ^*\cos Kh} = \frac{\sum_{n=-\infty}^{\infty}\frac{KG}{\Upsilon_n^*(G+T)}\coth\Upsilon_n^* b\int_0^{G+T}E\exp[-\Gamma_n^* x]dx\int_0^{G+T}E^*\exp[\Gamma_n^* x]dx + \sum_{m=1}^{\infty}\frac{2K}{\gamma_m}\int_0^G E\cos\frac{m\pi x}{G}\,dx\int_0^G E^*\cos\frac{m\pi x}{G}\,dx}{\int_0^G E dx\int_0^G E^* dx}. \quad (14)$$

By a similar procedure, (8) can be expressed entirely in terms of the unknown field H, giving

$$\frac{j\omega\mu\sin Kh + KZ\cos Kh}{j\omega\mu\cos Kh - KZ\sin Kh} = \frac{\sum_{n=-\infty}^{\infty}\frac{\Upsilon_n}{K}\cdot\frac{G}{G+T}\tanh\Upsilon_n b\int_0^{G+T}H\exp[\Gamma_n x]dx\int_0^{G+T}H^*\exp[-\Gamma_n x]dx + \sum_{m=1}^{\infty}\frac{2\gamma_m}{K}\int_0^G H\cos\frac{m\pi x}{G}\,dx\int_0^G H^*\cos\frac{m\pi x}{G}\,dx}{\int_0^G H dx\int_0^G H^* dx}. \quad (15)$$

A test of the stationary character of (14) and (15) is identical with the procedure given for a similar problem[3] and will not be presented. It is sufficient to say that if Z is entirely imaginary, (15) is stationary with respect to arbitrary variations about the true field H. If, in addition, $T\to 0$, (14) becomes stationary also.

Although neither (14) nor (15) is stationary unless Z is imaginary (or zero), they must both be satisfied by the true field. To test the accuracy of the fundamental mode as an approximation to the true field, the trial function $E=-A_0\sinh\Upsilon_0 b\cdot\exp[-\Gamma_0 x]$ is inserted in (14) and the asymptotic formula

$$\frac{j\omega\mu\cos Kh + KZ^*\sin Kh}{j\omega\mu\sin Kh - KZ^*\cos Kh} = \frac{G+T}{G}\cdot\frac{K}{\Upsilon_0^*}\coth\Upsilon_0^* b \quad (16)$$

is obtained as $G+T\to 0$. Similarly, when the companion trial function $H=-(K^2A_0/j\omega\mu\Upsilon_0)\cosh\Upsilon_0 b\cdot\exp[-\Gamma_0 x]$ is inserted in (15), the asymptotic formula

$$\frac{j\omega\mu\cos Kh - KZ\sin Kh}{j\omega\mu\sin Kh + KZ\cos Kh} = \frac{G}{G+T}\,\frac{K}{\Upsilon_0}\coth\Upsilon_0 b \quad (17)$$

results when $G+T\to 0$. Previous work by the Stanford group on a similar problem[4] indicates that these formulas are good representations for $\lambda_0/(G+T)\geq 10$.

It can be observed that for $T=0$ the two formulas are conjugates of each other, and the fundamental mode is the true field. Hence, if $\lambda_0/(G+T\geq 10$ and $G/(G+T)\approx 1$, it is reasonable to expect that the fundamental mode is the principal part of the true field. How far one can depart from these two requirements before it is no longer proper to consider only the fundamental mode has not been investigated theoretically.

Eq. (17) was chosen as the characteristic equation because, for $T>0$, it is more nearly stationary than (16). If Z and the waveguide geometry are known, (17) will yield a value for Υ_0. Use of (2) gives the complex propagation constant Γ_0 and the fundamental mode is then entirely described by the $n=0$ terms of (1).

An Evaluation of Z

Eq. (17) cannot be solved for Υ_0 without a knowledge of Z. It is, therefore, necessary to specify the external environment and determine those factors which influence the nature and behavior of Z. The analysis to be presented follows a line of attack used previously by the Ohio State group.[5,6] It is assumed that the serrated wall of the waveguide is imbedded in an infinite ground plane, and that T is exceedingly small. In the strip defined by $y=-h$, $-\infty<x<\infty$, $-a/2\leq z\leq a/2$, the wave disturbance is taken to be

$$E_x = \cos\frac{\pi z}{a}\exp[-\Gamma_0 x]. \quad (18)$$

The ground plane can be accounted for by the method of images. When this is done, the electromagnetic field in the half-space $y\leq h$ may be considered to be terminated by the magnetic current sheet

$$\vec{J}_m = -\vec{u}_z 2\cos\frac{\pi z}{a}\cdot\exp[-\Gamma_0 x] \quad (19)$$

located in the plane $y=-h$ within the limits $-\infty<x<\infty$, $-a/2\leq z\leq a/2$.

Referring to Fig. 2, if (x', y', z') is any point in the half-space $y<-h$, then the electric vector potential is given by

$$\vec{F}(x', y', z', t) = -\int_{-\infty}^{\infty}dx\int_{-a/2}^{a/2}\frac{\vec{u}_z 2\cos\frac{\pi z}{a}\exp[-\Gamma_0 x - jkr]}{4\pi r}dz \quad (20)$$

in which

$$r = \sqrt{(x'-x)^2 + (y'+h)^2 + (z'-z)^2}. \quad (21)$$

[3] R. S. Elliott, "On the theory of corrugated plane surfaces," Hughes Res. Labs. Tech. Memo. No. 317, revised; October, 1953. See Appendix.

[4] "Ridge and Corrugated Antenna Studies," Second Quart. Prog. Rep., Stanford Res. Inst.; October, 1949–January, 1950.

[5] J. N. Hines, V. H. Rumsey, and C. H. Walter, "Traveling wave slot antennas," Proc. IRE, vol. 41, pp. 1624–1631; November, 1953.

[6] V. H. Rumsey, "Traveling wave slot antennas," *J. Appl. Phys.*, vol. 24, pp. 1358–1365; November, 1953.

Eq. (20) may be written in the form

$$\vec{F}(x', y', z', t) = -\frac{\vec{u}_z}{2\pi}\exp\left[-\Gamma_0 x'\right]\int_{-a/2}^{a/2}\cos\frac{\pi z}{a}\,dz \int_{-\infty}^{\infty}\frac{\exp\left[-jkr+\Gamma_0(x'-x)\right]}{r}dx \quad (22)$$

$$= -\frac{\vec{u}_z}{2\pi}\exp\left[-\Gamma_0 x'\right]\int_{-a/2}^{a/2}\cos\frac{\pi z}{a}\,dz \cdot \int_{-\infty}^{\infty}\exp\left[-jkR\cosh\xi+\Gamma_0 R\sinh\xi\right]d\xi \quad (23)$$

in which

$$R = \sqrt{(y'+h)^2+(z'-z)^2} \quad (24)$$

and

$$x' - x = R\sinh\xi. \quad (25)$$

But

$$k\cosh\xi + j\Gamma_0\sinh\xi = \sqrt{k^2+\Gamma_0^2}\cosh\left[\xi - \tanh^{-1}\frac{\Gamma_0}{jK}\right] \quad (26)$$

and[7]

$$\int_{-\infty}^{\infty}\exp\left\{-jR\sqrt{k^2+\Gamma_0^2}\cosh\left[\xi-\tanh^{-1}\frac{\Gamma_0}{jK}\right]\right\}d\xi = -j\pi H_0^{(2)}(\kappa R) \quad (27)$$

where $H_0^{(2)}$ is the Hankel function of the second kind and

$$\kappa = \sqrt{k^2+\Gamma_0^2}. \quad (28)$$

Therefore,

$$\vec{F}(x', y', z', t) = -\frac{\vec{u}_z}{2j}\exp\left[-\Gamma_0 x'\right]\int_{-a/2}^{a/2}\cos\frac{\pi z}{a}\cdot H_0^{(2)}(\kappa R)\,dz. \quad (29)$$

Since

$$\vec{H} = \frac{1}{j\omega\mu}\nabla\times\nabla\times\vec{F},$$

$$H_z(x', y', z', t) = +\frac{\exp\left[-\Gamma_0 x'\right]}{2\omega\mu}\int_{-a/2}^{a/2}\cos\frac{\pi z}{a}\left[\left(\frac{\partial^2}{\partial z'^2}+k^2\right)H_0^{(2)}(\kappa R)\right]dz \quad (30)$$

$$= \frac{\exp\left[-\Gamma_0 x'\right]}{2\omega\mu}\int_{-a/2}^{a/2}\cos\frac{\pi z}{a}\left[\left(\frac{\partial^2}{\partial z^2}+k^2\right)H_0^{(2)}(\kappa R)\right]dz \quad (31)$$

$$= K^2\frac{\exp\left[-\Gamma_0 x'\right]}{2\omega\mu}\int_{-a/2}^{a/2}\cos\frac{\pi z}{a}H_0^{(2)}(\kappa R)\,dz + \frac{\exp\left[-\Gamma_0 x'\right]}{2\omega\mu}\cdot\frac{\pi}{a}\cdot\sin\frac{\pi z}{a}\cdot H_0^{(2)}(\kappa R)\Big|_{-a/2}^{a/2}. \quad (32)$$

Thus,

$$Z = \frac{+2\omega\mu}{K^2\int_{-a/2}^{a/2}\cos\frac{\pi z}{a}H_0^{(2)}(\kappa|z|)\,dz + \frac{2\pi}{a}H_0^{(2)}\left(\frac{\kappa a}{2}\right)} \quad (33)$$

or

$$Z = \frac{+\omega\mu}{K^2\int_{0}^{a/2}\cos\frac{\pi z}{a}H_0^{(2)}(\kappa z)\,dz + \frac{\pi}{a}H_0^{(2)}\left(\frac{\kappa a}{2}\right)}. \quad (34)$$

A Computation of Γ_0

Eq. (17) indicated that Γ_0 was dependent on Z through Υ_0, whereas (34) reveals that Z is dependent on Γ_0 through κ. An iterative procedure is required, and to facilitate computations, (34), (17), (2), and (28) are rewritten as follows:

$$\frac{\omega\mu}{KZ} = \frac{\frac{K}{k}}{\frac{\pi}{ka}}\int_0^{\pi/2}\cos x H_0^{(2)}\left[\frac{\frac{K}{k}}{\frac{\pi}{ka}}x\right]dx + \frac{\frac{\pi}{ka}}{\frac{K}{k}}H_0^{(2)}\left[\frac{\kappa}{K}\cdot\frac{ka}{2}\right] \quad (35)$$

$$\frac{\frac{\omega\mu}{KZ}\cos Kh + j\sin Kh}{\frac{\omega\mu}{KZ}\sin Kh - j\cos Kh}\cdot\frac{\frac{K}{k}}{\frac{\Upsilon_0}{k}}\cdot\coth\left(\frac{\Upsilon_0}{k}\cdot kb\right) \quad (36)$$

$$\left(\frac{\Gamma_0}{jk}\right)^2 = \left(\frac{\Upsilon_0}{k}\right)^2 + \left(\frac{K}{k}\right)^2 \quad (37)$$

$$\left(\frac{\kappa}{k}\right) = \sqrt{1-\left(\frac{\Gamma_0}{jk}\right)^2}. \quad (38)$$

The iterative procedure begins by assuming $\kappa/k = \pi/ka$ and solving (35) for a first approximation to $\omega\mu/KZ$. This value of $\omega\mu/KZ$ is then inserted in (36), yielding a first approximation to Υ_0/k. Eq. (37) then gives a first approximation to $(\Gamma_0/jk)^2$ which can be used in (38) to produce a second approximation to κ/k. This whole

[7] G. N. Watson, "A Treatise on the Theory of Bessel Functions," 2nd ed., Cambridge Univ. Press, Cambridge, Eng.; 1952. See p. 180.

process is repeated until the desired accuracy in the value of Γ_0 is obtained.

For standard X-band waveguide (id 0.900 inch by 0.400 inch), for the frequencies 8700, 9000, and 9300 mc, and for the wall thicknesses

$$Kh = \frac{\pi}{6}, \frac{\pi}{3}, \frac{\pi}{2}, \frac{2\pi}{3}, \frac{5\pi}{6}, \pi,$$

the above procedure was iterated seven times to give Γ_0/k correct to three significant figures. The results of these computations are given in Table I.

TABLE I

THE COMPLEX PROPAGATION CONSTANT, Γ_0/k, VS FREQUENCY AND WALL THICKNESS FOR THE FUNDAMENTAL MODE IN A SERRATED GUIDE

Wall Thickness, Kh, (Radians)	Γ_0/k for 8700 mc	Γ_0/k for 9000 mc	Γ_0/k for 9300 mc
$\pi/6$	$0.265+j0.776$	$0.268+j0.786$	$0.267+j0.793$
$\pi/3$	$0.361+j0.511$	$0.330+j0.546$	$0.308+j0.576$
$\pi/2$	$0.254+j0.514$	$0.244+j0.545$	$0.235+j0.572$
$2\pi/3$	$0.202+j0.551$	$0.198+j0.576$	$0.193+j0.596$
$5\pi/6$	$0.180+j0.602$	$0.176+j0.621$	$0.171+j0.636$
π	$0.187+j0.669$	$0.183+j0.683$	$0.176+j0.694$

An alternative way of displaying this information is by means of Fig. 3. Setting $\Gamma_0=\alpha_0+j\beta_0$, the relative phase velocity β_0/K and the leakage α_0 are plotted as functions of wall thickness for the three frequencies. The phase velocity is seen to be relatively insensitive to frequency but responsive to wall thickness. For example, at 9000 mc, it appears possible to obtain a phase velocity ranging from 125 to 185 per cent of light velocity, using wall thickness as the parameter.

α_0 is also seen to be fairly independent of frequency but variable with wall thickness. It is gratifying to see that for all three frequencies and for any wall thickness, the leakage is greater than would be required in the design of any practical traveling-wave antenna. This assures that by varying G/T and L, the complete range of leakage needed in design is available.

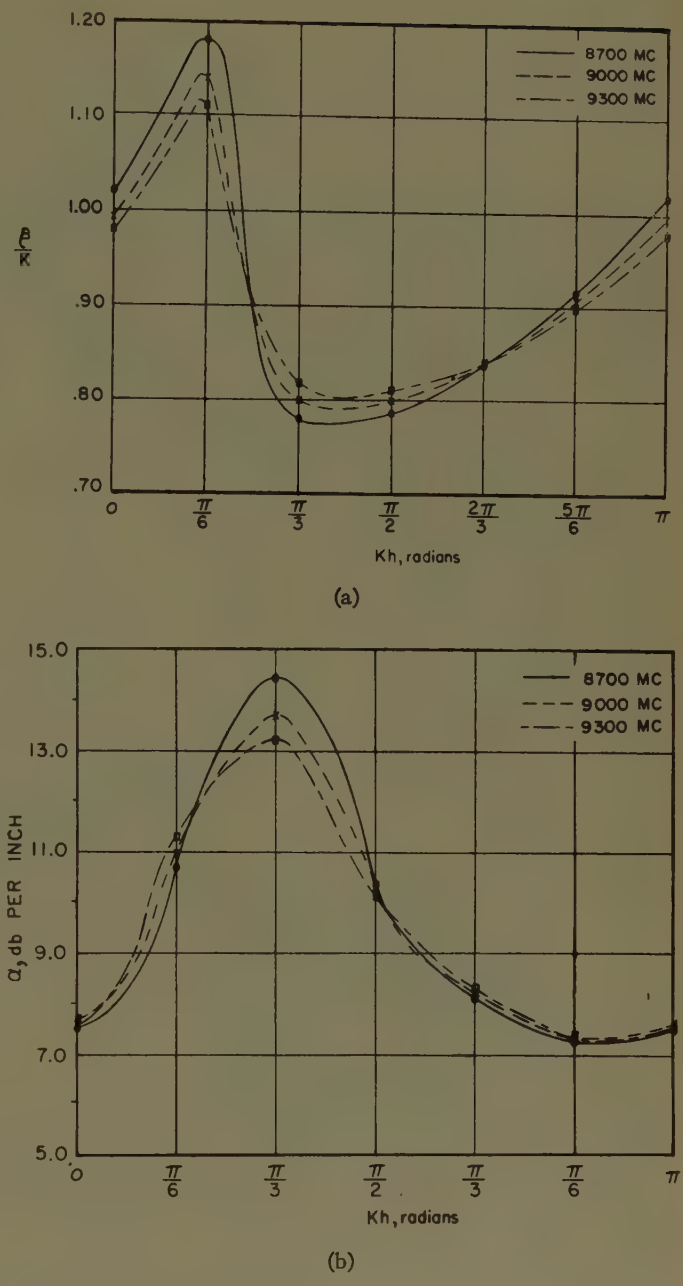

Fig. 3—(a) Relative phase constant vs wall thickness and frequency for X-band serrated waveguide. (b) Leakage vs wall thickness and frequency for X-band serrated waveguide.

CONCLUSION

An analysis of serrated waveguides for the case of full-width serrations ($L=a$) and narrow teeth has revealed that the fundamental mode has a complex propagation constant insensitive to frequency but modestly sensitive to wall thickness. The leakage is greater than would be required in practical antenna designs. The case of zero-width serrations ($L=0$) is also the case of the corrugated waveguide, a problem which has been worked out by several authors.[2,8] For the case $L=0$, the propagation constant is purely imaginary, there being no leakage, and the relative phase velocity ranges from zero to infinity as a function of h. This suggests that, as L increases, α increases and the range of β/K vs h decreases. It seems reasonable to expect that by choosing L, G/T, and h as control parameters, a practical range of both α and β can be achieved. This more general geometry poses difficulties which hamper a theoretical analysis, but the problem is being investigated. Meanwhile, the experimental evidence[9] strongly supports the hypothesis of adequate range for both α and β and this waveguide structure appears to offer an interesting new approach to many antenna problems.

[8] H. Goldstein, "Cavity Resonators and Waveguides Containing Periodic Elements," Ph.D. Thesis, Mass. Inst. of Tech.; 1943.

[9] K. C. Kelly and R. S. Elliott, "Serrated waveguide—Part II: experiment," this issue, pp. 276–283.

Serrated Waveguide—Part II: Experiment*

K. C. KELLY† AND R. S. ELLIOTT‡

Summary—Groups of nonresonant closely-spaced slots, cut in the broad wall of a rectangular waveguide, have been studied in a series of experiments. The name "serrated waveguide" has been applied to such structures. The complex propagation constant of the fundamental mode in a serrated waveguide has been measured as a function of slot size and spacing. The results have been used in the design of traveling-wave antennas with various aperture distributions These antennas can be used for flush-mounted applications.

Introduction

MICROWAVE antennas are required to satisfy a multitude of conditions, and as often as not the physical requirements exert a greater influence on the design than the electrical specifications. This is particularly true of flush-mounted antennas. The shape of the structure on which the antenna is to be placed is usually fixed by aerodynamic considerations, thus removing the shape of the antenna as a design parameter, unless radomes are utilized. Accepting the aerodynamic shape for the antenna surface, one must devise methods of exciting the proper currents in the surface to produce the desired pattern. If the phase and amplitude of current at each point along a line in the surface were controlled, the radiation pattern could be shaped in one plane. Similar control of current flow over an area of the surface would permit pattern shaping throughout a volume in space. The ultimate objective in antenna problems of this type is, therefore, to find a single flush-mounted antenna element which can act as the building block for the synthesis of arbitrary aperture distributions. It must be a simple matter to feed an aggregate of these antenna elements with a wide variety of amplitude and phase distributions if the antenna element is to be truly useful. A single antenna element which may be integrated to satisfy all foreseeable requirements will probably never be found. However, recent researches have uncovered several interesting approaches.[1–3]

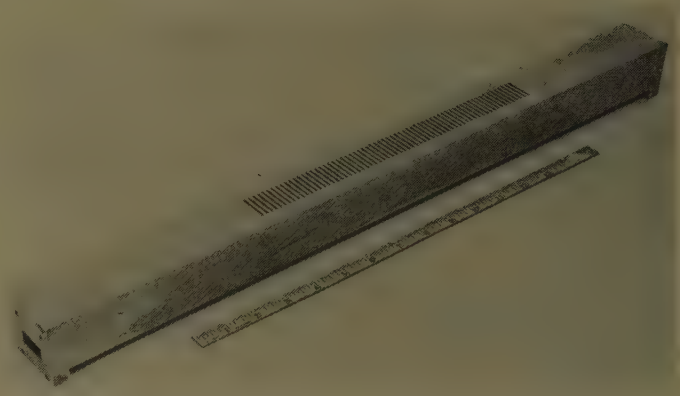

Fig. 1—Experimental thick-walled serrated waveguide.

The purpose of this paper is to describe experiments with an antenna element which shows promise as a solution for some flush-mounted applications. The element to be described consists of a series of transverse, nonresonant, closely-spaced slots[4] cut in the broad wall of a rectangular waveguide. The resulting antenna has been called a serrated waveguide for brevity. By varying the slot size and wall thickness, it is possible to achieve line aperture distributions of considerable arbitrariness in both amplitude and phase. An array of serrated waveguides will likewise yield a flexible area distribution. The sections which follow will describe the basic design experiments and the construction and testing of several successful antennas of this type.

The Basic Serrated Waveguide

The first paper of this series[5] presented an analysis of a serrated waveguide for the limiting case $L=a$, $t\to 0$, $T\to 0$, $G+T\to 0$, $G/T\to\infty$ (see Fig. 2 of Elliott[5]). A rigorous solution for $\Gamma=\alpha+j\beta$, the complex propagation constant of the fundamental serrated waveguide mode, was obtained and computations were displayed in a series of graphs covering the X-band range of frequencies (see Fig. 3 of Elliott[5]).

A good experimental corroboration of the theory was hampered by the G/T requirement. Experiments were conducted at X band and $G+T$ was chosen to be 5/32 inch to make $G/(G+T)\cong 10$. Machining difficulties forced the choice $G/T=2/3$, a far departure from the assumption of the theory. This led to the prediction that measured α would fall far below the theoretical value.

The experimental test section of the serrated waveguide is shown in Fig. 1. Constructional details are illus-

* Manuscript received by the PGAP, April 7, 1956; revised manuscript received, January 15, 1957. The research reported in this paper was supported in part by the Air Force Cambridge Res. Ctr. under contract with the Hughes Res. Labs.

† Hughes Aircraft Co., Culver City, Calif.

‡ Rantec Corp., Calabasas, Calif.

[1] J. N. Hines, V. H. Rumsey, and C. H. Walter, "Traveling-wave slot antennas," PROC. IRE, vol. 41, pp. 1624–1632; November, 1953.

[2] L. A. Kurtz, "Some Results Obtained Using Incremental Slot Characteristics in the Design of Linear and Planar Arrays," Rep. No. RSML-1-142, Res. Labs., Hughes Aircraft Co., Culver City, Calif.; July, 1954.

[3] W. Rotman, "A study of single surface corrugated guides," PROC. IRE, vol. 39, pp. 952–959; August, 1951.

"Ridge and Corrugated Antenna Studies," Quart. Progress Reps. 2–6, Stanford Res. Inst.; October, 1949—January, 1951.

R. S. Elliott, "On the theory of corrugated plane surfaces," IRE TRANS., vol. AP-2, pp. 71–81; April, 1954.

R. S. Elliott, "Pattern Shaping with Surface Wave Antennas," Tech. Memo. No. 360, Res. Labs., Hughes Aircraft Co., Culver City, Calif.; April, 1955.

[4] G. C. Southworth, U. S. patent application 2,405,242 on microwave radio transmission; 1941.

[5] R. S. Elliott, "Serrated waveguide—part I: theory," this issue, p. 270–275.

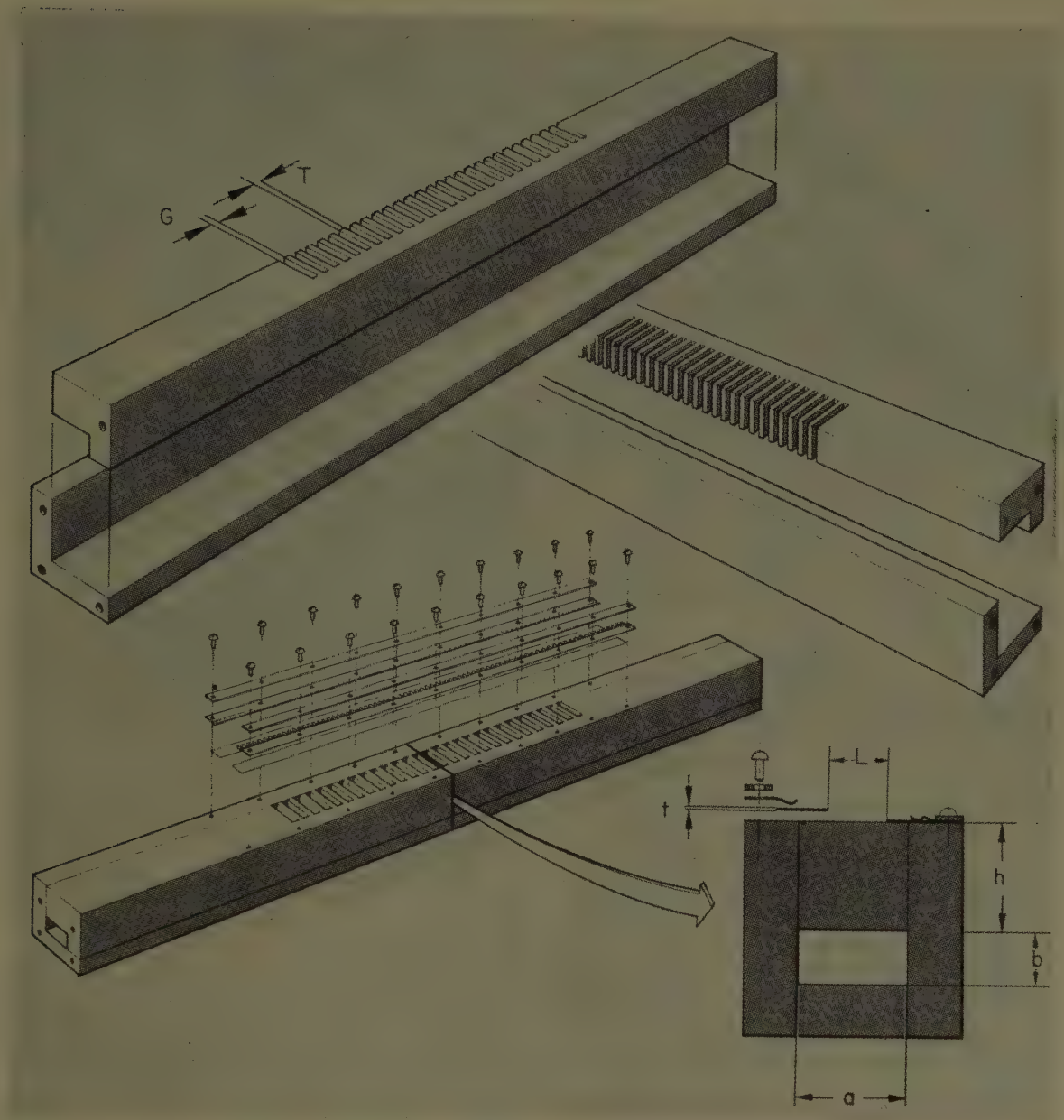

Fig. 2—Constructional details of thick-walled serrated waveguide.

trated in Fig. 2. This two-piece construction was adopted because one-piece construction, though very desirable, calls for a difficult broaching operation, and, end-milling small slots through the thick wall is prohibitively difficult. It later became apparent that imperfect solder joints in the two-piece section were affecting the leakage, and it is felt that the values of α obtained were reliable in their order of magnitude but were not highly precise.

The experimental procedure for measuring α is discussed in the Appendix. At 9000 mc, for $Kh=\pi$, a value $\alpha=5.4$ db/inch was recorded, as contrasted with a theoretical $\alpha=7.7$ db/inch. The reduction can easily be explained in terms of $G/T=2/3$, but the small amount of reduction was surprising. This result was consistently repeated for smaller values of Kh. It was concluded that varying G/T was not a profitable way to obtain a dynamic range for α, since the smaller, useful values of α correspond to values of G too small to provide ease in machining.

Because of the extremely rapid attenuation of the fields in this test section, no effort was made to measure β.

The theoretical curves indicate that for $L=a$, α is too high for all values of h and β/K performs a modest excursion around unity as h is varied. If L was equal to zero, the corrugated waveguide case would prevail with $\alpha=0$ and β/K ranging from zero to infinity [assuming $b\leq(\lambda g_0/4)$].[6] This reasoning indicates that a useful dy-

[6] If $b>\lambda g_0/4$, the corrugated waveguide can act as a pass band filter. λg_0 is the guide wavelength of the corresponding ordinary guide.

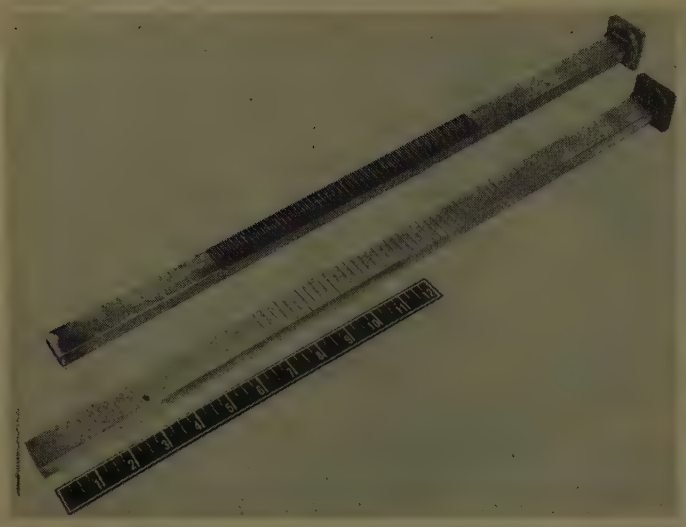

Fig. 3—Experimental thin-walled serrated waveguides with full width slots.

namic range of both α and β should be possible through proper variation of both L and h.

This idea was pursued experimentally with the test section of Fig. 1. The strips of thickness $t=0.015$ inch were held in place by fingered clamps as shown in Fig. 2. Their widths were varied to provide the change in L, and h was varied by removing the strips from the test section and planing down the serrated broad wall. The electrical imperfections (poor soldered joints) of the test unit made it impossible to gather precise data. However, indications of the effectiveness of this approach are found in the fact that β/K values as low as 0.39 and as high as 1.4 were observed. These figures are not thought to be the limits obtainable but are already well beyond the theoretical limits for the case where $L=a$. Further work on this form of the serrated guide was postponed until a suitable fabrication procedure could be found.

Thin-Walled Serrated Guides—Design Data

The experimental findings with the thick-walled test section can be summarized by two remarks: 1) It was found that controlling α through varying G/T was impractical, because the useful values of α corresponded to values of G which were too small for ease of machining. 2) When h and L were used as control parameters, another machining problem was created, since milling serrations in a thick wall forced a two-piece fabrication and poor electrical continuity.

These difficulties caused the initiation of a new series of experiments with thin-walled serrated waveguides in which L was the principal parameter. Standard X-band waveguide was used, and Fig. 2 of Elliott[5] applies with $h=0$, $t=0.050$ inch, $b=0.400$ inch, and $a=0.900$ inch.

A check was first made on G/T as a controlling parameter of α by setting $L=1.000$ inch. This procedure afforded an extremely simple and rapid machining technique. With circular milling saws, one or several on the arbor, slits were cut through the waveguide broad wall

Fig. 4—Experimental thin-walled serrated waveguides with slot length as the parameter.

across the entire width of the outside dimension of the waveguide. Fig. 3 shows two such waveguides. On the various test units, $G+T$ was varied over small limits and G/T varied over wide limits by simply choosing the thickness of the milling cutter and the spacing of the cuts. It was found that with $G+T=1/16$ inch and $G/T=1$, α was 3.8 db/inch, while with $G+T=\frac{1}{4}$ inch and $G/T=1/62$, α was down to 0.25 db/inch. It was not feasible to make G/T any lower, although smaller values of α were desired. The 62:1 variation in G/T produced only a 15:1 variation in α so once again there was cause to think that sufficient control of α was not to be obtained using G/T as the parameter.

Another approach was tried. In the serrations, the maximum E field is longitudinal and is on the centerline of the broad wall. It was reasoned that a metal strip placed on the outer surface of the waveguide, soldered at each serration and centered on the broad wall, would force E to be zero where it was once a maximum, and thus the leakage could be greatly reduced. Such strips proved effective and considerable control resulted when G/T was held at unity and the width of the strip was varied. However, the results were not wholly consistent. Since it appeared that strip centering and strip soldering were too critical, this method was abandoned.

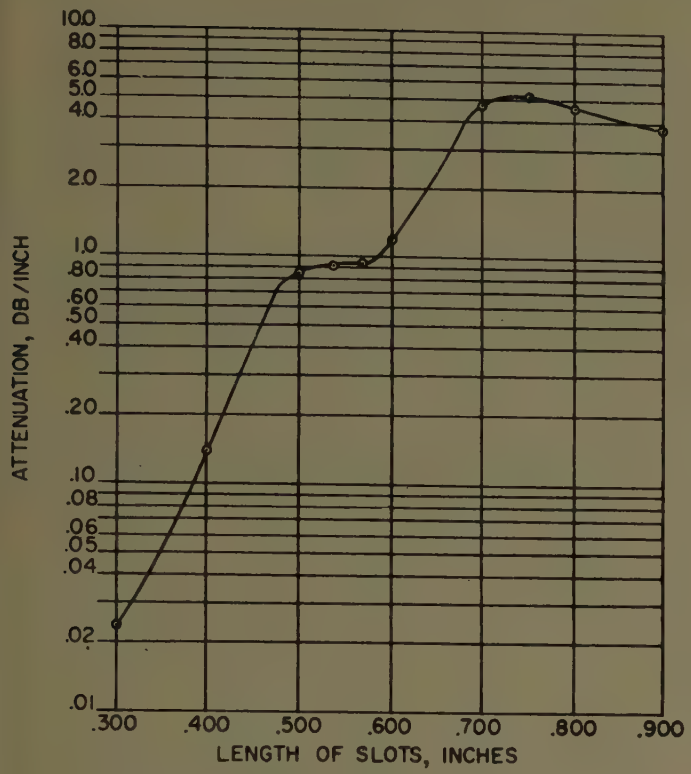

Fig. 5—Radiation in db/inch vs slot length with $G/T=\frac{1}{4}$.

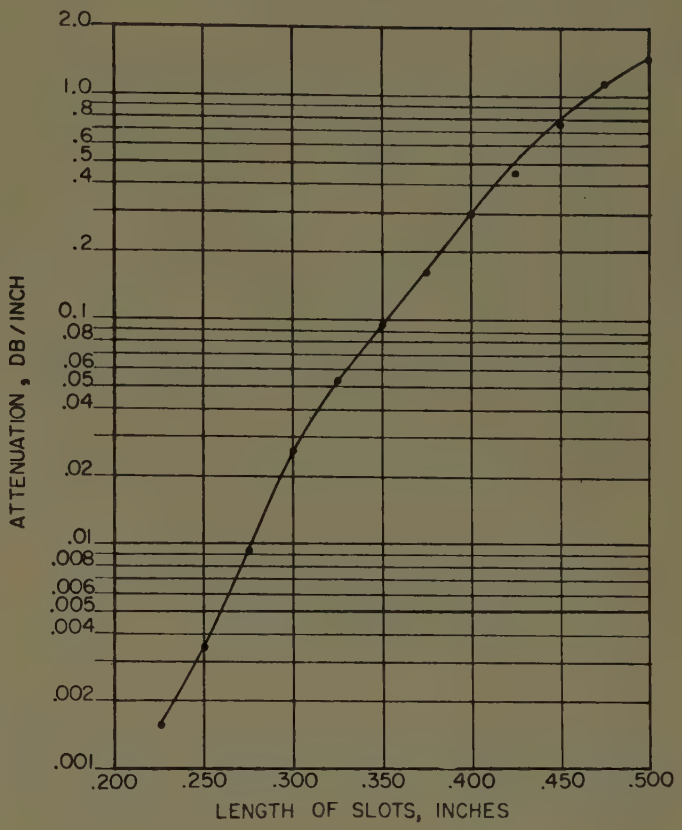

Fig. 6—Radiation in db/inch vs slot length with $G/T=\frac{2}{3}$.

A family of test sections for investigating serrated guides with L as the parameter is shown in Fig. 4. All slots in any one guide have the same L dimension, but L is different for each member of the family. An extension of the data obtained earlier with $L=1.000$ inch enabled a choice of $G/T=\frac{1}{4}$ and $G+T=5/32$ inch so that when $L=0.900$ inch, α would be slightly larger than the maximum value anticipated for the design of useful aperture distributions. It was expected that α would then decrease steadily to zero as $L\rightarrow 0$. This reasoning proved fallacious since, despite the tight mutual coupling between slots, a resonance effect was observed while testing at 9000 mc. Therefore, while α did reduce to zero with L, it did not do so monotonically, as evidenced by Fig. 5.

To eliminate the double-valued region of α vs L and to reduce the frequency sensitivity of α (when L goes through resonance), the upper limit of L was set just below resonance, and G/T was adjusted to obtain the required maximum value of α. Values of $G/T=\frac{2}{3}$ and $G+T=5/32$ inch proved satisfactory. With no further difficulties, the behavior of α with L was noted, and the findings are presented in Fig. 6. The data were taken at 9000 mc; however, patterns taken on arrays designed for 9000 mc show little pattern deterioration over the 8400 to 9600-mc band.

While α was quite responsive to changes in L, β was observed to be essentially constant with L (see Fig. 7). One of the important early objectives of this program was to find means to exert wide control on β as well as on α. The thick-walled serrated guide is capable of such control through h, but it was necessary to consider other means to vary β in the thin-walled guide.

Varying the waveguide width offers a method to control β, but it is limited by the passage of higher-order modes at one extreme and by cutoff for the fundamental mode at the other. Decreasing a will lower the value of β from the value obtained at a given frequency with a standard guide. Types of loading which will increase the value of β include the insertion of a dielectric or the presence of a ridge. Equations for the wavelength in lossless waveguides which have the characteristics that result from any of the above modifications may be found in several handbooks.[7] From a transmission line point of view, the radiation from a serrated guide makes it a lossy line, and the question arises as to the applicability of the handbook expressions. It had been found that the short-slot serrations did not cause a drastic change from the phase constant of the unslotted guide (Fig. 7). This characteristic suggested that the same might be true for other waveguide cross sections. To check this theory, a partial-filling dielectric plug was designed to cause a specified phase constant in an unserrated guide, and the phase constant was then measured with this plug in a serrated guide. The ordinary guide phase constant was

[7] For example, N. Marcuvitz, ed., "Waveguide Handbook," M.I.T. Rad. Lab. Ser., McGraw-Hill Book Co., Inc., New York, N. Y., vol. 10, pp. 388–402; 1951.

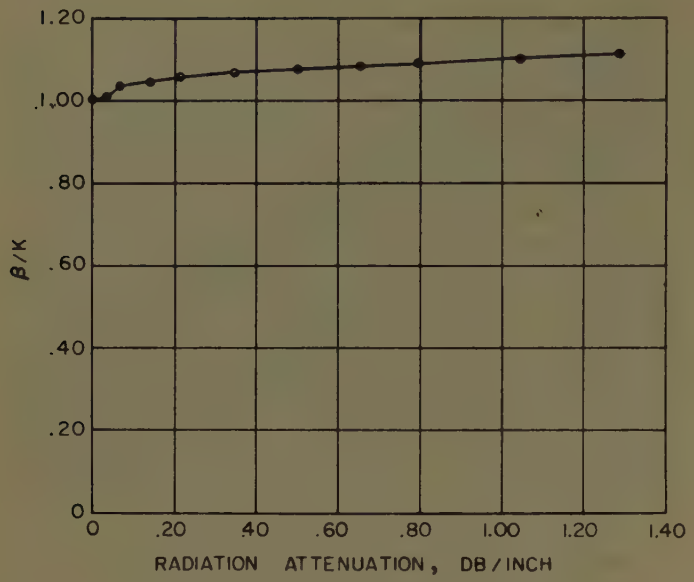

Fig. 7—Phase constant vs radiation in db/inch for $G/T=\frac{2}{3}$.

4.64 radians/inch with the dielectric in place. The serrated guide, loaded with the dielectric, had a phase constant of 4.60 radians/inch as determined from the angular position of the beam in Fig. 8. (See Appendix.)

For computations of moderate precision these data indicate that, when determining changes in waveguide geometry to control β, perhaps it is reasonable to neglect the leakage. For precision work, refinements may be made through complete analysis or extensive experimental information.

Thin-Walled Serrated Guides—Applications

Before the experimental findings could be applied to produce a specified amplitude distribution in an antenna aperture, it was necessary to mathematically relate the leakage, $\alpha(x)$, to the desired amplitude distribution $A(x)$.

With variable serrations, the power present in the guide can be expressed as

$$P(x) = B^2 \exp\left[-2\int_0^x \alpha(\xi)d\xi\right] \tag{1}$$

with B a constant which describes the initial magnitude. Differentiating and rearranging gives

$$\frac{1}{P(x)}\frac{dP(x)}{dx} = -2\alpha(x). \tag{2}$$

If the phase velocity is constant and if the aperture extends from $x=0$ to $x=D$, $P(x)$ is related to the aperture distribution by

$$P(x) = P_{\text{in}} - \int_0^x A^2(\xi)d\xi \tag{3}$$

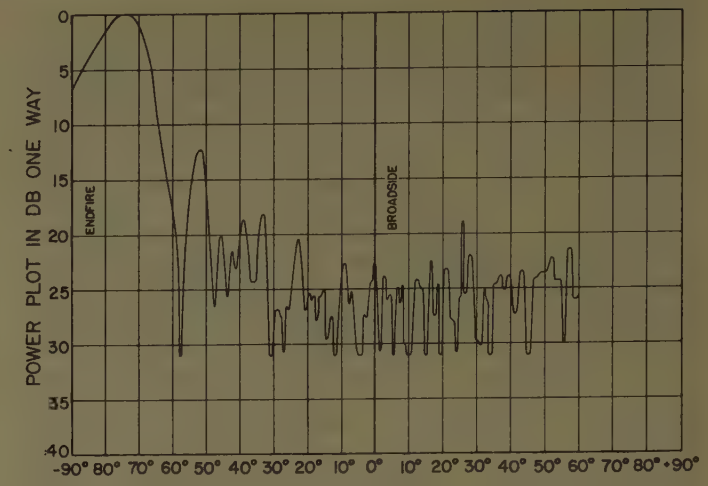

Fig. 8—Radiation pattern of dielectric-loaded serrated waveguide.

in which $A^2(\xi)$ is the power density in the aperture and

$$P_{\text{in}} = \int_0^D A^2(\xi)d\xi + P_{\text{load}}. \tag{4}$$

It is assumed that the traveling-wave array is terminated in a flat load which absorbs a fraction, f, of the input power ($P_{\text{load}}=fP_{\text{in}}$). Then (3) becomes

$$P(x) = \frac{1}{1-f}\int_0^D A^2(\xi)d\xi - \int_0^x A^2(\xi)d\xi \tag{5}$$

so that

$$2\alpha(x) = \frac{A^2(x)}{\frac{1}{1-f}\int_0^D A^2(\xi)d\xi - \int_0^x A^2(\xi)d\xi}. \tag{6}$$

When $A^2(x)$ is specified, (6) may be used as a design equation for $2\alpha(x)$, the leakage in nepers/unit length. This equation can then be related to the experimentally obtained relation between leakage and slot length which was displayed in Fig. 6. The result is a curve of slot length vs x from which the array can be constructed.

The first experimental array was chosen to have $A(x)=1+\sin(\pi x/D)$. The terminating load was designed to take 10 per cent of the power ($f=0.1$) as a compromise between antenna efficiency and a moderate peak value for $\alpha(x)$. The array length, D, was set at 10.14 inches, and $\alpha(x)$ was computed from (6). Next, employing Fig. 6, a curve was plotted of slot length vs. x. The axis of the abscissa was then divided into 5/32-inch intervals (5/32 inch being the distance $G+T$), and the length of each slot read off and tabulated (Fig. 9). When fabrication was completed, the radiation patterns were taken and are reproduced in Fig. 10. The theoretical sidelobe level for this amplitude distribution is 17.7 db, and the patterns show that this level is approached. Endfire and broadside angles on all patterns

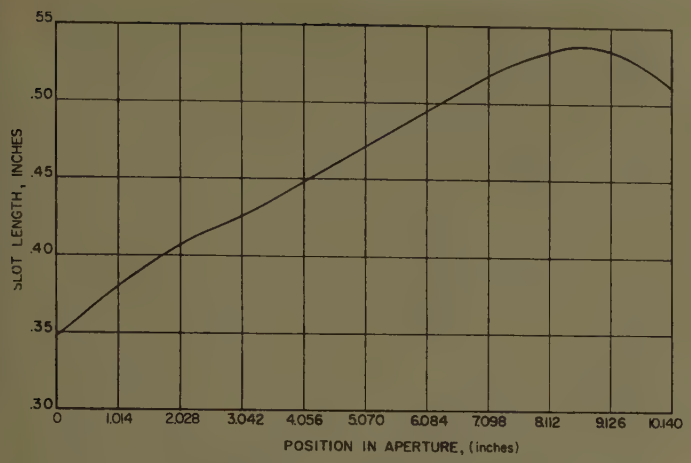

Fig. 9—Design curve for slots of $1+\sin(\pi x/D)$ aperture distribution.

in this report are as shown on Fig. 8. Since beam maxima occur at an angle $\theta=\cos^{-1}(\beta/k)$ off endfire (see Appendix) the beam shifts approximately 10° over the frequency range 8400 to 9600 mc. This frequency effect exists for all arrays of this type. It is minimized by making the wide dimension as large as possible consistent with higher-order mode suppression. Such a choice will, however, cause the average position of the beam to be nearer endfire for the same frequencies. Conversely, arrays of this type may have their beam positions quite sensitive to changes in frequency by operating the waveguide near cutoff. The average beam position would then be nearer broadside.

There is considerable interest in arrays capable of producing cosecant-squared radiation patterns. A uniform phase progression and a sawtooth amplitude distribution result in an approximation to a cosecant squared beam.[8]

By letting $A(x)=1-(x/D)$ a new array was constructed using the design data. This array radiated the power pattern shown in Fig. 11. The theoretical power pattern[8] for this amplitude distribution falls below a cosecent-squared curve at larger angles. In view of this fact, the experimental pattern has been compared to a $\csc^2\cos^{1/2}$ curve. The $\cos^{1/2}$ factor depresses the $\csc^2$ at larger angles (1.46 db at 60°). Naturally, the half-power beamwidth may be reduced by increasing the array length. The high sidelobe towards endfire is believed to be a result of edge diffraction and presumably could be reduced if the ground plane terminating the array were extended.

In gathering data on α as a function of slot length, no measurable difference resulted when a ground plane was positioned beside the serrated guide. This fact suggested that, should a two-dimensional or planar array be formed from several identical serrated guides soldered adjacently and fed in phase, the mutual coupling between guides would be so small that the E-plane pattern of the aggregate would be the same as the pattern of any one. This property was demonstrated to be essentially true when the array pictured in Fig. 12 was tested and

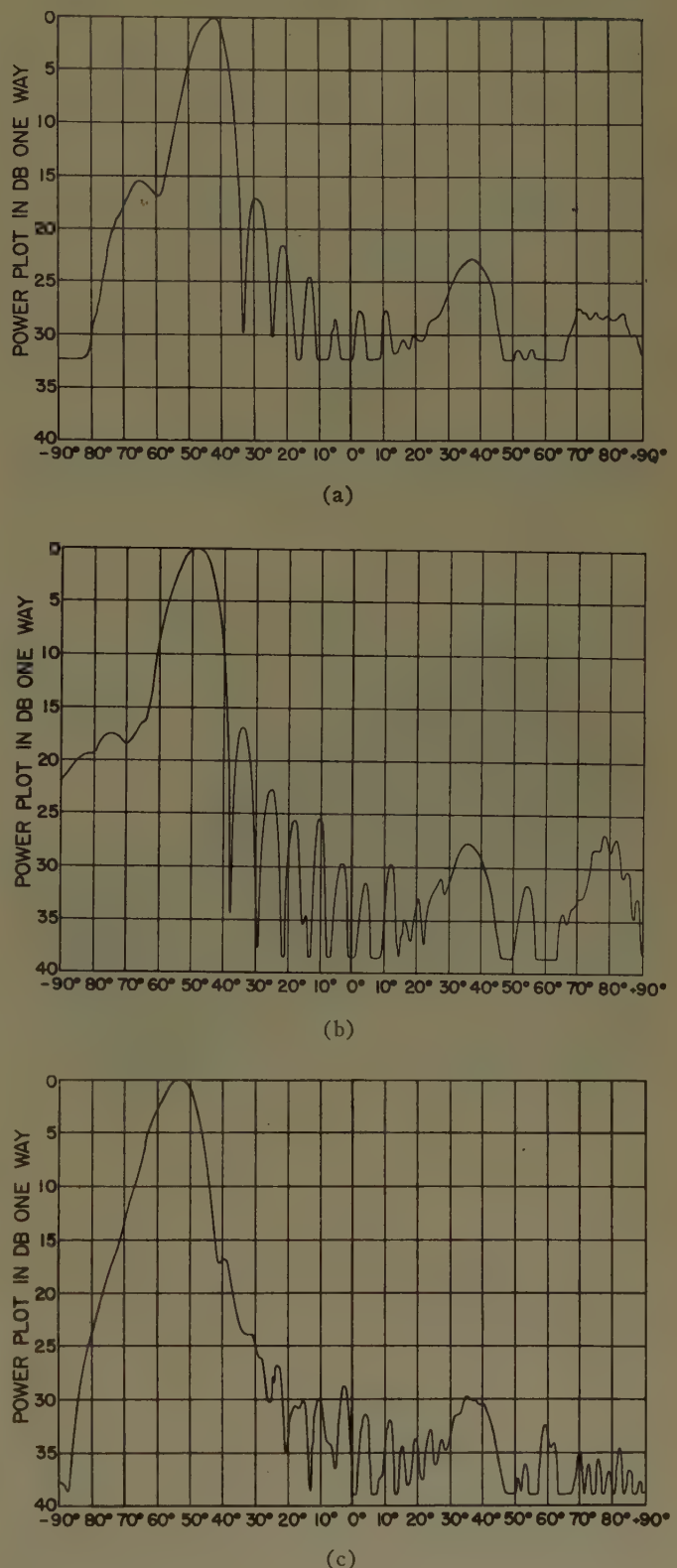

Fig. 10—E-plane patterns of serrated waveguide, $A(x)=1+\sin \pi x/D$. (a) 8400 mc, (b) 9000 mc, and (c) 9600 mc.

[8] A. S. Dunbar, "Uniform Progressive-Phase Antennas Having Asymmetric Amplitude Distributions," Tech. Rep. No. 188-13, Stanford Res. Inst.; September, 1950.

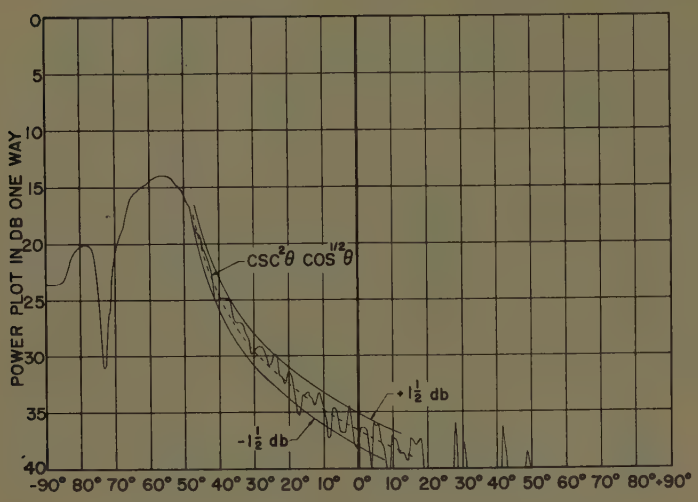

Fig. 11—*E*-plane pattern of serrated waveguide, $A(x)=1-(x/D)$.

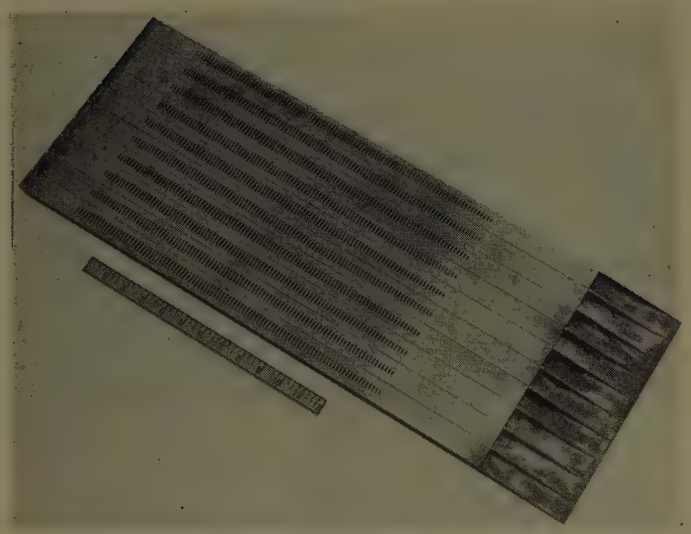

Fig. 12—Planar array showing taper to feed horn.

the *E*-plane pattern proved to be identical with that of one element. The amplitude distribution of each serrated guide was made approximately a sine taper, and the *E*-plane patterns obtained for three frequencies are shown in Fig. 13. The shape of the *H*-plane pattern is controlled by the amplitude distribution set up by the feeding system. The array pictured has the narrow walls tapered to a point. This tapered end was inserted into a hoghorn. The object was to have a feed which would cause the *H*-plane beam position to be fixed with frequency while the *E*-plane beam position executes its shift with frequency. *H*-plane patterns for the extreme frequencies are shown in Fig. 14. It can be noticed that the beam position is maintained with frequency change. The transition from the hoghorn to the waveguides was not very gradual; thus, the reflection in the hoghorn caused asymmetries in the *H*-plane patterns.

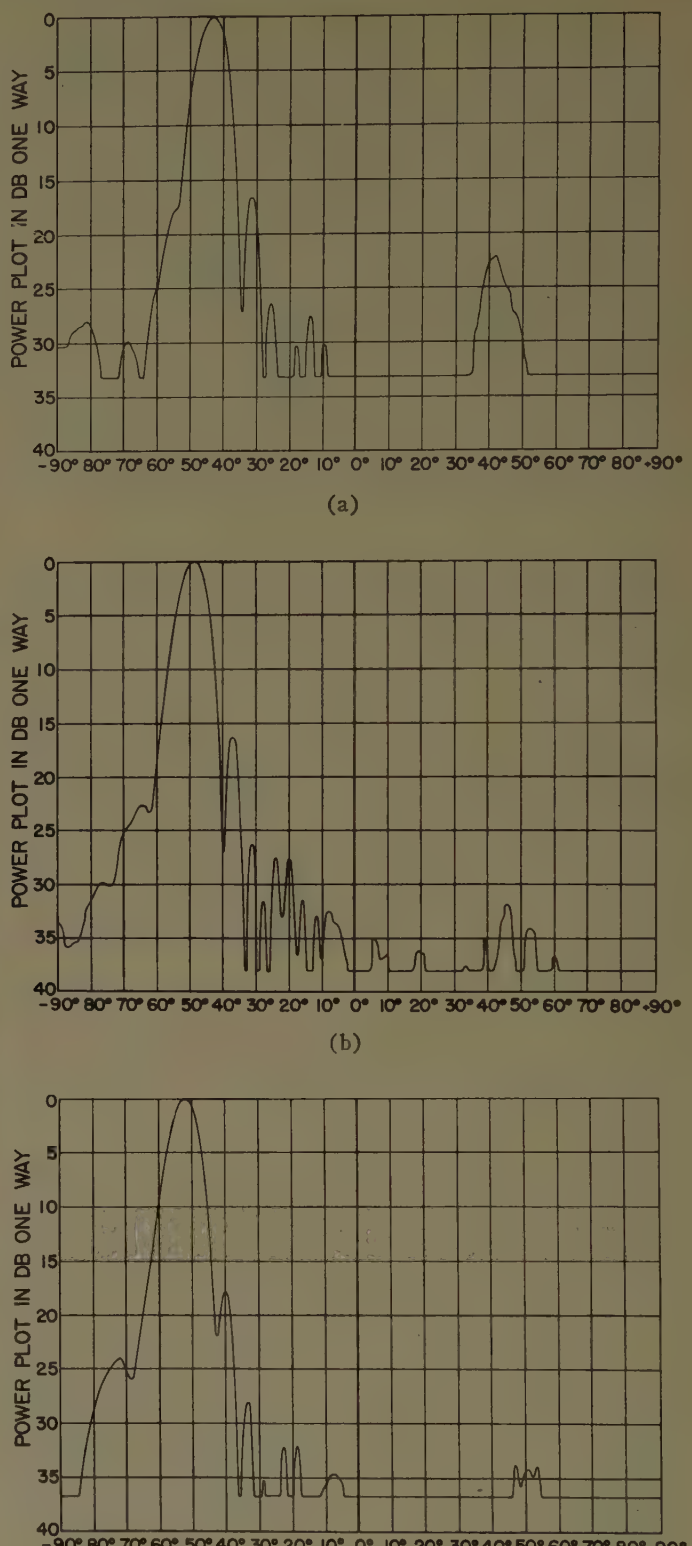

Fig. 13—*E*-plane patterns of planar array. (a) 8400 mc, (b) 9000 mc, and (c) 9600 mc.

Most amplitude tapers of interest result in distributions of transverse slot length which start small at the input end. A natural match to the uncut guide is ob-

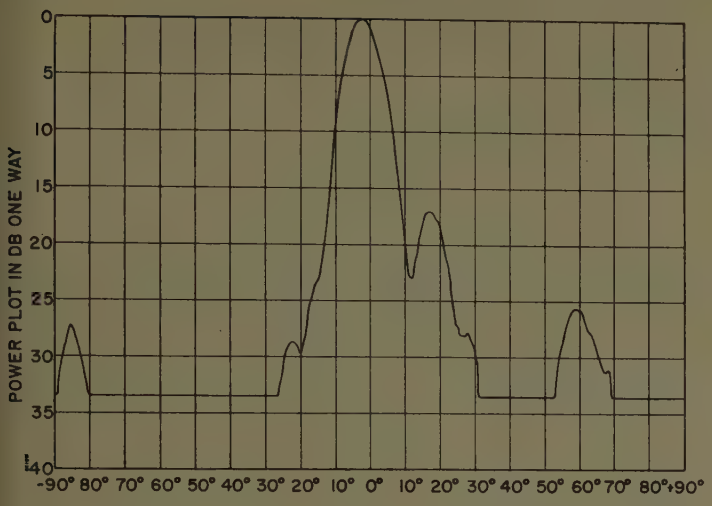

(a)

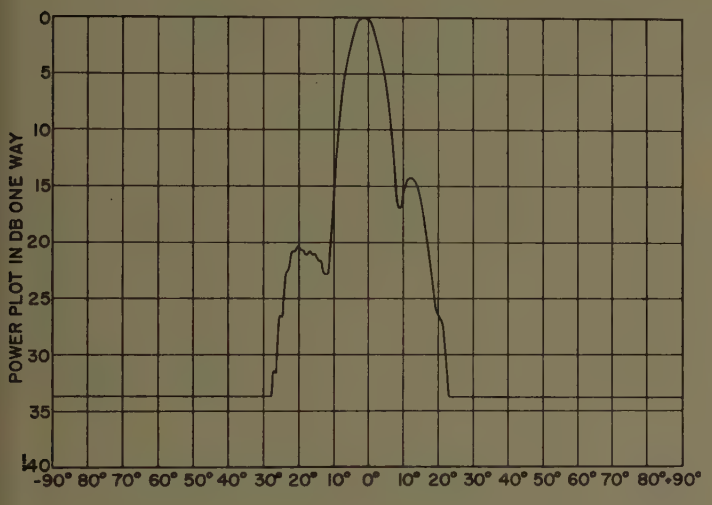

(b)

Fig. 14—*H*-plane patterns of planar array. (a) 8400 mc and (b) 9600 mc.

tained thereby. The vswr looking into each waveguide of the planar array is plotted as a function of frequency in Fig. 15. Excellent impedance characteristics are seen to exist. Even the sawtooth distribution, whose amplitude distribution has a maximum at the input end, has a vswr of 1.14 or less over the band.

Conclusion

It appears that the original objective of wide control of phase and amplitude over a slotted waveguide aperture is electrically possible with the serrated waveguide. However, fabrication of the most general serrated unit is extremely difficult.

A standard rectangular waveguide, when slotted to create a special case of the general serrated waveguide geometry, offers some useful pattern shaping capabilities and excellent impedance characteristics.

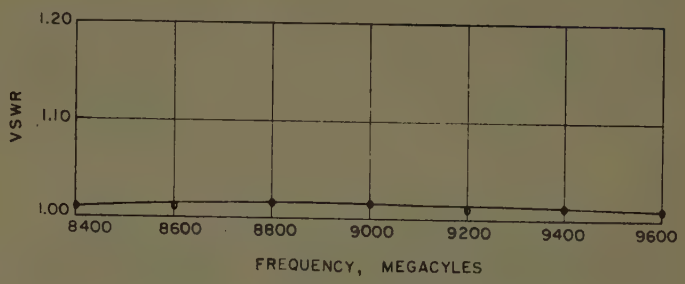

Fig. 15—VSWR of each serrated waveguide of planar array.

Appendix

Measurements

The attenuation constant, α, of a serrated guide was measured by treating uniformly serrated guides as uniform transmission lines and measuring the loss in the entire length. These test sections were made several wavelengths long, in order to minimize the errors caused by the perturbations at the junctions between the serrated guide and the standard guide feeding and terminating it.

Where the attenuation in a section was 1.0 db or less, the attenuation was measured by shorting the section and measuring the impedance looking into it. If the attenuation of the section was over 1.0 db but less than 40 db, measurement of the insertion loss of the section by modulated oscillator and bolometer detector proved satisfactory. For larger values of section attenuation, a spectrum analyzer was used in connection with an insertion loss type of measurement. Details of each of these techniques are given by Montgomery.[9]

After the attenuation of a section was measured, the figure was corrected for the effects of junction vswr and wall losses so that an attenuation figure representing radiated power could be obtained. This figure was then divided by the length of the serrated portion to obtain a pre-unit-length value for α.

Measurement of β was accomplished by a study of the radiation patterns of uniformly serrated test sections. When the position, θ, of the beam maximum is noted, β may be determined with good accuracy[10] by the equation

$$\beta = k \cos \theta \tag{7}$$

where k is the free-space phase constant and θ is the angle off endfire.[11] Alternatively, one may write

$$\theta = \cos^{-1} (\beta/k) = \cos^{-1} (\lambda_0/\lambda_g). \tag{8}$$

[9] C. C. Montgomery, ed., "Technique of Microwave Measurements," M.I.T. Rad. Lab. Ser., McGraw-Hill Book Co., Inc., New York, N. Y., vol. 11, pp. 804–853; 1947.

[10] This equation assumes that the serrated section is long enough to permit a good approximation using the method of stationary phase.

[11] A. S. Dunbar, "On the theory of antenna beam shaping," *J. Appl. Phys.*, vol. 23, p. 848; August, 1952.

A Technique for Controlling the Radiation from Dielectric Rod Waveguides*

J. W. DUNCAN† AND R. H. DuHAMEL‡

Summary—**This paper describes a technique for controlling the radiation from a dielectric rod waveguide by placing obstacles or antenna elements at appropriate points along the waveguide. The HE_{11} mode on a dielectric rod was used to excite concentric rings and radial wires. The coupling of the obstacles to the HE_{11} mode was determined by constructing an image line with a slotted section for impedance measurements. This information was used to design several antenna arrays with different types of patterns. The measured patterns were very satisfactory.**

Introduction

DURING RECENT YEARS, increasing use has been made of surface wave antennas. Examples are corrugated surfaces, dielectric rods and tubes, dielectric coated conductors, dielectric slabs, etc. Most surface wave antennas have been designed for endfire or near endfire radiation. Only minor success has been obtained in controlling the radiation from surface wave antennas in directions other than endfire. The objective of this work has been to devise methods of modifying surface waveguides in such a manner that accurate control of the radiation can be obtained.

Mueller[1] succeeded in obtaining broadside radiation from a dielectric rod antenna by means of placing dielectric disks on the rod with approximately half-wavelength spacing between the disks. Although his simple array theory predicted the direction and width of the main beam with fair accuracy, control of the side lobe level could be obtained only on an empirical basis. A disadvantage of the dielectric disks was that the polarization was a function of the circumferential angle.

It is believed that the technique described in this paper will allow accurate designs of modified surface wave antennas. The method is similar to Mueller's in that obstacles or discontinuities are placed at appropriate points along the waveguide in order to force and control the radiation. If an obstacle, such as a piece of metal, is placed near an excited surface waveguide, it will radiate and will also excite surface waves. By choosing the proper waveguide dimensions and/or choosing obstacles with a certain symmetry, all surface wave modes except one may be made negligible. The antenna system may then be represented by a single transmission line loaded at the appropriate point by the equivalent obstacle four-pole network. If the axial length of the obstacle is small, its equivalent admittance is a simple shunt element. Knowledge of the radiation pattern and the equivalent admittance of the obstacle would allow a simple, straightforward design of arrays of the obstacles to produce specified patterns. In some cases it may also be necessary to take into account the effect of the mutual admittance between the obstacles.

Briefly, the work to be described is the following: the coupling of wires and rings to the HE_{11} mode on a dielectric rod waveguide was measured. This information was then used to design several arrays to produce various types of patterns. The arrays were constructed and tested. Good agreement between the predicted and measured patterns was obtained.

The Dielectric Rod Waveguide

The dominant HE_{11} (or dipole) mode[2] on a dielectric rod is a hybrid mode which has axial components of both the electric and magnetic field intensities, and is unsymmetrical in that all field components vary as the sine or cosine of the circumferential angle, θ. The electric field configuration of the HE_{11} mode on a dielectric rod is shown in Fig. 1. The cutoff wavelength of a particular

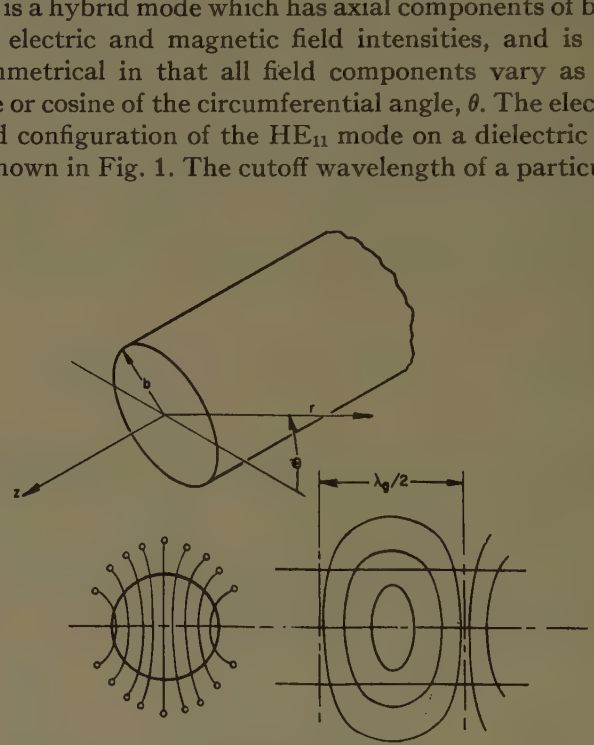

Fig. 1—Approximate electric field configuration of the HE_{11} mode on a dielectric rod waveguide.

mode on the dielectric rod is a function of the rod radius, b, and the operating frequency or wavelength, λ. Characteristic curves showing the variation of $\lambda g/\lambda$, the ratio

* Manuscript received by the PGAP, March 12, 1956; revised manuscript received, March 4, 1957.

† Antenna Lab., Dept. of Elec. Eng., University of Illinois, Urbana, Ill.

‡ Collins Radio Co., Cedar Rapids, Iowa; formerly at University of Illinois.

[1] G. E. Mueller, "A broadside dielectric antenna," PROC. IRE, vol. 40, pp. 71–75; January, 1952.

[2] R. E. Beam, "Final Report on Investigation of Multi-Mode Propagation in Waveguides and Microwave Optics," Army Signal Corps Contract No. W36-039 sc-38240, Microwave Lab., Northwestern University, Evanston, Ill., May 1, 1949 to November 30, 1950.

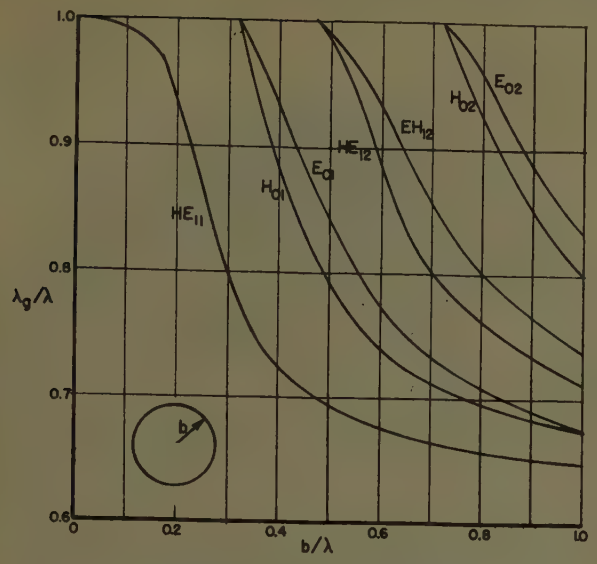

Fig. 2—Characteristic curves for symmetrical and unsymmetrical or hybrid modes on a dielectric rod.

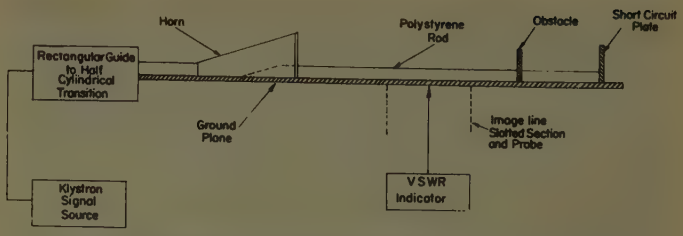

Fig. 3—Diagram of image line and associated equipment.

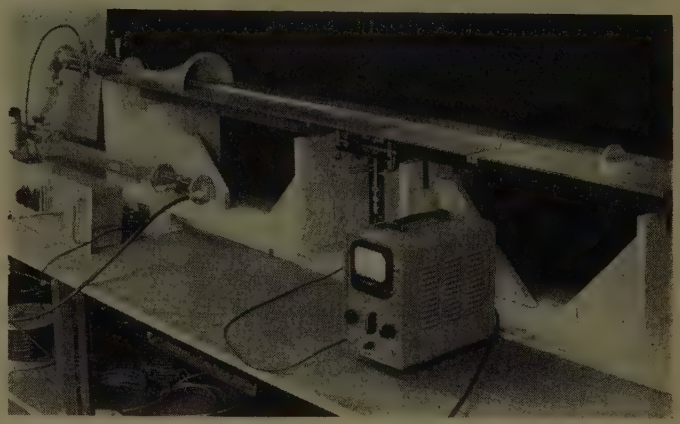

Fig. 4—Apparatus for measuring the coupling of obstacles to the dielectric rod waveguide.

of the guide wavelength to the operating wavelength as a function of the parameter b/λ are plotted in Fig. 2. The curves are for the symmetrical E_{01}, H_{01}, E_{02}, and H_{02} modes, and the unsymmetrical HE_{11}, HE_{12}, and EH_{12} modes. The symmetrical modes on a dielectric rod are either transverse electric or transverse magnetic and the field intensities are independent of the angle θ.

Measurement of the Obstacle Admittance

The dielectric rod waveguide was utilized to investigate modified surface wave antennas for two reasons. First, the rod has a simple geometry for which theoretical solutions are available. Second, by using an image system, accurate standing wave measurements may be made along the rod by means of a slotted section in the ground plane. Fig. 3 illustrates the arrangement of equipment which was used to measure the equivalent shunt admittance of the various types of obstacles. Fig. 4 is a photograph of the microwave equipment and dielectric image line. Shown from left to right are the signal oscillator and associated rectangular waveguide test equipment, the horn exciter, the dielectric rod image line, a ring type of obstacle, and a short-circuit plate. The launching horn is a half-conical horn approximately 25.4 cm long with a mouth diameter of 17.8 cm. It is fed by a 16.2-cm length of half-cylindrical waveguide. The launching horn and dielectric rod are mounted on a 0.64-cm brass plate which is 206 cm long and 25.4 cm wide. Utilizing the image principle, the polystyrene rod has been halved along its length and fastened to the brass plane by polystyrene pins. The total length of the dielectric image line was approximately 168 cm for most of the admittance measurements. The polystyrene pins are 0.32 cm in diameter and two pins are used for each 28-cm section of rod. The rod sections were machined to accurate length to realize a very tight fit between the interface of two sections and thereby minimize reflections from the discontinuity of the interface. Measurements indicated that reflections from such discontinuities were negligible. The polystyrene rod has a diameter of 2.22 cm and the operating wavelength was maintained near 4.5 cm. This results in a b/λ ratio of about 0.25 and reference to Fig. 2 shows that the guide wavelength of the HE_{11} mode was approximately 86 per cent of the operating or free space wavelength. The rod diameter and operating wavelength were purposely selected so that only the dominant HE_{11} mode was present on the rod waveguide; all higher order modes were cut off, as may be seen from Fig. 2. The short-circuit plate is silver-plated brass and has a radius of 4.45 cm.

The slotted section of the ground plane, which is located to the left of the ring obstacle, is shown in Fig. 5. The tapered slot is approximately 0.32 cm wide and 22.9 cm long. The probe is supported by a Hewlett-Packard Universal Probe Carriage which was modified and mounted on the underside of the brass plate. An inclined wire obstacle may be seen on the right side of the picture. The operation of the slotted section was quite satisfactory. The residual vswr was less than 0.2 db and vswr's of 40 db were obtained for the line terminated with the short-circuit plate.

Concentric rings were placed on the image line by means of the plates shown in Fig. 6. The obstacles were fabricated from 0.08-cm brass plate. These plates were inserted at a break in the ground plane (see Fig. 4) and the two sections of the ground plane were then clamped to make good electrical contact.

Fig. 5—The slotted section.

Fig. 6—Rings for the image line.

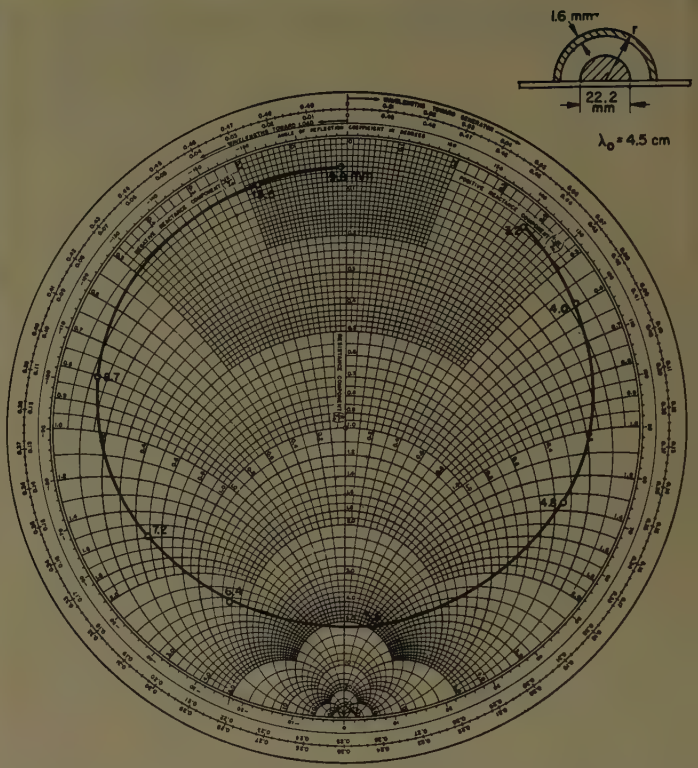

Fig. 7—Shunt admittance of a ring as a function of the mean ring radius.

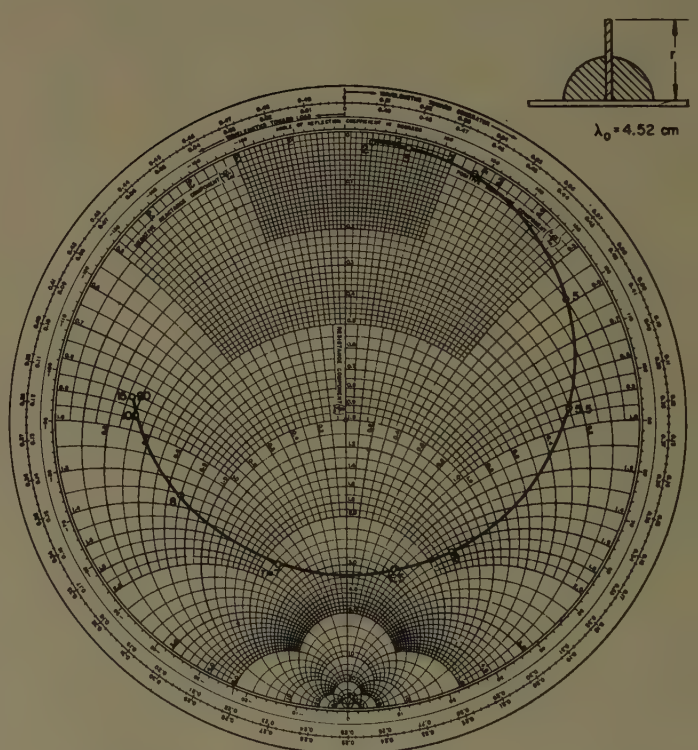

Fig. 8—Shunt admittance of a vertical wire as a function of the wire length

Since the existence of only a single mode was demonstrated, the admittance measurements were made in the same manner as that for a conventional waveguide and slotted section. The short-circuit plate was always placed an odd number of quarter-wavelengths past the obstacle. The measured normalized shunt admittance of a ring as a function of the mean ring radius is presented in Fig. 7. Since the maximum vswr that could be obtained with a short-circuit termination was 29 db for the ring measurements, the points at the top of the admittance chart are not very accurate. Fig. 8 shows the normalized shunt admittance of a vertical wire or monopole as a function of the wire length. For this series of measurements a vswr of 40 db could be attained for short-circuit termination of the line. It may be seen from Figs. 7 and 8 that the resonant ring and wire are strongly coupled to the line (conductances of 5.3 and 3.3, respectively).

In the design of an array it is certainly desirable, although not essential, to use resonant obstacles. In addition, the elements should be loosely coupled to the line, *i.e.*, the conductance should be considerably less than one. It is readily seen that the ring and protruding wire do not satisfy these requirements. A study of the field distribution of the HE_{11} mode makes apparent two methods of controlling the coupling of resonant obstacles to the rod. First, since the fields decay exponentially away from the rod, a resonant obstacle could be displaced from the rod to reduce the coupling. Second, since the fields vary sinusoidally with the circumferential angle, certain types of resonant obstacles, such as wires, could be oriented or rotated about the axis of the guide to control the coupling. The work to be described below illustrates these methods.

In Fig. 9 there is plotted the normalized shunt admittance of a wire normal to and displaced 3 mm from the

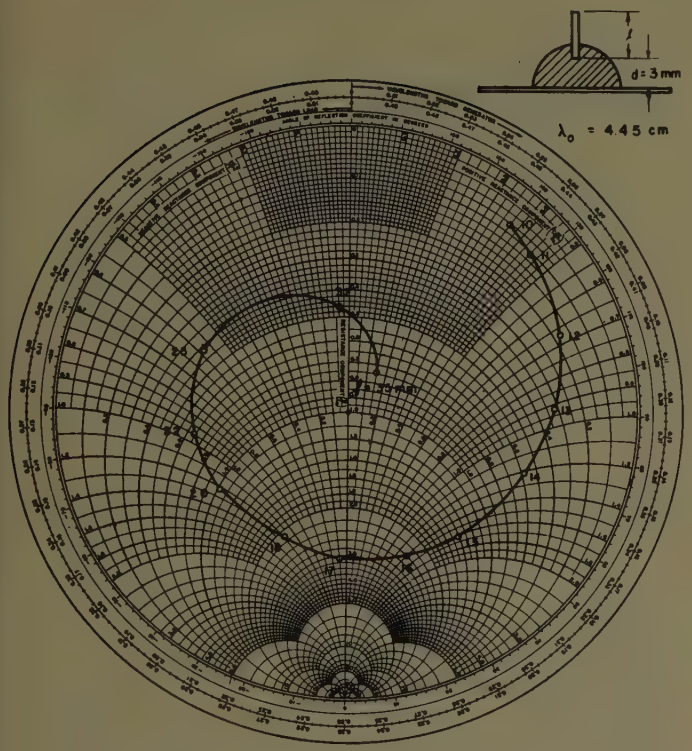

Fig. 9—Shunt admittance of a wire as a function of the wire length.

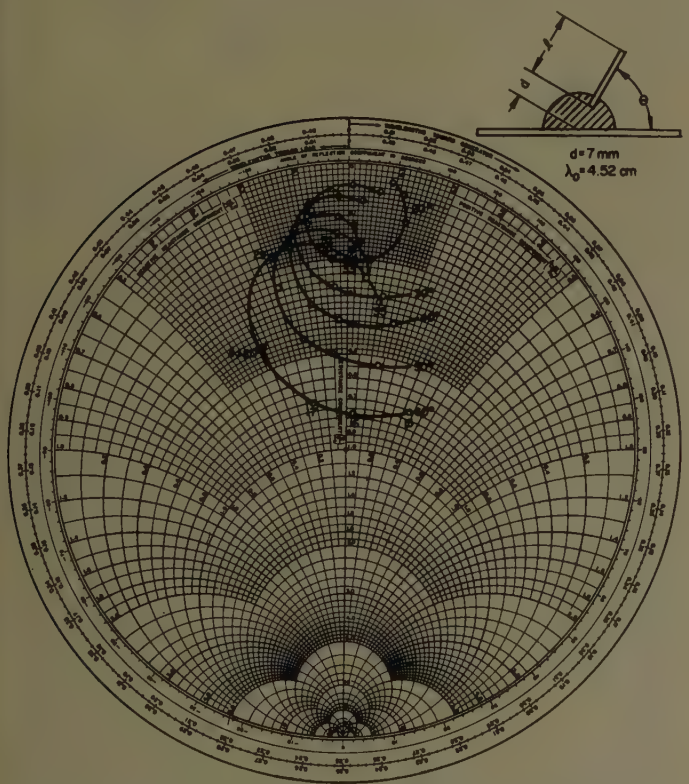

Fig. 10—Shunt admittance of an inclined wire as a function of the wire length.

slab as a function of the wire length. For these and the following measurements, the vswr on the line with the short-circuit plate was at least 37 db. Thus the points near the top of the chart are more accurate than some of those shown previously. The wire passed through the

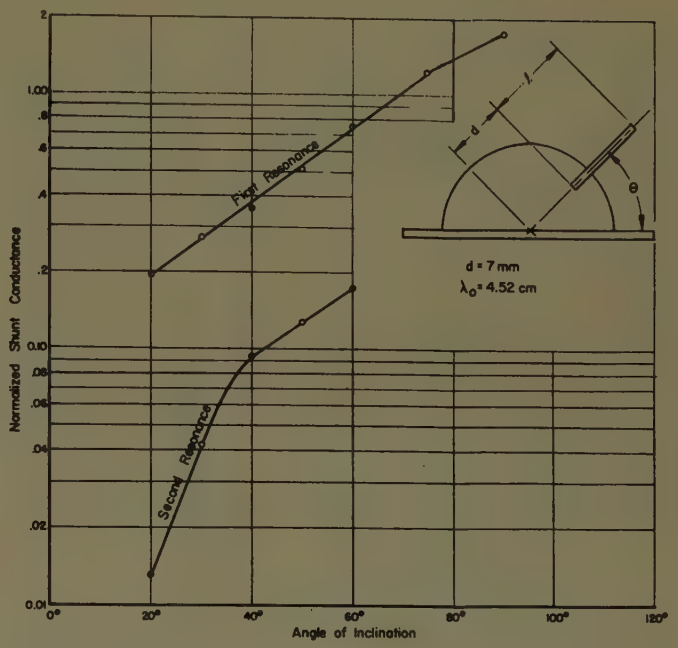

Fig. 11—Normalized shunt conductance of a resonant wire as a function of the angle of inclination.

first and second resonances when its length was 0.38 λ and 0.72 λ, respectively. This measurement was repeated for two other displacements. It was found that the conductance decreased to 1.1 and 0.2 at the first and second resonances respectively when the spacing was increased from 3 to 9 mm. Although control of the conductance can be obtained in this manner, it was apparent that the wire had to be placed completely outside of the rod in order to obtain conductances of 0.1 or less. Additional support of the wire would then have to be provided.

Fig. 10 shows the normalized admittance loci of an inclined wire as a function of the wire length for several angles of inclination. This data was used to construct the curves of Fig. 11, which show the normalized shunt conductance of a resonant wire as a function of the angle of inclination. It may be seen from the curve for the second resonance that a wide range of small conductances may be obtained.

Since only a single element was used, the measurements are not accurate for the second resonance curve for angles of 30° or less. For accurate results, several elements in tandem should be measured, as is done for loosely coupled slots in rectangular waveguides. This technique has the added advantage that it takes into account the incremental conductance due to the mutual coupling of the elements. It was found that the resonant length of the wire changed slightly with the angle of inclination, as is illustrated in Fig. 12.

Array Designs and Results

Since the inclined wire had the most desirable properties of the obstacles tested, it was used in the design of the arrays to be described. Now, given a prescribed

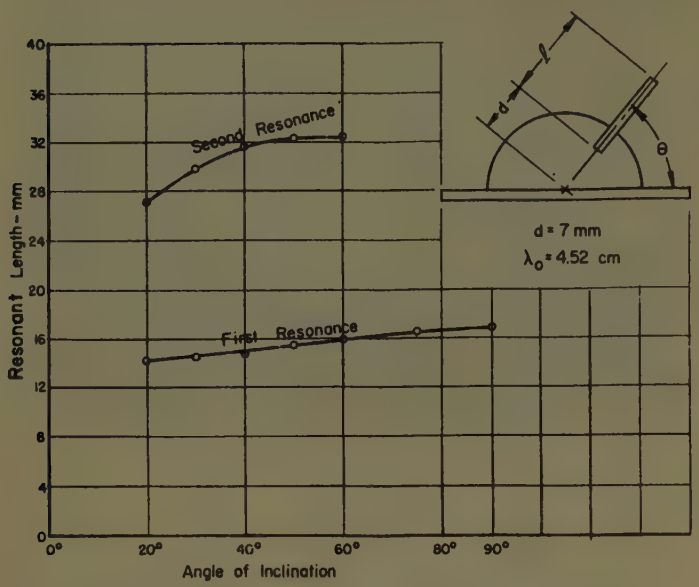

Fig. 12—Length of resonant wire as a function of the angle of inclination.

Fig. 13—An end view of the Dolph-Tchebycheff array.

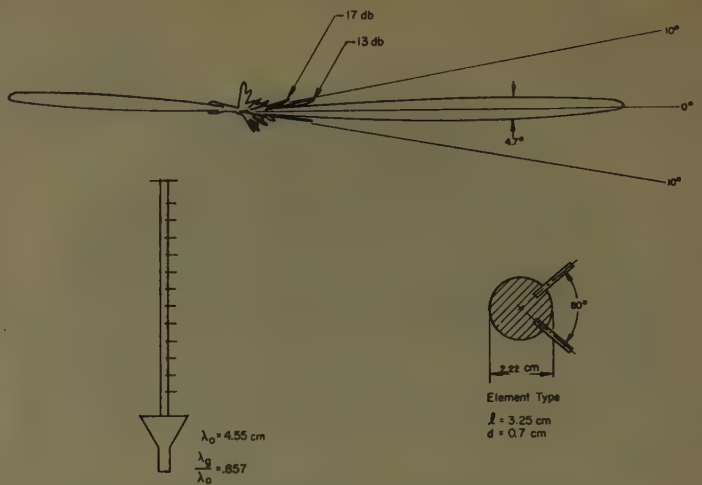

Fig. 14—Radiation pattern of a uniform broadside array with 12 elements at guide wavelength spacing.

pattern, the conventional linear array synthesis methods may be used to determine the array length, element spacings, and the equivalent shunt conductance of the antenna elements. Then, using Figs. 11 and 12, the angle θ and the wire length may be determined for each element. A 20-db Dolph-Tchebycheff broadside array is shown in the photograph of Fig. 13. Notice that for the complete rod the image wire has been added so that each element consists of two wires with an included angle of 2θ. The horn feed wire is oriented so that the electric field of the HE_{11} mode is normal to the plane bisecting the angle between the wires. For the Tchebycheff array a two-inch diameter short-circuit plate proved quite satisfactory.

The radiation patterns which are presented below represent a first attempt. That is, the array was designed from Figs. 13 and 14, constructed, and tested without any adjustments being made. Since conventional methods have been used, little will be said about the method of design for the various types of arrays.

First consider the pattern in Fig. 14 of the uniform array with 12 identical elements at guide wavelength spacing. The pattern was measured in the longitudinal plane which bisects the angle between the wires. The beam width and sidelobe levels are very close to the theoretical values. The small lobe pointing towards the top of the figure represents the stray radiation from the horn exciter. A similar pattern was obtained with a similar array for which the half angle between the wires was 60° instead of 40°. The transverse radiation patterns for the two arrays are shown in Fig. 15. It will be noticed that the patterns for the two cases are considerably different. Theoretically, the patterns should be symmetrical about a vertical line. The discrepancy is due to a misalignment of the feed horn and slight variations in the wire length and inclination. Aside from the asymmetry the transverse patterns are probably not suitable for practical applications. However, it is felt that further experimentation would lead to antenna elements with various types of useful transverse patterns.

The design data and radiation pattern for the 20-db Dolph-Tchebycheff broadside array for 12 elements with guide wavelength spacing are shown in Fig. 16. The element conductances were made proportional to the square of the calculated excitation coefficients of the array. Note the excellent agreement between the predicted and measured sidelobe level. The variation of the angle between the wires is readily apparent in the photograph of Fig. 13.

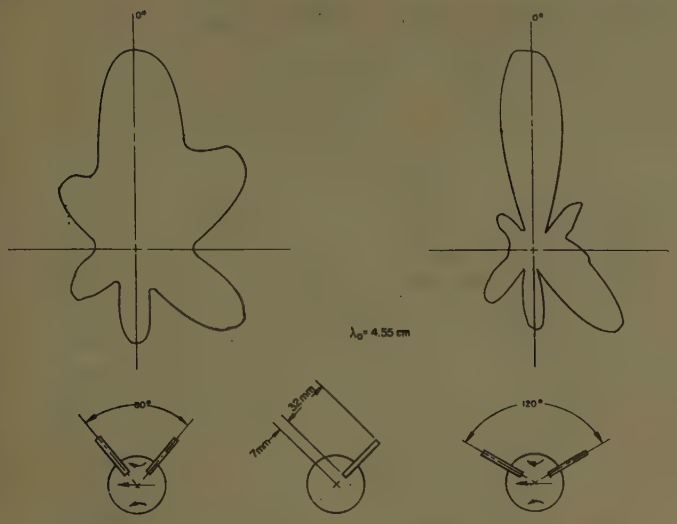

Fig. 15—Transverse radiation patterns for uniform arrays.

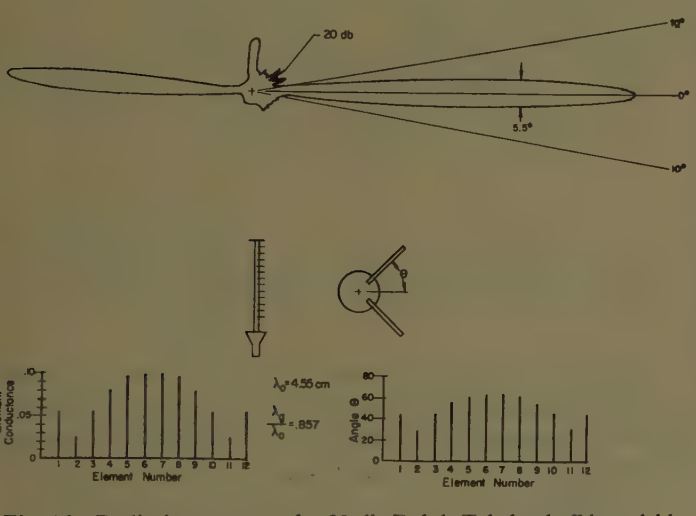

Fig. 16—Radiation pattern of a 20-db Dolph-Tchebycheff broadside array for 12 elements with guide wavelength spacing.

Similar data are presented in Fig. 17 for a nonresonant uniform array of 12 elements with an element spacing of 0.75 λ_g. Since the purpose of this work has been to illustrate the method of design rather than to develop a practical antenna, the array was designed so that 40 per cent of the input power to the array was absorbed in a matched resistance card termination on the dielectric rod. This simplifies the design calculations considerably for a short array since the vswr along the line may be considered to be unity for design purposes. Larger array efficiencies could be obtained by a more refined design procedure. The direction of the beam and the beam width are in excellent agreement with the theoretical values. However the first side lobe is only 10 db down instead of 13 db down and the stray radiation from the horn is at a higher level than before. This latter effect is due to the reduction of the antenna gain which results from the absorption of power in the matched load.

As a final example, a nonresonant array was designed to approximate a cosecant pattern. The design required

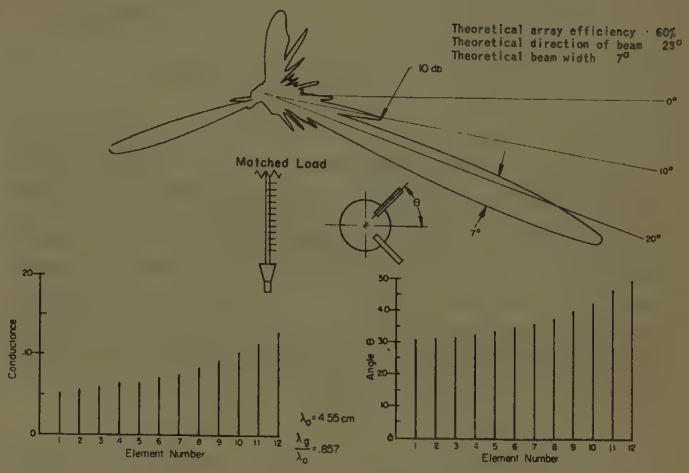

Fig. 17—Radiation pattern of a nonresonant uniform array with 12 elements with an element spacing of 0.75 λ_g.

a ten-to-one variation of element conductance and hence the angle θ for the elements was varied from 19° to 60°. The agreement between the predicted and experimental patterns was rather poor. Although an approximate synthesis method was used, the discrepancy was due mostly to the large variation of the angle θ. That is, it had been assumed in this design method that all the element patterns are identical. This is certainly not true for this case. In fact, it is rather surprising that the agreement for the two previous designs was so good since there was considerable variation of the angle between the wires for those cases.

Conclusion

The measurements have proven the feasibility of obtaining accurate control of the radiation from a dielectric rod waveguide in the longitudinal plane by means of placing obstacles along the waveguide. Since only a few types of obstacles have been investigated, it is likely that considerable control of the pattern in the transverse plane may be obtained by utilizing other types of obstacles such as dielectric pins, holes, or slots in the rod, and more suitable arrangements of intersecting wires. It should be possible to apply the same technique to other types of surface waveguides with equal success. The basic requirements needed for applying the design procedure are the following: an efficient surface wave exciter, the existence of only a single mode on the surface waveguide, an accurate means of determining the equivalent network for the coupling of the obstacle to the surface waveguide, and, of course, the discovery of obstacles for which the coupling may be varied over a wide range with only a moderate effect on the individual obstacle pattern. Conventional array design methods may then be used to obtain various types of patterns.

Acknowledgment

It is a pleasure to acknowledge the support of the Wright Air Development Center through Contract No. AF 33(616)-3220 for this work.

A Circularly-Polarized Corner Reflector Antenna*

OAKLEY M. WOODWARD, JR.†

Summary—**Unidirectional, circularly-polarized radiation may be obtained by tilting a dipole in a corner reflector. Inherent advantages of this antenna are the simplicity of both the construction and adjustment. The theory of images is employed to develop the basic theory of the antenna for the cases of greatest practical interest. An experimental investigation has been made on the radiation characteristics of a practical-sized antenna as a function of its geometric parameters. From this data, an antenna producing unidirectional, circularly-polarized radiation has been designed and constructed.**

Introduction

PAST EXPERIENCE has shown that more reliable transmission may be obtained in certain applications by the use of circular polarization. In general, antennas of this type may be classed as either omnidirectional or unidirectional. This paper is concerned only with the latter group.

One example of an unidirectional antenna having circularly polarized radiation is given by a single turnstile[1] layer supported parallel to a metal reflecting screen. Another type on which extensive work has been done is the helix.[2] The work described herein is concerned with the development of another type consisting of a corner reflector and a single dipole.

A simple theoretical analysis employing the theory of images may be used as a guide in the antenna design for this particular application. A mathematical analysis for the general case has been developed by Klopfenstein.[3]

Image Theory of Operation

Although the theory of images provides a simple method of analysis for the assumed idealized conditions, it is to be realized that the results obtained are not strictly applicable to antennas of finite dimensions. However, as will be demonstrated later, the method does serve as a useful guide in the antenna design.

The drawing of Fig. 1 illustrates the antenna geometry. The corner is formed by two vertical, sheet metal planes of height H and length L intersecting at an angle, β. The balanced dipole is symmetrically located within the corner angle at a distance, S, from the apex and tilted in the vertical plane at an angle, α, with respect to the corner bisector plane.

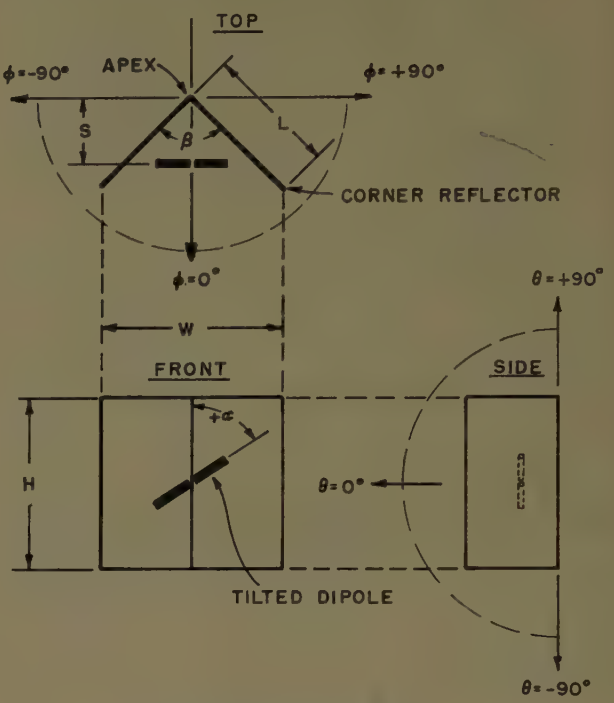

Fig. 1—Geometry of antenna.

A spherical-coordinate system, well-suited for experimental measurements, is employed for the distant field determination with the azimuth and elevation reference planes being designated as the ϕ plane and θ plane, respectively.

In order to analyze the antenna operation by the conventional theory of images, it must be assumed that the metal planes have perfect conductivity, are infinite in extent, and intersect at an angle equal to $180°/n$, where n is an integer. A further simplification in this application is obtained by resolving the current flowing in the tilted dipole into horizontal and vertical components as shown in Fig. 2(a).

For a chosen corner angle of 90° ($n=2$), the image representation of the separated components may be drawn as in Figs. 2(b) and 2(c). In the first case [Fig. 2(b)], the vertical component, a, produces three images, b, c, and d, of alternating polarity and equidistant from the apex. In the broadside direction ($\phi=\theta=0°$), the far-field, vertically-polarized radiation intensity may be found by combining the contributions from the four sources. This addition is illustrated in Fig. 2(d), where the reference or X axis is taken with respect to the apex of the corner reflector. It is seen that the total vertically polarized component is 180° out-of-phase with respect to the reference for all values of S.

Similarly, the horizontal component, a, of Fig. 2(c) produces three symmetrical images, b, c, and d, with

* Manuscript received by the PGAP, May 8, 1956; revised manuscript received, February 4, 1957. This paper was presented at the URSI-IRE Spring meeting, Washington, D. C.; May 2, 1956.

† RCA Laboratories, Princeton, N. J.

[1] G. H. Brown, "The turnstile antenna," *Electronics*, vol. 9, p. 15; April, 1936.

[2] J. D. Kraus, "Antennas," McGraw-Hill Book Co., Inc., New York, N. Y., ch. 7; 1950.

[3] R. W. Klopfenstein, "Corner reflector antenna with arbitrary dipole orientation and apex angle," paper presented at the URSI-IRE Spring meeting, Washington, D. C.: May 2, 1956. (*Note:* The geometric notation and terminology of these two reports are not identical due to the different methods of approach to the problem.)

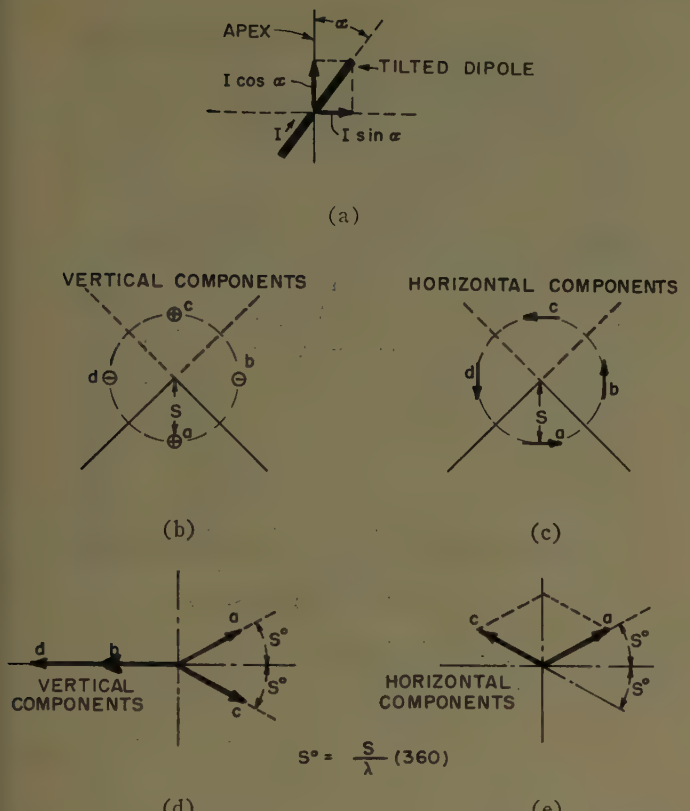

Fig. 2—(a) Resolving dipole current into horizontal and vertical components. (b), (c) Image representation of 90° corner reflector. (d), (e) Vector addition of the far-field components for $\theta=0°$ and $\phi=0°$.

currents flowing as in a continuous loop. In this case, the images, *b* and *d*, have a null in the broadside direction, so that the total horizontally-polarized radiation for $\phi=\theta=0°$ is found by summing the contributions from the out-of-phase components, *a* and *c*. This operation is performed in Fig. 2(e) using the same reference axis as before. Here it is seen that a quadrature relationship exists between the summation and the reference axis for all values of S.

On comparing the radiation in the broadside direction of the horizontal and vertical components, we have, for $\beta=90°$,

$$F_H/F_V = j\frac{2(I\sin\alpha)(\sin S^0)}{(I\cos\alpha)(2\cos S^0-2)} = j\tan\alpha\frac{\sin S^0}{\cos S^0-1}$$

$$= -j\frac{\tan\alpha}{\tan(S^0/2)} \qquad (1)$$

where $S^0=S/\lambda\ (360)$.

Therefore, for the case of a 90° corner reflector, the vertically-polarized and horizontally-polarized components are in quadrature in the broadside direction for all values of the dipole spacing, S. This fulfills two of the requirements for circular polarization, *i.e.*, that perpendicular components are in phase quadrature. The third requirement of equal magnitudes may be easily satisfied for all values of S (except for those cases where one or both of the magnitudes are zero) by adjusting the tilt angle, α, of the dipole to be equal to $S^0/2$.

Information is also supplied in (1) as to the rotation direction of the field intensity vector. Using the geometric notation of Fig. 1, the radiation is defined as a right-hand elliptically-polarized wave if F_H leads F_V, and is defined as a left-hand elliptically-polarized wave if F_H lags F_V.

The radiation properties of a corner reflector for other values of n may be determined using the theory of images in a similar manner. However, as n increases, the expressions become increasingly cumbersome. From an analysis of these results, it can be shown that circular polarization in the broadside direction may be obtained independent of S for any corner angle equal to a submultiple of 90°, such as 45°, 30°, 22½°, etc.

Theoretical Power Gain

The power gain of the 90° corner antenna in the broadside direction may be determined as a function of the vertical and horizontal component gains. Referring again to the vector diagrams of Figs. 2 (d) and 2 (e) the field gains of the vertical and horizontal arrays compared to an isolated reference dipole may be written, respectively, as follows:

$$F_V/F_O = 2(I\cos\alpha)(\cos S^0-1)/I_0 \qquad (2)$$

and

$$F_H/F_O = 2(I\sin\alpha)(\sin S^0)/I_0 \qquad (3)$$

where I_0 is the reference dipole current.

For a power gain measurement, the far fields are compared for equal input powers to the test antenna and the reference dipole. Hence, for the vertical component,

$$(I\cos\alpha)^2R_V = I_0^2R_0 \qquad (4)$$

and for the horizontal component,

$$(I\sin\alpha)^2R_H = I_0^2R_0 \qquad (5)$$

where R_V and R_H are radiation resistances of the vertical and horizontal components, respectively.

On eliminating the currents and squaring the field ratios, we obtain the power gains relative to a half-wave dipole for the two component arrays as

$$\text{P.G.}_V = 4R_0(\cos S^0-1)^2/R_V \qquad (6)$$

and

$$\text{P.G.}_H = 4R_0(\sin S^0)^2/R_H. \qquad (7)$$

The relations of (6) and (7) are plotted in Fig. 3 for dipole-to-axis spacings up to one wavelength. Available mutual impedance data were used to determine the radiation resistances of the components. Larger spacings were not considered in this particular application because of the greatly increased size requirements. The abscissa is calibrated in a logarithmic scale to better illustrate the relative bandwidths at various values of S. These curves are calculated assuming no losses in the

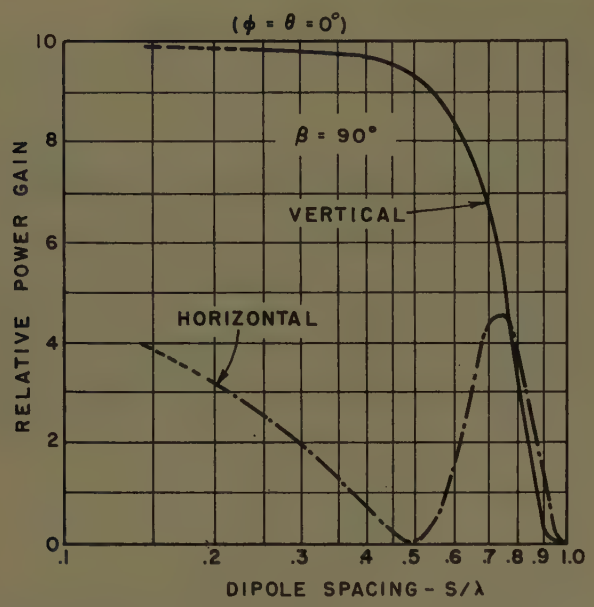

Fig. 3—Theoretical power gain of vertical and horizontal components compared to a half-wave dipole.

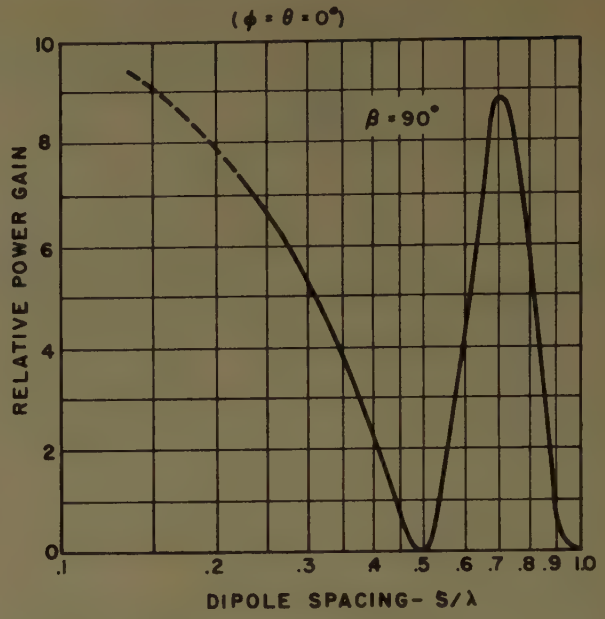

Fig. 4—Theoretical power gain of circularly polarized corner reflector compared to a circularly-polarized, isotropic source.

corner sides. In actual practice, these losses cause both of the gain curves to drop off rapidly as the dipole spacing is reduced to small values.

It is seen that a spacing in the region of 0.75λ has much less bandwidth than one in the vicinity of 0.25λ, where the reduced slopes of the curves indicate a more constant power gain with frequency change.

The next step is to determine the relative power gain of the actual array adjusted to produce circular polarization. Returning for the moment to the concept of two separate array components, the effective radiated power of each, as measured with a linearly-polarized dipole at a distant point in the broadside direction, is equal to the product of the relative power gain and the input power. In addition, these two measured powers must be equal for circular polarization.

Therefore,

$$(P_V)(\text{P.G.}_V) = (P_H)(\text{P.G.}_H) \tag{8}$$

where P_V and P_H are the input powers to the vertical and horizontal components, respectively.

If equal input powers are now applied to the circularly-polarized array and to a vertically-polarized reference dipole, the measured relative gain (P.G._{CP}) will be equal to the gain of the vertical component of the array reduced by the factor, $(P_V)/(P_V+P_H)$, or

$$\text{P.G.}_{CP} = (\text{P.G.}_V)\frac{P_V}{P_V + P_H}. \tag{9}$$

On combining (8) and (9), the power gain of the circularly-polarized corner reflector is obtained with respect to a linearly-polarized dipole in terms of the relative gains of the vertical and horizontal components of the array as

$$\text{P.G.}_{CP} = \frac{\text{P.G.}_V}{1 + \dfrac{\text{P.G.}_V}{\text{P.G.}_H}}. \tag{10}$$

This gain comparison, however, leads to a rather pessimistic impression of the gain value since one half of the input power to the corner array is wasted in the test with a linearly polarized reference dipole. Logically, a circularly-polarized antenna should be compared to a circularly-polarized standard antenna. Hence, a simple relation between the two references may be shown as follows.

A half-wave dipole has a relative gain of 1.096 with respect to an infinitesimal dipole, and the latter has a gain of 1.5 relative to a linearly-polarized, isotropic source. Therefore, the right-hand term of (10) must be multiplied by the constant 3.29 ($=1.096\times1.5\times2$) to obtain the corner array gain compared to a circularly-polarized, isotropic source.

The gain data of Fig. 3 is used with (10) and this constant to calculate the gain curve of Fig. 4. In this case, the tilt angle of the dipole is adjusted for each value of the dipole spacing to produce circularly-polarized radiation.

Theoretical Field Patterns of the 90° Corner Reflector

The theoretical relative field patterns may be easily obtained from the image representation of Fig. 2(b) and 2(c) in terms of paired couplets.

For the vertical components, the relative azimuth and elevation patterns are given, respectively, by

$$F_V \underset{(\theta=0^0)}{=} C_1 \cos\alpha[\cos(S^0\cos\phi) - \cos(S^0\sin\phi)] \tag{11}$$

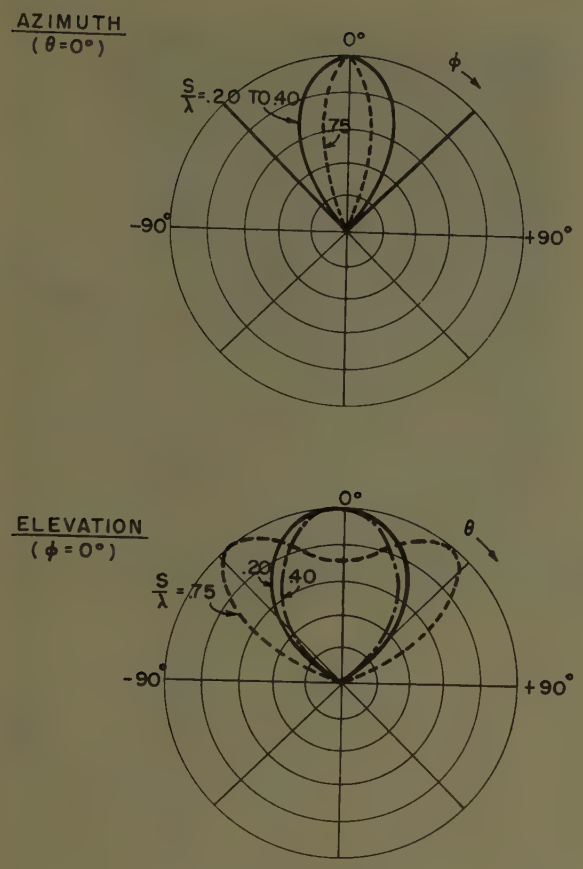

Fig. 5—Theoretical relative field patterns of vertical components for $\beta=90$.

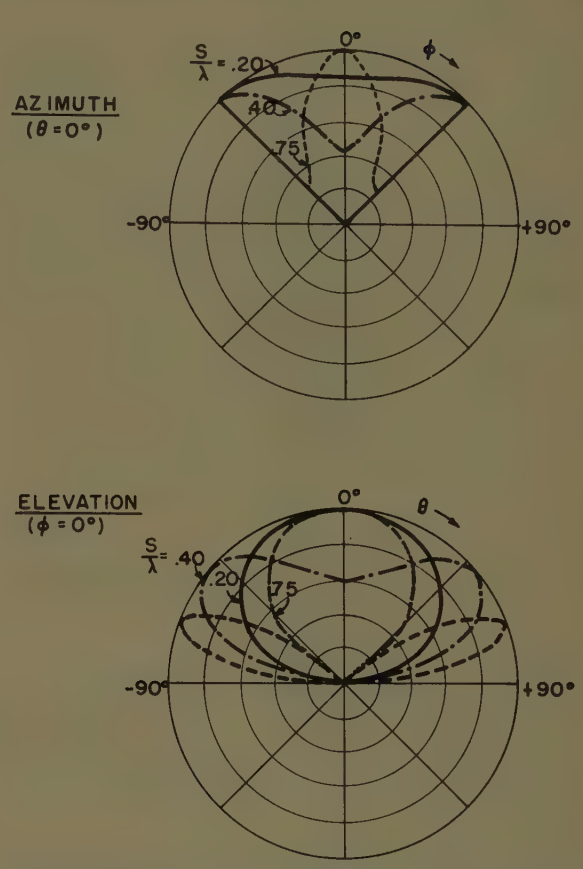

Fig. 6—Theoretical relative field patterns of horizontal components for $\beta=90$.

and

$$F_V = C_2 \cos\alpha[\cos(S^0 \cos\theta) - 1]\cos\theta. \quad (12)$$
$$(\phi=0^\circ)$$

Similarly, for the horizontal components,

$$F_H = C_3 \sin\alpha[\cos\phi \cdot \sin(S^0 \cos\phi) + \sin\phi \cdot \sin(S^0 \sin\phi)] \quad (13)$$
$$(\theta=0^\circ)$$

and

$$F_H = C_4 \sin\alpha \sin(S^0 \cos\theta)] \quad (14)$$
$$(\phi=0^\circ)$$

where the constants, C, are normalizing factors.

In order to simplify these expressions, a short dipole having a cosine form factor is assumed.

Theoretical patterns for several values of dipole spacing are plotted in Figs. 5 and 6 as calculated from these equations. Only the quadrant of particular interest enclosed by the corner reflector has been shown for the azimuth data, and only the forward half of the patterns for the elevation data.

It is noted that undesired high side lobes are produced for the 0.75λ dipole spacing in the elevation pattern of Fig. 6. It is also seen in Fig. 6 that the 0.20λ spacing produces a more unidirectional pattern than the 0.40λ spacing.

Polarization Measurements

The polar characteristics may be measured in the broadside direction of the transmitting corner reflector by rotating a distant receiving dipole in the plane normal to the line joining the antennas. For the general case of elliptically-polarized radiation, two parameters are obtained at the receiving site: the axial ratio equal to the ratio of the minimum and maximum magnitudes of the dipole terminal voltage, and the orientation of the dipole with respect to the corner vertex for maximum or minimum received signals.

Although the measured polarization data may be presented in several different ways, a system described by Rumsey[4] is especially well suited for plotting the two measurements as a single point on a graph. This method employs the Smith-Carter impedance chart with altered coordinates for representation of elliptical polarization. The standing wave ratio is equivalent to the axial ratio (R), and the distance toward the generator (in electrical degrees) is equivalent to the orientation (ψ_M) of the maximum received signal. Thus, it is seen that a linearly-polarized wave is represented by a point on the great circle and a circularly-polarized wave by the center of the diagram.

[4] V. H. Rumsey, "Part I—transmission between elliptically polarized antennas," Proc. IRE, vol. 39, pp. 535–540; May, 1951.

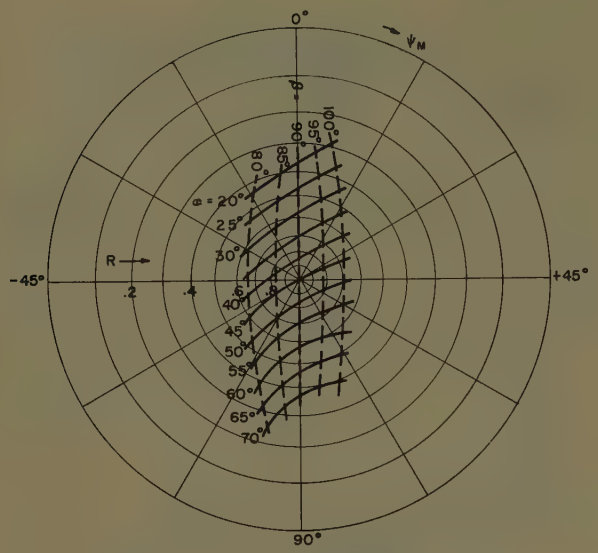

Fig. 7—Polarization chart theoretical curves for $S/\lambda = 0.25$.

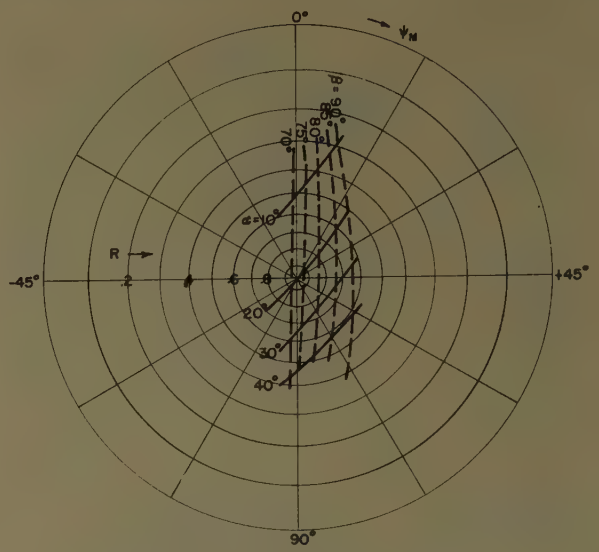

Fig. 8—Polarization chart measured curves for $L = 9$ inches, $H = 15$ inches, $f = 800$ mc, $S/\lambda = 0.25$.

Since the image theory applies only for certain corner angles, additional information on the radiation characteristics as a function of the corner angle was obtained from Klopfenstein's analysis and plotted on the polarization chart of Fig. 7 to serve as a guide in the experimental measurements. Two families of curves are given showing the elliptical polarization produced by various dipole tilt angles and corner reflector angles for a fixed dipole spacing.

Experimental Measurements

Having found the various corner angles for which circular polarization may be obtained, independent of S, the next problem is the choice of angle for a practical antenna design. Corner angles of 30° or less were not considered because of the extreme criticalness of the phase adjustment with change in the corner angle. Since the dipole spacing is the only frequency-dependent parameter of the system, it is desirable to keep it as small as possible for greater bandwidth as well as decreasing the physical size of the array. However, a practical limit is approached as the dipole becomes closer to the sides of the corner because of the decreased radiation resistance of the dipole and the increased ohmic losses in the sides. On considering these various limitations, the 90° corner angle was chosen rather than the 45° value as a good compromise design.

Starting with a 90° corner reflector constructed with fairly large sides, polarization measurements were taken in the broadside direction as the dimensions of the sides were reduced in steps. A test frequency of 800 mc was arbitrarily chosen to provide an antenna of convenient and easily handled dimensions.

The corner antenna was mounted on a turntable with the beam directed up toward a linearly polarized receiving antenna supported above the turntable by means of a horizontal boom.

For each reduction in the corner side dimensions, data were taken for various values of corner angle, dipole tilt angle, and dipole spacing. In general, a reduction in the corner sides gave a shift of the β-family curves to the right, and of the α-family curves downward. The adjustment for circular polarization became increasingly critical and the spillover became excessive for very small sides.

A practical compromise was chosen based on the measured data of Fig. 8. The photograph of Fig. 9 shows the final antenna as constructed of sheet aluminum. Solid or mesh sides are necessary in this application since the sides must perform as a reflector for both horizontal and vertical polarizations. Mechanical dimensions to produce circular polarization at 800 mc are given in Fig. 10. The apex was altered as indicated to facilitate the dipole support mounting.

Azimuth and elevation field patterns were measured on this antenna for both polarizations and the results plotted in Figs. 11 and 12. These patterns were taken by rotating the antenna in an arc while mounted on the test turntable. Hence, the backward radiation could not be obtained accurately because of ground reflections.

For vertical polarization, the measured patterns of Fig. 11 check reasonably close with the theoretical patterns of Fig. 5 having distinct nulls in the plane of the sides. Since the theoretical azimuth pattern for the horizontal components (Fig. 6) is almost omnidirectional, no relationship could be deduced as to the shape of the experimentally determined pattern obtained from a finite screen reflector.

Of interest also is the departure from circular polarization as the antenna orientation is changed. Ellipticity measurements were made at 800 mc as the antenna was rotated in the azimuth and elevation planes. Axial ratio contours are given in the projection plot of Fig. 13 (p. 296) in terms of the angular departure from the broad-

Fig. 9.

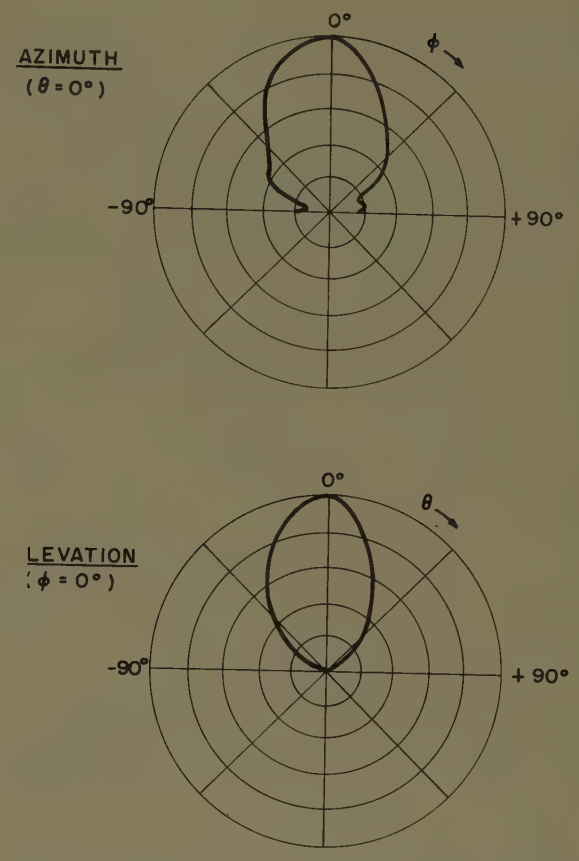

Fig. 11—Measured relative field patterns of vertical components. $f = 800$ mc.

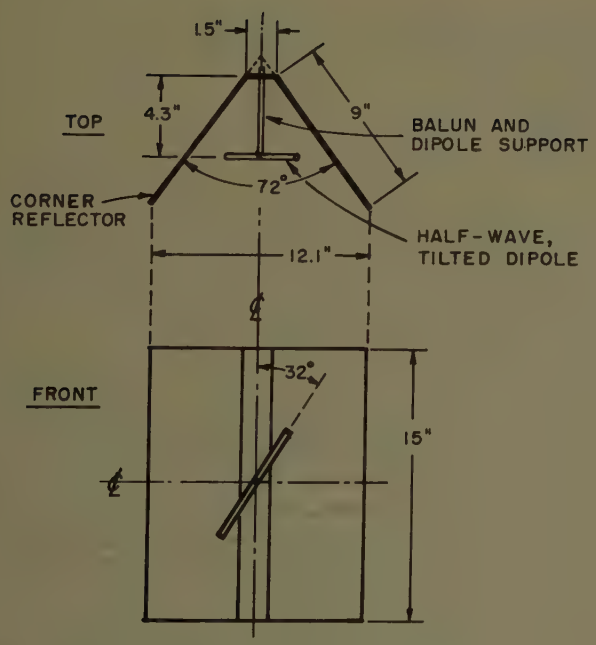

Fig. 10—Circularly polarized corner reflector.

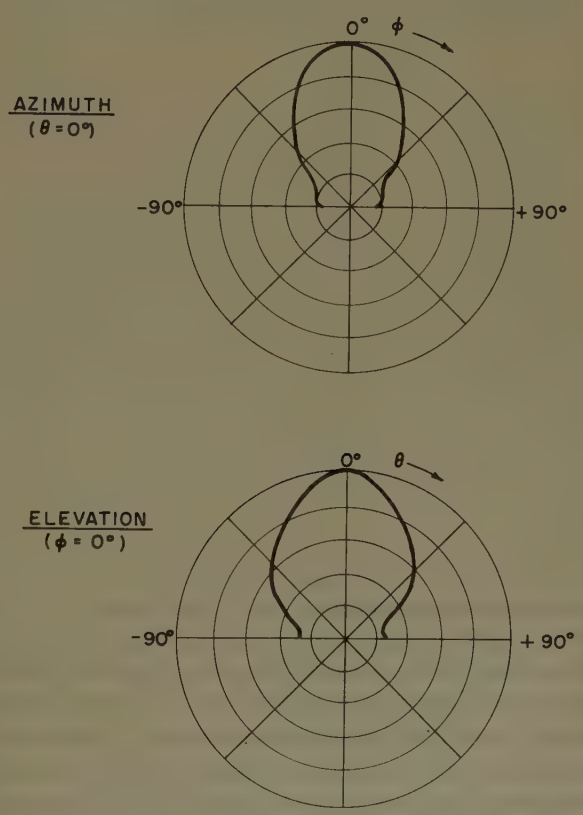

Fig. 12—Measured relative field patterns of horizontal component. $f = 800$ mc.

side direction. It is noted that the circularity remains more constant in the azimuth plane.

The previous tests were conducted at the midband frequency of 800 mc. The upper curve of Fig. 14 shows the change in the axial ratio in the broadside direction

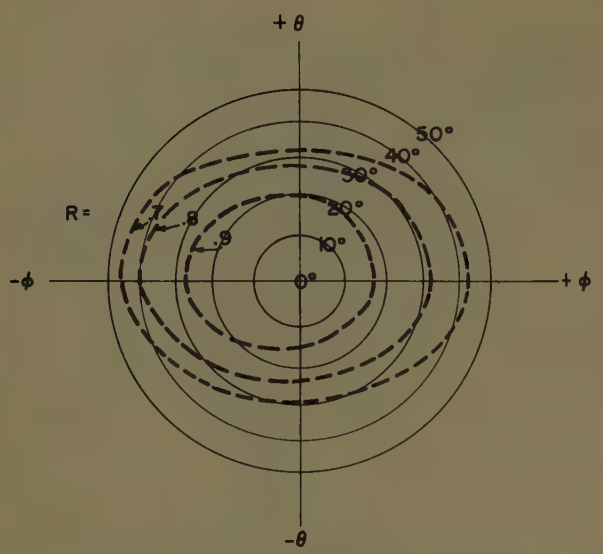

Fig. 13—Measured variation of axial ratio. $f=800$ mc.

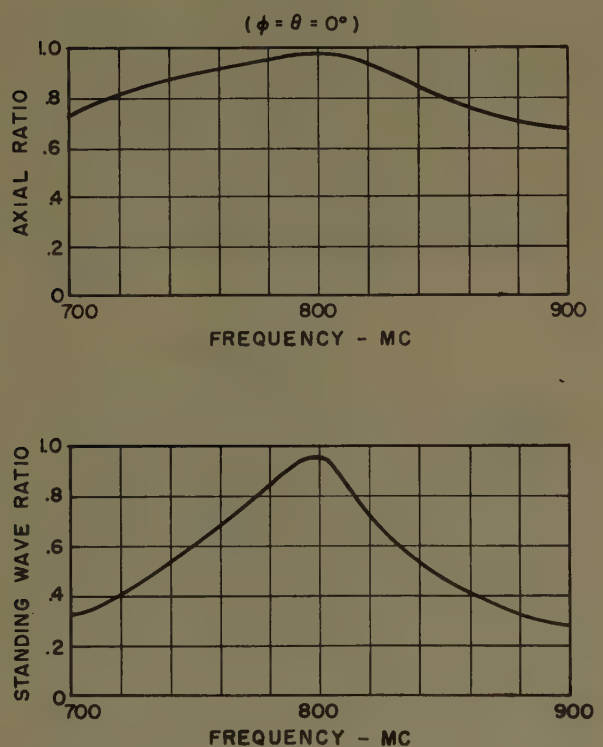

Fig. 14—Measured values of axial ratio and standing wave ratio vs frequency.

as the frequency is changed. It is seen that the circularity bandwidth is quite broad.

The standing wave ratio as measured on the 52-ohm coaxial input line to the antenna is plotted in the lower curve of Fig. 14. The rather narrow bandwidth obtained may be partially attributed to the narrow-band balun used in the dipole design. Since the emphasis of this work was in the antenna radiation field, no particular effort was exercised in improving the impedance characteristics. However, it is believed that considerable bandwidth improvement could be obtained by suitable design of the dipole shape and the balun.

Gain measurements were made two different ways. In the first method, the distant field strength of the corner array was compared with that from a linearly-polarized, standard antenna of known relative gain. This standard consisted of a dipole mounted one-quarter wave in front of a flat screen reflector. The measured gain compared to a free-space, half-wave dipole in this test was 2.6. On multiplying by the constant 3.29, a gain figure of 8.55 is obtained with respect to a circularly polarized, isotropic source.

In the second experiment, two identical, 90° corner antennas were adjusted for circular polarization and tested by the absolute gain method. The results of this test showed the power gain of the array to be 7.56 compared to a circularly-polarized, isotropic source.

The dipole spacing of 4.3 inches (Fig. 10) is equivalent to 0.29 wavelength at 800 mc. Referring to the curve of Fig. 4, the theoretical gain for this spacing is 5.7. The discrepancy between the two measured values may be partially attributed to experimental errors. However, a comparison of the measured and calculated field patterns indicate that the gain of a corner array of finite dimensions might be somewhat different from that of the ideal case having infinite sides.

Simplified Field Adjustment of Corner Antenna

In the previously described experiments, circular polarization was obtained from the corner array by adjusting the geometric parameters to produce a constant received voltage at a dipole for all orientations in the ψ plane. For each change in the antenna, this involved the steps of finding the maximum and minimum fields by rotating the dipole, and then taking the ratio of the two readings. In the course of the work, a simpler method was developed which is especially well adapted for field adjustment of the antennas for a circularly-polarized transmission link.

Fig. 15 illustrates the setup employing transmitting and receiving corner antennas oriented for maximum transmission and having their apex lines parallel. All mechanical dimensions and geometric parameters are identical for the two arrays with the exception that the dipoles are tilted in the opposite directions. Thus, since the receiving antenna has been reversed in direction to face toward the transmitting antenna, the dipoles will remain parallel for all tilt angles.

The test procedure simply involves rotating the dipoles together until a null is reached at the receiver and if necessary, to alter one of the other parameters to achieve this null. The only requirement is that the same adjustment be made on both antennas.

An explanation may be furnished by separating an elliptically-polarized, transmitted wave into circularly-polarized and linearly-polarized components. The rotation direction of the circularly-polarized component is

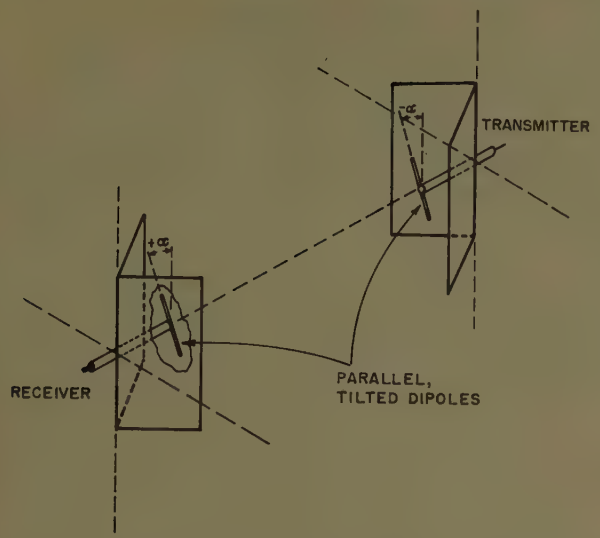

Fig. 15—Field adjustment of corner reflectors to produce circular polarization.

reversed by changing the dipole tilt angle from $+\alpha$ to $-\alpha$. Hence, the receiving antenna is blind to the transmitted, circularly-polarized component, and only the linearly-polarized component is received. The symmetry of the arrangement insures that the linearly-polarized components of both antennas lie in the same plane for maximum transmission independent of the magnitude of α.

A null at the receiver therefore indicates that both antennas are adjusted for circular polarization but of opposite sense of rotation. For use in a transmission link, then, it is only necessary to reverse the direction of the tilt angle of one of the antennas to obtain maximum transmission.

Conclusion

The theory of images has been used to develop the basic theory of the antenna for the cases of greatest practical interest. From this data, the parameters of a circularly-polarized radiator were designed. Numerous experiments were conducted to determine the modifications and dimensions of a practical antenna satisfying the electrical requirements.

Inherent advantages of this type of antenna are the simplicity of both the construction and the adjustment.

Acknowledgment

The author wishes to acknowledge the assistance of R. K. Long who gathered most of the experimental data for this project.

Corner Reflector Antennas with Arbitrary Dipole Orientation and Apex Angle*

RALPH W. KLOPFENSTEIN†

Summary—**This paper is concerned with the determination of corner reflector characteristics for reflectors of arbitrary apex angle excited by any infinitesimal dipole source which is tangent to a circular cylinder having the reflector axis as its axis. Use is made of the dyadic Green's functions for the perfectly conducting wedge recently given by Tai, and the results are obtained as infinite series of Bessel functions.**

The quantities of interest are the relative phase and magnitude of vertical and horizontal components of electric field, the directive gain of the antenna, and the radiation resistance of the dipole source. These have been computed for a continuous range of apex angles from 30° to 180° for dipole-to-axis spacings up to about a wavelength.

The results of this general analysis are useful not only for the determination of reflector characteristics for apex angles not subject to image analysis, but also for the obtaining of certain limiting forms for small apex angles which are not readily apparent from the image analyses.

Introduction

THE CORNER reflector antenna excited by a half-wave dipole forms a compact, high-gain antenna of moderate bandwidth. The mathematical model from which the performance characteristics of such antennas are calculated consists of two semi-infinite conducting planes intersecting in a line at an angle from zero to 360°. The excitation of the wedge is normally accomplished by placement of a half-wave dipole antenna within the wedge. In practice, of course, the semi-infinite planes of the mathematical model are truncated to some finite extent, and, ordinarily, they are made as small as possible. The value of the mathematical model lies in the experimentally observed fact that it predicts the performance of the practical antenna so long as the reflecting sheets are only moderately large relative to the exciting dipole and its spacing from the apex of the reflector.

The initial work in regard to the corner reflector antenna consisted of an analysis of the fields for on-center excitation by a dipole source oriented parallel to the axis for corner reflectors whose central angles were submultiples of 180°.[1] For these cases, the analysis can be car-

* Manuscript received by the PGAP, May 8, 1956.
† RCA Laboratories, Princeton, N. J.

[1] J. D. Kraus, "The corner-reflector antenna," Proc. IRE, vol. 28, pp. 513–519; November, 1940.

ried out through the theory of images. These results have recently been put into a general form applicable to all such apex angles.[2] It is perhaps less generally known that a similar image analysis can be carried out for horizontal orientation of the dipole, *i.e.*, orientation such that the dipole lies in a plane perpendicular to the corner reflector axis and is perpendicular to a line in this plane connecting the dipole location with the reflector axis.[3] This dipole orientation has received relatively little attention to date probably because of its apparently lower gain potentiality. It has recently been pointed out, however, that for certain dipole orientations the corner reflector antenna serves as a circularly polarized radiator.[4] This has led to renewed interest in corner reflector characteristics for arbitrary dipole orientations and arbitrary apex angles.

Analyses have previously been given for the corner reflector of arbitrary apex angle excited by a line source,[3] and, more recently, for the corner reflector of arbitrary apex angle excited by an infinitesimal vertical dipole source.[5] This paper is concerned with the determination of corner reflector characteristics for reflectors of arbitrary apex angle excited by any infinitesimal dipole source which is tangent to a circular cylinder having the reflector axis as its axis as shown in Fig. 1. Field expressions have been obtained as well as expressions for the power gain and radiation resistance of such antennas. The values of these quantities have been computed for a suitable range of antenna dimensions, and the results of these computations are given in graphical form. The analysis has been restricted to excitation by an infinitesimal dipole because of the essential similarity of these results to those for any dipole length (at least through a half-wavelength) and because of the simplification thus obtained. The question of the current distribution on the radiating element has thus been avoided.

The analysis for arbitrary apex angle is valuable because of its generality. Especially useful are certain limiting forms of the results which can be readily observed in the results given here. In addition, the results of image analyses besides being restricted to apex angles which are submultiples of 180° have the property of becoming more and more involved as the apex angle decreases. The results obtained here, on the other hand, become increasingly simplified as the apex angle decreases. For small apex angles one would probably choose to use the results of the more general analysis because of its relative computational simplicity even through the apex angle was such that an image analysis could be used.

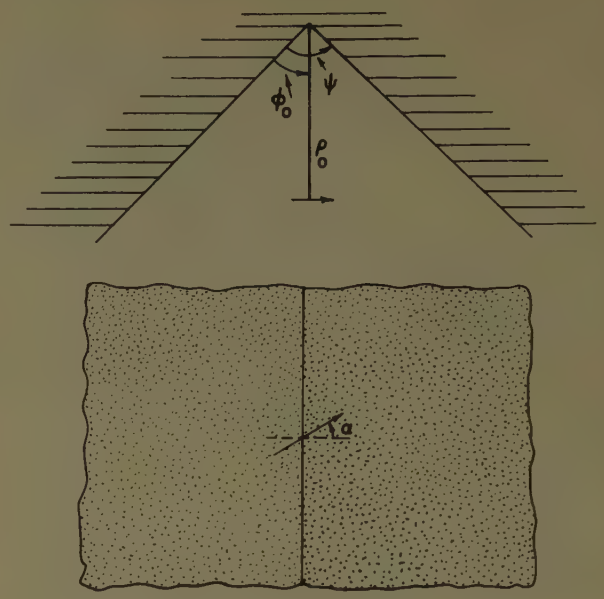

Fig. 1—Corner reflector antenna with infinitesimal dipole excitation.

Field Components for Arbitrarily Oriented Dipole Excitation

The corner reflector geometry under consideration is shown in Fig. 1. With reference to this figure the fields are to be found for arbitrarily specified ρ_0, ϕ_0, ψ, and α. Due to the principle of superposition, the consideration of arbitrary α can be immediately reduced to the consideration of only two values of α. In particular, it suffices to determine the fields for vertical and horizontal orientation of the dipole, *i.e.*, for $\alpha=\pi/2$ and $\alpha=0$. The field, $\overline{E}_\alpha$, for any value of α can be obtained from $\overline{E}_v(\alpha=\pi/2)$ and $\overline{E}_h(\alpha=0)$, *viz.*,

$$\overline{E}_\alpha = \overline{E}_h \cos(\alpha) + \overline{E}_v \sin(\alpha). \quad (1)$$

The use of dyadic Green's functions permit the determination of electromagnetic fields due to current distributions and apertures in the presence of diffracting bodies.[6] The dyadic Green's functions for a number of diffracting bodies including the infinite perfectly conducting wedge have recently been given by Tai.[7] In terms of the dyadic Green's function, $G_e(P, P')$, the electric field, $\overline{E}(P)$, due to a current distribution, $J(P')$ in the presence of a diffracting body is given by

[2] J. J. Epis, "Corner Reflector Standard Gain Antennas for 800 to 1600 Megacycles," Div. of Elec. Eng., University of California, Berkeley, Calif.; Inst. of Eng. Res., Ser. 60, Issue No. 118; July 15, 1954.

[3] E. B. Moullin, "Radio Aerials," Oxford University Press, London, Eng., pp. 125–170, 181–183; 1949.

[4] O. M. Woodward, Jr., "A circularly polarized corner reflector antenna," this issue, pp. 290–297.

[5] J. R. Wait, "On the theory of an antenna with an infinite corner reflector," *Can. J. Phys.*, vol. 32, pp. 365–371; June, 1954.

[6] C. T. Tai, "Radiation from Current Elements and Apertures in the Presence of a Perfectly Conducting Half Plane Sheet," Tech. Rep. No. 45, Stanford Res. Inst., Stanford, Calif.; June, 1954.

[7] C. T. Tai, "A Glossary of Dyadic Green's Functions," Tech. Rep. No. 46, Stanford Res. Inst., Stanford, Calif.; July, 1954.

$$\overline{E}(P) = i\omega\mu \iiint \overline{J}(P') \cdot \mathbf{G}_e(P, P')dv, \qquad (2)$$

where the volume integral is taken over the volume in which the current is distributed. In the case of an electric dipole source of strength $\overline{A}$ then, the electric field is

$$\overline{E}(P) = i\omega\mu \overline{A}(P') \cdot \mathbf{G}_e(P, P'). \qquad (3)$$

The corner reflector is described in terms of a cylindrical coordinate system (ρ, ϕ, z) as indicated in Fig. 2. For the case of a horizontally oriented dipole source at $(\rho_0, \phi_0, 0)$, $\overline{A} = \hat{\phi}A$ so that

$$\overline{E}(P) = i\omega\mu A\hat{\phi} \cdot \mathbf{G}_e(P, P'). \qquad (4)$$

The procedure involved in the actual substitution of the dyadic Green's function into (4) is lengthy but straightforward so that it will not be reproduced in detail here. The terms of the resulting field components of order $1/R$ $(R = \sqrt{\rho^2+z^2})$ are given by

$$E_\rho = -\frac{\pi\mu\omega}{2k^2\rho_0\psi^2} \sum_{n=0}^{\infty} \epsilon_n n \cos(n\pi\phi_0/\psi) \sin(n\pi\phi/\psi)$$

$$\cdot \int_{-\infty}^{\infty} J_{n\pi/\psi}(\lambda\rho_0) H_{n\pi/\psi}^{(1)'}(\lambda\rho) \frac{h^2}{\lambda} e^{ihz} dh,$$

$$E_\phi = -\frac{\mu\omega}{2\psi} \sum_{n=0}^{\infty} \epsilon_n \cos(n\pi\phi_0/\psi) \cos(n\pi\phi/\psi)$$

$$\cdot \int_{-\infty}^{\infty} J_{n\pi/\psi}'(\lambda\rho_0) H_{n\pi/\psi}^{(1)'}(\lambda\rho) e^{ihz} dh,$$

and

$$E_z = \frac{i\pi\mu\omega}{2k^2\rho_0\psi^2} \sum_{n=0}^{\infty} \epsilon_n n \cos(n\pi\phi_0/\psi) \sin(n\pi\phi/\psi)$$

$$\cdot \int_{-\infty}^{\infty} J_{n\pi/\psi}(\lambda\rho_0) H_{n\pi/\psi}^{(1)}(\lambda\rho) e^{ihz} dh, \qquad (5)$$

where $\epsilon_n = \frac{1}{2}$ for $n = 0$, and $\epsilon_n = 1$ for all other n. The primed Bessel functions denote differentiation with respect to their arguments, and λ is defined by $\lambda = \sqrt{k^2 - h^2}$.

The integrals in (5) may be evaluated for large values of ρ by the method of saddle points, and when this is done it is found that

$$E_\rho = \frac{\mu\omega}{\psi} \frac{e^{ikR}}{R} \cos^2(\theta) G_2,$$

$$E_\phi = \frac{\mu\omega}{\psi} \frac{e^{ikR}}{R} G_1,$$

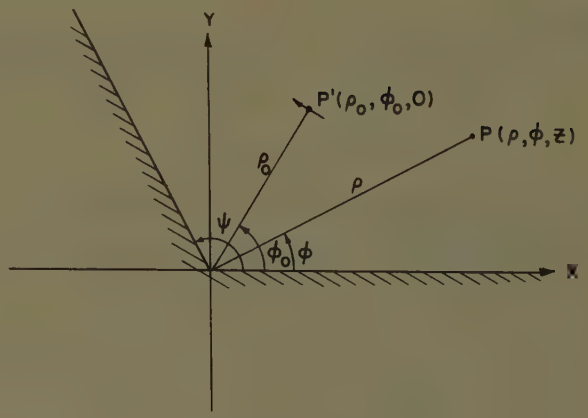

Fig. 2—Cylindrical coordinate system associated with corner reflector antenna.

and

$$E_z = -\frac{\mu\omega}{\psi} \frac{e^{ikR}}{R} \sin(\theta) \cos(\theta) G_2,$$

where

$$G_1 = \sum_{n=0}^{\infty} \epsilon_n \exp\left[\left(-i\frac{n\pi}{\psi}\right)\frac{\pi}{2}\right],$$

$$\cos(n\pi\phi_0/\psi) \cos(n\pi\phi/\psi) J_{n\pi/\psi}'(k\rho_0 \sin\theta),$$

and

$$G_2 = \sum_{n=1}^{\infty} \left[\frac{n\pi}{\psi k\rho_0 \sin\theta}\right] \exp\left[\left(-i\frac{n\pi}{\psi}\right)\frac{\pi}{2}\right]$$

$$\cos(n\pi\phi_0/\psi) \sin(n\pi\phi/\psi) J_{n\pi/\psi}(k\rho_0 \sin\theta). \qquad (6)$$

In (6) R and θ are the spherical coordinates of a point P in the far field. The field components themselves are more compactly written in terms of spherical coordinates in the far field. Thus,

$$E_\phi = \frac{\mu\omega}{\psi} \frac{e^{ikR}}{R} G_1,$$

and

$$E_\theta = \frac{\mu\omega}{\psi} \frac{e^{ikR}}{R} \cos\theta(G_2). \qquad (7)$$

Eq. (7) gives the results which were the object of this analysis. It gives the far field components due to a horizontal infinitesimal dipole arbitrarily located within a corner reflector of arbitrary apex angle.

An exactly similar process can be carried out for excitation by a vertical infinitesimal dipole source by setting $\overline{A} = \hat{k}A$. When this is done it is found that the far field is given by

$$E_\theta = +\frac{i\mu\omega}{\psi} \frac{e^{ikR}}{R} \sin(\theta) G,$$

where

$$G = \sum_{n=1}^{\infty} \exp\left[\left(-i\frac{n\pi}{\psi}\right)\frac{\pi}{2}\right] \sin(n\pi\phi_0/\psi) \qquad (8)$$
$$\sin(n\pi\phi/\psi) J_{n\pi/\psi}(k\rho_0 \sin\theta).$$

This checks the results obtained by a somewhat different method by Wait.[5]

The infinite series G, G_1, and G_2, involve Bessel functions of fractional order in the general case. Until recently these functions have been only sketchily tabulated, but new tables,[8-10] have greatly increased the usefulness of expressions such as those obtained for the corner reflector fields. In the case that the apex angle of the reflector is a submultiple of 180°, the series above involve Bessel functions of integral order only. Comparison of these results with those of image analysis then furnish a family of identities involving infinite series of Bessel functions. Some of these identities are well known while others, particularly those corresponding to the smaller apex angles, are not generally recognized.

The forward fields due to horizontal and vertical elements centrally located in a corner reflector ($\phi_0 = \psi/2$) have been computed from (6) and (8) for spacings of the dipole elements from the apex up to about one wavelength. Of particular interest in this connection is the ratio (in magnitude and phase) of the horizontal and vertical fields in the forward direction. When these fields are in phase quadrature, circularly polarized radiation in the forward direction can be obtained by suitable adjustment of the tilt angle α. In fact, the required tilt angle is simply the inverse cotangent of the ratio of the magnitudes of the fields. Curves showing the magnitude and phase of the field ratio are given respectively in Figs. 3 and 4. The dotted lines in Fig. 4 show the points at which circularly polarized radiation may be obtained.

The convergence of the series of (6) and (8) is fairly rapid. Three-decimal accuracy is given by the leading term only for $k\rho_0 \leqq 2(\pi/\psi - 1.25)$ in the case of vertical dipole excitation, and for $k\rho_0 \leqq 1.5\ (\pi/\psi - 2.5)$ in the case of horizontal dipole excitation. The above inequalities apply in the case that $k\rho_0$ is between 1 and 6 which is the range in which computational experience was gained here.

Directive Gain for Horizontal and Vertical Dipole Excitation

The directive gain can be found in the usual way by comparing the radiation intensity in the preferred direction to the total radiated power. Thus,

$$D(\theta_1, \phi_1) = \frac{4\pi I(\theta_1, \phi_1)}{\int_0^{\psi}\int_0^{\pi} I(\theta, \phi) \sin\theta d\theta d\phi} \qquad (9)$$

where D is the directive power gain in the direction (θ_1, ϕ_1), and I is the radiation intensity in any direction (θ, ϕ).

For the vertical infinitesimal dipole excitation this relationship can be written as

$$D_v(\theta_1, \phi_1) = \frac{4\pi \sin^2(\theta_1) \left| G(\theta_1, \phi_1) \right|^2}{\int_0^{\psi}\int_0^{\pi} \left| G(\theta, \phi) \right|^2 \sin^3(\theta) d\theta d\phi}. \qquad (10)$$

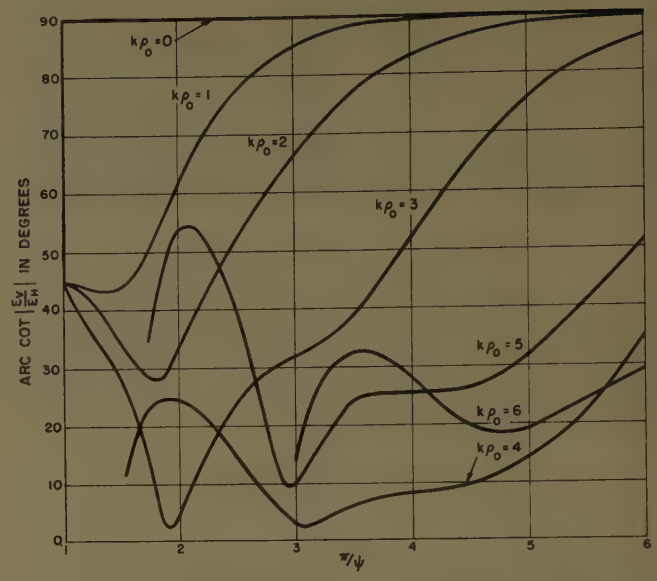

Fig. 3—Ratio of magnitudes of E_v and E_h in forward direction as a function of corner angle for various dipole-to-apex spacings. ($\phi_0 = \psi/2$).

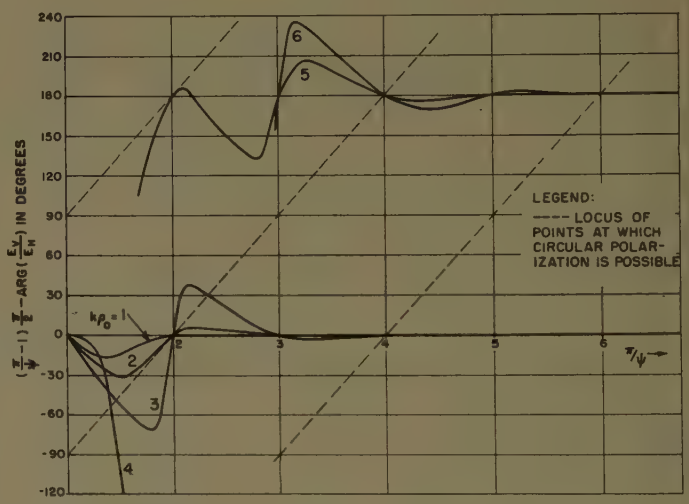

Fig. 4—Phase difference between E_v and E_h in forward direction as a function of corner angle for various dipole-to-apex spacings. ($\phi_0 = \psi/2$).

[8] E. Cambi, "Eleven and Fifteen-Place Tables of Bessel Functions of the First Kind to All Significant Orders," Dover Publications, New York, N. Y.; 1948.

[9] Mathematical Tables Project, "Tables of Spherical Bessel Functions," Columbia University Press, New York, N. Y., 2 vols.; 1947.

[10] National Bureau of Standards, "Tables of Bessel Functions of Fractional Order," Columbia University Press, New York, N. Y., vol. 1; 1948.

In the denominator the integration with respect to ϕ can be carried out explicitly, and considerable simplification results due to the orthogonality of the trigonometric functions involved in $G(\theta, \phi)$ on the interval $[0, \psi]$. Upon integration it is found that

$$D_v(\theta_1, \phi_1) = \frac{4\pi \sin^2(\theta_1) \left| G(\theta_1, \phi_1) \right|^2}{\psi \sum_{n=1}^{\infty} \sin^2(n\pi\phi_0/\psi) \int_0^{\pi/2} J_{n\pi/\psi}{}^2(k\rho_0 \sin\theta) \sin^3(\theta) d\theta} \tag{11}$$

where for a central location of the dipole ($\phi_0 = \psi/2$) alternate terms of the series vanish thus increasing the rate of convergence.

For small spacing of the dipole from the apex of the corner reflector ($k\rho_0 \ll 1$), (11) can be evaluated by considering the leading terms of its power series expansion to obtain

$$D_v(\theta_1, \phi_1) \approx \frac{8\sqrt{\pi}\Gamma[(\pi/\psi) + (5/2)]}{\Gamma[(\pi/\psi) + 2]} \sin^2(\pi\phi_1/\psi)(\sin\theta_1)^{(2\pi/\psi)+2}, \tag{12}$$

where $\Gamma(x)$ denotes the gamma function. It is seen that for small spacing the maximum directive gain always occurs at $\theta_1 = \pi/2$, $\phi_1 = \psi/2$, and is independent of the dipole angular location specified by ϕ_0. For larger spacing this is no longer true, and displacement of the dipole from $\phi_0 = \psi/2$ will introduce beam deflection. For the small spacing case, the maximum directive gain then is given by

$$D_v \approx \frac{8\sqrt{\pi}\Gamma[(\pi/\psi) + (5/2)]}{\Gamma[(\pi/\psi) + 2]} \tag{13}$$

which can be further simplified in case the apex angle is small to

$$D_v \approx \frac{8}{\sqrt{\pi}}\left[\frac{\pi}{\psi} + \frac{7}{12}\right]^{3/2} \tag{14}$$

by the introduction of asymptotic expansions for the gamma functions. These last two formulas furnish convenient guides for the determination of corner reflector gains in the relatively small spacing case. Exact values can be obtained from (11) for larger spacings.

A similar analysis can be carried out for horizontal infinitesimal dipole excitation using the field expressions of (7) to obtain

$$D_h(\theta_1, \phi_1) = \frac{8\pi\left[\left|G_1(\theta_1, \phi_1)\right|^2 + \cos^2\theta_1 \left|G_2(\theta_1, \phi_1)\right|^2\right]}{\psi\left\{\int_0^{\pi/2} J_1{}^2(k\rho_0 \sin\theta) \sin\theta d\theta + \frac{1}{2}\sum_{n=1}^{\infty} \cos^2(n\pi\phi_0/\psi) \int_0^{\pi/2} \left[(A - B)^2 + (A + B)^2 \cos^2\theta\right] \sin\theta d\theta\right\}},$$

where

$$A = J_{n\pi/\psi - 1}(k\rho_0 \sin\theta),$$

and

$$B = J_{n\pi/\psi + 1}(k\rho_0 \sin\theta). \tag{15}$$

The formidable appearance of this last expression is somewhat deceiving, and actually it is as readily handled numerically as is (11). In the small angle case only the leading term of the denominator is needed.

Small spacing expressions similar to those of (12)–(14) can also be obtained for this case by considering the leading term of the power series expansion of (15). In this case, what constitutes the leading term depends upon the apex angle as well as upon the direction of observation. However, in the event that $\psi < \pi/2$ (or in case $\phi_0 = \psi/2$ if $\psi < \pi$) the choice of the leading term is unambiguous and it is found that for small spacings

$$D_h(\theta_1, \phi_0) \approx \frac{3\pi}{\psi} \sin^2(\theta_1), \tag{16}$$

and that the maximum directive gain which occurs for $\theta_1 = \pi/2$ is

$$D_h \approx 3\pi/\psi. \tag{17}$$

Thus, it is seen that the corner reflector excited by an infinitesimal horizontal dipole element behaves essentially like a continuous loop antenna when the apex angle is sufficiently small, as one would suspect from the image analysis.

The directive gains of corner reflectors excited by vertical and horizontal dipole elements have been computed for dipole-to-apex spacings up to about one wavelength from (11) and (15). The integrations involved were carried out with the aid of a planimeter. These results are displayed as a function of ψ with the dipole spacing as a parameter in the curves of Figs. 5 and 6.

Radiation Resistance for Horizontal and Vertical Dipole Excitation

A direct computation of the radiation resistance for the infinitesimal dipole which excites a corner reflector

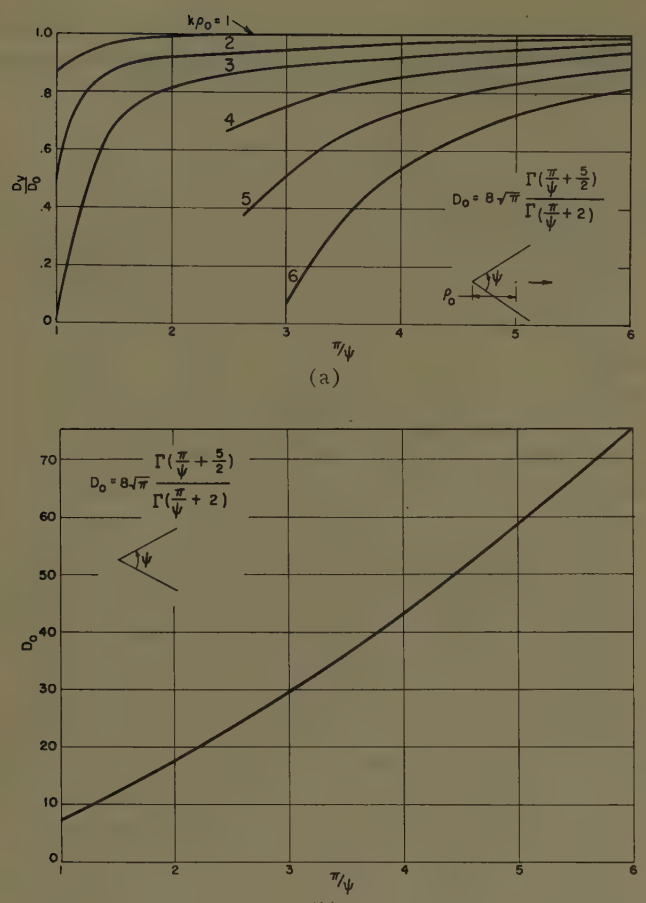

Fig. 5—(a) Forward gain of corner reflector excited by vertical infinitesimal dipole source. ($\phi_0 = \psi/2$). (b) Zero spacing gain of corner reflector excited by vertical infinitesimal dipole source.

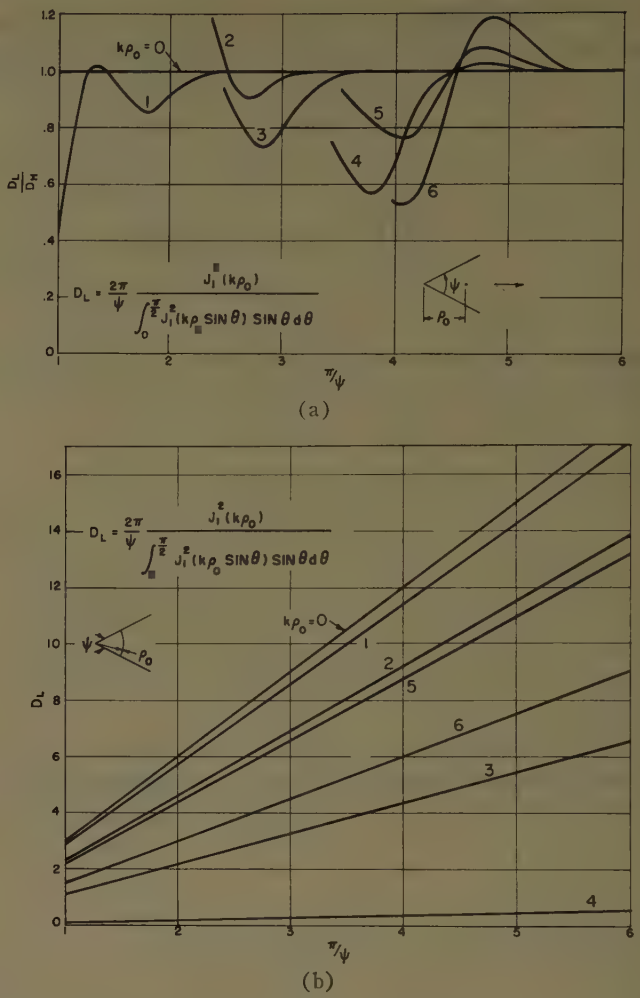

Fig. 6—(a) Forward gain of corner reflector excited by horizontal infinitesimal dipole source. ($\phi_0 = \psi/2$). (b) Gain of sector of circular loop in corner reflector.

would have little meaning since it would turn out to be zero in every case just as it does for an isolated infinitesimal dipole. This is a reflection of the fact that an assumed infinite current radiates a finite amount of power. The meaningful quantity which can be obtained in this case is a comparison of the radiation resistance of an infinitesimal dipole located in the corner reflector to that of an isolated infinitesimal dipole. This ratio while only exact in the zero length limit gives approximate results for all short dipoles, and it is surprisingly close even in the case of half-wavelength dipoles.

A comparison between the radiation resistances of two antennas can be obtained through

$$\frac{R_1}{R_0} = \frac{D_0(\theta_1, \phi_1) I_1(\theta_1, \phi_1)}{D_1(\theta_1, \phi_1) I_0(\theta_1, \phi_1)} \tag{18}$$

where R_1, R_0 are the respective radiation resistances, D_1, D_0 are the respective directive gains, and I_1, I_0 are the respective radiation intensities in an arbitrarily specified direction θ_1, ϕ_1. The radiation intensities are evaluated for equal currents at the points of reference at which the radiation resistances are evaluated.

The radiation field of an isolated infinitesimal dipole source of unit strength placed at the origin and oriented along the Z axis of a spherical coordinate system is given by

$$E_\theta = \frac{i\mu\omega}{4\pi} \sin\theta \frac{e^{ikR}}{R}, \tag{19}$$

and, it has a directivity gain in the $\theta_1 = \pi/2$ direction of

$$D_0(\pi/2, \phi_1) = 1.5. \tag{20}$$

When an isolated infinitesimal dipole is compared to a co-oriented infinitesimal dipole in a corner reflector by means of (18) making use of (8), (11), (19), and (20) it is found that

$$\frac{R_v}{R_0} = \frac{6\pi}{\psi} \sum_{n=1}^{\infty} \sin^2(n\pi\phi_0/\psi) \cdot \int_0^{\pi/2} J_{n\pi/\psi}{}^2(k\rho_0 \sin\theta) \sin^3(\theta) d\theta, \tag{21}$$

where the infinite series is the same as that involved in the denominator of (11). A similar process may be carried out making use of (7), (15), (19), and (20) to obtain for the horizontal infinitesimal dipole in a corner reflector

$$\frac{R_h}{R_0} = \frac{3\pi}{\psi}\left\{\int_0^{\pi/2} J_1^2(k\rho_0 \sin\theta)\sin\theta d\theta + \frac{1}{2}\sum_{n=1}^{\infty}\cos^2(n\pi\phi_0/\psi) \cdot \int_0^{\pi/2}[(A-B)^2 + (A+B)^2\cos^2\theta]\sin\theta d\theta\right\}, \quad (22)$$

where A and B are as defined in (15).

The radiation resistances of horizontal and vertical dipole elements centrally located in a corner reflector ($\phi_0 = \psi/2$) have been computed from (21) and (22) for spacings of the dipole elements from the apex up to about one wavelength. The integrations are the same as those involved in the directive gain calculations so that no additional numerical integrations were required. These results are displayed as a function of ψ with the dipole spacing as a parameter in the curves of Figs. 7 and 8.

The convergence of the series of (21) and (22) is quite rapid. In the case of a vertical exciting element it was found that the leading term was sufficient for $k\rho_0 \leqq 3(\pi/\psi - 1)$ in the range up to one wavelength spacing while in the case of a horizontal exciting element only a single term was necessary for $k\rho_0 \leqq 2(\pi/\psi - 1.5)$ in the same range of spacings.

As in the case of the directive gain, approximate expressions for the radiation resistance which hold for small spacings of the dipole element from the corner reflector apex may be obtained by considering the leading term of the power series expansions of (21) and (22). For excitation by a vertical dipole element it is found that

$$\frac{R_v}{R_0} = \frac{3\sqrt{\pi}(k\rho_0/2)^{2\pi/\psi}\left(\frac{\pi}{\psi}+1\right)}{\Gamma\left(\frac{\pi}{\psi}\right)\Gamma\left(\frac{\pi}{\psi}+\frac{5}{2}\right)}, \quad (23)$$

while for excitation by a horizontal dipole element it is found that

$$\frac{R_h}{R_0} \approx \frac{2\pi}{\psi}(k\rho_0/2)^2. \quad (24)$$

Eq. (24) applies in the case $\psi < \pi/2$ (if $\phi_0 = \psi/2$ for $\psi < \pi$) only.

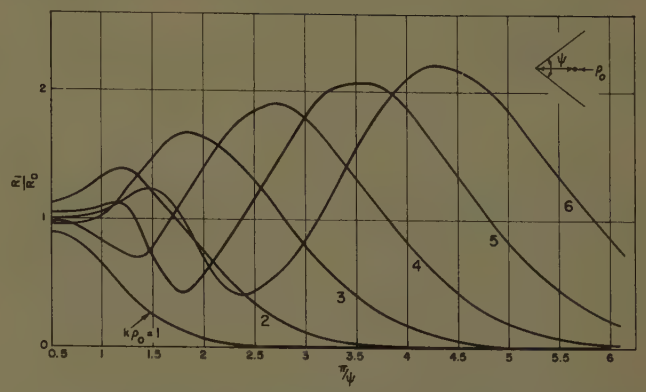

Fig. 7—Radiation resistance of short vertical dipole in corner reflector compared to free space radiation resistance.

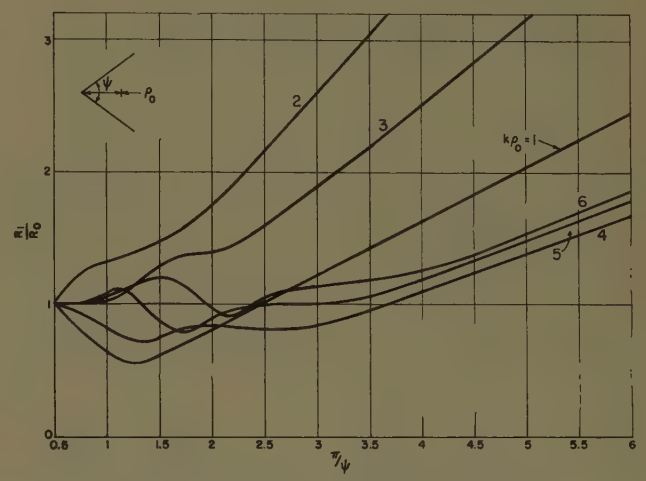

Fig. 8—Radiation resistance of short horizontal dipole in corner reflector compared to free space radiation resistance.

Directive Gain and Radiation Resistance for Arbitrary Dipole Orientation

It was seen previously that when the fields were known for a corner reflector excited by horizontally and vertically oriented infinitesimal dipoles, the corresponding fields for a dipole element arbitrarily oriented tangent to a circular cylinder whose axis is the reflector axis could be easily found [see Fig. 1 and (1)]. In this section similar results will be obtained for the directive gain and radiation resistance of a corner reflector excited by such an arbitrarily oriented infinitesimal dipole source.

A unit dipole source oriented at an angle α (as shown in Fig. 1) may be considered as the superposition of a horizontally oriented dipole source of magnitude $\cos\alpha$ and a vertically oriented dipole source of magnitude $\sin\alpha$. The power inputs to these dipole elements are

$$P_h = C\cos^2\alpha R_h,$$

and

$$P_v = C\sin^2\alpha R_v, \quad (25)$$

where C is a constant, and the total input to the arbitrarily oriented unit dipole source is

$$P = C[\cos^2 \alpha R_h + \sin^2 \alpha R_v]. \quad (26)$$

The justification for (25) and (26) lies in the fact that there is no mutual resistance coupling between the vertical and horizontal component dipole elements, or, in other words, that the two component dipole elements radiate power independently. This fact is quite evident intuitively, but it can also be shown directly by an integration of the Poynting vector due to the field of (1). This decoupling exists only for the vertical and horizontal directions and not for other mutually perpendicular directions which might be chosen.

From (26) it is seen that the radiation resistance of an arbitrarily oriented dipole source is given by

$$R_\alpha = \cos^2 \alpha R_h + \sin^2 \alpha R_v. \quad (27)$$

The radiation resistance thus oscillates, as the dipole is rotated, between the extreme values which correspond to vertical and horizontal orientation. In particular, if R_h and R_v are equal, the radiation resistance (but not necessarily the radiation reactance) will be independent of the angle α.

Similar considerations applied to the radiation intensities of the component dipole sources will lead to a corresponding result for the directive gain of an arbitrarily oriented unit dipole source. The radiation intensities in a given direction (θ_1, ϕ_1) due to the component dipole sources are

$$I_h(\theta_1, \phi_1) = K \cos^2 \alpha R_h D_h(\theta_1, \phi_1),$$

and

$$I_v(\theta_1, \phi_1) = K \sin^2 \alpha R_v D_v(\theta_1, \phi_1), \quad (28)$$

where K is constant. The total radiation intensity cannot in general be obtained by simply adding the component intensities; but on the equator $(\theta = \pi/2)$, in this case, the two fields are mutually perpendicular so that the corresponding radiation intensities can be directly added. In this case, then:

$$I_\alpha(\pi/2, \phi_1) = K[\cos^2 \alpha R_h D_h(\pi/2, \phi_1) + \sin^2 \alpha R_v D_v(\pi/2, \phi_1)],$$

$$= KR_\alpha \frac{\cos^2 \alpha R_h D_h(\pi/2, \phi_1) + \sin^2 \alpha R_v D_v(\pi/2, \phi_1)}{\cos^2 \alpha R_h + \sin^2 \alpha R_v}, \quad (29)$$

in which it can be observed that

$$D_\alpha(\pi/2, \phi_1) = \frac{\cos^2 \alpha R_h D_h(\pi/2, \phi_1) + \sin^2 \alpha R_v D_v(\pi/2, \phi_1)}{\cos^2 \alpha R_h + \sin^2 \alpha R_h}. \quad (30)$$

Eqs. (27) and (30) now permit the determination of the properties of a corner reflector excited by an arbitrarily oriented infinitesimal dipole source from the corresponding properties for horizontally and vertically oriented dipole sources. The directivity gain of (30), of course, does not allow for any polarization loss, and it is only available if the receiving antenna is elliptically polarized in the same manner as the transmitting antenna.

Of particular interest is the corner reflector whose radiation in the $(\pi/2, \psi/2)$ direction is circularly polarized. For certain apex angles such that the horizontal and vertical components of radiation are in phase quadrature, the tilt angle α can be adjusted so that they have equal magnitude, and the resultant radiation is then circularly polarized. This occurs when the radiation intensities, $I_h(\pi/2, \psi/2)$ and $I_v(\pi/2, \psi/2)$ are of equal magnitude, or, from (28), when

$$\cos^2 \alpha R_h D_h(\pi/2, \psi/2) = \sin^2 \alpha R_v D_v(\pi/2, \psi/2). \quad (31)$$

This relation permits the elimination of α from (27) and (28), and it is found that for a circularly polarized corner reflector antenna

$$D_{cp}(\pi/2, \psi/2) = \frac{2}{\frac{1}{D_h(\pi/2, \psi/2)} + \frac{1}{D_v(\pi/2, \psi/2)}}, \quad (32)$$

and

$$R_{cp} = \frac{\frac{1}{D_h(\pi/2, \psi/2)} + \frac{1}{D_v(\pi/2, \psi/2)}}{\frac{1}{R_h D_h(\pi/2, \psi/2)} + \frac{1}{R_v D_v(\pi/2, \psi/2)}}. \quad (33)$$

The relation in (32) is particularly interesting in that it shows that the directive gains of the horizontal and vertical components combine exactly like parallel resistances, the directive gain of the resulting circularly polarized antenna being twice as large as the parallel combination.

The gains and radiation resistances of circularly polarized corner reflector antennas have been computed through the relations given in (32) and (33) from the data shown in Figs. 5–8. The results of these computations are shown in Figs. 9 and 10. With only a few exceptions, circular polarization is only possible for corner reflectors whose apex angle is a submultiple of 90°, but for those apex angles circular polarization is possible at any dipole-to-apex spacing except where the horizontal and vertical component has a zero in its radiation pattern in the direction $(\pi/2, \psi/2)$.

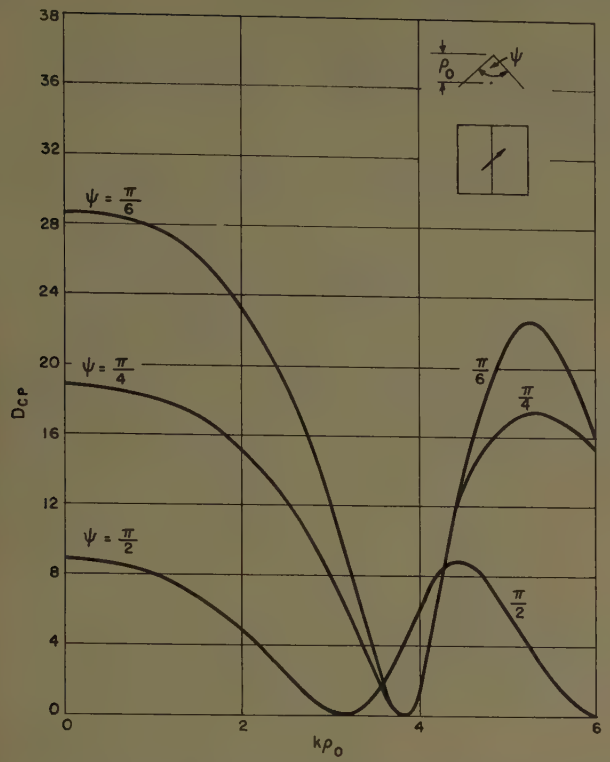

Fig. 9—Directive gain vs dipole spacing for circularly polarized corner reflector antenna with various apex angles.

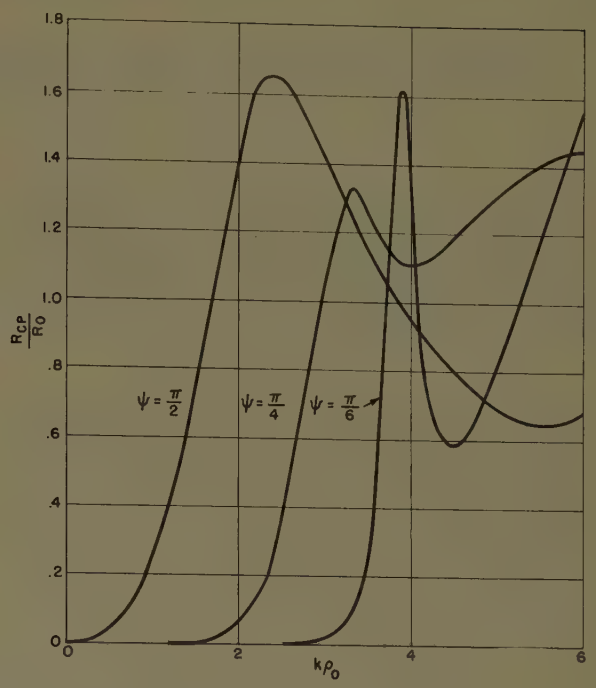

Fig. 10—Radiation resistance vs dipole spacing for circularly polarized corner reflector antenna with various apex angles.

Conclusion

The theory of the corner reflector has been thoroughly developed for excitation by an infinitesimal dipole source which is tangent to a circular cylinder having the corner reflector as its axis. These results are applicable to reflectors of arbitrary apex angle. The electromagnetic fields, directive gains, and radiation resistance have been found in terms of an infinite series of Bessel functions. These series are especially suitable for computation for the smaller apex angles although the convergence of the series is reasonably rapid for all apex angles. Computations of corner reflector properties with dipole-to-apex spacings up to about a wavelength have been carried out, and the results are given in a series of curves.

Of particular interest are the configurations which lead to circularly polarized radiation in the direction of maximum gain. It has been shown that, with a few exceptions, this is possible only for corner reflectors whose apex angles are submultiples of 90°. However, for such reflectors circular polarization is possible for every dipole-to-apex spacing except those for which the horizontal or vertical gain has a zero in the forward direction.

Mutual Impedance of Unequal Length Antennas in Echelon*

HOWARD E. KING†

Summary—**The expression is developed for the mutual impedance between two staggered parallel center-fed, infinitely thin antennas of unequal lengths. Heretofore unpublished curves are presented here which display the mutual impedance characteristics for a variety of unequal antenna lengths in echelon.**

Introduction

THE antenna engineer is often confronted with the problem of predetermining the input impedance of each radiator of a directional array. In addition he must frequently determine the interference pattern due to parasitic wires or antennas adjacent to the fed antenna. To find the input impedance and/or to find the induced currents on other wires, it is necessary to determine the mutual impedance between elements. Carter[1] has presented the mutual impedance between two wires in echelon where each antenna is an odd number of $\frac{1}{2}$ wavelengths long. The mutual impedance expression between two identical nonstaggered parallel center-fed antennas of Brown[2] is now a classic. The work of Brown was carried further by Cox[3] who determined the mutual impedance between parallel antennas of unequal lengths.

Thus, sufficient data has been presented in the past to solve the conventional problems. However, the antenna engineer may often require a knowledge of the mutual impedance between staggered parallel antennas of arbitrary length. The purpose of this paper is to present an expression which combines the work of Carter and Cox from which may be calculated the mutual impedance between any two infinitely thin center-fed parallel antennas of any length whether they be nonstaggered, staggered, or collinear.

As with all the formulas cited in the references, the mutual impedance equations apply accurately to infinitely thin antennas only, but nonetheless serve as a practical approximation for real antennas of finite thickness.

Determination of Mutual Impedance

The problem on hand is illustrated in Fig. 1. Two center-fed antennas of half-lengths l_1 and l_2 are shown separated by a distance d, and staggered by the height, h. The mutual impedance between the two antennas of Fig. 1 is defined by

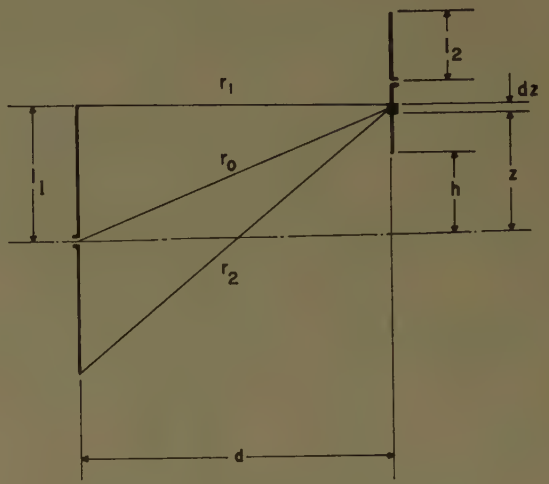

Fig. 1—Two parallel antennas of arbitrary length in echelon.

$$Z_{21} = -\frac{V_{21}}{I_{1b}} \tag{1}$$

where V_{21} is the open-circuit voltage at the terminals of antenna 2, due to a base current I_{1b} in antenna 1. The open-circuit voltage at the terminals of antenna 2 which results from the voltages induced in all the elemental lengths of the antenna may be found, by application of the reciprocity[4] theorem, to be

$$V_{21} = \frac{1}{I_{2b}}\left(\int_{h}^{l_2+h} E_{z1}I_2(z)dz + \int_{l_2+h}^{2l_2+h} E_{z1}I_2(z)dz\right), \tag{2}$$

where I_{2b} is the base (*i.e.*, feed point) current of antenna 2, and E_{z1} is the component of electric intensity parallel to the axis of the antenna at a point z along antenna 2, due to a current in antenna 1. The antenna current distribution $I_2(z)$ is assumed to be sinusoidal and given by

$$\begin{aligned} I_2(z) &= I_{2m}\sin\beta(z-h) && h < z < l_2 + h \\ I_2(z) &= I_{2m}\sin\beta(2l_2 + h - z) && h + l_2 < z < 2l_2 + h \end{aligned} \tag{3}$$

where I_{2m} is the value of current at the current loop or current maximum. The expression[2] for parallel component of electric field, is given as

* Manuscript received by the PGAP, July 14, 1956.
† The Ramo-Wooldridge Corp., Los Angeles 45, Calif.
[1] P. S. Carter, "Circuit relations in radiating systems and application to antenna problems," Proc. IRE, vol. 20, pp. 1004–1041; June, 1932.
[2] G. H. Brown, "Directional antennas," Proc. IRE, vol. 25, pp. 81–145; January, 1937.
[3] C. R. Cox, "Mutual impedance between vertical antennas of unequal heights," Proc. IRE, vol. 35, pp. 1367–1370; November, 1947.
[4] See, for example, E. C. Jordan, "Electromagnetic Waves and Radiating Systems," Prentice-Hall, Inc., New York, N. Y., p. 349; 1950.

$$E_{z1} = 30I_{1m}\left[\frac{-je^{-i\beta r_1}}{r_1} + \frac{-je^{-i\beta r_2}}{r_2} + \frac{2j\cos\beta l_1 e^{-i\beta r_0}}{r_0}\right]. \quad (4)$$

Eq. (1) gives the mutual impedance referred to the base or feed point. The mutual impedance related to the loop currents will be given by

$$Z_{12\,\text{loop}} = \frac{I_{1b}I_{2b}}{I_{1m}I_{2m}} Z_{12\,\text{base}}. \quad (5)$$

Inserting (2)–(4) into (1), and in view of (5), the expression for the mutual impedance referred to the loop currents becomes

$$Z_{12} = -30\left[\left\{\int_h^{l_2+h} \sin\beta(z-h) + \int_{l_2+h}^{2l_2+h} \sin\beta(2l_2+h-z)\right\}\left(\frac{-je^{-i\beta r_1}}{r_1} + \frac{-je^{-i\beta r_2}}{r_2} + \frac{2j\cos\beta l_1 e^{-i\beta r}}{r_0}\right)dz\right]. \quad (6)$$

The geometry of Fig. 1 reveals that

$$r_0 = \sqrt{d^2+z^2} \quad (7)$$

$$r_1 = \sqrt{d^2+(l_1-z)^2} \quad (8)$$

$$r_2 = \sqrt{d^2+(l_1+z)^2}. \quad (9)$$

The real part of the complex expression (6) gives the mutual resistance and the imaginary part gives the mutual reactance. Eq. (6) can be evaluated by mechanical integration; however, to make possible arithmetical computations the integration is done mathematically so that a convenient form is available for calculations.

Substituting the relations (7)–(9) into (6), and following the integrations in a manner similar to that outlined in the Appendix, the most general expressions for the mutual impedance between two thin parallel center-fed antennas of any arbitrary half-length l_1 and l_2, spaced a distance d apart, and staggered by the value h, are:

where

$$u_0 = \beta(\sqrt{d^2+(h-l_1)^2} + (h-l_1))$$
$$v_0 = \beta(\sqrt{d^2+(h-l_1)^2} - (h-l_1))$$
$$\mu_0' = \beta(\sqrt{d^2+(h+l_1)^2} - (h+l_1))$$
$$v_0' = \beta(\sqrt{d^2+(h+l_1)^2} + (h+l_1))$$
$$\mu_1 = \beta(\sqrt{d^2+(h-l_1+l_2)^2} + (h-l_1+l_2))$$
$$v_1 = \beta(\sqrt{d^2+(h-l_1+l_2)^2} - (h-l_1+l_2))$$
$$\mu_2 = \beta(\sqrt{d^2+(h+l_1+l_2)^2} - (h+l_1+l_2))$$
$$v_2 = \beta(\sqrt{d^2+(h+l_1+l_2)^2} + (h+l_1+l_2))$$
$$u_3 = \beta(\sqrt{d^2+(h-l_1+2l_2)^2} + (h-l_1+2l_2))$$
$$v_3 = \beta(\sqrt{d^2+(h-l_1+2l_2)^2} - (h-l_1+2l_2))$$
$$u_4 = \beta(\sqrt{d^2+(h+l_1+2l_2)^2} - (h+l_1+2l_2))$$
$$v_4 = \beta(\sqrt{d^2+(h+l_1+2l_2)^2} + (h+l_1+2l_2))$$
$$w_1 = \beta(\sqrt{d^2+h^2} - h)$$
$$y_1 = \beta(\sqrt{d^2+h^2} + h)$$
$$w_2 = \beta(\sqrt{d^2+(h+l_2)^2} - (h+l_2))$$
$$y_2 = \beta(\sqrt{d^2+(h+l_2)^2} + (h+l_2))$$
$$w_3 = \beta(\sqrt{d^2+(h+2l_2)^2} - (h+2l_2))$$
$$y_3 = \beta(\sqrt{d^2+(h+2l_2)^2} + (h+2l_2)).$$

Considerable reduction in the length of (10) and (11) results if the length $l_1=\lambda/4$. Furthermore, note that once R_{12} is obtained one can find X_{12} by the following relations. Let

$$R_{12} = X_{12}$$
$$\text{Ci}(x) = -\text{Si}(x)$$
$$\text{Si}(y) = \text{Ci}(y).$$

Mutual Impedance Curves

The antenna configurations used in this presentation are illustrated in Fig. 2. In all the curves the mutual

---

$$\begin{aligned}R_{12} = 15\{&\cos\beta(l_1-h)(\text{Ci}(u_0)+\text{Ci}(v_0)-\text{Ci}(u_1)-\text{Ci}(v_1))+\sin\beta(l_1-h)(-\text{Si}(u_0)+\text{Si}(v_0)+\text{Si}(u_1)-\text{Si}(v_1))\\
&+\cos\beta(l_1+h)(\text{Ci}(u_0')+\text{Ci}(v_0')-\text{Ci}(u_2)-\text{Ci}(v_2))+\sin\beta(l_1+h)(-\text{Si}(u_0')+\text{Si}(v_0')+\text{Si}(u_2)-\text{Si}(v_2))\\
&+\cos\beta(l_1-2l_2-h)(-\text{Ci}(u_1)-\text{Ci}(v_1)+\text{Ci}(u_3)+\text{Ci}(v_3))+\sin\beta(l_1-2l_2-h)(\text{Si}(u_1)-\text{Si}(v_1)-\text{Si}(u_3)+\text{Si}(v_3))\\
&+\cos\beta(l_1+2l_2+h)(-\text{Ci}(u_2)-\text{Ci}(v_2)+\text{Ci}(u_4)+\text{Ci}(v_4))+\sin\beta(l_1+2l_2+h)(\text{Si}(u_2)-\text{Si}(v_2)-\text{Si}(u_4)+\text{Si}(v_4))\\
&+2\cos\beta l_1\cos\beta h(-\text{Ci}(w_1)-\text{Ci}(y_1)+\text{Ci}(w_2)+\text{Ci}(y_2))+2\cos\beta l_1\sin\beta h\,(\text{Si}(w_1)-\text{Si}(y_1)-\text{Si}(w_2)+\text{Si}(y_2))\\
&+2\cos\beta l_1\cos\beta(2l_2+h)(\text{Ci}(w_2)+\text{Ci}(y_2)-\text{Ci}(w_3)-\text{Ci}(y_3))+2\cos\beta l_1\sin\beta h\,(2l_2+h)(-\text{Si}(w_2)+\text{Si}(y_2)+\text{Si}(w_3)-\text{Si}(y_3))\}\end{aligned} \quad (10)$$

$$\begin{aligned}X_{12} = 15\{&\cos\beta(l_1-h)(-\text{Si}(u_0)-\text{Si}(v_0)+\text{Si}(u_1)+\text{Si}(v_1))+\sin\beta(l_1-h)(-\text{Ci}(u_0)+\text{Ci}(v_0)+\text{Ci}(u_1)-\text{Ci}(v_1))\\
&+\cos\beta(l_1+h)(-\text{Si}(u_0')-\text{Si}(v_0')+\text{Si}(u_2)+\text{Si}(v_2))+\sin\beta(l_1+h)(-\text{Ci}(u_0')+\text{Ci}(v_0')+\text{Ci}(u_2)-\text{Ci}(v_2))\\
&+\cos\beta(l_1-2l_2-h)(\text{Si}(u_1)+\text{Si}(v_1)-\text{Si}(u_3)-\text{Si}(v_3))+\sin\beta(l_1-2l_2-h)(\text{Ci}(u_1)-\text{Ci}(v_1)-\text{Ci}(u_3)+\text{Ci}(v_3))\\
&+\cos\beta(l_1+2l_2+h)(\text{Si}(u_2)+\text{Si}(v_2)-\text{Si}(u_4)-\text{Si}(v_4))+\sin\beta(l_1+2l_2+h)(\text{Ci}(u_2)-\text{Ci}(v_2)-\text{Ci}(u_4)+\text{Ci}(v_4))\\
&+2\cos\beta l_1\cos\beta h(\text{Si}(w_1)+\text{Si}(y_1)-\text{Si}(w_2)-\text{Si}(y_2))+2\cos\beta l_1\sin\beta h(\text{Ci}(w_1)-\text{Ci}(y_1)-\text{Ci}(w_2)+\text{Ci}(y_2))\\
&+2\cos\beta l_1\cos\beta(2l_2+h)\,(-\text{Si}(w_2)-\text{Si}(y_2)+\text{Si}(w_3)+\text{Si}(y_3))+2\cos\beta l_1\sin\beta(2l_2+h)(-\text{Ci}(w_2)+\text{Ci}(y_2)+\text{Ci}(w_3)-\text{Ci}(y_3))\}\end{aligned} \quad (11)$$

Fig. 2--Two parallel antennas in (a) nonstaggered, (b) staggered, and (c) collinear arrangement.

impedance is referred to the loop currents. Fig. 3 (opposite) shows the mutual impedance between two $\lambda/2$ dipoles (half-length $l_1=l_2=\lambda/4$). Note that Fig. 3(a) for the nonstaggered case (or $h=-\lambda/4$) is the plot normally seen in all standard references for two parallel antennas. Figs. 3(b) and 3(c) show the deviation from Fig. 3(a) when the antennas are in echelon, *i.e.*, staggered by $h=0$ and $h=\lambda/4$, respectively. The shape is generally the same with a decrease in magnitude.

Fig. 4 (pp. 309–310) illustrates the mutual impedance between two antennas of half-lengths $l_1=\lambda/4$ and $l_2=\lambda/6$ for the nonstaggered case ($h=-l_1=-\lambda/4$), and for two staggered cases ($h=0$, and $h=l_1=\lambda/4$). Fig. 5 (pp. 310–311) depicts corresponding results for the case where the half-lengths are $l_1=\lambda/4$ and $l_2=\lambda/8$.

Special Cases

Collinear Array

A special case of echelon antennas is the arrangement of Fig. 2(c) where $d=0$ in (10) and (11). This gives rise to an indeterminate form of $\infty-\infty$. By taking the limit of the expression as d approaches zero, the mutual resistance and reactance are obtained as

$$\begin{aligned}R_{12} = 15\Big\{&\cos\beta(h-l_1)\Big[\mathrm{Ci}\,(u_0)-\mathrm{Ci}\,(u_1)+\ln\frac{h-l_1+l_2}{h-l_1}\Big]+\sin\beta(h-l_1)\,[\mathrm{Si}\,(u_0)-\mathrm{Si}(u_1)]\\
&+\cos\beta(h+l_1)\Big[\mathrm{Ci}\,(v_0')-\mathrm{Ci}\,(v_2)+\ln\frac{h+l_1+l_2}{h+l_1}\Big]+\sin\beta(h+l_1)\,[\mathrm{Si}\,(v_0')-\mathrm{Si}\,(v_2)]\\
&+\cos\beta(h-l_1+2l_2)\Big[-\mathrm{Ci}\,(u_1)+\mathrm{Ci}\,(u_3)+\ln\frac{h-l_1+l_2}{h-l_1+2l_2}\Big]+\sin\beta(h-l_1+2l_2)\,[-\mathrm{Si}\,(u_1)+\mathrm{Si}\,(u_3)]\\
&+\cos\beta(h+l_1+2l_2)\Big[-\mathrm{Ci}\,(v_2)+\mathrm{Ci}(v_4)+\ln\frac{h+l_1+l_2}{h+l_1+2l_2}\Big]+\sin\beta(h+l_1+2l_2)\,[-\mathrm{Si}\,(v_2)+\mathrm{Si}\,(v_4)]\\
&+2\cos\beta l_1\cos\beta h\Big[-\mathrm{Ci}\,(y_1)+\mathrm{Ci}\,(y_2)+\ln\frac{h}{h+l_2}\Big]+2\cos\beta l_1\sin\beta h[-\mathrm{Si}\,(y_1)+\mathrm{Si}\,(y_2)]\\
&+2\cos\beta l_1\cos\beta(h+2l_2)\Big[\mathrm{Ci}\,(y_2)-\mathrm{Ci}(y_3)+\ln\frac{h+2l_2}{h+l_2}\Big]+2\cos\beta l_1\sin\beta(h+2l_2)\,[\mathrm{Si}\,(y_2)-\mathrm{Si}(y_3)]\Big\}\end{aligned}\tag{12}$$

and

$$\begin{aligned}X_{12} = 15\Big\{&\cos\beta(h-l_1)\,[-\mathrm{Si}\,(u_0)+\mathrm{Si}\,(u_1)]+\sin\beta(h-l_1)\Big[\mathrm{Ci}\,(u_0)-\mathrm{Ci}\,(u_1)+\ln\frac{h-l_1}{h-l_1+l_2}\Big]\\
&+\cos\beta(h+l_1)\,[-\mathrm{Si}\,(v_0')+\mathrm{Si}\,(v_2)]+\sin\beta(h+l_1)\Big[\mathrm{Ci}\,(v_0')-\mathrm{Ci}\,(v_2)+\ln\frac{h+l_1}{h+l_1+l_2}\Big]\\
&+\cos\beta(h-l_1+2l_2)\,[\mathrm{Si}(u_1)-\mathrm{Si}\,(u_3)]+\sin\beta(h-l_1+2l_2)\Big[-\mathrm{Ci}\,(u_1)+\mathrm{Ci}\,(u_3)+\ln\frac{h-l_1+2l_2}{h-l_1+l_2}\Big]\\
&+\cos\beta(h+l_1+2l_2)\,[\mathrm{Si}\,(v_2)-\mathrm{Si}\,(v_4)]+\sin\beta(h+l_1+2l_2)\Big[-\mathrm{Ci}\,(v_2)+\mathrm{Ci}\,(v_4)+\ln\frac{h+l_1+2l_2}{h+l_1+l_2}\Big]\\
&+2\cos\beta l_1\cos\beta h[\mathrm{Si}\,(y_1)-\mathrm{Si}\,(y_2)]+2\cos\beta l_1\sin\beta h\Big[-\mathrm{Ci}\,(y_1)+\mathrm{Ci}\,(y_2)+\ln\frac{h+l_2}{h}\Big]\\
&+2\cos\beta l_1\cos\beta(h+2l_2)\,[-\mathrm{Si}\,(y_2)+\mathrm{Si}\,(y_3)]+2\cos\beta l_1\sin\beta(h+2l_2)\Big[\mathrm{Ci}(y_2)-\mathrm{Ci}(y_3)+\ln\frac{h+l_2}{h+2l_2}\Big]\Big\}.\end{aligned}\tag{13}$$

Eqs. (12) and (13) represent the mutual impedance for two collinear antennas of any arbitrary lengths l_1 and l_2, providing $h>l_1$. Figs. 6–8 (p. 311) represent the mu-

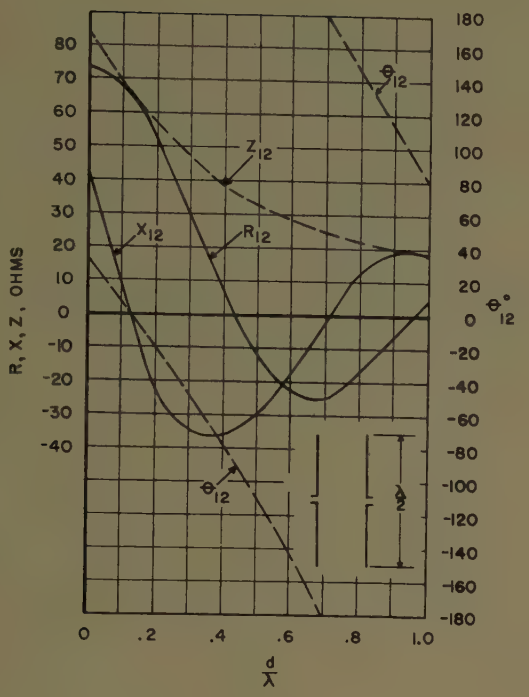

(a)

Fig. 3(a)—Mutual impedance curves for two parallel half-wavelength antennas, nonstaggered.

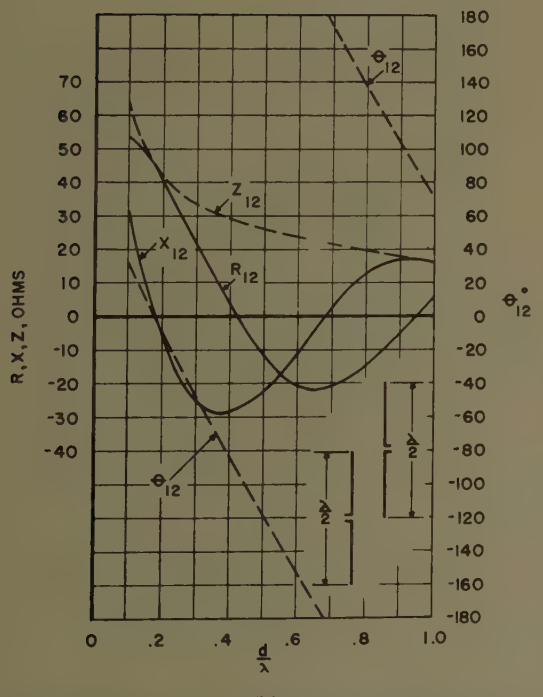

(b)

Fig. 3(b)—Mutual impedance curves for two parallel half-wavelength antennas staggered by $h=0$.

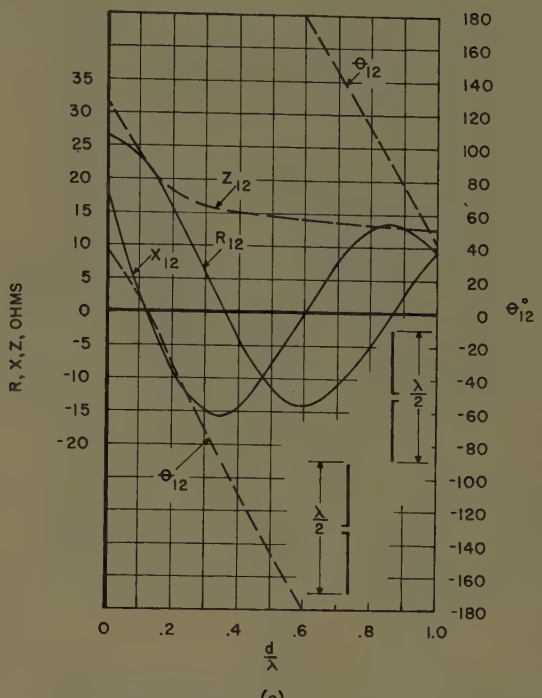

(c)

Fig. 3(c)—Mutual impedance curves for two parallel half-wavelength antennas staggered by $h=\lambda/4$.

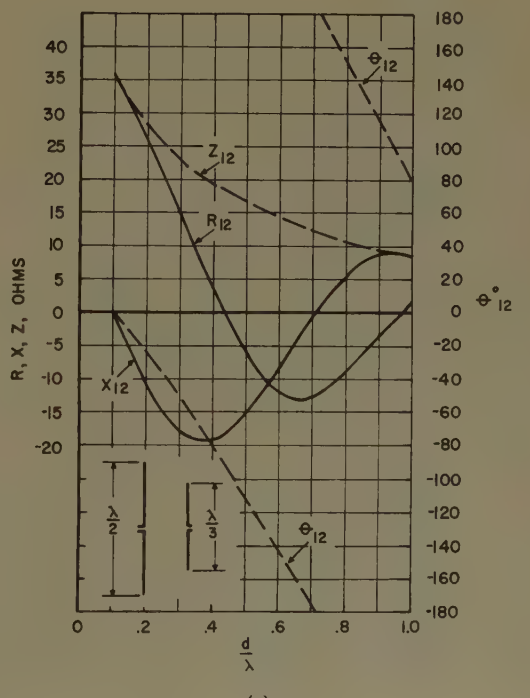

(a)

Fig. 4(a)—Mutual impedance curves between two parallel antennas of lengths $\lambda/2$ and $\lambda/3$, nonstaggered (referred to the loop currents).

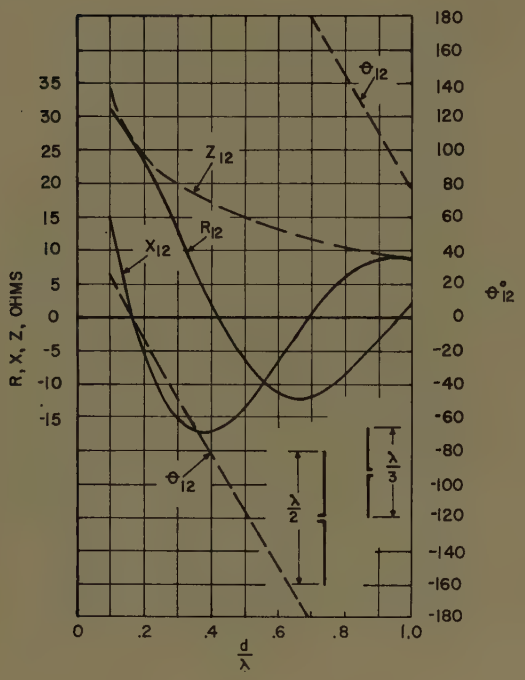

Fig. 4(b)—Mutual impedance curves between two parallel antennas of lengths λ/2 and λ/3, staggered by $h=0$ (referred to the loop currents).

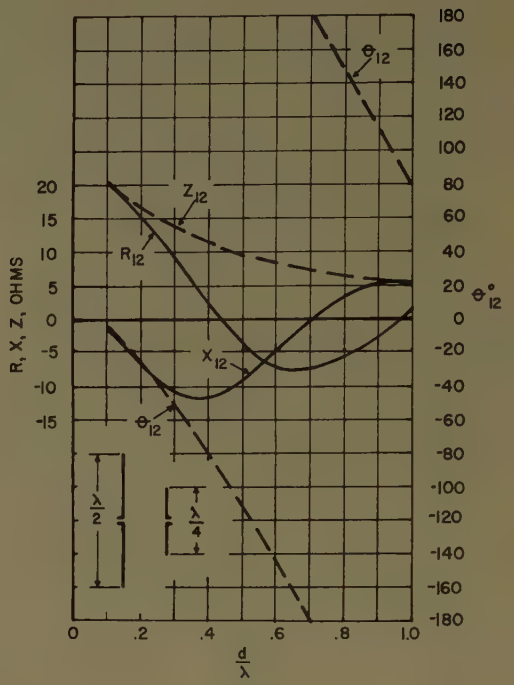

Fig. 5(a)—Mutual impedance curves between two parallel antennas of lengths λ/2 and λ/4, nonstaggered (referred to the loop currents).

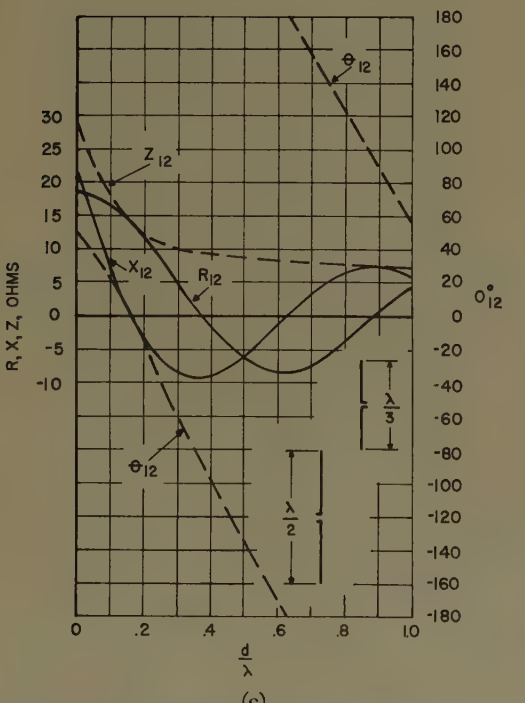

Fig. 4(c)—Mutual impedance curves between two parallel antennas of lengths λ/2 and λ/3, staggered by $h=\lambda/4$ (referred to the loop currents).

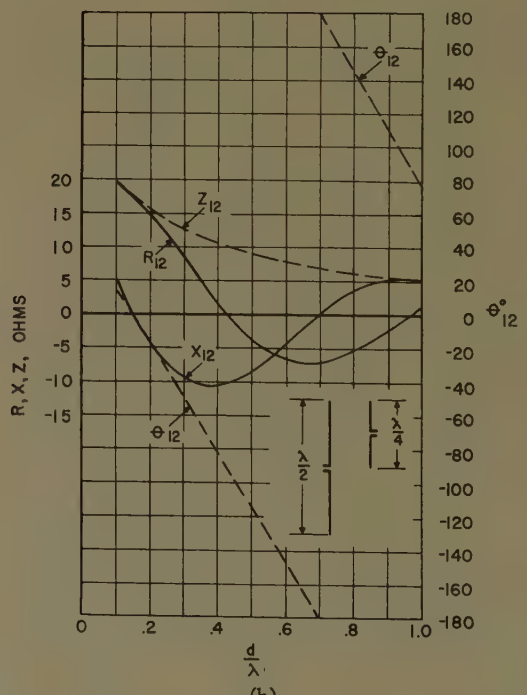

Fig. 5(b)—Mutual impedance curves between two parallel antennas of lengths λ/2 and λ/4, staggered by $h=0$ (referred to the loop currents).

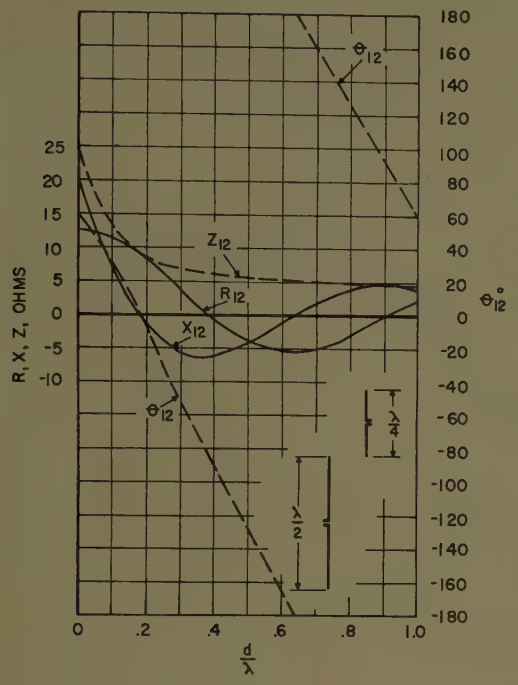

(c)

Fig. 5(c)—Mutual impedance curves between two parallel antennas of lengths $\lambda/2$ and $\lambda/4$, staggered by $h=\lambda/4$ (referred to the loop currents).

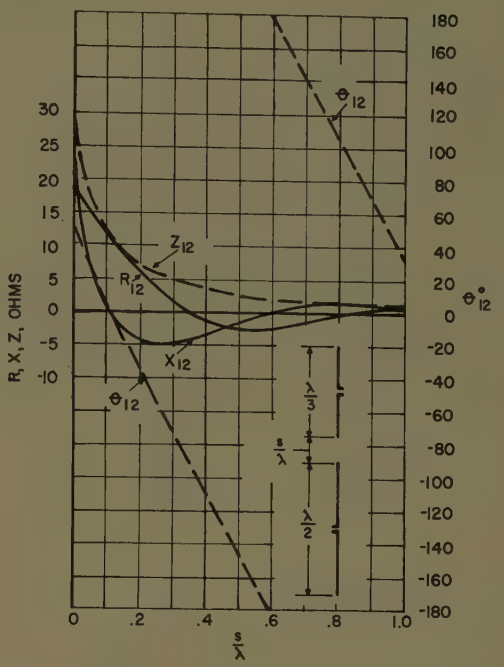

Fig. 7—Mutual impedance curves between two antennas of lengths $\lambda/2$ and $\lambda/3$ in a collinear arrangement.

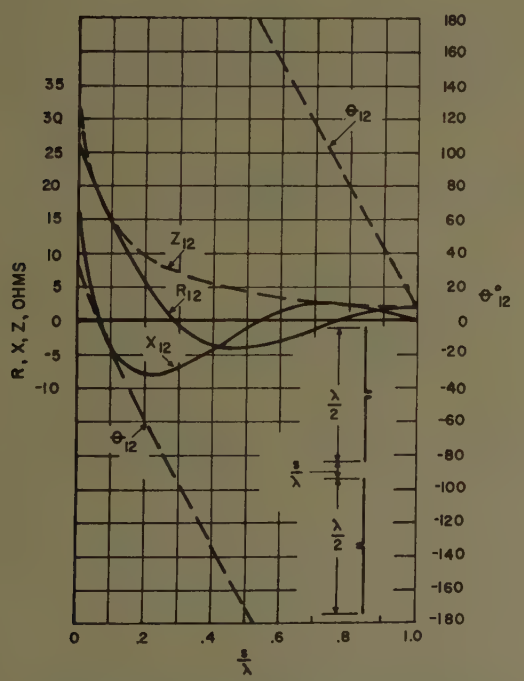

Fig. 6—Mutual impedance curves between two half-wavelength antennas in a collinear arrangement.

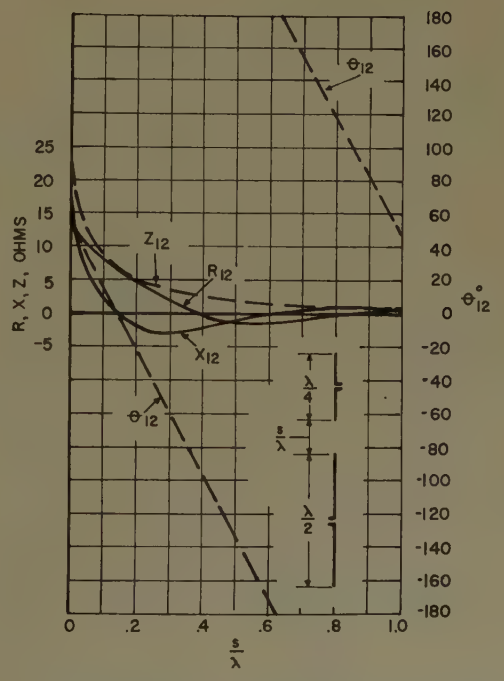

Fig. 8—Mutual impedance curves between two antennas of lengths $\lambda/2$ and $\lambda/4$ in a collinear arrangement.

tual impedances between an antenna with its half-length $l_1=\lambda/4$, and antennas of half-lengths corresponding to $l_2=\lambda/4$, $\lambda/6$, and $\lambda/8$.

The mutual resistance and reactance of two collinear $\lambda/2$ dipoles ($l_1=l_2=\lambda/4$) can be written from (12) and (13), respectively, as

$$R_{12}=30\{\cos 2\beta l_1[\mathrm{Ci}\,(u_0)+\mathrm{Ci}\,(v_0)-2\,\mathrm{Ci}\,(u_1)-2\,\mathrm{Ci}\,(v_1)+2\,\mathrm{Ci}\,(\beta d)]+\sin 2\beta l_1[-\mathrm{Si}\,(u_0)+\mathrm{Si}\,(v_0)+2\,\mathrm{Si}\,(u_1)-2\,\mathrm{Si}\,(v_1)]+[-2\,\mathrm{Ci}\,(u_1)-2\,\mathrm{Ci}\,(v_1)+4\,\mathrm{Ci}\,(\beta d)]\} \quad (18)$$

$$R_{12}=15\left\{\sin\beta h\left[\mathrm{Ci}\,2\beta(h-l_1)-2\,\mathrm{Ci}\,2\beta(h+l_1)+\mathrm{Ci}\,2\beta(h+3l_1)+\ln\frac{(h+l_1)^2}{h^2+2hl_1-3l_1^2}\right]+\cos\beta h[-\mathrm{Si}\,2\beta(h-l_1)+2\,\mathrm{Si}\,2\beta(h+l_1)-\mathrm{Si}\,2\beta(h+3l_1)]\right\} \quad (14)$$

and

$$X_{12}=15\left\{\sin\beta h[-\mathrm{Si}\,2\beta(h-l_1)+2\,\mathrm{Si}\,2\beta(h+l_1)-\mathrm{Si}\,2\beta(h+3l_1)]+\cos\beta h\left[-\mathrm{Ci}\,2\beta(h-l_1)+2\,\mathrm{Ci}\,2\beta(h+l_1)-\mathrm{Ci}\,2\beta(h+3l_1)+\ln\frac{(h+l_1)^2}{h^2+2hl_1-3l_1^2}\right]\right\}. \quad (15)$$

Non-Staggered Arrays

[See Fig. 2(a).] Referring to (10) and (11), if $h=-l_2$, then R_{12} and X_{12} will reduce to the equations given by Cox for parallel antennas of unequal height which are

$$\begin{aligned}R_{12}=30\{&\cos\beta(l_1+l_2)[\mathrm{Ci}\,(u_0)+\mathrm{Ci}\,(v_0)-\mathrm{Ci}\,(u_1)-\mathrm{Ci}\,(v_1)-\mathrm{Ci}\,(w_1)-\mathrm{Ci}\,(y_1)+2\,\mathrm{Ci}\,(\beta d)]\\&+\cos\beta(l_1-l_2)[\mathrm{Ci}\,(u_0')+\mathrm{Ci}\,(v_0')-\mathrm{Ci}\,(\mu_1)-\mathrm{Ci}\,(v_1)-\mathrm{Ci}\,(w_1)-\mathrm{Ci}\,(y_1)+2\,\mathrm{Ci}\,(\beta d)]\\&+\sin\beta(l_1+l_2)[-\mathrm{Si}\,(u_0)+\mathrm{Si}\,(v_0)+\mathrm{Si}\,(u_1)-\mathrm{Si}\,(v_1)-\mathrm{Si}\,(w_1)+\mathrm{Si}\,(y_1)]\\&+\sin\beta(l_1-l_2)[-\mathrm{Si}\,(u_0')+\mathrm{Si}\,(v_0')+\mathrm{Si}\,(u_1)-\mathrm{Si}(v_1)+\mathrm{Si}(w_1)-\mathrm{Si}\,(y_1)]\}\end{aligned} \quad (16)$$

and

$$\begin{aligned}X_{12}=30\{&\cos\beta(l_1+l_2)[-\mathrm{Si}\,(u_0)-\mathrm{Si}\,(v_0)+\mathrm{Si}\,(u_1)+\mathrm{Si}\,(v_1)+\mathrm{Si}\,(w_1)+\mathrm{Si}\,(y_1)-2\,\mathrm{Si}\,(\beta d)]\\&+\cos\beta(l_1-l_2)[-\mathrm{Si}\,(u_0')-\mathrm{Si}\,(v_0')+\mathrm{Si}\,(u_1)+\mathrm{Si}\,(v_1)+\mathrm{Si}\,(w_1)+\mathrm{Si}\,(y_1)-2\mathrm{Si}\,(\beta d)]\\&+\sin\beta(l_1+l_2)[-\mathrm{Ci}\,(u_0)+\mathrm{Ci}\,(v_0)+\mathrm{Ci}(u_1)-\mathrm{Ci}\,(v_1)-\mathrm{Ci}\,(w_1)+\mathrm{Ci}(y_1)]\\&+\sin\beta(l_1-l_2)[-\mathrm{Ci}\,(u_0')+\mathrm{Ci}\,(v_0')+\mathrm{Ci}\,(u_1)-\mathrm{Ci}\,(v_1)+\mathrm{Ci}\,(w_1)-\mathrm{Ci}\,(y_1)]\}.\end{aligned} \quad (17)$$

If the radiators are equal in length ($l_1=l_2$) and with $h=-l_2$, then the mutual resistance and reactance for two parallel center-fed thin antennas simplify to

and

$$X_{12}=30\{\cos 2\beta l_1[-\mathrm{Si}\,(u_0)-\mathrm{Si}\,(v_0)+2\,\mathrm{Si}\,(u_1)+2\,\mathrm{Si}\,(v_1)-2\,\mathrm{Si}\,(\beta d)]+\sin 2\beta l_1[-\mathrm{Ci}\,(u_0)+\mathrm{Ci}\,(v_0)+2\,\mathrm{Ci}\,(u_1)-2\,\mathrm{Ci}\,(v_1)]+[2\,\mathrm{Si}\,(u_1)+2\,\mathrm{Si}\,(v_1)-4\,\mathrm{Si}\,(\beta d)]\}, \quad (19)$$

which are the formulas given by Brown.

Conclusion

The mutual impedance relations for collinear or echelon arrays with elements of arbitrary lengths were presented. The expressions are only approximate because sinusoidal current distributions on both elements were assumed. However, the information in this paper should be useful for practical antenna array design.

Appendix

A typical term of (6) reduces to

$$A=30\int_h^{l_2+h}\frac{\sin\beta r_1}{r_1}\sin\beta(z-h)\,dz=30\int_h^{l_2+h}\frac{\sin\beta\sqrt{d^2+(l_1-z)^2}}{\sqrt{d^2+(l_1-z)^2}}\sin\beta(z-h)\,dz. \quad (20)$$

By change in the variable of $x=l_1-z$, and use of trigonometric identity for the product of angles one obtains

$$\begin{aligned}A=15\int_{l_1-h}^{l_1-l_2-h}&[\cos\beta(l_1-h)\cos\beta(\sqrt{d^2+x^2}-x)\\&-\sin\beta(l_1-h)\sin\beta(\sqrt{d^2+x^2}-x)\\&-\cos\beta(l_1-h)\cos\beta(\sqrt{d^2+x^2}+x)\\&-\sin\beta(l_1-h)\sin\beta(\sqrt{d^2+x^2}+x)\\&\cdot\frac{dx}{\sqrt{d^2+x^2}}.\end{aligned} \quad (21)$$

A second change in the variables of

$$u = \beta(\sqrt{d^2 + x^2} - x)$$
$$v = \beta(\sqrt{d^2 + x^2} + x) \qquad (22)$$

gives

$$A = 15\int_{u_0}^{u_1}\left[-\cos\beta(l_1 - h)\frac{\cos u}{u}\,du + \sin\beta(l_1 - h)\frac{\sin u}{u}\,du\right]$$
$$+ 15\int_{v_0}^{v_1}\left[-\cos\beta(l_1 - h)\frac{\cos v}{v}\,dv - \sin\beta(l_1 - h)\frac{\sin v}{v}\,dv\right] \qquad (23)$$

where u_0, v_0, u_1, and v_1 are defined in (10) and (11). The integrals of (23) are recognized as cosine and sine integrals, and it can be rewritten as

$$A = 15\{\cos\beta(l_1 - h)[\mathrm{Ci}\,(u_0) + \mathrm{Ci}\,(v_0) - \mathrm{Ci}\,(u_1) - \mathrm{Ci}\,(v_1)]$$
$$+ \sin\beta(l_1 - h)[-\mathrm{Si}\,(u_0) + \mathrm{Si}\,(v_0) + \mathrm{Si}\,(u_1) - \mathrm{Si}\,(v_1)]\}. \qquad (24)$$

Following this procedure, (10) and (11) were derived for mutual resistance and reactance.

Corrections

The following correction to "Exterior Electromagnetic Boundary Value Problems for Spheres and Cones," by L. L. Bailin and S. Silver, which appeared on pages 5–16 in the January, 1956 issue of these TRANSACTIONS, has been called to the attention of the authors by Dr. Leopold Felsen.

The expressions for the field produced by a slot in a cone given in the above paper are incomplete. We overlooked the contribution made to the TE modes in the external field by an excitation in the radial direction along the cone. It is necessary to add a term to our function Π^*, given by (52) on page 12, that represents the contribution of the E_R component of excitation in the aperture. The complete expression is

$$\Pi^*(r, \theta, \phi) = \left(\frac{\epsilon}{\mu}\right)^{1/2}\sum_{m=0}^{\infty}\sum_{i=1}^{\infty}\frac{(2\nu_i' + 1)P_{\nu_i'}^{m}(\cos\theta)}{\nu_i'(\nu_i' + 1)\sin^2\theta_0\left.\dfrac{\partial^2 P_\nu^m}{\partial\theta\partial\nu}\right|_{\substack{\theta=\theta_0\\ \nu=\nu_i'}}\pi(1 + \delta_{0m})}$$
$$\left\{\int_{r_1}^{r_2}\int_{\phi_1}^{\phi_2} mf_1(r', \phi')\Gamma_1(r, r')\sin m(\phi' - \phi)\,dr'd\phi' + \nu_i'(\nu_i' + 1)\sin\theta_0\int_{r_1}^{r_2}\int_{\phi_1}^{\phi_2} f_2(r', \phi')\Gamma_2(r, r')\cdot\cos m(\phi' - \phi)\,dr'd\phi'\right\}$$

where $f_1(r', \phi')$ is the E_R component of the excitation in the aperture and $f_2(r', \phi')$ is the E_ϕ component; and

$$\Gamma_1(r, r') = j_{\nu_i'}(kr)\frac{d}{dr'}[r'h_{\nu_i'}^{(2)}(kr')] \qquad r < r'$$
$$= \frac{j_{\nu_i'}(kr')\dfrac{d}{dr'}[r'h_{\nu_i'}^{(2)}(kr')]h_{\nu_i'}^{(2)}(kr)}{h_{\nu_i'}^{(2)}(kr')} \qquad r > r'$$

and

$$\Gamma_2(r, r') = j_{\nu_i'}(kr)h_{\nu_i'}^{(2)}(kr') \qquad r < r'$$
$$= j_{\nu_i'}(kr')h_{\nu_i'}^{(2)}(kr) \qquad r > r'.$$

A circumferential slot such as is shown on page 13 in Fig. 3(a) of the paper, in general generates both TM and TE type modes. The total field contains terms derived from the function Π and the function Π^*. When the slot runs completely around the circumference and is excited uniformly (*i.e.*, has no variation in ϕ), the function Π^* reduces to zero and the field consists of only TM waves. A slot along a generator of the cone such as is shown in Fig. 3(b) gives rise to only TE waves and its field is obtained from the function Π^*; the results for such a slot remain as in the paper.

James R. Wait, author of "The Transient Behavior of the Electromagnetic Ground Wave on a Spherical Earth," which appeared on pages 198–202 of the April, 1957 issue of these TRANSACTIONS, has brought the following corrections to the attention of the editors.

In (3), $(2\pi)^{1/2}X$ should be replaced by $(2\pi X)^{1/2}$.

In (12), a should be replaced by 2.

In Fig. 3, the curve for 1500 mi. was misplotted; it should be essentially the same as the corresponding curve in Fig. 4.

communication

Determination of HF Skywave Absorption*

GERALD L. PUCILLO†

Summary—**A graphical method is employed as a means for facilitating the determination of hf skywave absorption for any given transmission path at any given time.**

THE EXISTING method for determining hf skywave absorption, employed by Laitinen and Haydon,[1] requires the use of several different charts and nomographs. This method is cumbersome and laborious, particularly when a large number of absorption determinations are required.

As a means of simplifying the procedure, a single combined graph, Fig. 1, opposite, has been devised. The graph not only facilitates the determination of absorption but also serves as a visual aid in the understanding of the parts played by the various parameters affecting the absorption. Application of the graph is limited to those cases in which the maximum usable frequency (muf) and the ionospheric layer height are known.

The graph is a solution of the following two equations used by Laitinen and Haydon:[1]

$$\cos\psi = \sin L_1 \sin L_2 + \cos L_1 \cos L_2 \cos\Omega \qquad (1)$$

and

$$A = \text{absorption (db)} = \frac{\text{cn sec } \phi(\cos a\psi)^m(1 + bs)}{(f + f_H)^d}. \qquad (2)$$

In (1)

L_1 = latitude of the ionosphere reflection point,
L_2 = latitude of the sun's subsolar point,
Ω = hour angle of the sun referred to the ionosphere reflection point,
ψ = solar zenith angle at the ionosphere reflection point.

In (2),

ψ = solar zenith angle at the ionosphere reflection point,
a = constant = 0.881,
b = constant = 0.0037,
c = constant = 615.5,
m = constant = 1.3,
d = constant = 1.98,
f = operating frequency (also called wave frequency),
f_H = gyro-frequency at a 100-km height,
n = number of ionospheric reflections ($n = 1$ in graph),
ϕ = angle at a 100-km height between a perpendicular to the earth and the ray path,
s = 12 month running average sunspot number.

The solar zenith angles were computed by using (1) and taking subsolar points for the fifteenth and thirtieth days of each month from the declination of the sun given in the Nautical Almanac of 1955.

The angle, ϕ, at a 100-km height between a perpendicular to the earth and the ray path was computed from geometrical considerations.

The procedure to be followed in using the graph is indicated in the upper right-hand corner of the graph.

The absorption determinations resulting from the use of this graph differ, on the average, by 1.4 db from the values obtained by using the previous method cited.[1] This average difference was determined as the result of differences arising from sixty comparison checks.

* Manuscript received by the PGAP, November 5, 1956.
† U. S. Navy Underwater Sound Lab., Fort Trumbull, New London, Conn.
[1] P. O. Laitinen and G. W. Haydon, "Analysis and Prediction of Skywave Field Intensities in the High Frequency Band," Radio Propagation Unit Tech. Rep. No. 9; August, 1950.

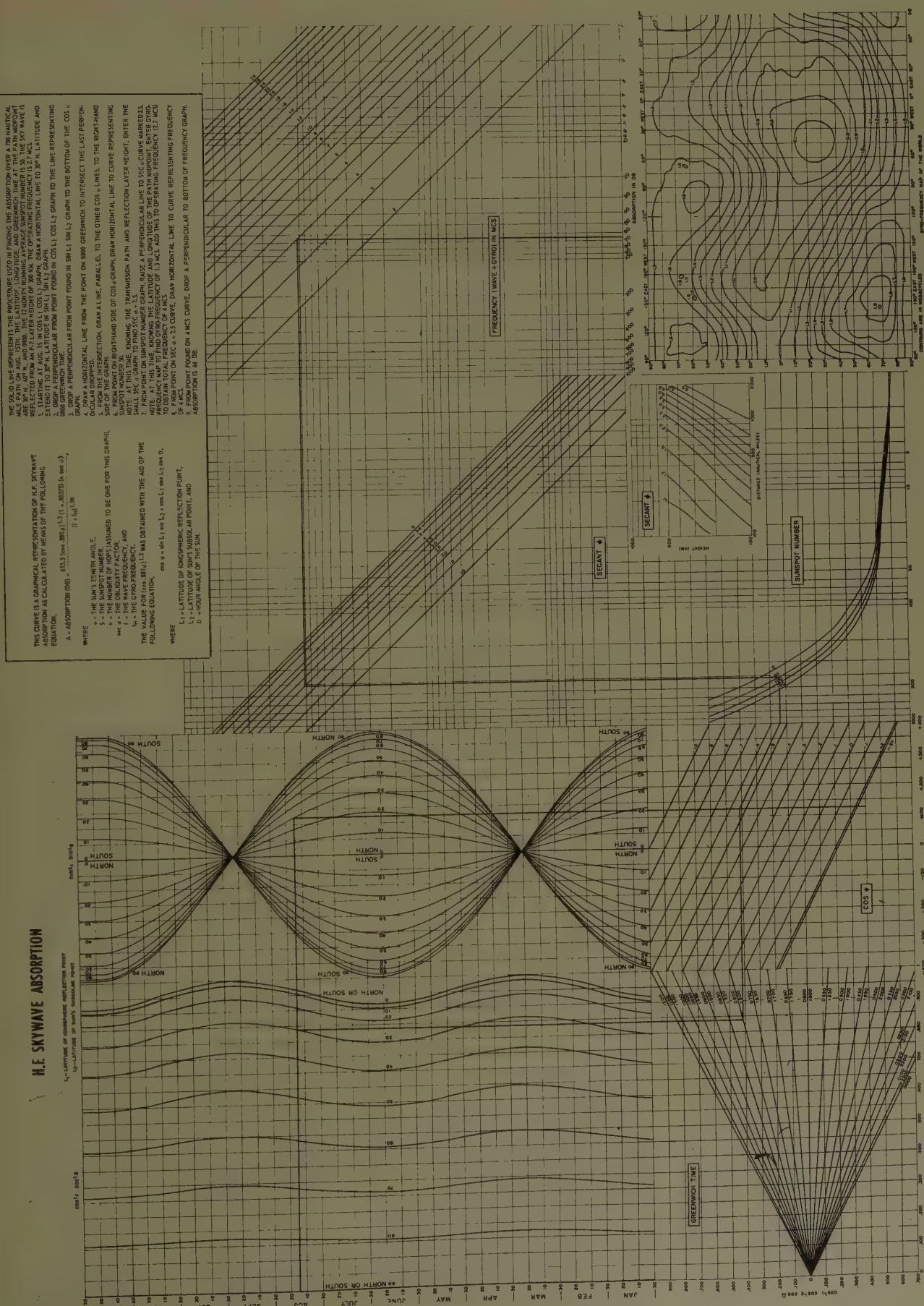
H.F. SKYWAVE ABSORPTION
THE SOLID LINE REPRESENTS THE PROCEDURE USED IN FINDING THE ABSORPTION OVER A 700 NAUTICAL MILE PATH ON JULY 15, 1957. THE LATITUDE AND LONGITUDE OF THE PATH MIDPOINT ARE 30° N., 60° W., AND 0800 GREENWICH TIME AT THIS PATH MIDPOINT. THE 12 MONTH RUNNING AVERAGE SUNSPOT NUMBER IS 50. THE SKY WAVE IS REFLECTED FROM AN F-2 LAYER HEIGHT OF 300 KM. THE OPERATING FREQUENCY IS 2.7 MCS.
1. STARTING AT AUG. 15 IN COS L1 COS L2 GRAPH DRAW A HORIZONTAL LINE TO 30° N. LATITUDE AND EXTEND THIS LINE TO THE SIN L1 SIN L2 GRAPH.
2. DROP A PERPENDICULAR FROM POINT FOUND IN COS L1 COS L2 GRAPH TO THE LINE REPRESENTING 0800 GREENWICH TIME.
3. DROP A PERPENDICULAR FROM POINT FOUND IN SIN L1 SIN L2 GRAPH TO THE BOTTOM OF THE COS ν GRAPH.
4. DRAW A HORIZONTAL LINE FROM THE POINT ON 0800 GREENWICH TO INTERSECT THE LAST PERPENDICULAR DROPPED.
5. FROM POINT OF INTERSECTION, DRAW A LINE, PARALLEL TO THE OTHER COS ν LINES, TO THE RIGHT-HAND SIDE OF THE GRAPH.
6. FROM POINT ON RIGHT-HAND SIDE OF COS ν GRAPH, DRAW HORIZONTAL LINE TO CURVE REPRESENTING SUNSPOT NUMBER 50.
7. FROM POINT ON SUNSPOT NUMBER GRAPH, RAISE A PERPENDICULAR LINE TO SEC ϕ CURVE MARKED 2.5. NOTE: AT THIS TIME, KNOWING THE PATH LENGTH AND HEIGHT OF REFLECTING LAYER, THE SECANT OF THE ANGLE OF INCIDENCE MAY BE FOUND.
8. FROM POINT ON SEC ϕ = 2.5 CURVE, DRAW HORIZONTAL LINE TO CURVE REPRESENTING FREQUENCY OF 4 MCS. ADD THIS TO OPERATING FREQUENCY (2.7 MCS) TO OBTAIN TOTAL FREQUENCY OF 6 MCS.
9. FROM POINT FOUND ON 6 MCS CURVE, DROP A PERPENDICULAR TO BOTTOM OF FREQUENCY GRAPH.
10. FROM POINT FOUND ON 4 MCS CURVE, DRAW HORIZONTAL LINE TO CURVE REPRESENTING FREQUENCY OF 6 MCS. FROM POINT OF INTERSECTION, DROP A PERPENDICULAR TO BOTTOM OF FREQUENCY GRAPH.
11. FROM POINT FOUND ON 6 MCS CURVE, DRAW HORIZONTAL LINE TO CURVE REPRESENTING FREQUENCY OF 6 MCS. FROM POINT OF INTERSECTION, DROP A PERPENDICULAR TO BOTTOM OF FREQUENCY GRAPH.
ABSORPTION IS 64 DB.
THIS CURVE IS A GRAPHICAL REPRESENTATION OF H.F. SKYWAVE ABSORPTION AS CALCULATED BY MEANS OF THE FOLLOWING EQUATION.
A = ABSORPTION (DB) = 615.5 (cos .881ψ)^1.3 (1 + .00375 S sec ϕ) / (f + f_H)^1.98
WHERE
ψ = THE SUN'S ZENITH ANGLE,
S = THE SUNSPOT NUMBER,
ϕ = THE ANGLE OF INCIDENCE, ASSUMED TO BE ONE FOR THIS GRAPH,
n = THE OBLIQUITY FACTOR,
f = THE WAVE FREQUENCY, AND
f_H = THE GYRO-FREQUENCY.
THE VALUE FOR (cos .881ψ)^1.3 WAS OBTAINED WITH THE AID OF THE FOLLOWING EQUATION,
cos ψ = sin L1 sin L2 + cos L1 cos L2 cos D,
WHERE
L1 = LATITUDE OF IONOSPHERIC REFLECTION POINT,
L2 = LATITUDE OF SUN'S SUBSOLAR POINT, AND
D = HOUR ANGLE OF THE SUN.
FREQUENCY (WAVE + GYRO) IN MCS
SECANT ϕ
SUNSPOT NUMBER
COS ψ
GREENWICH TIME
NORTH OR SOUTH
JAN FEB MAR APR MAY JUNE JULY AUG SEPT OCT NOV DEC

Fig. 1.

Abstracts of Papers From the IRE-URSI Symposium Held May 22–25, 1957—Washington, D.C.

Microwave Antenna and Waveguide Techniques Before 1900—J. F. Ramsay, *Canadian Marconi Company*—Between the years 1888, when Hertz first launched electromagnetic radiation in the radio spectrum, and 1900, when Marconi was successfully establishing communication by radio, the scientific investigators of the time turned their attention to microwaves. Later, when it was found that the longer waves were more suited to long-distance communication, interest in the microwaves waned. Between 1888 and 1900, however, microwave devices and techniques had a rich development anticipating much of present-day practice. It is the object of the present paper to review the antennas and waveguides of the period with some reference to the associated microwave techniques then developed.

Apart from Hertz's dipole, with or without a plane reflector, the principal microwave antennas evolved were the cylindrical parabola, the dielectric lens, the waveguide cavity radiator, the radiating iris, and the electromagnetic horn.

Among the waveguides produced were the round, square, and rectangular forms, the open end being used as a radiator. The experimental development of these hollow pipe radiators appears to have anticipated Rayleigh's theoretical paper on waveguides by a number of years, Lodge discovering the mode property experimentally in 1894.

Many of the associated microwave components were of the "free-space" or quasi-optical type, rather than of the constrained or bounded type as common today, since the investigators between Hertz and Marconi were profoundly interested in the representation of optical phenomena at microwave frequencies, Hertz himself being the founder of "microwave optics," a classical subject being revived today.

Thus we find the Hertzians making and using polarized mirrors, "cut-off" metal-plate gratings, quarter-wave and half-wave plates, artificial dielectrics, microwave absorbers, prisms of wax, ice, or liquid filled, or of artificial dielectric, totally reflecting prisms, lenses of sulphur ebonite, wax, pitch, and so on, a wealth of microwave components only partly exploited today.

In the field of systems, measuring arrangements preponderated and included microwave spectrometers, interferometers, diffraction gratings plane or curved, transmission test sets, recorders, polarimeters. With the polarimeter, J. C. Bose established microwave analog physics, with macroscopic models of molecules subjected to microwave radiation. Otherwise, representations of optical phenomena were made with the enormous scale advantage arising from the use of microwaves. The properties of dielectrics, particularly anomalous dispersion, were extensively studied and measured.

All of this microwave work was carried out using spark discharge generators, often of considerable peak power, and with surprising accuracy. For detection many devices were investigated, the most popular being the semiconducting coherer and the gaseous discharge tube.

A New Technique for the Study of Magnetic-Ionic Duct Propagation at Very Low Frequencies*—R. A. Helliwell and E. Gehrels, *Radio Propagation Laboratory, Stanford University*—An experiment has been performed to test the theory that signals from vlf transmitters can be propagated along lines of the earth's magnetic field in the manner of whistlers. The test was made using pulses of one-quarter second duration transmitted from station NSS at Annapolis on 15.5 kc. The signals were observed at Cape Horn, about 10,000 km from the transmitter but close to the transmitter's magnetic conjugate point. The regular "ground-ionosphere" signal was received at all times. At night, about 50 per cent of the time, there was heard a long-delayed echo whose intensity ranged from 10 to 30 db below the regular signal. The measured delay averaged about 0.65 second, closely in accord with whistler delays measured at 15.5 kc at Stanford. Whistlers were usually observed at Cape Horn but were not always present when the NSS echo was detectable.

These results support the theory that vlf signals can be propagated to distant points not only along the ground but also by way of the outer ionosphere in what might be called the magneto-ionic duct. This appears to be the first controlled test giving support of Storey's theory of the path of whistlers and provides a new technique for the systematic study of magneto-ionic duct propagation and the exploration of the outer ionosphere. Details of the results and correlations with whistlers and other phenomena will be described.

We gratefully acknowledge the help and cooperation of Commander Neely and his staff of the Naval Communications Division, Chief of Naval Operations, in providing special pulse transmissions from NSS. We are indebted to General Canas, Colonel Stegmaier, and Dr. Lomnitz of the Chilean AGI Committee for assistance in setting up the receiving station at Cape Horn.

Experimental Investigations of the Angular Scattering and Multipath Delays for Transmissions Beyond the Horizon†—J. H. Chisholm, J. F. Roche, and W. J. Jones, *Lincoln Laboratory, Massachusetts Institute of Technology*—Previous experiments have shown that the potential bandwidth and the antenna performance of tropospheric communications systems depend upon the differential multipath delays occasioned by components arriving over an angular spectrum. A series of experiments is described which utilized 0.25-microsecond pulses at 3670 mc and narrow-beam antennas to measure the differential delay of pulses as a function of simultaneous angular movement of the antennas in azimuth and elevation over a 188-mile path. Similar angular measurements, utilizing 2290-mc cw transmissions have been performed over 188- and 350-mile paths.

In evaluating propagation data for the prediction of system performance, it is difficult to isolate the effective gain realization from the frequency dependence. A series of experiments are described in which transmissions were made over 188-mile and 350-mile paths at 417 mc and 2290 mc during the winter of 1956–1957. Various combinations of antenna apertures were utilized for the 2290-mc transmissions ranging from antenna gain products (G_rG_t) of 32 db to 86 db, relative to isotropic antennas. Simultaneous transmissions were performed over the 188-mile path at 417 and 2290 mc utilizing antennas of approximately equal beamwidths to investigate the degree of frequency dependence relative to free space. Results are given for gain realization for symmetrical and asymmetrical beamwidths for the transmitting and receiving antennas.

The Radio Noise Environment Resulting from Extra-Terrestrial Sources—L. R. Hughes, *Smyth Research Associates*—A preliminary analysis of the statistics of the extremely variable solar radio emissions is described. The results are given as a description of part of the radio noise environment in which high-sensitivity radio communications systems are expected to operate. Data are presented which describe the probability and degree of solar radio interference with the operation of an arbitrary receiving system.

Since further investigations into the detail of extraterrestrial noise interference depend upon a more complete description of the variable solar emissions, the parameters of many of the equipments used to routinely record these emissions are discussed as they relate to this problem.

A Stable High-Q Parallel-Resonant Circuit—J. C. Seddon, *U. S. Naval Research Laboratory*—A new piezoelectric crystal circuit is described which has proven useful in radio receivers and oscillators. Over an appreciable range of frequencies it is equivalent to a parallel LC circuit of high Q and low L/C ratio. As it may be tuned with a parallel capacitor or inductor, the circuit may be used in stable oscillators tunable over a moderate range. The circuit has been used extensively in double-tuned transformers in intermediate frequency amplifiers up to 5 mc. The response curve of a critically coupled 850-kc amplifier is shown where the

* This work was supported in part by the Office of Naval Res. under Contract Nonr-225(27) and in part by a grant from the Natl. Science Foundation.

† The research in this document was supported jointly by the U. S. Army, Navy, and Air Force under contract with the Mass. Inst. Tech.

bandwidth is $\frac{1}{2}$ kc and the bandwidth factor is 4.9. The narrow bandwidth makes possible continuous unattended recordings of atmospheric noise uncontaminated by appreciable man-made signals. Reduced data are shown of atmospheric noise at WSPG, N.M., at a frequency of 4.27 mc illustrating the solar control of transmission at this frequency. A portion of a record taken in the auroral zone at 58°N shows the sudden, extreme variations in noise characteristic of that region at night.

The local oscillator in a 300-cycle bandwidth receiver was replaced by a sawtooth sweep oscillator in order to convert it to a spectrum analyzer. The output of the analyzer when connected to an antenna shows fsk, icw, and cw signals with a sweep of 3.6 kc/cm near $7\frac{3}{4}$ mc.

Electromagnetic Field Theory as Applied to Radio Interference Measurements—W. Jarva, *Filtron Company, Inc.*—Present methods of making radiated radio interference measurements in accordance with military specifications are subject to inaccuracies as great as 40 db. It has only recently been realized that practically all of the seemingly unpredictable variations in measurements are due to the test methods being incompatible with certain types of field which can be emitted by practical interference sources. An exposition of the problem is provided in terms of electromagnetic field theory for distances small compared with a wavelength and suggestions are made for minimizing the effects of present sources of inaccuracy.

The importance of the magnetic field in dealing with general radio interference problems and with shielding problems in particular is becoming increasingly recognized. Procedures which are now being used to calibrate loop antennas of commercial field intensity and radio interference meters do not provide means for making meaningful measurements in the induction field. A discussion is presented concerning the basis of the problem and a more desirable calibration system is suggested.

An All Transistor PDM Telemetry Coder—J. S. Sherwin, *U. S. Naval Ordnance Test Station*—Description of a transistor voltage-controlled delay multivibrator (dmv) and a "clamp" which prevents averaging of the input signal during the information pulse; for use in a 1/10 per cent sled borne pdm telemetry system. The dmv coder utilizes silicon transistors in a circuit which presents a 100-K ohm load to the voltage source, exhibits a linearity of better than 1 per cent, can be calibrated to 1/10 per cent, and has negligible drift. The clamp is in essence a memory circuit which retains, throughout the time of the information pulse, a constant value of signal voltage as read at the incidence of a trigger pulse. The voltage at the memory is transferred to the coder by an emitter follower stage having an input impedance of approximately 10 M ohm in order to maintain the memory voltage within 1/10 per cent of initial value for the longest pulse width encountered. One germanium and three silicon transistors are used in the clamp. The pulse rate generator utilizes a germanium transistor in a blocking oscillator circuit. Pulse rate stability is 1–2 per cent, and the entire system linearity can be calibrated to 1/10 per cent prior to use.

Digital Rate Synthesis—A Method for the Precise Measurement and Control of Frequency—T. J. Rey, *Glen Burnie, Md.*—Digital rate synthesis is a transformation of conventional frequency synthesis (beat methods) from the frequency to the time domain; pulse techniques take the place of filtering and mixing.

The signal whose period is to be measured or controlled is in the form of pulse train no. 1. A single reference source drives a rate generator, which consists of one or more dividing stages in fixed cascade; train no. 2 from the generator is a sequence of nonuniformly spaced pulses, the average repetition rate of which is known from the independently controllable connections between the individual stages and the no. 2 bus.

A rate difference detector compares the rate of no. 1 with the average rate of no. 2. The smoothed detector output has the proper sign and serves to indicate the magnitude of the difference, or to reduce the difference in a closed loop.

The range of direct operation is limited by pulse techniques, but can be extended with the aid of beat methods. In the application to frequency control, digital and conventional synthesis can be combined with phase-locking methods to stabilize an oscillator over a practically unlimited band of frequencies, with a precision and purity approaching that of the reference source.

Data Reduction Equipment for a "Forward Scatter" Link—D. Eadie, *University of Florida*—It is expected that a great deal can be learned about the mechanism of tropospheric scatter propagation from studies of the amplitude distribution of the rapidly fluctuating component of the signal level. The average signal or long time trend must be extracted first in order that the amplitude distributions are centered on this average level.

Equipment which will automatically extract this long time trend of the average signal level and at the same time determine the amplitude distribution of the rapidly fluctuating component has been put into operation at Orange Hill on New Providence Island, Bahamas, by the University of Florida group studying this phenomena. Both continuous wave and pulsed signals can be analyzed. The distributions, which are obtained in real time and in cumulative form, are simultaneously printed on adding machine tape and punched on paper tape.

A block diagram of the equipment is presented. Briefly, the average trend level is extracted by adjustment of an attenuator in the receiver. The setting of this attenuator is one of the data inputs to the printout system.

The distribution of the fluctuating component is determined by sampling the signal at thirty different amplitude levels. If the signal amplitude exceeds each particular level, pulses are admitted to the accumulator for that particular level; consequently, thirty accumulators are required for the thirty levels.

A distribution is obtained by analyzing one thousand samples of the signal level. A gate, located between the receiver and the amplitude level sorters, is opened by a "starting" pulse and closed by the output pulse from a one-thousand count preset counter. The output pulse from this counter also starts the print-out cycle. The printer-punch records the following information: 1) the time of day, 2) the attenuator setting, and 3) the data stored in the thirty levels of the accumulator.

The level sorters are of special design. The accumulators, preset counter, etc., employ dekatron glow tubes. The gate, linear amplifier, and switching control employ, in many cases, packaged circuits. The design has been a joint effort between the Baird Associates-Atomic Instrument Co. and the University of Florida. The bulk of the equipment has been built by Baird-Atomic. The printer-punch will be furnished by Clary Corporation.

The equipment began limited operation in November, 1956. Further improvements are presently being made. Examples of data print-out are described. Punched information on the tape can be transferred to IBM cards for further analysis in the IBM 650 computer located at Gainesville.

Future plans call for the design and installation of an automatic servosystem of novel design for setting the attenuator. This will release the operator of the necessity of manually adjusting the present remotely controlled attenuator unit.

A Recent NRL Rocket Measurement of Ionospheric Electron Densities—J. A. Kane and J. E. Jackson, *U. S. Naval Research Laboratory*—Electron densities in the ionosphere above White Sands, N. M., were measured continuously from the E region up to the lower F_2 region with the Aerobee-Hi NRL-50. The results are in agreement with previous NRL flights, namely, the daytime ionosphere remains dense between the E and F_2 regions, with only minor valleys in the electron-density profiles.

The NRL rocket technique for obtaining the ionospheric electron densities provides eight externally independent profile measurements. These eight measurements arise from the fact that the Doppler frequencies for both polarization components of a continuous wave are measured at two ground stations during both the ascent and descent of the rocket.

Corrections due to the effects of a nonvertical propagation path have been calculated. In the altitude region between 160 and 260 km, a comparison of the eight independent electron profile measurements after these correction terms have been applied reveals variations of a random nature of the order of 5 per cent. In the absence of any additional large systematic errors, the 5 per cent random variation indicates the upper limit to which the experiment in the region above 160 km could be affected by ionospheric irregularities.

Electron Distribution in a New Model of the Ionosphere—H. K. Kallmann, *Institute of Geophysics, University of California at Los Angeles*—A theoretical analysis of the formation of the ionosphere has been made which has led to a new model of the ionized regions between 90 and 300 km above the earth's surface. The study is based primarily on a new model of pressure, density, and temperature distributions,* derived from rocket

* H. K. Kallmann, W. D. White, and H. E. Newall, *J. Geophys. Res.*, vol. 61, p. 513; 1956.

observations, as well as on the Chapman theory of ionized layer formation. Some of the simplifying assumptions, usually made in evaluating this theory have been eliminated. As a result, a picture of the ionosphere has been obtained which agrees rather well with the experimental results obtained by means of rockets.* These results show that the ionosphere does not consist of ionized layers but rather of continuously densely ionized regions, except for the bottom of the E region. Furthermore they show that the true height of reflection of radio waves is considerably lower than the apparent height. the difference being as much as 340 km in the F_2 region. The calculations were carried out on the high-speed digital computer at the Rand Corporation.

Differential Absorption in the D and Lower-E Regions—J. C. Seddon, *U. S. Naval Research Laboratory*—The measurment of the absorption of radio waves in the ionosphere with the aid of rockets has proven to be surprisingly difficult. However, a new method has been devised for measuring differential absorption of a wave transmitted from the rocket to a ground station. This method involves the measurement of the amplitude of the signals received on two crossed dipoles as the rocket rolls about its long axis. A maximum signal on one antenna with a simultaneous minimum on the other provides the values of the sum and differences of the two magneto-ionic components from which the ratio of the extraordinary component to the ordinary component may be calculated, and from this the differential absorption $T_x - T_0$. Measurements of these quantities were made at 7.75 mc on June 29, 1956, at 12:09 MST using an Aerobee-Hi Rocket. No appreciable differential absorption was noted until an altitude of 88 km was attained. The differential absorption then increased slowly to 94 km, where it then increased rapidly to a value of one half per kilometer at 96 km. The appearance of the previously-reported additional components with approximately unity index of refraction prevented measurements at higher altitudes.

As a high frequency of 46.5 mc is also transmitted from the same antenna, the measurement of the relative rotation of the plane of polarization of the 7.75-mc signal provides a means of measuring electron densities as low as 1000 el/cc. The electron density first became noticeable at 75 km, and showed a very sharp increase at 86.5 km. The results then obtained at higher altitudes agree with those obtained by the usual NRL method where the beat frequencies are large enough to be measured.

The Effect of Various Radiations on the E Layer of the Ionosphere †—R. E. Houston, Jr., *Ionosphere Research Laboratory, The Pennsylvania State University*—In the course of recent rocket flights, experimental values for the intensity of incoming radiations in the far ultraviolet and X-ray regions have been obtained. During this same interval, experimental values of absorption cross sections for radiations in the same wavelength regions have become available. Utilizing these values, the contribution to the electron density of the ionosphere due to Lyman alpha, Lyman beta, and X rays is calculated. The resulting electron distribution is compared with rocket, 75 kc and 150 kc pulsed, vertical incidence radio wave, and other radio propagation results.

Measurement and Interpretation of Tidal Effects in the Equatorial Ionosphere—G. J. Gassmann, *Ionospheric Physics Laboratory, Geophysics Research Directorate, Air Force Cambridge Research Center*—Sequences of ionospheric records taken on individual days simultaneously by several equatorial stations and by airborne equipment are analyzed with respect to layer heights, ion densities, and other features. The obtained ionospheric cross sections show the pronounced effect of the solar air tide. The interpretation of the measurements indicates that the solar tidal current system varies considerably from day to day in strength and location and reveals that the usual statistical treatment of ionospheric and magnetic data will obscure or diminish these effects.

Inclusion of the Earth's Magnetic Field in a Simple and Rapid Method for Reducing h'-f Curves to Electron-Density-Height Profiles*—E. R. Schmerling, *Ionosphere Research Laboratory, The Pennsylvania State University*—The simplest technique for reducing h'-f curves to electron-density-height profiles, without making assumptions about profile shape, is due to Kelso.† In his method the magnetic field is neglected, and the h'-f curve is sampled at fixed multiples of the frequency f_v at which the true height is desired, this height being obtained simply by taking the average of the sampled h' values. If the field is included, Kelso's method of deducing sampling points breaks down. In a method due to Budden,‡ true heights can be derived, including the magnetic field, by a matrix multiplication, in which the matrix coefficients are all different. A method is described for deducing sampling frequencies from the coefficients of the Budden matrix, such that the simplicity of Kelso's approach is retained. Different ratios of f_v are required for different magnetic latitudes, and the ratios change slowly with f_v. The variation is slow enough for the h'-f curve to be divided into about 3 parts, in each of which the true reflection height is given by sampling at fixed ratios of f_v, and taking the average of the h' values. Once the sampling ratios are found, the reduction of h'-f curves proceeds simply and rapidly without further computing aids.

On the Measurement of Virtual Height[1]—I. Kay, *New York University, Institute of Mathematical Sciences*—A time dependent definition of the virtual height of a reflected wave train is suggested. This definition is such that its accuracy increases as the width of the incident pulse increases. Moreover, it is theoretically possible to obtain an estimate of the virtual height with as small an error as desired to matter what the nature of the reflecting medium.

Suppose an incident pulse having width W and a carrier frequency ω_0 produces a reflected wave which, when measured at a fixed point $x=0$ in space, is $R(\omega_0, W, t)$. The suggested definition of the virtual height $h'(\omega_0)$ is

$$h'(\omega_0) = c \lim_{W\to\infty} \frac{\int_{-\infty}^{\infty} t\,|R(\omega_0, W, t)|^2 dt}{\int_{-\infty}^{\infty} |R(\omega_0, W, t)|^2 dt},$$

where c is the free space velocity of light. This relation for $h'(\omega_0)$ holds for any physically reasonable incident wave train and is independent of its envelope shape.

An example is given of a reflected wave whose virtual height cannot be determined by inspection in the usual manner. The expression given here for the virtual height provides the correct result.

Some Solar Observations with the Cornell Narrow-Band Radio Polarimeter—M. H. Cohen and E. R. Schiffmacher, *Cornell University*—A correlation type radio polarimeter has been constructed at the Cornell Radio Observatory. The center frequency is 201.5 mc; bandwidth, 9 kc; antenna, a 17-foot paraboloid with crossed dipoles diplexed to give simultaneous right and left circular components. The instrument has been in partial operation since December 15, 1956, and observations have been made of the sun on both quiet and active days. This instrument has a substantially narrower bandwidth than the polarimeter used by Hatanaka *et al.** (100 kc at 200 mc), and the polarization measuring interferometer used by Payne-Scott and Little† (150 kc at 97 mc), but to date no significant bandwidth effects have been observed. In particular, many unpolarized bursts have been seen, some of them in time association with small flares. Several outstanding events with polarizations changing rapidly with time have been recorded.

A Further Analysis of a Solar-Terrestrial Correlation—K. Toman—In a previous paper‡ the distribution in time of a 180-pair correlation coefficient of daily values of the final Zurich sunspot member Z and the planetary K-index, ΣK_p, was reported.

With this paper, the r distribution has been completed and extended to cover the period from 1940 to 1954. Correlation intervals were successively advanced by ten days.

For the same period and with ten-day separations, correlograms were successively obtained lagging the data of Z and ΣK_p with respect to each other so as to include more than one solar rotation. Time displacements and magnitudes of optimum correlation coefficients are interpreted. The solar rotational period is analyzed and the correlogram technique is evaluated. Positive and negative correlation coefficients are discussed in terms of the longitudinal distribution of sunspots and M regions.

* J. S. Seddon, A. D. Pickar, and J. E. Jackson, *J. Geophys. Res.*, vol. 59, p. 513; 1954.
† The research reported in this paper has been sponsored by the Geophys. Res. Dir. of the AF Cambridge Res. Center, Air Res. and Dev. Command, under Contract AF19(604)-1304.

* The research reported in this paper has been sponsored by the Geophys. Res. Dir. of the AF Cambridge Res. Center, Air Res. and Dev. Command, under Contract AF19(604)-1304.
† J. M. Kelso, *J. Geophys. Res.*, vol. 57, p. 357; 1952.
‡ K. G. Budden, "The Physics of the Ionosphere," Report on Phys. Soc. Conference, p. 332; 1955.
[1] The research reported in this article has been sponsored by the AF Cambridge Res. Center, Air Res. and Dev. Command, under Contract No. AF 19(604)-1717.

* Hatanaka, Suzuki, and Tsuchiya, *Proc. Japan Acad.*, vol. 31, p. 81; 1955.
† Payne-Scott and Little, *Aust. J. Sci. Res.*, vol. 4, p. 508; 1951.
‡ K. Toman, "A Solar-Terrestrial Correlation," presented at the URSI Meeting, Berkeley, Calif.; October 11–12, 1956.

Fluctuations in the Apparent Amplitude and Position of Extra-Terrestrial Radio Sources, as Observed near the Auroral Zone*—J. M. Lansinger, C. G. Little, R. P. Merritt, and E. Stiltner, *Geophysical Institute of the University of Alaska*—Continuous-tracking phase-switch interferometer systems have been set up on 223 mc and 456 mc at the Geophysical Institute of the University of Alaska, College, Alaska, to observe the fluctuations in amplitude and position of localized extraterrestrial radio sources ("radio stars"). The equipment parameters and experimental procedures are described and examples of the records obtained are presented. Analysis of the first data shows that the amplitude variations are typically less than ±2 db at 223 mc and ±1 db at 456 mc. The extreme variations observed during the strongest scintillations in amplitude range from +5 db to −14 db (223 mc) and +2 db to −4 db (456 mc). Although the irregular angular deviations are typically less than the minimum detectable value (approximately 0.25 minutes of arc), irregular deviations of as much as 3.5 minutes of arc at 456 mc have been observed. These preliminary observations are in general agreement with the expected λ^2 dependence of ionospheric refraction.

X-Ray Flares and Sudden Ionospheric Disturbances—T. A. Chubb, H. Friedman, and J. E. Kupperian, Jr., *U. S. Naval Research Laboratory*—When the sun is quiet, *D* region is ionized by the hydrogen Lyman Alpha line (1215.7A). During a solar flare, the *D*-region ionization is increased with resulting SID. It has been proposed that Lyman Alpha is also responsible for the increased ionization produced by the flare. However, sudden phase anomalies and magnetic crochets cannot be explained satisfactorily by Lyman Alpha alone. An X-ray flare offers a better explanation of these phenomena.

During the summer of 1956 a rocket was launched during a Class I flare and both Lyman *a* and X rays were measured simultaneously. Ten minutes after start of the flare Lyman Alpha had returned to normal, but a strong X-ray flux was still present in *D* region with a short wavelength limit between 3A and 4A.

Antenna Resolution as Limited by Atmospheric Turbulence—C. M. Angulo, *Brown University*, and J. P. Ruina, *University of Illinois*—Spatial variations of the index of refraction of the atmosphere introduce fluctuations in the phase and amplitude of a wave propagating through it. The effect of these fluctuations on the resolution capability of microwave antennas is discussed in this paper. The measure of resolution used in the calculations is the beamwidth which is defined as the square root of the second moment about the mean of the normalized antenna pattern. This measure simplifies the calculations greatly and results in a simple expression for the beam broadening due to the variation of the refractive index. This broadening is dependent on the distance to the target, the scale of the turbulence, and the variance of the refractive index, and is relatively insensitive to the shape of the spatial correlation function of the refractive index. Measurements by others of the nature of the refractive index spatial variation are then used to obtain numerical estimates of the ultimate resolution capability of a microwave antenna as limited by atmospheric turbulence.

* This work was sponsored by the Rome Air Dev. Center, Air Res. and Dev. Command, under Contract No. AF 30(635)-82887.

On Multiple Scattering of Waves by Plane Bounded Volume Distributions—V. Twersky, *Sylvania Electronic Defense Laboratory*—This paper gives an approximate theoretical treatment for a plane wave exciting a "uniformly random" distribution of fairly arbitrary scatterers in a volume of space bounded by two parallel planes. Coherent multiple scattering is taken into account to obtain simple approximations of the coherent transmitted, reflected, and internal fields; these forms also hold approximately for a "one mode" treatment of a periodic array of close spaced scatterers, provided the scattering parameters of the isolated elements are stripped of radiative loss terms. Corresponding approximations are obtained for the "differential scattering cross section per unit volume" (*i.e.*, the incoherent scattering), and for the "differential scattering cross section per unit area of face plane." The parameters of the final results are the average number of scatterers in unit volume, the thickness of the "equivalent slab," the angle of incidence, the presumably known scattering amplitudes of the isolated elements, etc. This work generalizes an earlier treatment* by using a simplification of the formalism of Foldy† and Lax.‡

A New Approach to Diffraction of High-Frequency Waves by Ellipsoids of Revolution—N. A. Logan, *Antenna Laboratory, Air Force Cambridge Research Center*—The cartesian components of the electromagnetic field in a rotationally symmetric coordinate system with an element of arc length

$$ds^2 = h_1^2 du^2 + h_2^2 dv^2 + \rho^2 d\phi^2$$

are expanded in a Fourier series with respect to the angle ϕ.

The Fourier coefficients are expanded in terms of an infinite series of solutions of the scalar wave equation in which coefficients are determined by the boundary conditions on the surface of a diffracting obstacle and the radiation condition at infinity. The formidable problem presented by rigorous determination of these coefficients can be avoided by using certain physical concepts together with the present formulation to extract a solution that is valid for high frequencies. For points not too close to the polar axis the solution is expressed in terms of the solutions of the scalar wave equation satisfying the conditions

$$u = 0 \quad \text{and} \quad \frac{\partial}{\partial n}(\rho u) = 0$$

on the surface of the obstacle. The caustic near the polar axis is examined and the solution then extended to include points near the axis. The application of this approximate method of solution to the case of spheres with $ka = 10$ and $ka = 20$ leads to results in close agreement with the exact solution.

Effects of Satellite Spin on Ground-Received Signals*—J. T. Bolljahn, *Stanford Research Institute*—The man-made satellites to be launched during the International Geophysical Year will each be equipped with an antenna in the form of a crossed dipole pair driven in phase quadrature. A spin at a rate of the order of 3 cps is to be imparted to the satellite prior to separation from the launching vehicle. Because of the dissymmetry of the forces applied to separate the satellite from the final rocket stage, it is expected that the spin axis will not remain aligned with the axis of symmetry of the antenna.

This paper describes the nature of the signal received in ground antennas having various polarization characteristics from the spinning satellite for arbitrary angles between the satellite spin axis and its axis of symmetry and for arbitrary observation angles. It is found that, in general, three signal components are received consisting of the original carrier frequency plus an upper and a lower sideband spaced from the carrier by the spin frequency. In experiments which require counting rf cycles in the received composite signal, spin errors will be produced for some combinations of ground antenna polarization, spin axis orientation, and observation angle.

An Analytical Study of Scattering by Thin Dielectric Rings†—L. L. Philipson, *Hughes Aircraft Company*—An analysis of the scattering effect of a thin dielectric ring on an electromagnetic field is developed in a rigorous manner under two assumptions: the incident field is the free space field of the source, and the scattered field tends asymptotically to zero as the radial thickness of the ring approaches zero. When an integral equation of Barrar and Dolph,‡ derived directly from Maxwell's equations, is employed, a formal expansion of the field in powers of the thickness is obtained, and then it is proved that the linear approximation obtained from it is indeed asymptotically equal to the total field. The sufficiency of this approximation is justified by experimental evidence. The far-zone pattern function of the ring is next obtained, and the resulting formulas are applied to the situation where the incident field is generated by a dipole antenna coaxial with the ring for which experimental comparisons are possible.

Perturbation Method for Calculating Diffraction by an Almost Ideal Obstacle—C. B. Shaw, Jr., *Hughes Aircraft Company*—A perturbation method has been developed for treating the diffraction problem of an arbitrary electromagnetic field incident from an exterior region on a dielectric medium, which is assumed to constitute an "almost ideal" obstacle. An "ideal" obstacle is one for which the diffraction problem can be solved; "almost ideal" implies that the

* V. Twersky, "Multiple Scattering of Waves by a Volume Distribution of Parallel Cylinders," Inst. of Math. Sciences, New York Univ. Res. Rep. No. EM-59; October, 1953.

† L. L. Foldy, "The multiple scattering of waves," *Phys. Rev.*, vol. 67, pp. 107–119; February, 1945.

‡ M. Lax, "Multiple scattering of waves," *Rev. Mod. Phys.*, vol. 23, pp. 287–310; 1951.

* The work reported herein was sponsored by the Ballistic Res. Lab., U. S. Army Ordnance, under Contract DA 04-200-ORD-273.

† Extracted from Tech. Memo. No. 416, Res. Lab., Hughes Aircraft Co.; January 3, 1956.

‡ R. B. Barrar and C.L. Dolph, "On a three-dimensional transmission problem of electromagnetic theory," *J. Rational Mechanics and Analysis*, vol. 3, pp. 725–743; November, 1954.

actual (perturbed) obstacle produces a diffracted field not differing too greatly from that of the ideal. Comparison of integral equations for the total fields in the ideal and almost ideal cases establishes a series expansion of the perturbed field, each term of which has a straightforward physical interpretation. When the almost ideal obstacle differs from the ideal only by the presence of a cavity of dimensions small in terms of wavelength, the first-order perturbation formula can be given a quite simple form, particularly useful when the ideal diffraction problem has been solved for plane waves incident at certain angles. Discussion will cover the detail in which the solution of the ideal problem must be known in order to apply the perturbation method, and an example of its use in studying transmission of a plane wave through a plane dielectric sheet containing a small cavity.

An Analysis of the Time and Space Scale Problems in Radio Meteorology—A. Engelman and L. Colin, *Rome Air Development Center*—The problems of where and how often to sample the atmosphere in order to determine optimum time and space instrumentation scales is attacked. For the determination of the refraction at an initial elevation angle of 13°, three rawinsonde sites were installed over a forty-mile range from Syracuse to Rome, N. Y. In addition, teletype information for several other northeastern United States sites was used in the analysis. The data is reduced into index of refraction as a function of height profiles and then integrated by planimeter. Comparisons between a simply defined index profile and one derived properly by isoplething in the *X-Z* direction is discussed. Use is also made of analog computation of the refraction correction.

It is concluded from this investigation, that if one eliminates the large scale differences in surface values of the refractive index, the space scale factor is at least greater than forty miles. With a similar restriction the time scale factor is about six hours. Removing the ground measurement qualification a time delay of about three hours may be used as the scale.

A 216-Mile 2700-MC Scatter Link—L. H. Doherty, *National Research Council (Canada)*—An experimental 2700-mc radio link was in operation between Ottawa and Toronto for the period April, 1955, to December, 1956. Yearly median level was 80 dbm. Monthly median signal during the best summer month was about 12 db above the median for the poorest winter month. The signal was usually Rayleigh distributed, but departures from this distribution were observed at all median levels. Average fading rate was approximately 1 cps with extremes at one fifth and five times this frequency.

Measurements made with antennas of apertures of 4, 8, 12, 16, and 20 feet show an increase in aperture to medium coupling loss with increasing size. It is also observed that fading rate decreases with increasing antenna size.

A Statistical Model for Forward Scattering of Waves Off a Rough Surface*—L. M. Spetner, *The Johns Hopkins University*—Using methods of physical optics, a statistical description of the scattering of waves off a rough surface is obtained. The rough surface is assumed to consist of a large number of independent point scatterers which fluctuate randomly in vertical position and also disappear and appear at random. The surface is divided into cells so that no more than one scatterer can occupy a cell, and the events in any two different cells are independent of each other. The average scattered signal, the mean square fluctuation, and the time covariance of the fluctuating portion of the signal are computed in terms of the mean square scatterer height, the grazing angle, the radiation wavelength, the decay time for disappearance of scatterers, the time autocorrelation of a scatterer height, and the *a priori* probability of finding a given cell occupied by a scatterer.

* This work was supported by the Bureau of Ordnance, U. S. Navy, Contract NOrd 7386.

High Altitude VHF Tropospheric Field Strengths Measured to Great Distances Beyond the Radio Horizon—L. A. Ames, N. L. Conger, J. W. Frazier, E. J. Martin, and T. F. Rogers, *Air Force Cambridge Research Center*—The overwater airborne measurement of 220-mc field strengths is continuing at the Air Force Cambridge Research Center. Improvements in equipment have permitted these field strengths to be recorded beyond 600 statute miles. Also, the employment of a B-29 aircraft enabled measurements to be obtained at altitudes very near the tropopause in the winter of 1955–1956.

Data have now been gathered for heights between 500 and 30,000 feet. Certain conclusions may be drawn relative to the general behavior of signal level as a function of both distance and height over a smooth earth. In particular, a simple picture is drawn of the height-gain function for great heights. Simultaneous flights were made at 3000 and 30,000 feet verifying this picture.

Investigation of Long-Distance Overwater Tropospheric Propagation at 400 MC*—H. E. Dinger and W. E. Garner, *U. S. Naval Research Laboratory*; D. H. Hamilton, Jr. and A. E. Teachman, *M.I.T., Lincoln Laboratory*—The Naval Research Laboratory in cooperation with the M.I.T. Lincoln Laboratory conducted an investigation of overwater tropospheric propagation under both summer and winter conditions. The transmissions were from the M.I.T. Round Hill Field Station near New Bedford, Mass., to a vessel traveling along great circle courses extending to a maximum distance of 630 nautical miles (724 statute miles) from the transmitter.

During July, 1955, a 10-kw, 385.5-mc transmitter was used with a 28-foot paraboloid antenna. In January, 1956, the same transmitter was used, supplemented by a 40-kw transmitter feeding a 60-foot paraboloid for use at the greater distances. The frequency used for the winter period was 412.85 mc. Aboard ship the receiving antenna consisted of a 17-foot paraboloid, directionally controlled from the ship's gyro. Horizontal polarization was used throughout.

The data obtained are presented to show 1) the median signal level vs distance for the powers used, and 2) the median path loss vs distance for the case of antennas which were approximately 100 feet above the earth's surface. The data appear to show that the attenuation rate was variable with distance. The signals were also analyzed with respect to fading characteristics in an attempt to predict the median level to be expected in the absence of superrefraction. For this purpose, signals with a short-time fading characteristic, which was well represented by a Rayleigh distribution, were used. Fast-fading Rayleigh-type signals prevailed a higher percentage of the time during the winter than during the summer, and in general, were accompanied by windy weather. Meteor bursts were observed and recorded at 600 statute miles from the transmitter.

* Part of the research in this document was supported jointly by the U. S. Army, Navy, and Air Force under contract with the Mass. Inst. Tech.

Flight Measurements of Transmission Loss at 38.5 MC—I. H. Gerks, *Collins Radio Company*—Measurements have been made of field strength as a function of distance at 38.5 mc over a distance range of 0 to about 1100 miles. The transmitter is rated at 20-kw carrier level or peak envelope power. Radiation is either cw or SSB modulation. The transmitting antenna is a 4V antenna with a gain of 19 db over a dipole. The receiver is specially designed for SSB and cw reception. The bandwidth is either 4 kc or 70 cps. The receiving antenna is a *V* mounted on a Beechcraft airplane in such a manner as to give a favorable directional pattern.

Enough flights have been made to obtain a fairly reliable sampling of the field strength over the entire distance range. It was found that F-layer propagation caused severe contamination of the scatter signal quite regularly during daylight hours. Later results were obtained at night. Most flights have been made at 5000-feet elevation. Results are also reported on SSB voice quality, height gain in the ionospheric scatter region, and cross-course field distribution.

An Experimental Investigation of Ionospheric Forward Scattering at HF—D. A. Hedlund and L. C. Edwards, *Raytheon Manufacturing Company*—The results of cw field strength measurements in the 20–30 mc band over a 1350-km East-West path are presented. Measurements have been made almost continuously since September, 1956, up to the present time. Operation in this frequency band during a peak period of the sunspot cycle has allowed comparison of ionospheric scatter and normal *E* and F_2 layer transmission. Long term variations in received signal level and short term fading characteristics are described.

Two-way pulse tests have been conducted over the same path in an attempt to locate the scattering region more accurately. Measurements made over several 24-hour periods indicate no significant diurnal variation in transmission time of the scatter mode. Interpretation of these transmission time measurements in terms of midpoint scattering leads to heights approaching 100 km; however, if scattering from points off the great circle path, such as might be produced by meteors, is considered, lower heights are indicated. A comparison of these two possibilities for the system in use is presented.

On the Reception of HF Waves Above the Classical MUF*—M. Balser, *M.I.T. Lincoln Laboratory*—Several observers have noted that when an (h', f) curve is recorded

* The research in this document was supported jointly by the U. S. Army, Navy, and Air Force under contract with the Mass. Inst. Tech.

using a remote swept-frequency transmitter, a "nose" appears on the curve, extending beyond the muf expected from the meeting of high and low rays or determined from a midpath vertical sounding. It is tentatively proposed that this phenomenon can be explained simply on the basis of geometrical optics. It is well known that random variations in the index of refraction cause random departures from the mean ray paths determined by the smooth medium, and that inhomogeneities in the electron density of the ionosphere cause such variations. The order of magnitude of the departure from the mean path can be estimated from angle of arrival experiments as a couple of degrees. Departures of this amount from the mean path of a skip ray could produce reception at points within the skip distance for which the classical muf may be of the order of a megacycle lower.

The Reflection-Scatter MUF—E. Warren and L. Hagg—In the past few years the Defense Research Telecommunications Establishment has carried out preliminary measurements using oblique incidence ionospheric sounders.

It has been found that the highest practical frequency for high-frequency sky-wave propagation is that above which the mechanism of propagation by reflection plus scatter becomes inefficient. This frequency is, on the average, more than fifteen per cent higher than that predicted by the transmission slider method. An empirical scaling method has been devised and a theoretical explanation is presented.

A Fading Origin Experiment for Radio Waves Reflected from the Ionosphere*—T. N. Gautier, R. S. Lawrence, W. F. Utlaut, and B. Wieder, *National Bureau of Standards*—The fading of radio wave pulses transmitted via one-hop reflection from the ionosphere between a transmitter and a receiver located 6 km apart has been correlated with the fading of pulses at the same radio frequency transmitted by vertical incidence reflection between a second transmitter and receiver located at the midpoint of the 6-km path. It is argued that if scattering is introduced mainly at or near the level of reflection, the diffraction pattern around the first receiver in the waves from the first transmitter should be nearly identical with the diffraction pattern around the second receiver in the waves from the second transmitter. Thus, the fading of the pulses transmitted over the slightly oblique path should be well correlated with the fading of the pulses transmitted over the vertical incidence path. On the other hand, a lack of correlation would strongly imply that the scattering was taking place well below the level of reflection.

Beginning in October, 1956, a number of pairs of fading records have been made at frequencies between 2.5 mc and 6 mc, during daytime and at night. During daytime, frequencies below about 3.5 mc were reflected from the E layer, while higher frequencies were reflected from the F layer. At night all frequencies in this range were usually reflected from the F layer, although occasionally the lower frequencies were reflected by sporadic E. In a large majority of the cases of E-layer reflection the fading was well-correlated. In all cases of F-layer reflection the fading was poorly correlated. In one instance at night successive records were made at the same frequency, first of the fading of a sporadic E echo and then of the fading of the echo from the F layer seen through the sporadic E. The sporadic-E fading was well-correlated, but the fading of the F-layer echoes were poorly correlated. We conclude that in nearly all cases the fading of F-layer echoes was caused by scattering well below the level of reflection, possibly in the E region.

A variation of the experiment is being carried out to locate the height at which the scattering occurs. This involves two paths to the ionosphere which intersect at a level which can be varied by moving one of the receivers.

These results, of course, will have important implications for the interpretation of drift measurements by the fading method.

A Theory of Radio Star Scintillation Based on Ionospheric Turbulence—H. G. Booker, *Cornell University*—On the basis of the model of a turbulent ionosphere previously presented by Booker,* calculations have been made concerning the effect of ionospheric turbulence on the amplitude and phase of signals from discrete sources of cosmic radio noise. For a magnetic dip of $\pm 60°$, results are as follows:

1) There seems no possibility of star scintillation occurring above the level of maximum electron density in the F region if scintillation is caused by ionospheric turbulence.

2) It is unlikely that even the under side of the F layer plays a major part in star scintillation since the size and shape of the possible irregularities are inappropriate and the diurnal variation is incorrect.

3) The fluctuations in absolute phase at ground level are introduced primarily on the under side of the E layer and should have a diurnal variation with a maximum shortly after midday. It should be remembered, however, that the fluctuations in absolute phase are not what are measured in practice.

4) For the reasons given by Hewish,† the fractional amplitude fluctuations are less than the absolute phase fluctuations. However the extent of this reduction varies radically with height in a way not considered by Hewish. Amplitude fluctuations due to irregularities at E-region levels are drastically curtailed because the macroscale of irregularities at this level is so large. Above about 140 km, however, the earth's magnetic field greatly reduces the size of the electronic irregularities measured in the direction perpendicular to the field, and this greatly reduces the Hewish suppression factor above about 140 km. The upshot is that the interval of height between the E and F regions plays a major role in causing amplitude fluctuations even though fluctuations in absolute phase are produced primarily on the under side of the E region.

5) The strength of the amplitude fluctuations depends to a large extent on the "potential" gradient of electron density between the E and F regions (that is, the gradient corrected for adiabatic variation of density with height). The night time maximum of star scintillation can therefore be explained qualitatively if the height interval that is responsible for amplitude fluctuations is on the top side of a well-developed E layer during the daytime but on the tail of the F layer at night.

6) The order of magnitude of the amplitude fluctuations predicted by the above model is very roughly in accordance with observations and can be adjusted by reasonable changes in the model. The same is true for the size and shape of irregularities.

This theory of radio star scintillation carries with it the implication that the fading of hf radio waves reflected from the F layer is largely due to multiple scattering below the F layer, and that "spread F" is due to an unusually large amount of multiple scattering between the E and F regions.

Post-CMP Geomagnetic Effects of Solar Event-Producing Regions—M. B. Wood, *National Bureau of Standards*—Solar regions which produce noise in time association with flares and regions which produce importance 3+flares unsorted as to radio burst productivity have been studied in terms of geomagnetic effects. Post-event effects and post-central meridian passage (cmp) effects of the event-producing regions have been compared. The results indicate that 1) in general the post-cmp geomagnetic effects are as strong as the post-event effects and 2) 460 mc radio burst-flare events are as strongly associated with geomagnetic disturbances as are 200-mc flare events, both in terms of post-event effects and post-cmp effects.

Radar Scattering by Meteor Trails—H. Brysk, *University of Michigan*—The scattering of radar waves by "underdense" meteor trails has been calculated in detail. It is found that the restriction to the precisely specular case can be seriously misleading (in the absence of diffusion it leads to an upper bound to the scattering intensity; where diffusion is considerable, it has led to wrong conclusions). The effects of the beam pattern (*e.g.*, sharp cutoff, Gaussian) and of non-turbulent diffusion have been examined. In the case of velocity measurements based on the diffraction pattern, it is found that although the theoretical analysis that has been used is questionable the results are essentially valid.

Radar Echoes from Overdense Meteor Trails Under Conditions of Severe Diffusion—G. S. Hawkins and D. F. Winter, *Harvard College Observatory*—A theoretical study has been made of the diffusion of meteor trails where the electron density is greater than the critical density. It was found that, to a first approximation, the reflecting surface was a prolate spheroid with the major axis coinciding with the direction of motion of the meteor. The scattering cross section was computed for a radar situated on the minor axis and was found to be equivalent to that of a sphere with diameter equal to the major axis of the spheroid. The power scattered back to receiver was found to be proportional to the sixth power of the wavelength and inversely proportional to the fourth power of range. When diffusion of the trail is severe, the radar cross section of an over-

* The work was supported in part by the Western Development Division, USAF. References: R. M. Gallet and R. A. Helliwell, "A theory of the production of vlf noise (so-called dawn chorus) by traveling wave amplification in the exosphere of the earth," VLF Symposium, February, 1957; and *J. Geophys. Res.* R. M. Gallet and D. L. Jones, "A systematic classification of natural vlf noises other than whistlers."

* Booker, *J. Geophys. Res.*, vol. 61, p. 673; 1956.
† Hewish, *Proc. Roy. Soc. A*, vol. 209, p. 81; 1951.

dense trail is algebraically identical to that of an underdense trail.

Refraction, Scintillation, and Absorption Measurements at Microwave and Meter Wavelengths—J. Aarons, J. Castelli, and W. Barron, *Air Force Cambridge Research Center*—Simultaneous solar measurements over the ocean were made during the summer of 1956 with 218-mc, 3-cm, and 8-mm radiometers. The data has been analyzed from the viewpoint of atmospheric absorption, refraction, and scintillations in the microwave wavelengths and refraction in the meter wavelengths. Refractive errors at 218 mc, determined from null readings on a sea interferometer, were greater than at the microwave wavelengths. Microwave measurements in the X and Ka bands were measured by means of varied altitude positions of two antennas feeding Dicke radiometers. Attenuations recorded centered around 0.018 db/km in the X band and 0.03 db/km in the Ka band. Tropospheric scintillations with periods ranging from 3–70 seconds were seen at lower angles in the microwave measurements, particularly at X band.

Radiation from Slots on Dielectric Clad and Corrugated Cylinders—J. R. Walt and A. M. Conda, *National Bureau of Standards*—The radiation from slots on smooth circular cylinders of perfect conductivity is now well understood. However, if the cylindrical surface is coated with a thin dielectric film, the patterns can be appreciably modified. The calculation of the radiation characteristics, however, is extremely tedious due to the complexity of the rigorous formula.* For this reason, it seems worthwhile to modify the final expressions for the field by making several approximations on the basis that the thickness of the dielectric film is small. Furthermore, it is of interest to consider the problem by using approximate boundary conditions. This latter method can also be used to treat the corrugated cylinder under the restriction that the teeth are closely spaced with respect to the wavelength.

The numerical results in this paper include radiation patterns for axial slots on a dielectric clad cylinder by using both exact and approximate techniques for cylinder circumferences of 2 and 3 wavelengths. The close similarity of the two methods lends confidence to the validity of the approximate formulas for pattern calculation of large dielectric clad and corrugated cylinders. Examples of these are shown for a cylinder circumference of eight wavelengths.

Transverse Resonance Analysis of Flush-Mounted Antennas—R. C. Honey, *Stanford Research Institute*—This paper describes the application of the transverse resonance method to the analysis of large flush-mounted antennas and the experimental confirmation of the technique. In contrast to the more usual methods of array design, the complete two-dimensional array is treated as a unit rather than as a sum of a large number of discrete radiators. The solution of a suitably generalized transverse resonance equation determines the complex propagation constants both transverse to and along the array. The method has been applied to two types of large flat flush-mounted antennas polarized parallel to the plane of the antenna: the first consisting of a capacitive sheet spaced over a conducting ground plane, and the second of an inductive sheet spaced over a conducting ground plane.

The experimental tests of the latter type of antenna verify the theoretical predictions in every detail. The low-sidelobe pencil beam from the antenna scans in the H plane from 70° to 30° above the plane of the antenna as the frequency changes from 7 to 13 kmc. The H-plane beamwidth of the antenna stays virtually constant over most of this band. The E-plane radiation patterns of the antenna are essentially the same as the E-plane patterns of the line source used to feed the antenna.

A New Broadband Conical Helix Antenna—M. Nussbaum, *American Electronic Laboratories Inc.*—A unique conical helix antenna is presented which represents a major improvement, from both the electromagnetic and mechanical viewpoints, over the conventional cylindrical helix. Usable bandwidths of greater than 4:1 have been achieved.

The antenna configuration is an inverted conical frustrum, apex fed by a rigid transmission line, whose axis coincides with the axis of the helix, and which terminates in a small disk at the top of the antenna. The transmission line prevents the center conductor from radiating and also provides a convenient location for matching transformers. The former function prevents interaction between the feed line and the helix coil while the latter eliminates matching transformers behind the base plate. The ground plane of the conical helix is plastic because reflection of energy occurs at the larger coil diameters and unlike the base fed cylindrical helix which requires a large ground plane, the conical helix functions properly with no ground plane.

Conical helixes have been constructed for use in the region 250–10,000 mc up to this time. The high-frequency limitation is due to the small physical size required; conversely, the low-frequency limit depends upon the largest physical size which one con siders acceptable.

This paper discusses the basic helix design, the selection of initial parameters, the effect of parameter variations, the standard models which exist, and the prospective improvements either contemplated or in process.

Measured data on three typical helixes is presented to illustrate the manner in which the characteristics such as beam width, beam tilt, axial ratio, side lobe level, and vswr vary with frequency. These three helixes cover the total range 400–4500 mc and illustrate graphically the evolution of the helix from a tall, thin helix having 2:1 bandwidth to a short, fat antenna having 4:1 bandwidth.

Some Results Concerning the Fresnel Region of Constant Phase Rectangular Apertures*—C. Polk, *RCA Laboratories, Princeton, N. J.*—The far field of constant phase rectangular apertures has been described by relatively simple formulas given in Silver's book on "Microwave Antenna Theory and Design" (page 187). Analogous information describing the Fresnel region of such apertures must necessarily be more complex since the radiation pattern and the "gain" vary with distance from the aperture. Based upon the Kirchhoff diffraction formula however, it is possible to derive solutions in closed form and to plot "universal" curves which are applicable to many combinations of wavelength, aperture size, and distance.

Fresnel region "gain correction functions" have been defined and computed for constant phase rectangular apertures with uniform, triangular, "roof-top," cosine, and cosine squared illumination. The examination of these correction functions permits interesting conclusions concerning the variation of Fresnel region fields with distance and the significance of the common $2L^2/\lambda$ limit for various aperture distributions.

Formulas for relative power patterns in the Fresnel region in planes parallel to the aperture have also been obtained and "universal" curves have been plotted.

The computational results have been checked by laboratory and field experiments which are described briefly.

Characteristics of Thin Wire Loop and Biconical Antennas with Spherical Ferrite Core—J. Herman, *Diamond Ordnance Fuze Laboratories*—The problem of radiation from a thin wire loop antenna in air and with a finite spherical core of material other than air has been solved quite rigorously. The equations for the fields have been expressed in general spherical wave functions, or modes. It has been found that three families of waves are present: one TE, and two TM families. The solution holds for any diameter loop, for any frequency and for any core material, including losses, whose characteristics are homogeneous and isotropic, including air. Expressions in mode series for the input impedance, radiated power, and efficiency of radiation, have been derived. A particular ferrite has been used for experimental check of the theory. A ball of this material, about 3¼ inches in diameter, with a thin silvered loop flush with its surface, was fabricated, and input impedance over a frequency range of 90 to 250 mc was measured. The results yielded very good agreement with theoretically calculated values using the measured characteristics of the material.

As predicted, the use of ferrite effectively increases the electrical size of the antenna. While an impedance transformation results, highly useful especially for very small antennas, losses in the commercially available materials tend to diminish the advantage gained over an air loop of the same dimensions. However, the ferrite loop is still much better than the air loop.

As better materials are developed, the use of this type of radiator and receiver of energy will be notably advantageous.

An Automatic Phase Measuring Circuit for Microwaves—R. Mittra, *The Pennsylvania State University*—The paper describes the theory and performance of a microwave circuit assembly for automatic measurement of phase of microwave signals. The circuit is

* J. R. Wait and W. E. Mientka, "Slotted-cylinder antenna with a dielectric coating," to be published in *NBS J. Res.*, vol. 58.

* This work has been made possible by the support of the USAF Air Res. and Dev. Command, Rome Air Dev. Center, under Contract AF30(602)-583 with the Moore School of Electrical Engineering, Univ. of Pennsylvania.

useful for diffraction and scattering measurements and can be employed to measure the space variation of the amplitude and phase of the field automatically without requiring any adjustments of the instruments for individual readings. Most of the presently known circuits for phase measurement employ a calibrated phase shifter and an attenuator which have to be adjusted for every measurement in order to obtain the phase shift by the null method, which involves adjusting a reference signal so that it is equal in amplitude and opposite in phase with respect to the received signal. In the present method, by employing a single-sideband modulated signal as reference, the phase information at microwaves is transferred to the modulating audio signal. The phase of the detected wave when compared with a reference audio wave in an audio frequency phase meter yields the required phase shift. Arbitrary phase shifts are measurable without any adjustment. The circuit adjustment has been built and tested and has been found satisfactory for a fair degree of accuracy.

An Adjustable Sliding Termination for Rectangular Waveguide—R. W. Beatty, *National Bureau of Standards*—A new adjustable sliding termination for rectangular waveguide has been developed. The termination consists of a strip of dissipative material which can be rotated in the waveguide and slide relative to a short-circuiting plunger. Individual mechanical control of the motions is provided and the elements may be locked in any desired position. The termination is of simple design and can easily be adjusted to produce reflection coefficients from zero to nearly unity in magnitude, and any desired phase. In addition to the usual applications of adjustable sliding terminations, it provides a suitable design for an adjustable secondary standard of impedance for rectangular waveguide systems.

Measurements of the Refractive Index of Various Aerosols at a Frequency of 9400 Megacycles—C. M. Crain, J. E. Boggs, and D. Thorn, *The University of Texas*—This paper describes the apparatus used and the results obtained for measurements of the refractive indices of silver iodide, oil smoke, powdered iron, and plastic aerosols for densities in the range from 0 to 50 micrograms per cc. The sensing element used was a 9400-mc cavity resonator. A continuous flow process was employed.

The density of particles in the cavity resonator was determined by passing the gas containing the suspended particles through a particle filter and flow meter and by weighing the residue deposited in the filter for a measured flow in cc. The refractive index of the aerosol was determined by using an EERL microwave refractometer and measuring the change in difference frequency between two cavity resonators caused by introducing the aerosol of known concentration into one of the cavity resonators.

The contributions of particles to the total refractive index of the various aerosols measured were proportional to particle density and were 0.15, 0.74, 0.46, and 0.18 N^* units per microgram per cc for silver iodide, oil smoke, plastic spheres, and powdered iron, respectively. The values obtained in all cases were in reasonable agreement with those indicated by theory for spherical particles.

A discussion of some of the many practical problems associated with the measurements will be presented.

* $N=(n-1)10^6$ where n is the index of refraction.

Frequency Stabilization of Variable Oscillators—D. Makow, *National Research Council (Canada)*—A circuit is described where a single quartz crystal exercises considerable control over a range of continuously variable frequencies.

Two self-excited oscillators generate voltages having frequencies f_A and f_B, respectively. The sum frequency $f_A+f_B=f_C$ is obtained in a mixer and is applied to a crystal-controlled discriminator centered at $f_{CO}=f_C$. The oscillators are physically similar and their frequencies drift alike as a result of temperature, humidity, or power supply variations. The sum f_C then changes accordingly, and the crystal discriminator produces a dc output proportional to the deviation of f_C from f_{CO}. The dc voltage is fed back to the oscillators in such a manner as to correct the drift in f_A and f_B. Tuning is accomplished by shifting the frequencies of the two oscillators in opposite directions, thus not changing the sum frequency.

An experimental circuit shows a five to ten fold improvement in frequency stability with temperature and power supply variations, and the frequency resetting error is reduced.

Design of Narrow Band Microwave Filters—J. J. Taube and B. F. Bogner, *Airborne Instruments Laboratory*—In designing band-pass filters of the constant k type where the percentage bandwidth is small, say less than 5 per cent, one is often confronted with the fact that the designs which assume lossless resonant circuits*† do not apply. In narrow band filters, it becomes important to consider dissipation effects in order to achieve the desired filter amplitude-frequency response. This technique has been called predistortion and is due to Darlington‡ and Bode.[1] Dishal[2] derived the general equations for dissipative band-pass filters consisting of one to four coupled resonant circuits.

Since microwave filters are conveniently represented by coupled circuits, the Dishal approach has become especially useful. The design presented herein is an extension of Dishal's design equations. There are infinite sets of solutions to these equations. A particular solution was derived which represents a filter having the exact relative amplitude-frequency response (usually Butterworth or Tchebycheff) with *minimum midband insertion loss*. Complete design information is presented for the minimum insertion loss case for Butterworth and Tchebycheff responses. Examples of three-resonator waveguide and stripline filters designed from this approach will be presented. Their performance will be compared with the theory.

Although minimum insertion loss designs have only been computed up to four resonant circuits, the principles behind its completion for any number of resonant circuits are clear. The possibilities of extension of this design will be discussed.

* M. Dishal, "Two new equations for the design of filters," *Elec. Commun.*, vol. 30, pp. 324–337.

† W. Mumford, "Maximally flat filters in waveguide, *Bell Sys. Tech. J.*, vol. 27, pp. 684–713.

‡ S. Darlington, "Synthesis of reactance four-poles," *J. Math. Phys.*, vol. 18, pp. 257–353.

[1] H. W. Bode, "Network Analysis and Feedback Amplifier Design, D. Van Nostrand Company, Inc., New York, N. Y., Section 10.11.

[2] M. Dishal, "Design of dissipative band-pass filters producing desired exact amplitude frequency characteristics," PROC. IRE, vol. 37, pp. 1050–1069; September, 1949.

Some Preliminary Characteristics of Meteor Echoes as Determined by Radar Investigations at Frequencies of 100, 200, and 400 MC—A. M. Peterson, R. L. Leadabrand, and R. A. Rach, *Stanford Research Institute*—Results of amplitude time measurements of meteor reflections are presented which were made using radars at frequencies of 100 mc at Stanford and at 200 and 400 mc at College, Alaska. Results of the investigation of the number of meteor reflections as a function of direction and time of day are also presented, giving information about the rates and radiants of sporadic meteors.

The Fading of Meteoric Radio Echoes—L. A. Manning, *Stanford University*—A theory of the fading of enduring meteoric radio echoes has been developed based on the assumption that after formation the trails are distorted sinuously by a wind profile having the properties of Gaussian noise. Before distortion, an echo is possible only from the perpendicular reflection point, but as distortion progresses, reflecting "glints" appear within an ever-widening length of trail. Fading starts after a median 0.4 seconds (Greenhow) when the second glint is created, and is due to the difference in wind velocity at the active glints. An ensemble of trails has an "aperture distribution" of glints having a Gaussian power reflection coefficient along the trail and linearly increasing width. The rate of growth of the aperture has been found from measurements of the cross correlation of fading envelopes at ground stations separated up to 1000 feet at 61 mc. The correlation over the ensemble is Gaussian in product of time by spacing, and yields a minimum significant scale of the wind structure of one or two kilometers.

The expected rate of fading depends on the number of active glints, and has been found as predicted to increase with time until the number of glints is reduced by trail shrinkage at the end of the echo. The height differential required to cause zero correlation in wind velocity is thus found to be a little over 6 km. Values are also found for rms wind velocity and velocity gradient consistent with those photographed by Whipple.

Application of the theory explains fully the delay in appearance of off-perpendicular echoes found by McKinley and Millman. It also has implication as to the number of detectable long-duration echoes, and their decay properties. It enables prediction of oblique path diversity requirements for reduction of fading in meteor propagation.

Forward Scattering by Reflections from Meteor Trails of a UHF Signal over an 830-Mile Path*—J. H. Chisholm, M. Loewenthal, and A. E. Teachman, *M.I.T., Lincoln Laboratory*—A number of experiments have been performed over an 830-mile path between the M.I.T. field stations at Round Hill, Mass., and Elberton, Ga., to investigate

* The research in this document was supported jointly by the U. S. Army, Navy, and Air Force under contract with the Mass. Inst. Tech.

meteor echoes at uhf. The equipment consists of a 48-kw cw klystron transmitter operating into a steerable 60-foot parabola and a receiving antenna with multiple feeds connected to a duplicate pair of sensitive narrow-band receivers and high-speed tape recorders.

In the most interesting of these experiments, the receiving feeds were set to receive signals elevated 6° above the horizon and 6° east and west of the great circle path to the transmitter. The steerable antenna was pointed at fifteen-minute intervals successively 6° to the east, center, and west of the path. (The elevation was again 6°.) The character of the echoes, the variation in meteor signal rate during the period of observation, and the relative distribution either side of the path (of bearing 236°) are described.

Simultaneous with the above data, records were taken at a similar site located in Winston-Salem, N. C., 630 miles away.

On the Diurnal Changes of the Optimum Antenna Bearings for Meteor Burst Propagation: Part I, Measurements for N-S and E-W Paths*—A. M. Peterson and W. R. Vincent, *Stanford Research Institute*—Measurements have been made of the directions of arrival of radio signals propagated over long paths via reflections from individual meteor ionization trails. In particular, meteor-propagated signals from television stations KTVK in Phoenix, Ariz., and KHQ-TV in Spokane, Wash., have been recorded at Stanford, Calif. At the receiving site, the bearing of a directional antenna is programmed to sample the echoes arriving from various azimuths.

Certain gross features of the diurnal changes in the favored directions of arrival have been repeated in each test. For the Phoenix-Stanford path (approximately east-west), most meteor bursts arrive from the north side of the great-circle path during the morning hours, while most of the bursts arrive from the south side of the path during the evening hours. For the Spokane-Stanford path (approximately north-south) most bursts arrive from the west side of the great-circle path during the night, while the east side of the path is favored during the daytime hours. The off-path angle from which most meteor echoes arrive may be as great as 30°.

In addition to the general diurnal variations in the angles of arrival of meteor bursts outlined above, there are on occasion sudden, short-lived fluctuations in the meteor echo rate and the directional characteristics of the signals. In one example of such a variation, the number of echoes arriving from a particular azimuth increased by a factor of ten in less than an hour. After less than two hours, the rate was back to normal. This sudden enhancement, presumably associated with a heretofore undetected meteor shower of very short duration, was not repeated on the preceding or following day.

On the Diurnal Changes of the Optimum Antenna Bearing for Meteor Burst Propagation: Part II, Predictions Based on Theory and Radar Measurement of the Meteor Radiant Distribution*—V. R. Eshleman and R. F. Mlodnosky, *Stanford University*—Because of the directivity of the radio reflections from the straight, long columns of ionization formed by meteoric particles, the paths of propagation from transmitter to receiver via meteor trails depend upon the directions of travel (radiants) of the particles into the upper atmosphere. Certain features of the diurnal, seasonal, and geographical variations of the sporadic meteor radiant distribution have been deduced from considerations of possible and probable distributions of meteor orbits around the sun, and the manner in which the earth sweeps through interplanetary space. Single-station radar measurements of the range and azimuth distributions of meteor echoes have been analyzed to obtain information on diurnal variations of the radiant distribution.

The results of the experimental and theoretical determinations of the meteor radiant distribution are used to predict the salient directional features of meteor propagation over several representative oblique paths. These predictions correspond to the directional measurements discussed in Part I of this paper.

In addition to the gross features which are repeated each day, the radar measurements reveal important fluctuations in the radiant distribution which appear to be random. If these fluctuations are indeed random, it would not be possible to determine in advance how individual variations of this type would affect meteor burst propagation. In order to determine the feasibility of an "instantaneous prediction" of the optimum antenna bearing for meteor burst propagation, a simultaneous radar and oblique path test was performed. From the results of this test, it appears tht a radar at one end of a meteor burst path could be used to continually monitor the changing radiant distribution, and that this information could be used to adjust the bearings of the antennas used in the oblique path so as to maximize the rate of reception of meteor echoes.

Radar Studies of Meteors Down to 15th Magnitude*—P. B. Gallagher and V. R. Eshleman, *Stanford University*—Present-day knowledge of the ionizing effects of meteoric particles is confined to those sizes corresponding to about 10th visual magnitude and larger. Little is known concerning the behavior of those meteors between 10th magnitude meteors and micrometeorites (20th magnitude) owing to the lack of a sufficiently sensitive tool for a study.

This paper concerns a recently constructed sensitive radar at Stanford University, designed to help fill this gap in knowledge concerning the meteor spectrum. The system features a high-gain 23.1-mc double-line broadside array of 96 four-element Yagi antennas. The array generates a fan-shaped radiation pattern that has lobe structure in the meridian plane, and has a measured transverse half-power beam width of 1.5°. This array, in conjunction with an available 90-kw pulsed transmitter, comprises a system theoretically capable of detecting ionization trails created by meteors of sizes down to an estimated 15th visual magnitude.

Initial data with the array half complete indicates that meteor ionization trails having line-densities as low as 10^{10} electrons per meter (corresponding to about 15th magnitude) can be detected as individual events. Average hourly rates of total meteor activity observed in the array during early morning hours are above 4000. New experimental data for the meteor rate-amplitude law extended down to the limit of sensitivity of this radar will be presented, together with the implications of these results to meteor astronomy and meteor propagation. Details of the antenna system and its other potential reseached applications will also be described.

The Clustering of Meteor Bursts at Twenty Megacycles over a 608-Kilometer Path—L. R. Wylie, *Wittenberg College*, and H. T. Castillo, *Wright Air Development Center*—The field strength of the 20-mc transmissions from the Bureau of Standards radio station WWV has been recorded between 0200 and 0300 hours over the 608-km path between Washington, D. C., and Springfield, Ohio. Bursts of signal were received that could not be explained by conventional ionospheric propagation theories. Simultaneous radio and visual observations established that the bursts were the results of meteoric ionization.

An omnidirectional antenna, conventional communications receiver, dc amplifier, and Esterline-Angus recorder were used to collect data. A mean of 175 bursts per hour was recorded. Practically all of the meteors were below naked eye visibility. The average duration of a burst was about two seconds. The noise level of the receiver was 0.10 μv and about half of the meteors had amplitude 0.11 μv or less.

A Poisson distribution was fitted to the observed data and a significant difference between observation and theory was noted, signifying that the incoming meteors are not randomly distributed, but are clustered.

An Experimental System for Studying the Zeros of Gaussian Noise—G. M. White, *Harvard University*—Gaussian noise is generated by the shot-effect and amplified by video amplifiers. Then a band around 600 kc is transferred to the audio region and shaped by a filter so that the power spectrum of the noise is either

$$1/1 + 2\left(\frac{f}{f_0}\right)^2 + \left(\frac{f}{f_0}\right)^4 \text{ or } 1/1 + \left(\frac{f}{f_0}\right)^4 (f_0 = 1 \text{ kc}).$$

This filtered noise is then passed through several stages of clippers and expander-amplifiers and a quarter-μsec pulse placed at each of the zero crossings of the filtered noise. The zero-crossing pulses are then used to obtain an experimental verification of Rice's formula for having a zero crossing in an interval Δt, t seconds after a zero crossing has occurred.* Close agreement to the theoretical curves are obtained for the two spectrums considered.

Lightning Discharge Measurements—M. M. Newman, *Lightning & Transients Research Institute*—Atmospheric interference reduction and lightning protection development for aircraft brought out the need for as yet unavailable data on lightning

* This work was supported by the AF Cambridge Res. Center, Air Res. and Dev. Command.

* This work was supported by the AF Cambridge Res. Center, Air Res. and Dev. Command.

* S. O. Rice, "Mathematical analysis of random noise," *Bell Sys. Tech. J.*, vol. 24, p. 58; 1945.

channel resistivities, surge impedances, velocities of pulse advance, and consequent rates of charge transfer. To facilitate intercepting natural lightning discharges for detailed study, a special mobile artificial lightning generator installation has been designed and installed on an ocean-going schooner.

Some experiments are planned for this summer on the Great Lakes where we will have room enough to follow a storm, and utilize lifeline throwing rockets for launching wires toward charged clouds, so as to channel lightning discharges through measurement equipment. Superimposing artificial pulses on the natural lightning channel should upon analysis of reflection times and attenuation of coefficients provide necessary, heretofore unavailable, basic data.

Parallel studies of artificial lightning pulse radiation using balloon supported channel conductor equivalents are expected to prove useful in lightning sferics propagation studies, particularly as it is calculated it will be possible to produce short-time pulse trains of radiated powers of the order of 100 megw in the 10-kc frequency range of interest in the "whistler" type propagation theory.

Periodicity in Dawn Chorus—H. E. Dinger, *U. S. Naval Research Laboratory*—Observations of musical atmospherics over a number of years have shown that the time between a lightning stroke and the resultant long whistler is generally from two to four seconds. Storey's theory attempts to explain this delay and is currently accepted as a logical explanation.

Dawn chorus generally shows no periodicity; however, at times one may observe a phenomenon, which is probably a form of the dawn chorus, consisting of several musical tones slowly descending in frequency with an apparent period of repeatability of three to four seconds. This period corresponds to the delay of most long whistlers. The observed results suggest that there may be a connection between this phenomenon and the normal whistler propagation path, possibly in such a manner as to give rise to an oscillation system supplied by energy from an extraterrestrial source and having a period determined by the magnetic path. An important experiment will be that of determining what is happening simultaneously at the magnetic conjugate point when the effect is being observed. To date no observations have been recorded of the normal dawn chorus and the type described here appearing simultaneously.

Unusual Sferic Phenomenon Observed During Tornado Season of 1956—H. L. Jones, *Oklahoma A & M College*—Some 20,000 feet of sferic records were obtained during the tornado seasons of 1956. Several new features found in these records introduced some interesting sidelines pertinent to the nature of the severe storms that are characteristic of the Great Plains Area.

As the surface temperature increased during June and July, 1956, a new type of sferic activity became apparent. During the preceding months the recorded directional pips were separate and distinct. This was not the case for numerous recordings made during the months of June and July. In these recordings it is apparent that some type of flare discharge accompanied the individual directional pips in such a way that the directional pips are recorded against a "flare" background. This phenomenon resulted in large values on the stroke counter.

The Bryan, Texas, tornado produced a high stroke rate on the records obtained at the Tornado Laboratory. The High-Frequency Directional Finder located this storm within one half of 1° of the azimuth of Bryan.

Film records of directional pips indicate that these pips occur in "bursts" that are separated by intervals of one to three seconds. These intervals corresponded with visual observations for the occurrences of the volume discharges that appear in the cloud mass at approximately 10,000 feet.

Orthogonality Properties of Modes in Uniform Waveguides Containing Anisotropic Media—A. D. Bresler and N. Marcuvitz, *Polytechnic Institute of Brooklyn*—The solution of discontinuity and excitation problems in general uniform waveguides requires a knowledge of the orthogonality properties of the (source free) guided modes (eigenvectors) of the waveguides. It is shown that, in general, a statement of orthogonality properties involves both the modes of the given waveguide and those of an appropriate "adjoint" waveguide. A description is given for the adjoint waveguides associated with uniform waveguides containing dissipative inhomogeneous anisotropic media and bounded, if at all, by combinations of electric walls, magnetic walls, anisotropic sheath walls, and general impedance walls. The eigenvalue problem defining the modes is classified as hermitian or symmetric according as the (hermitian or symmetric) adjoint waveguide is identical with the original waveguide. For these special cases, relations between different eigenvalues and their associated eigenvectors are deduced.

Modal representations for arbitrary field distributions are, in general, of the traveling-wave type and do not reduce to the familiar transmission line representations wherein the voltage and current are direct measures of the transverse electric and magnetic fields, respectively. The latter representations arise only in waveguides which exhibit reflection symmetry. This class of waveguides is delimited. An indication is given of the manner in which reflection symmetry simplifies the general orthogonality property and permits the introduction of conventional transmission line representations.

Theory of Mode Coupling, Part I: Derivation of the Mode Coupling Formalism—H. A. Haus and L. N. Howard, *Research Laboratory of Electronics, M.I.T.*—Devices (such as the traveling-wave tube and the helix-helix coupler) consisting of two or more subsystems, each of which is capable of slow wave propagation can be conveniently analyzed by the coupling of modes formalism as originally suggested by J. R. Pierce. It is shown that the coupling of modes formalism is based on an expansion of the fields in terms of the modes of the individual subsystems. A method for such an expansion is established. Coupled transmission line equations result among the expansion coefficients of the field. The coupling terms are found from integral expressions involving the fields of the modes of the subsystems, interrelations among the coupling coefficients are shown and explained. This formalism lends itself to simple approximate calculations of the slow modes of a composite system once the modes of the subsystem are known. An application to the analysis of the traveling-wave tube with a thick beam is presented.

Theory of Mode Coupling, Part II: Mode Coupling as an Eigenvalue Problem—L. N. Howard and H. A. Haus, *Research Laboratory of Electronics, M.I.T.*—Problems in coupling of modes lead to a generalized eigenvalue problem of the form $H\chi - \lambda P\chi$ where H and P are hermitian matrices. If P is positive definite the eigenvalues are all real and the problem can in fact be reduced directly to an ordinary hermitian eigenvalue problem. The physical meaning is that the coupling leads to purely propagating normal modes. But if P is not positive definite this is not always possible. Some of the eigenvalues may be complex. In this paper we discuss canonical forms for the pair of matrices H, P, and their physical interpretation in terms of the resulting normal modes of the system. In the case of nonrepeated roots one can simultaneously achieve a diagonal form for P and a form for H which is diagonal for the real eigenvalues and has 2×2 blocks for each pair of conjugate complex eigenvalues. A representative physical situation is the exponentially growing and decaying pair of waves in a traveling wave tube.

Radiation from a Rectangular Waveguide Filled with Ferrite—G. Tyras, *Boeing Airplane Company* and G. Held, *University of Washington*—This paper presents an approximate analytical solution to the problem of radiation from a ferrite-filled rectangular waveguide. The problem is approached in the following manner: first, it entails a solution to Maxwell's equation for the aperture field distribution which is assumed to be the same as that of the waveguide containing a magnetized ferrite and second, the vector Huygen's principle is applied to find the radiation field from the previously determined aperture distribution.

The solution to the problem is found in this manner for the cases of longitudinal and transverse magnetization of a ferrite. The transverse magnetization case is supplemented with a discussion of a specific numerical example which includes plots of the aperture field distribution and phase angle as well as plots of the far-zone radiation field. The experimentally known phenomenon of the effect of the applied magnetization upon the shift of the main lobe* is demonstrated and verified analytically.

The Internal Magnetic Field of a Ferrite Ellipsoid—R. A. Hurd, *National Research Council (Canada)*—A method developed by Stevenson† for the solution of scattering problems in power series in $(\text{wavelength})^{-1}$ is extended to apply to anisotropic bodies such as ferrite ellipsoids. It is assumed that the direction of the static magnetic field applied to the ferrite is along one of the ellipsoid principal axes. The first two terms of the power series have been found for the general ellipsoid. In the case of a spheroid three terms have been computed. The zero order (static) approximation yields the ferromagnetic resonance conditions obtained

* D. J. Angleakos and M. M. Korman, "Radiation from ferrite-filled apertures," PROC. IRE, vol. 44, pp. 1463–1468; October, 1956.

† A. F. Stevenson, *J. Appl. Phys.*, vol. 24, pp. 1134–1151; September, 1953.

by Kittel,* while the higher order terms exhibit different resonance conditions. The effects of the size of the ellipsoid on the apparent permeability are considered.

The Spectrum of Turbulent Mixing and its Application to Scatter Propagation—R. Bolgiano, Jr., *Cornell University*—The process of turbulent mixing in a stratified atmosphere has been analyzed as a general diffusion phenomena. This has led to a scale law for radio scattering of L^{γ}, $\gamma \leq 11/3$, in disagreement with Villars & Weisskopf's L^5 law.

The essence of the development here employed is that, in the presence of steady-state turbulence, fluctuations of all sizes of an atmospheric property ψ, such as specific humidity, are introduced by the interaction of the turbulence with the mean gradient of that property. These fluctuations are then converted to other, on the average, smaller scales by the mixing action of the turbulent velocity components. Finally, at very small sizes the fluctuations are "dissipated" by molecular diffusion. Thus, at such scales that molecular effects are negligible, $S\psi$, the average rate of transfer of mean square fluctuations from larger to smaller scales, must be an inverse function of L or, at best, approximately constant. Under the similarity hypothesis of statistical turbulence theory, namely, the patterns of the turbulent-eddy disturbances are dynamically similar so that only the length scale and magnitude scale for each disturbance remain undetermined, the spectral intensity of mean square fluctuations, $E\psi(k)$ is given, in order of magnitude, by $LS\psi(k)\tau_L(k=2\pi/L)$. τ_L, the "lifetime" of a disturbance of size L, is proportional to $L^{2/3}$ according to the universal equilibrium theory. Since radio analyses indicate that the scattering coefficient, σ, is proportional to $L^2E_{\psi}(k)$, this leads to the conclusion that σ is proportional to $L^{11/3}$, or to a smaller power of L.

Numerical examples have been worked out for both the troposphere and the ionosphere. The results are in fair agreement with experiment, though on the basis of the gradients assumed the predicted signal levels exceed somewhat the measured values.

The Fading of Radio Waves Scattered by Dielectric Turbulence—R. A. Silverman, *New York University*—The fading of radio waves scattered by dielectric turbulence is shown to be the results of two effects. The first is time variation of the scattering eddies as seen in a coordinate system moving with the local wind velocity. The second is Doppler shifting produced by the convection of the scattering eddies by the mean wind and by the macro-eddies. In the troposphere, the scattering eddies lie in the inertial range of statistical turbulence theory. This makes it possible to find the envelope fading rate of the received scattered signal to within a constant of proportionality by using dimensionality and similarity arguments. The result is an expression for the fading rate as a function of carrier frequency which departs significantly from that found with "scattering blob" models.

The Relation of Radio Measurements to the Spectrum of Tropospheric Dielectric Fluctuations—A. D. Wheelon, *The Ramo-Wooldridge Corporation*—The size spectrum of isotropic fluctuations in the troposphere's dielectric constant is related to quantities measured by radio means. Two classes of experiments are analyzed: 1) line-of-sight phases and amplitude instability, and 2) refractometer measurements of dielectric fluctuations. This analysis is independent of models for the dielectric fluctuations and provides a system from which the spectrum can be estimated from experimental data. The measured quantities are expressed as weighted integrals of the spectrum, many of which may be inverted to give the spectrum directly in terms of the data. Antenna smoothing by the receivers and finite data sample effects are studied, in addition to the basic propagation mechanisms.

Meteorological Correlations with a Scatter Signal—W. S. Ament, F. C. Macdonald, and D. L. Ringwalt, *U. S. Naval Research Laboratory*—During the week of December 3–8, 1956, the Naval Research Laboratory's Flying Laboratory and the University of Florida conducted joint 1250-mc scatter propagation measurements on a 262 (nautical) mile link from Patrick Air Force Base, Fla., to Nassau, Bahamas. Meteorological and refractometer soundings were taken on a six-hourly schedule at selected points along the path. The weather was consistent and refractometer profiles showed a consistent 40–50 N-unit "inversion" at altitudes 4000–6000 feet corresponding with a temperature inversion, a haze layer, and the base of cumulus clouds. The latter imposed a 10–40 mile mesometeorological scale and scatter in details of the profiles. Ground-to-air scatter signals show a 5–15 db height-gain maximum at "inversion" height, a 0.17 db per mile attenuation rate, and a Rayleigh fading characteristic with underlying slower fades at inversion height and above. Ground-to-ground signal levels correlate suggestively with wind-shear across the inversion. The indicated propagation mechanism is multiple scatter and partial ducting at the irregular N-curve break. This work was sponsored under ONR Contract Nonr 580(04) and was possible only through the cooperation of Air Force Missile Test Center, Patrick Air Force Base, Fla., and Naval Air Development Unit. South Weymouth, Mass., with contributions from Air Force Cambridge Research Center, Applied Physics Laboratory, M.I.T. Lincoln Laboratory, and Office of Naval Research.

Theory of Scattering from a Nearly Transparent Anomaly—V. W. Bolie, *Collins Radio Company*—Recent advances in the design of uhf and microwave communication equipment, coupled with the increasing need for expanding the usable frequency spectrum, have generated considerable interest in making use of scattered signals which are propagated beyond the radio horizon. Although a large amount of experimental measurements have been reported in the literature, much theoretical work in interpreting the basic scattering phenomena remains to be done. In order to gain a more detailed insight to the scattering mechanism, an approximate equation of propagation of electromagnetic energy in a nearly transparent medium is applied to the case in which the medium contains a dielectric inhomogeneity in the form of an isolated Gaussian-shaped perturbation in the refractive index. Equations for the scattering caused by the perturbing blob are illustrated graphically. The energy extracted from the incident wave by the blob is illustrated graphically by a plot of the total scattering cross section as a function of blob size.

Ionospheric Effects of the Great Solar Cosmic Ray Event of February 23, 1956—A. H. Shapley and R. W. Knecht, *National Bureau of Standards*—A widely reported solar outburst occurred on February 23, 1956. At 0334 UT, a bright flare was observed in progress on the sun (Kodiakanal, India). An unprecedented increase in cosmic ray intensity began at 0350 UT (at Chicago) reaching the highest level ever recorded, and requiring up to 18 hours for the return to normal. Ionospheric soundings data from both the dark and daylight hemispheres have been examined.

Soundings data from 12 stations in the dark hemisphere north of geomagnetic latitude 60° have revealed a large absorption effect whose beginning somewhat lags the start of the solar event and which lasts up to 48 hours. The effect is greatest above 65° and nonexistent below 50°. Between about 51° and 59°, the increase in absorption does not appear in time association with the solar event, but rather as an augmentation of the usual daylight absorption during the sunlit hours of the following day (February 23). Except for a moderate effect that was observed at two stations at about 0400, magnetic conditions were generally quiet throughout the period of high absorption until a severe disturbance began 47 hours after the solar event. The apparent mechanism is a steady influx of solar-associated charged particles in the mev energy range producing an excess of free electrons in the D region or in a sub-ionospheric layer.

Soundings taken in the daylight hemisphere at Okinawa, Guam, Baguio, and Adak show the usual increase in absorption coincident with the flare. At Okinawa, however, a discontinuity in foF2, amounting to a 17 per cent increase in the F2 layer maximum electron density, occurred at the time of the solar event. Lack of the appearance of this effect at the three other locations suggests caution in its interpretation.

Observations of the Geographical Position and Extent of Regions of Anomalous High-Latitude Absorption*—H. Leinbach and C. G. Little, *University of Alaska*—Investigations of high-latitude absorption have been made at the Geophysical Institute of the University of Alaska, using 30 mc extraterrestrial radiation. Three observing techniques have been used: 1) observations using a rotating, horizontally directed antenna, 2) comparison of observations with fixed, vertically directed antennas at Barrow and College, north and south of the auroral maximal zone respectively, and 3) comparison of observations of galactic noise received at a single site on vertically-directed, broad and narrow beam antennas.

The rotating antenna observations at College typically showed greater absorption

* C. Kittel, *Phys. Rev.*, vol. 73, pp. 155–161; January, 1948.

* This work was sponsored in part by the National Science Foundation and in part by the Army Signal Corps, Fort Monmouth, under Contract Number DA-36-039-SC71137.

to the north than to the south of the station. On the other hand, the two-station data indicate that on the average absorption is greater at College than at Barrow. These two results lend support to the suggestion that the anomalous high-latitude absorption reaches a maximum near the zone of most frequent auroral activity.

The observations have also shown the presence of irregularities in the absorption varying from less than 60 km to greater than 800 km in extent.

398 McAuroral Echoes Observed at College, Alaska—A. M. Peterson, R. L. Leadabrand, and R. B. Dyce, *University of Alaska*—Echoes from the aurora have been detected at College, Alaska, at a frequency of 398 mc using a radar with 60-kw peak power, 0.5-millisecond pulse width, 3-kc receiver bandwidth, and a 61-foot diameter steerable parabolic reflector. The signal strengths of the echoes were as great as 27 db above receiver noise level (receiver noise figure 6 db). Echoes have been observed within the following limits: bearings: 50°W to 50°E of magnetic north, elevation angles: 0° to 13°, ranges: 400 to 100 km.

The 3° vertical beamwidth of the antenna allows height determination of the reflecting auroral ionization. The heights were found to lie between 80 and 130 km with an average height of 105 km.

Reflection geometry indicates that echoes can be observed when the angle between the transmitted ray and the magnetic field lines departs as much as 6° from perpendicular. These new experimental data will require further refinements to the theory of scattering from auroral ionization.

UHF Auroral Observations*—S. J. Fricker, R. P. Ingalls, M. L. Stone, and S. C. Wang, *Lincoln Laboratory, M.I.T.*—A 412-mc bistatic pulsed radar system has been set up in Massachusetts, with which auroral returns have been observed at ranges of the order of 900 to 1300 km. Results from some early work with this system are given, including:

1) Typical *A*-scope and intensity modulated film records.
2) Average frequency of occurrence, and variation of occurrence rate with azimuth.
3) Diurnal variation of occurrence rate.

A method is outlined for mapping the regions from which returns may be observed at a given site. This is based on the postulate that the radar beam must be perpendicular to the earth's actual magnetic field in the auroral region for returns to be observed. The positions of the observed echoes are seen to overlap the computed regions, thus giving some idea of the stringency of the perpendicularity condition at this frequency. Possible height limitations are indicated, particularly an upper limit of approximately 165 km.

Some VHF Sporadic-E Results—R. M. Davis, Jr., J. W. Finney, E. K. Smith, Jr., and D. H. Zacharisen, *National Bureau of Standards*—Recordings with wide dynamic range have been made for a period of ten months on two frequencies (27.775 and 49.8 mc) over the Cedar Rapids to Sterling path. Additional data on 49.8 mc using the ionosphere scatter receiver are available since March, 1951. Information as to the intensity distribution and frequency dependence has been extracted from the records for this circuit.

Sporadic-*E*, as observed on ionosphere scatter circuits, follows much the same magnetic activity dependence as is found for vertical incidence sporadic-*E*. A study of sporadic-*E* on the Cedar Rapids to Sterling circuit reveals that much more is recorded on magnetically quiet than on magnetically disturbed days.

The problem of extrapolating vhf oblique incidence sporadic-*E* information from ionosonde data is complicated by the fact that their temporal variations are not always simply related. This problem is considered here in connection with the reliability of world *Es* maps based on vertical incidence data for predicting vhf sporadic-*E* field strengths pertinent to communication circuits.

Variations of E-Layer "Scatter" Receptions with EEs*—M. L. Phillips, *Lincoln Laboratory, M.I.T.*—If sporadic-*E* ionization is assumed to occur in patches having a sharp lower boundary, of approximately uniform reflectivity, with spatial and time probabilities of occurrence approximately equal, and if measurements of *fEs* are considered negligibly influenced by ionospheric absorption and characteristics of the measuring equipment, changes in received power from sporadic-*E* reflection may be estimated from *fEs* measurements. Comparison of such estimates with published data for *E*-layer "scatter" receptions shows good agreement with observed changes in received power due to changes in transmission frequency, length of transmission path, and with season, and time of day for temperate-zone observations, although there is poor agreement with diurnal change and seasonal change during night hours in auroral regions, for which a possible explanation is given.

Magnetic Storm Effects in the Inner and Outer Ionosphere—S. F. Singer, *University of Maryland*—Evidence is adduced for two types of magnetic storm effects. One, identified with the sudden commencement, is caused by currents flowing in the inner ionosphere and shows typical features associated with normal ionospheric currents. This current is set up by an interplanetary shock wave which penetrates by way of the auroral zone into the earth's atmosphere.

The second type is identified with the main phase of the magnetic storm and is caused by high-speed solar corpuscles which enter into the normally forbidden regions of the earth's dipole field, are trapped there, and execute motions and drifts which reproduce the hypothetical Störmer ring current. The distribution of this ring current can be calculated and shows a maximum in the vicinity of 7 earth radii. The time constant of the ring current is calculated to be 1–2 days.

Back Scattering from the Sea and Land at Centimeter and Millimeter Wavelengths—C. R. Grant and B. S. Yaplee, *U. S. Naval Research Laboratory*—The back scattering from the sea and from several land terrains has been measured at wavelengths of 3.2 cm, 1.25 cm, and 8.6 mm. σ°, the average radar cross section of sea or land echo per unit area of the surface, has been plotted as a function of the angle of incidence for the three wavelengths. A family of curves at each of the three wavelengths shows the change in σ° with wind velocity or sea state. σ° is also shown as a function of the angle of incidence for several land terrains. In general, σ° increases with frequency and also with wind velocity in the case of the sea surface.

A Comparison of Phase Modulated Interferometers—D. J. Farmer, *The Ramo-Wooldridge Corporation*—The operation of a phase-modulated radio interferometer is analyzed from the viewpoint of the random noise voltages appearing at the input rather than from the usual starting point of the corresponding noise powers. This approach demonstrates the efficacy of preamplifiers in reducing the over-all receiver background noise when such devices are placed in the separate arms of the interferometer; further, the method shows how noise signals due to the receiver, the galactic background, and a spatially localized source each contribute to the recorded output. Results, in terms of the signal-to-noise ratio at the recorder, are obtained for several forms of the phase modulating function, including the Ryle type instrument. An interpretation is given to the signal-to-noise ratio which can be used to describe the performance of the instruments and circumvents the subjective specification of signal "detectability."

The Results of the Observations of Jupiter's Radio Emissions on 18 and 20 MC in 1956 and 1957—R. M. Gallet, *National Bureau of Standards*—An account of Jupiter's radio emissions properties, from the observations obtained simultaneously on 18 and 20 mc during two years will be given. The equipment developed by K. Bowles has remarkable features, permitting to observe more than one complete rotation of Jupiter (10^H) consecutively, when the interference is not limiting the recording time. Thus, a very considerable amount of data was obtained with essentially the same equipment characteristics on both frequencies, a feature very important for differential measurements.

It has been possible to resolve several sources spaced in longitude. These sources do not move relatively to each other and maintained their activity over many years, by comparing with data obtained in 1951 by Shain in Australia. Thus, they are relative to the solid body of the planet beneath the visible clouds of the atmosphere; the rotation period of this solid body is established to a high degree of precision (to some tenths of a second at most) and is about 10 seconds shorter than the rotation of the clouds (system II).

The ionosphere of Jupiter is an important controlling factor of the reception of these emissions on the earth. The permitted cone of transmission varies in aperture with the solar activity and the percentage of time of the observed emissions diminishes when the solar activity increases; it has been possible to obtain the regression of the ionization in Jupiter's ionosphere in the

* The research in this document was supported jointly by the U. S. Army, Navy, and Air Force under contract with the Mass. Inst. Tech.

* The research in this document was supported jointly by the U. S. Army, Navy, and Air Force, under contract with the Mass. Inst. Tech.

average vs solar activity. A detailed investigation for each longitude of the same effect gives indications on the latitudes of the different sources.

This normalization of the data shows also the spectral properties. It is remarkable that for a 10 per cent variation in the frequency, the ratio of the total activity at 20 mc vs 18 mc is about 0.6 or less.

It is still not possible to discuss the mechanism of the production of the emissions, but numerous high-speed recordings of the pulses with time resolution of 1/100 second or better on magnetic tape, give many indications for future theories.

Observations of Radio Stars and Selected Regions of the Galactic Plane at 440 MC—N. G. Roman and B. S. Yaplee, *U.S. Naval Research Laboratory*—In June and July of 1956 and February of 1957, measurements of radio sources were made at 440 mc. Local interference restricted usable measurements to the stronger sources visible at night. These included among others Cassiopeia A, Cygnus A, Taurus A, Virgo A, Centaurus A, and the galactic center. Upper limits to the brightnesses of several other sources, including the moon, were also obtained.

Measurements of the increase in brightness of the Milky Way above the neighboring background were made in the Cygnus *X* region and near the galactic center between longitudes 320° and 345°. No absolute calibration of the background temperatures was possible.

High Frequency Scattering Based on the Fock Approximation, I—Theory—S. J. Rabinowitz, *The W. L. Maxson Corporation*—A universal function for the current induced on the surface of a conducting obstacle by a plane wave has been derived by V. Fock. The result is applicable to any scatterer for which all dimensions and all radii of curvature are large compared to wavelength. The Fock approximation is identical with the familiar Kirchhoff approximation everywhere on the surface except for a narrow belt located on both sides of the shadow-light interface.

Fock's analysis is reviewed. The electromagnetic field scattered by a sphere is calculated in detail based on the Fock current. The results are generalized for scattering by any large, smooth obstacle.

The total scattered field is obtained by integrating the fields radiated by the surface currents induced on the obstacle. For the large, smooth obstacles under consideration, the integral can be evaluated by the method of stationary phase integration. Two points of stationary phase exist, one in the illuminated region, and one in the shadow region of the scatterer. The scattered field is the sum of the fields radiated from the neighborhoods of these two points. Calculations for the fields scattered by two spheres and an ellipsoid of revolution have been made. The qualitative and quantitative differences between these calculations and calculations based on the Kirchhoff approximation are presented. The relationship between the Fock currents and the "creeping waves" of Deppermann and Franz are discussed.

High-Frequency Scattering Based on the Fock Approximation, II—Experiment—S. J. Rabinowitz, *The W. L. Maxson Corporation*—The electromagnetic field scattered by a large, smooth obstacle upon which a plane wave impinges can be calculated from the surface currents induced. Conversely, the surface currents can be found from the scattered field. The scattered field has been shown to depend primarily on the surface currents near two points of stationary phase, one in the shadow region, and one in the illuminated region of the obstacle. The contributions from these two points can produce an interference in the total scattered field considered as a function of angle. It is possible to separate the two contributions and to determine the surface current at the two points.

The design of an experiment suitable for measuring surface current by means of the scattered field is described. It is shown that the current of the entire surface, except for a region near the shadow-light interface, can be determined. This region is much smaller than that wherein the Fock currents differ from the currents given by the Kirchhoff approximation. Hence, the validity of Fock's approximations can be verified experimentally in this manner.

The experimental data obtained for the scattering cross section of three large bodies are in excellent qualitative and good quantities agreement with the analysis. The experiments were performed at 97.2 kmc. The apparatus is described in detail.

The Role of Fock Functions in the Theory of Diffraction by Convex Surfaces—N. A. Logan, *Air Force Cambridge Research Center*—Rigorous series expansions for the solutions of radiation and scattering problems involving perfectly conducting circular cylinders and spheres are replaced by a more convergent representation by means of the Poisson summation formula. The terms of the new series are expanded asymptotically in a series of inverse integral powers of ka in the illuminated region and in inverse fractional powers of ka in the penumbral and umbral regions.

The coefficients in the latter expansion are expressed in terms of a family of universal functions first introduced by Fock. Comparison of the two expansions leads to a modification of the latter expansion, extending its domain of applicability to include the illuminated region. Comprehensive tables have been prepared for six such functions which permit one to predict the effects of polarization and surface curvature when 1) both source and receiver are at infinity, 2) both source and receiver are on the obstacle, and 3) the source is at infinity and the receiver is on the obstacle, or vice versa.

Electromagnetic Back-Scattering Cross Sections of Dielectric-Coated Infinite Cylindrical Obstacles—C. C. H. Tang, *Gordon McKay Laboratory, Harvard University*—The electromagnetic back-scattering properties of an infinite cylindrical conductor coated with a lossless dielectric layer of thickness comparable to a wavelength is investigated both theoretically and experimentally. The theoretical problem is first formulated with three regions of arbitrary constants of materials and then reduced to the specific cases. The scattered field, total scattering cross section, and back-scattering cross section can all be expressed in compact fashion in terms of scattering amplitude coefficients.

The existing experimental methods for measuring back-scattering cross sections of two-dimensional obstacles fail to yield accurate results for obstacles of small scattering cross sections. The present investigation utilizes the parallel-plate-region technique modified to permit the application of Doppler-shift principle. The scattering obstacle is set in motion in the presence of a plane-wave electromagnetic field in the parallel-plate region, and the detected Doppler signal is proportional to the back-scattered field.

The theoretical and experimental results are in excellent agreement. Because of the complicated multiple scattering effect at the boundaries, the back-scattering behavior of the dielectric-coated cylinders does not present a pattern that can be predicted from a simple model; however, for cylinders of small inner radii a geometric-optical interpretation is possible. For cylinders of large inner radii nothing in general can be said.

Network Representation of Infinite Gratings for Obliquely Incident Waves—L. O. Goldstone and H. M. Altschuler, *Microwave Research Institute, Polytechnic Institute of Brooklyn*—The network representations of infinitely extended gratings formed by metallic obstacles of a variety of cross sections have been available for some time for cases where either the electric or magnetic field vectors of the incident wave are parallel to the uniform direction of the grating and where the direction of incidence is constrained to be perpendicular to the uniform direction. The present paper deals with the extension by simple means of such known solutions to cases where the transverse electric and magnetic field vectors of the incident wave are unrestricted and where the direction of incidence need not be perpendicular to the uniform direction. The method employs the known solutions as a starting point so that the resulting networks obtained embody the same limitations with respect to order of diffraction as the known solutions. The far reflected and transmitted fields can be readily inferred from the network description.

The transition from the earlier results to the extended ones is achieved by the introduction of a set of modes (guided waves) which differ from the familiar E and H modes in that they are characterized by the vanishing of the field components along a prescribed transverse direction. These modes, which have been designated as E-type and H-type modes, will be discussed briefly.

The Resonant Conductance of Slots in Linear and Two-Dimensional Arrays—G. C. McCormick, *National Research Council (Canada)*—Stevenson's work on the radiation and network properties of a slot in a waveguide refers to a single slot backed by an infinite plane conductor. In practical applications many slots may be used in linear or two-dimensional arrays. In some arrays the mutual coupling among slots can be neglected, but in two-dimensional arrays and in arrays radiating into a horn or parallel-plate region, the coupling is always significant. The resonant conductance or resistance of the slot can be determined by calculating the power radiated from the slot. This is done, assuming that the slots are excited to given voltages, by calculating the magnetic field in the neighborhood of each

slot by a semirigorous method. Results are given for several configurations of linear and two-dimensional arrays.

Wavelength Correction in a Microwave Interferometer—D. M. Kerns, *National Bureau of Standards*—Formulas are derived enabling correction for wavelength error due to diffraction and misfocussing effects in a microwave interferometer intended for high-accuracy measurements. Microwave energy is radiated by a waveguide-to-space transducer, reflected by a plane mirror at a distance d, received (and scattered) by the same transducer, and finally observed in interference with a suitable reference signal. Using a refinement and generalization of a method apparently first given by E. S. Dayhoff, a solution in terms of the radiating and the scattering properties of the transducer is obtained. The solution is a series in which successive terms correspond to successive multiple reflections between transducer and mirror. The first term yields the following useful results, valid for any (positive) d: the received signal is proportional to $\int_{-\infty}^{\infty}\int_{-\infty}^{\infty} k_z B(k_x,k_y)\cdot B(-k_x, -k_y)\exp(2ik_z d)\,dk_x dk_y$, where k_x, k_y are the transverse components of the propagation vector $k, k_z=\sqrt{k^2-k_x^2-k_y^2}$, and $B(k_x,k_y)$ is the two-dimensional Fourier transform of the complex vector amplitude of the electric field obtaining in the "aperture" plane with the mirror removed. The relationship of B to the far-field of the radiator affords a possible alternative method of determining B in the cases of present interest. Examples of the evaluation (approximate or otherwise) of the above integral will be given.

Characteristics of Signals Received on a Large Aperture Antenna in Propagation Beyond-the-Horizon*—W. H. Kummer and D. C. Hogg, *Bell Telephone Laboratories, Inc.*—The characteristics of the signal received on a 60-foot paraboloid operating in a 4.11-kmc, 171-mile beyond-the-horizon circuit are discussed. Data obtained by scanning the antenna in the horizontal and vertical planes show that most of the energy scattered toward the receiver is contained, on the average, within an angle of about one degree. Thus there is an apparent broadening of the free-space radiation pattern of the antenna; a relation between the broadened patterns and the ratio of the power received on the large antenna and on a small antenna is obtained. The results are discussed in relation to median signal level structure of the atmosphere, and profile of the propagation path. The scanning data are presented in the form of pictures of the signal photograph on an oscillograph.

Some Generalized Tropospheric Scattering Relationships as Applied to Transhorizon Microwave Propagation—A. T. Waterman, Jr., *Stanford University*—Although there has been a substantial accumulation of evidence indicating that the received signal in transhorizon microwave propagation consists of the sum of several noncoherently related components, interpretation of specific observations in terms of a specific scattering hypothesis has not always been free from ambiguities. In the present paper the assumption is made that there is an atmospheric scattering characterized by a cross section inversely proportional to an arbitrary power of the scattering angle. Various consequences are then deduced as regards the characteristics of the received signal which would be observed in various special circumstances.

The variation of received power with distance is derived for various inverse power dependencies on scattering angle and for the following beam-width configurations: 1) relatively broad beams at both ends of the transmission path, 2) relatively narrow beams at both ends, 3) a narrow beam at one end and broad at the other, and similar combinations in which an antenna may be broad-beam in one dimension and narrow in another. Correspondingly, the aperture-medium coupling loss is obtained as the ratio of received powers, not only the ratio of 1) and 2) above, but also of 1) to 3) and other possible pairings of the configurations considered. In addition, expressions are derived for diversity distances, again for various scattering-angle dependencies.

Where applicable and definitive, these results are compared with observational data.

To a large extent, this paper represents a generalization of results which have been presented previously. Its purpose is to find what factors are critical in interpreting experimental observations and to distinguish those phenomena which might have alternative explanations.

Resolution of Vertical Incidence Radar Return into Random and Specular Component—R. K. Moore, *University of New Mexico*—Postulating that the ground is made up of scatterers whose height above mean ground level is randomly distributed, leads to a summation of the electric field returned to a radar in which a random component and a reduced specular component may be isolated. The specular component is obtained by averaging the components of the individual signals in phase with the return which would be obtained from a point on the mean ground plane beneath (or above) the actual position of the scatterer. The random component is obtained by summing the phasors which must be added to the mean specular component for each scatterer to give the actual phasor associated with the displaced scatterer. When the standard deviation of the displacements of the scatterers from the mean is large compared with a wavelength, the random component greatly exceeds the specular. When the surface is almost smooth, the reverse is true.

In this first-order theory, the vector nature of the waves has been neglected for simplicity. Furthermore, it is assumed that the ground is made up of isolated scatterers whose position is not correlated with that of their neighbors. More sophisticated assumptions should lead to a better description of the actual phenomena, but it is believed these simplifying assumptions lead to a good qualitative description of the electromagnetic problem.

In developing the theory it was found desirable to determine distribution functions associated with a random walk in which the direction of each step was normally distributed about a mean direction, rather than being uniformly distributed as in the usual random walk problem. The distribution functions associated with this type of random walk have been calculated and are shown.

Comparison of Measured and Predicted Tropospheric Bending of Electromagnetic Waves—L. J. Anderson, L. G. Trolese, and J. B Smyth, *Research Associates*—Numerous methods are available for computing the amount of bending that electromagnetic waves should undergo when passing through an atmosphere with a given refractive index profile. This paper describes a comparison of experimentally determined bending by means of a sea-interferometer, with computed bending obtained by use of a method developed by L. J. Anderson. The computation method consists basically of dividing the arbitrary refractive index profile into a series of layers having linear gradients and obtaining the incremental bending in each layer by convenient graphical means. The experimental data was obtained by use of transmitters in an aircraft flying at a constant altitude of 30,000 to 40,000 feet and receivers situated 100 feet high on a cliff overlooking the sea. By use of the positions of interference minima at two frequencies in the proper manner, the total bending which takes place in the troposphere at low angles below 30,000 feet can be determined to an accuracy of ± milliradian. This region accounts for 90 per cent of the bending in passing through all of the troposphere. The measured and computed bending on a standard and three nonstandard days agree fairly well.

Propagation Through the Troposphere and Ionosphere—V. A. Counter and E. P. Riedel, *Lockheed Aircraft Corp.*—On May 2, 1956, V. A. Counter of Lockheed Missile Systems Division presented to a joint meeting of URSI and IRE a paper entitled, "Propagation Through the Troposphere and Ionosphere." The present paper is a continuation of this work using more refined and extensive models in both the troposphere and ionosphere and the 1103A computing machine to obtain refraction, attenuation, and range deviation results at frequencies above 50 mc, for elevation angles between 0.01 and 90° from zero to one thousand nautical miles above the earth.

Six tropospheric profiles of the refractive modulus, m, as a function of height, h, were studied, three having the general form: $m=a[1+b\exp ch/4]\exp -h/4$, where a, b, and c are constants. The other three profiles included a layer with tilt angles of ±1° and 0°.

Three profiles of electron density vs height were used representing minimum 2½ per cent, mean and maximum 2½ per cent points of ionospheric activity. Chapman functions were used to represent the general shape of the layers. The electron-ion collision was included in the calculations. The earth's magnetic field was neglected.

A Long-Distance Pulse Propagation Experiment on 20.1 Megacycles—R. Silberstein, *National Bureau of Standards*—Pulses from a megawatt transmitter at Sterling, Va., were recorded on Maui, T. H., and simultaneously at Boulder, Colo., in October, 1956. Vertical-incidence data were taken at Carthage, Ill., and some backscatter records at Sterling.

Since Boulder is approximately one-

* This work was supported in part by Contract AF18(600)-572 with the USAF Air Res. and Dev. Command.

third of the 7647-km distance from Sterling to Maui with an angle of departure of about 8°, one might expect a well-defined three-hop F_2 mode to fail at Maui when the one-hop mode failed at Boulder, leaving only a weak signal for the two-hop near-grazing-incidence signal.

The records showed strong signals at smaller delay times persisting for many hours after the three-hop failure, which itself was not always easy to distinguish in a single record. The lower-order modes would have had to include combinations of E and F_2 layer propagation. Records taken on different days were vastly different in the increase of retardation as modes began to fail, as well as in the modes themselves, showing great sensitivity to ionospheric conditions and a possible large role of lateral deviations and tilts.

Further experiments should include a receiver near Stanford which would enable identification of the two-hop mode and also afford a rough test of the two-control-point theory.

Numerical Computations from the Theory of VLF Noise Emissions and their Comparison with Observations—R. M. Gallet and A. Hessing, *National Bureau of Standards*—A theory for explaining the very low frequency emissions other than whistlers (so called hiss, dawn chorus, hooks, etc.) was presented by Gallet and Helliwell in a recent communication. This theory now has been developed in detail with the purpose of obtaining numerically the predicted spectra (frequency vs time) and to compare them with the observations presented in the preceding communication.

The physical model for these emissions is the following. A neutral bunch of incoming ionized particles from the sun with a velocity v is guided near the earth along a magnetic line of force, through the earth's exosphere. The electromagnetic interaction of these particles with the plasma of the exosphere, in the presence of the local magnetic field, excites electromagnetic waves according to the mechanism of a traveling-wave tube discussed by Gallet and Helliwell. The excited frequencies are given by:

$$f_{1,2} = \frac{f_H}{2}\left[1 \pm \sqrt{1 - \left(\frac{2v}{c}\right)^2 \frac{f_P^2}{f_H^2}}\right]$$

where f_p is the local plasma frequency defined by the electronic density present in the exosphere, and f_H is the gyrofrequency. These electromagnetic waves in turn propagate along the line towards the earth with the group velocity U of the whistler mode. Their time of flight t is given by:

$$t = \int_{\text{path}}^{ds/U}.$$

The total time of propagation of the frequencies is their time of flight t plus the time of travel γ of the particles along the magnetic line of force to the point of excitation of the frequency f.

A program for the total time $t+\tau$ vs frequency f has been developed on the electronic computer IBM650. The computations have been made with different models of the distribution of electronic density outside the earth. Computed curves and observed spectrograms will be shown and compared. A short discussion of the best models of the exosphere and of the velocity v from these results will be given.

A Systematic Classification of Natural VLF Noises Other than Whistles—R. M. Gallet and D. L. Jones, *National Bureau of Standards*—Starting at the beginning of 1956 an intensive program of observations of whistlers and other types of vlf noises, so-called hiss, dawn chorus, etc., was undertaken by the writers, with the help of J. Watts who is responsible for very valuable achievements in the recording technique and the securing of spectrograms. A very high sensitivity was achieved by using the one-mile loop antenna built for vlf sweep frequency ionospheric soundings by Watts. Since the beginning of 1957, simultaneous observations at Anchorage, Alaska, are available.

The magnetic tape recordings are taken at 35 minutes past every hour. A collection of about 10,000 spectrograms is now available and expands continuously. Besides the whistlers, a large number of other types of vlf noises have been recognized and systematically studied.

Their occurrence is essentially related to periods of geomagnetic activity, according to a progressive pattern of shape variations. A number of "families" have been established, by criteria of reproducibility of forms of spectrograms and progressive transitions around a general property such as the risers, the hooks, quasi-horizontal tones, tails, etc. Besides the shape the degree of sharpness or fuzziness is also important, going to the extreme case of the hiss, which appears as a solid band of noise on the spectrogram, continuous in time sometimes for hours. Many phenomenological properties have been established for the extra-terrestrial beams and bunches of ionized particles which seem to be responsible for their production.

An atlas of spectrograms of these vlf noises is in publication, and is intended to serve as a guide for IGY observations. The presentation of these data is relevant to a companion paper (see preceding abstract) related to the theory of these noises.

Computation of Group Indices and Group Heights for Low Frequencies*—J. J. Gibbons, *The Pennsylvania State University*—An approximate formula is derived from which the group index μ', including the effect of collisions, can be easily calculated as a function of μ and χ, the real and imaginary parts of the Appleton-Hartree index. This expression is quite accurate for the ranges of N and ν usual for frequencies below 1 mc. For a given frequency a set of $\mu'(N,\nu)$ curves can be constructed from which the group heights for any give N profile can be quickly determined by graphical methods. The method is applied to compute group delays for several possible models.

Ionospheric Reflection of Very Low Frequencies—H. Poeverlein, *Air Force Cambridge Research Center*—The reflection coefficient of an ionospheric layer can be studied or calculated by means of a theoretical formulation, which has been developed for wavelengths large compared to the layer thickness. The phase of the reflected wave as given by the complex reflection coefficient can be ascribed to a certain phase reflection level within the ionospheric layer.

With decreasing frequency both the amplitude reflection coefficient and the phase reflection height tend towards definite limit values. With increasing frequency the phase reflection height decreases until the transition to geometric-optical propagation is reached, where the reflection height turns to increase with increasing frequency.

Various simplified cases have been studied until now. The influence of the terrestrial magnetic field was taken into account in the case of vertical incidence and extremely low frequencies.

Spatial Areas of Fade Resulting from Ionospheric Polarization Rotation—I. B. Goldberg, *University of Michigan*—One if the most significant effects of the ionosphere on an electromagnetic wave is the rotation of its plane of polarization resulting from the presence of the earth's magnetic field. As a consequence of this phenomenon, commonly referred to as the Faraday effect, a radio signal scattered from positions in or above the ionosphere is subject to fading. The extent of this type of fading to P- and L-band radars is shown by spatial area contours in the ionosphere for a variety of circumstances.

The standard explanation for this effect may be cited in the following way for wave frequencies above 100 mc. An electromagnetic wave of plane polarization entering into the ionosphere in the presence of the earth's magnetic field is split into two waves nearly circularly polarized in opposite senses. Each component wave has a slightly different index of refraction which results in a differential phase shift between the two modes. As the component waves continue independently through the ionized region, there is a continuous alteration of phase between the two waves. Upon emergence from the ionized layer, the waves recombine to form a linearly polarized wave with its direction of polarization rotated by an amount proportional to the length of path in the medium and the difference in indices between the two modes. Thus, an echo from certain regions in the ionosphere would not be observed if the degree of rotation to that region and return was of particular magnitude to reduce the intensity of an echo by a sufficient amount. These ionospheric areas of fade may then be computed for any location. A model of the ionospheric cumulative electron density profile has been used based on information from a report by the Ionospheric Research Laboratory of Pennsylvania State University for Sylvania Electric Products, Inc. It is believed realistic for this purpose. These fading regions in space are shown for changes of wave frequency, geomagnetic latitude, and direction.

Effects of Ionospheric Layer Tilts on High-Frequency Radio Propagation*—S. Stein, *Stanford University*—The F layer, as is well known, has a complex global distribution of ion density. In addition to the

* The research reported in this paper has been sponsored by the Geophys. Res. Dir. of the AF Cambridge Res. Center, Air Res. and Dev. Command, under Contract AF19(604)-1304.

* This work was supported jointly by the U. S. Army, Navy, and Air Force under contract with Stanford University.

conventional ionospheric parameters, the F layer may be further characterized by an equivalent layer tilt, a function of frequency and takeoff angle. Low angle rays reflected from a tilted F layer may propagate beyond the bulge of the earth, without striking the ground, and illuminate the ionosphere again. When sufficient ion density exists at the second illuminated region, the rays will propagate on around the earth. A ray may be reflected several times before striking a properly oriented tilt so that the surface of the earth is illuminated. These modes are called ${}^nF$ modes, where n is the number of layer reflections. The theory of tilt supported modes has been successfully applied to the anomalous propagation across the equator.*

Theoretical Chapman layers and other models are investigated to find the ray trajectories and determine equivalent layer tilts. These results form the nucleus of a prediction scheme for tilt supported modes.

The characteristics of multiple-hop ground backscatter were investigated in order to assist in recognition of ${}^nF$ mode ground scatter. Detection of ${}^nF$ mode ground scatter occurs as a consequence of geometrical time-delay focussing and to a lateral beam effect. Under some conditions Peterson's "minimum-time-delay" focussing is also considered. Comparisons are made between calculations and experimental backscatter records obtained at the location of Stanford University.

Tilt supported rays may propagate long distances without the necessity of ground reflections and without reentering the absorbing D region except on the last leg where the earth's surface is illuminated. The radio frequency of ${}^nF$ mode propagation is examined in comparison with the conventional muf.

Coherent Integration of Doppler Echoes in Pulse Radar—B. D. Steinberg, *General Atronics Corporation*—It is well known that s/n improvement results from integration of radar echoes. For noncoherent or envelope detection the proper integrator is a low-pass filter, whether Doppler is present or not. Marcum analyzed the effectiveness of integration for noncoherent detection. This paper presents a comparable theory for the integration of coherent signals with Doppler.

Coherent integration requires a band-pass filter at the Doppler frequency, usually not known in advance. Hence, each range gate must feed a bank of narrow-band filters. Such equipment complexity can be justified only if considerable benefit results.

From the theory, calculations are made of coherent integration of Doppler signals. The measure used is absolute receiver sensitivity (input s/n for specified detection probability and false alarm interval). The parameters are input s/n, observation time, and detection probability. The theoretical results are presented graphically.

The theory also treats coherent integration when the dynamic range is reduced to polarity only. Harrington found a 1½ to 2-db loss in sensitivity due to one-bit quantization in the noncoherent case. The corresponding loss in sensitivity of a coherent receiver is 5 to 6 db.

Information Theory Applied to the Human Visual System—J. R. Singer, *National Scientific Laboratories, Inc.*—The complex phenomenon of visual form and pattern recognition with size invariance may be partially understood by comparison with an electronic apparatus which would accomplish the same task. In this treatment, the receptors of the eye are simulated by photoelectric cells; the bipolar, ganglion, and amacrine cells, by pulse coding circuitry; the optic nerves, by signal transmission channels; and the brain, by a digital computer. This analog system permits an application of Shannon's theorem* for the capacity of a signal channel containing white noise which is

$$C = W \log_2 \left(\frac{S+N}{N} \right)$$

for a binary transmission system.

It is shown that the maximum possible capacity of the transmission channels which are the analog to the optic nerves far exceeds the computer processing capacity (recognition speed of the brain) in binary units per second. The assumptions for this conclusion, however, bear further scrutiny since "reasonableness" is used as a guide wherever experimental data are unavailable. Experiments which would aid in further application of information theory to vision are suggested and outlined.

Impulse Response of Cascaded Double-Tuned Circuits—Y. Peless—In this paper a general formula for the impulse response envelope of a cascade of n identical double-tuned circuits is derived. The results are limited to the case of small fractional bandwidth, but are generally applicable for an arbitrary arrangement of the poles of the complex impedance function representing the transformer. The solution involves reduction of the four-pole to an approximate equivalent two-pole followed by complex integration. The results are presented in terms of 3 parameters, one fixing the average location of the two-pole in the complex plane, and two fixing the location of one pole with respect to the other. Tables and curves for low-order cases are presented. Finally, the relation between the pole location and the circuit constants is presented so that the design of the interstages for prescribed impulse response is determined.

Some Applications of the Isometric Circle Method to Impedance Transformations Through Lossless Two-Port Networks—E. F. Bolinder†—The isometric circle method is a graphical method of transforming a complex quantity by the linear fractional transformation. If the quantity is a complex impedance Z, then the linear fractional transformation

$$\frac{Z' - aZ + b}{cZ + d'} \quad ad - bc = 1 \qquad (1)$$

can be interpreted as an impedance transformation through a bilateral two-port network which, for a fixed frequency, is characterized by the four complex constants a, b, c, and d.

The isometric circle is defined as the circle which is the complete locus of points in the neighborhood of which lengths are unaltered in magnitude by (1). The isometric circle of the direct transformation, C_d, has its center at $O_d = -d/c$ and a radius $R_c = 1/|c|$; the isometric circle of the inverse transformation, C_i, has its center at $O_i = a/c$ and the same radius.

Mathematically, (1) is divided into two classes of transformations: the loxodromic transformation,* characterized by $a+d=$ complex, and the nonloxodromic transformation, characterized by $a+d=$real. The latter transformation is further divided into the hyperbolic, parabolic, and elliptic transformations specified by $|a+d| \gtrless 2$.

If the two isometric circles are drawn in the complex plane, the following graphical constructions yield a graphical method for the loxodromic case:

1) an inversion in the isometric circle of the direct transformation C_d;

2) a reflection in the symmetry line L to the two circles; and

3) a rotation around the center O_i of the isometric circle of the inverse transformation through an angle $-2 \arg (a+d)$.

If the bilateral two-port network is lossless, it is shown that the impedance transformation corresponds to a nonloxodromic transformation. In this case the third operation above is eliminated. A plotting of the isometric circles immediately specifies the nonloxodromic transformation. If the two circles intersect, the elliptic, above-cutoff, case exists; if the circles are tangent the parabolic, cutoff, case exists; and, finally, if the two circles are external the hyperbolic, below-cutoff, case exists.

The isometric circle method is applied to impedance and reflection coefficient transformations through some simple bilateral, lossless, two-port networks. The examples chosen are: a uniform transmission line, a lossless transformer, an exponentially tapered transmission line, and uniform waveguide sections (TE and TM modes). Graphical constructions for simple numerical examples are shown both in the impedance plane and the reflection coefficient plane (Smith chart). The connections between the constructions in the two planes are shown by mapping the planes stereographically on the unit sphere. It is shown that the transformation through the uniform transmission line is elliptic and that it corresponds to a rotation of the sphere around a line through the fixed points. The ideal transformer, on the other hand, is hyperbolic and corresponds to a stretching of the surface of the sphere along a line through the fixed points. Finally, the exponentially tapered line and the waveguide section may both be elliptic, parabolic, or hyperbolic depending on simple relations between the mechanical dimensions and the frequency.

* O. G. Villard, Jr., S. Stein, and K. S. Yeh, "New Evidence of Anomalous Transequatorial Ionospheric Propagation," paper presented at 1957 IRE National Convention, New York, N. Y.; March 18, 1957.

* C. E. Shannon and W. Weaver, "The Mathematical Theory of Communication," University of Illinois Press, Urbana, Ill., p. 67; 1949.

† This work was supported in part by the U. S. Army (Signal Corps), Air Force (Office of Scientific Res., Air Res. and Dev. Command), and the Navy (Office of Naval Res.).

* If a loxodromic transformation (Greek: loxo=oblique, dromos=a running course), centered around the origin of the complex plane, is stereographically mapped on a sphere, a curve is obtained that cuts the meridians under a constant angle. The curve, that uniformly turns around both poles an infinite number of times, is called a loxodrom.

On the Theory of Pulse Transmission and Reception*—N. DeClaris, *Cornell University*—The parameter representation of time and frequency domain functions as well as the associated network requirements for narrow pulse transmission and reception are discussed. It is shown that the density distribution function $\mu=(\gamma,\lambda)$ provides a basic tool for arriving at and dealing with the approximation and synthesis problems.

Thus, a single real function for network characterization, rational or transcendental, avoids the question of amplitude and phase frequency responses, and moreover, it places in evidence pronounced effects of network complexity imposed by small variations in pulse shape tolerance.

An example illustrates the above viewpoint for the case when part of the transmission system is preassigned.

Microwave Diagnostics for High-Temperature Plasmas†—C. B. Wharton, *University of California*—High-temperature plasma research, aimed mainly toward controlled thermonuclear reactions, has been greatly facilitated by the development of a number of microwave measuring techniques, called "microwave diagnostics." These schemes are based in part on previous plasma microwave studies but mostly on ideas generated at UCRL in conjunction with the AEC Project Sherwood, and are being presented here for the first time. The properties of a plasma measurable by these techniques are: average special density, density distribution, collision frequency, electron temperature, recombination, and other loss rates, all as a function of time, with or without magnetic fields present. A wide latitude in choice of geometry and operating conditions is possible. The quantities measured directly are the phase, an absorption coefficient of the dispersive propagation "constant," the cyclotron frequency, bremsstrahlung radiation power, and gyromagnetic radiation power. A brief theoretical derivation of the simple microwave properties of a plasma is given and experimental results indicating satisfactory correlation are presented. Experimental setups and millimeter wave equipment employed in the experiments are described.

General Synthesis of a Class of Waveguide Filters—H. J. Riblet, *Microwave Development Laboratories*—Necessary and sufficient conditions are given that a prescribed insertion loss function can be obtained exactly with a cascade of admittance inverters equally spaced on a uniform transmission line. In the limit of narrow bandwidth this procedure becomes "indeterminate" and the synthesis procedure simplifies to a form which can be shown to be necessary and sufficient for the existence of a low-pass ladder analog. In this limit, an exact equivalence between direct and quarter-wave coupled filters of the customary type can be shown. This equivalence permits a comparison in the accuracy of the two procedures. It is shown that the error in the insertion loss function, introduced by the simplifying assumption, is of the order of the square of the percentage bandwidth for the direct coupled filter by which the quarter-wave coupled filter differs further from it by terms which are of second or higher order in the percentage bandwidth. Finally the procedure is applied to the design of a slightly novel direct-coupled filter and experimental results are given.

The Approximate Parameters of Slot Lines and their Complement—G. H. Owyang and T. T. Wu, *Gordon McKay Laboratory, Harvard University*—The rigorous solution of the transverse problem encountered with parallel transmission lines constructed of coplanar strips with finite thickness involves very complicated functions such as hyperelliptic integrals. However, for a thickness very small compared with the width and the separation, an approximate answer may be obtained by a first-order perturbation method.

The contour of the conducting strips is transformed by the Schwarz-Christoffel mapping into infinitely thin strips whose properties are already known. The actual distribution of current density is then calculated approximately from the known current density on the infinitely thin strips and the mapping factor. From the current density and the surface resistance of the material, the ohmic loss, and hence the attenuation, is obtained. The line constants are obtained as part of the analysis.

The complementary problem of parallel slots in an infinite conducting plane of small but finite thickness is solved by a similar procedure.

Absorption of Plane Waves in an Optimum Nonuniform Medium Backed by a Metallic Surface—I. Jacobs, *Bell Telephone Laboratories*—The problem of coating a metallic surface so as to make the combination absorbing over a broad frequency band is considered from the point of view of nonuniform transmission line theory. An optimization argument is presented which leads to the consideration of a medium in which the fractional increase in dielectric constant per wavelength in the medium is constant. The nonuniform transmission line equations are solved exactly for this case and the results are expressed in terms of readily interpretable elementary functions. It is shown that a fixed geometrical length of line can lead to an arbitrarily large effective length without destroying the match to free space. Hence, in a nonuniform medium with a small loss tangent, all energy may be almost completely absorbed regardless of termination.

The line has a long wavelength cut-off given by approximately 4π times the actual length of the line. A return loss of greater than 10 db is obtained at all frequencies above 1.8 times the cut-off frequency. Practical limitations on maximum attainable dielectric constant necessitate the use of larger loss tangent materials which diminish the return loss. For a maximum relative dielectric constant of 4000, a return loss of 10 db is calculated at frequencies about five times the cut-off frequency.

Straight Tapers in Rectangular Waveguides: A Comparison of Principal Mode and Nonuniform Transmission Line Theories—T. J. Rey, *Glen Burnie, Md.*—Tapered sections are used for joining lines or guides that differ in cross section, particularly where the phase velocities are unequal.

In rectangular waveguides exhibiting changes of either height or width or both (with preservation of aspect ratio), it is convenient to use linear tapers. In these, cylindrical or spherical wave functions have been shown by Lewin* to describe the fields allowing the effect on the $TE_{0,1}$ mode in the uniform guide to be expressed by comparison of the principal modes. Lewin's work is revised, mainly with regard to the choice of wave-functions and their approximations.

An alternative approach to the problem is to regard the principal mode as expanding (or contracting) from one uniform guide into the other, through the tapered section that serves as a "nonuniform" transmission line. Theories of this nature are reviewed briefly.

The results of the two types of theory are compared, and show various measures of agreement.

On the Construction of the Green's Function for a Nonuniform Waveguide Region or for Waveguide Regions Filled with an Inhomogeneous Medium—R. Mittra, *Department of Electrical Engineering, The Pennsylvania State University*—The paper describes an integral equation method for the construction of the Green's function G for a nonuniform waveguide region. The method is also applicable, for certain modes of propagation, for constructing the Green's function of a waveguide region filled with an inhomogeneous medium. The method is limited in application to problems which can be reduced to two-dimensional scalar wave propagation only.

The discussion of the problem is divided into two parts. The first one considers the case when the nonuniformity of the waveguide is confined to a finite region and the dimensions of the waveguide are equal for large positive and negative distances. In the second part, a method is described which is useful for constructing the Green's function of a waveguide region with dissimilar dimensions at the two ends. An example of such a region is the tapered junction between two dissimilar guides. The method can be applied to such regions provided the walls of the waveguide form separable coordinate surfaces at large distances from the origin. Waveguide-to-horn junction is another example of a waveguide geometry for which the method can be used.

The integral equation for the Green's function is formulated in terms of a known Green's function and the metric of transformation which maps the nonuniform waveguide region conformally, into a parallel plate region. Approximate solutions of the integral equation are discussed and the equations for the field potential and the reflection coefficient are also derived. The techniques discussed can also be used in connection with certain resonator problems and those concerning free space diffraction by arbitrary cylinders. Also, for certain types of modes of propagation the method can be used to obtain Green's function for a waveguide region filled with a medium with two-dimensional inhomogeneity.

* Part of the work presented here was carried out while acting as a consultant to the General Electric Co., Advanced Electronics Center.

† Work performed under the auspices of the U. S. Atomic Energy Commission.

* L. Lewin, "Advanced Theory of Waveguides," Illiffe, London, England, pp. 114–120; 1951.
L. Lewin, "Reflection cancellation in waveguides," *Wireless Eng.*; August, 1949.

Contributors

M. G. ANDREASEN

Mogens G. Andreasen was born in Horsens, Denmark, on January 1, 1927. He received the M.S. degree in telecommunications engineering in 1952 and the technical licentiate degree in 1956, both from the Royal Technical University of Denmark. Then he was employed as an engineer in the Microwave Laboratory and from 1953 to 1956 as a research assistant in the Laboratory of Electromagnetic Theory, Technical University of Denmark. During 1953–1955, he taught microwave circuits. Since April, 1956, he has been with the Antenna Laboratory of Siemens & Halske, Munich, Germany.

He is a member of the Institution of Danish Civil Engineers.

❖

N. W. BROTEN

Norman W. Broten (S'47–A'51) was born on December 21, 1921 in Meacham, Saskatchewan, Canada. He studied at the University of Western Ontario, London, Canada, from which he received the degree of B.Sc. in 1950. Mr. Broten then joined the staff of the National Research Council of Canada at Ottawa, where he has been engaged in research in the field of radio astronomy.

He is a member of the Royal Astronomical Society of Canada.

❖

N. H. BRYANT

Nelson H. Bryant (A'53) was born in Greene, N. Y., on September 19, 1917. He received the B.E.E. degree from Cornell University in 1939 and joined Westinghouse Electric Corp., Bloomfield, N. J. There he did development engineering on vapor lamps and associated circuits and production engineering on transmitting tubes. In 1944, he joined the U. S. Naval Reserve and served as a radar officer. He returned to Cornell and received the M.E.E. degree. Since then, except when working on an over-the-horizon radio propagation problem at Stanford University Electronics Laboratory (1956–1957), he has been at Cornell where he is now an associate professor of electrical engineering.

He is a member of Tau Beta Pi and Eta Kappa Nu.

A. E. COVINGTON

Arthur E. Covington (M'49) was born in Regina, Saskatchewan, Canada, on September 21, 1913. He received the B.A. degree in physics and mathematics in 1938, and the M.A. degree in 1940 from the University of British Columbia. He took postgraduate studies at the University of California at Berkeley from 1940 to 1942.

Since then, Mr. Covington has been with the National Research Council of Canada at Ottawa. He is a member of the American Astronomical Society and the Royal Astronomical Society of Canada.

❖

R. H. DUHAMEL

Raymond H. DuHamel (A'53–M'57) was born in Tuscola, Ill., on October 11, 1922. He received the B.S. degree from the University of Illinois in 1947, the M.S. degree in 1948, and the Ph.D. degree in 1951, all in electrical engineering. While in graduate school, he held a research assistantship with the Radio Direction Finding Laboratory at the University, where he did research on antennas for rdf systems and on methods of antenna pattern synthesis.

From 1951 to 1952, Dr. DuHamel worked on television antennas at RCA Laboratories, Princeton, N. J. From 1952 to 1956, he was a research assistant professor in electrical engineering at the University of Illinois, where he was in charge of the Antenna Laboratory. Since 1956, he has been head of the Antenna Group at Collins Radio Company in Cedar Rapids, Iowa.

Dr. DuHamel is a member of Sigma Xi and Eta Kappa Nu.

❖

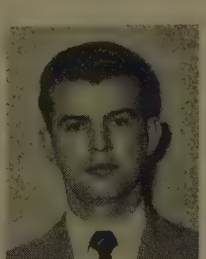

J. W. DUNCAN

James W. Duncan (A'53) was born in Decatur, Ill., on September 15, 1926. He received the B.S. degree from the University of Colorado in 1950 and the M.S. degree from the University of Illinois in 1955.

From 1950 to 1953, Mr. Duncan worked for Sandia Corporation, Albuquerque, N. M., as a development engineer. Since 1953, he has been a teaching and research assistant at the University of Illinois and is continuing graduate study for the Ph.D. degree in electrical engineering.

He is a member of Eta Kappa Nu, Tau Beta Pi, Sigma Tau, and Pi Mu Epsilon.

❖

R. S. ELLIOTT

Robert S. Elliott (S'51–A'52–SM'54) was born in Brooklyn, N. Y., on March 9, 1921. He was a Pulitzer Scholar at Columbia University, where he received the A.B. degree in 1942 and the B.S. degree in 1943.

From 1943–1946, he was employed by the Applied Physics Laboratory, serving as a junior engineer on problems in radar, guided missiles, and the proximity fuse. In 1946, he became a member of the electrical engineering staff at the University of Illinois, where his duties included undergraduate and graduate teaching and research in antennas and microwave tubes. While at Illinois, he received the M.S. degree (1947) and Ph.D. degree (1952).

Summer work in the antenna groups at Sperry (1949) and North American (1950) supplemented his Illinois employment. Upon leaving Illinois in 1952, Dr. Elliott served one year of active duty in the U. S. Navy and then joined the technical staff of the Hughes Aircraft Company at Culver City, Calif., where he headed the Antenna Research Section of the Microwave Laboratory. He left Hughes to help form the Rantec Corporation, Calabasas, Calif., where he is vice-president and technical director.

Dr. Elliott is a member of Tau Beta Pi and Sigma Xi.

❖

P. E. GUDMANDSEN

Preben E. Gudmandsen (A'51–M'56) was born on October 5, 1924 in Frederiksberg, Denmark. He received the M.Sc. degree in electrical engineering and telecommunication from the Royal Technical University of Denmark in 1950. Since then he has been a research engineer in the Microwave Laboratory, the Danish Academy of Technical Sciences, Copenhagen, Denmark. He has been concerned with propagation measurements within and beyond the radio horizon, statistical analysis of propagation measurements and evaluation of such data, and development of microwave components and other equipment, mainly for propagation measurements. He has acted as a consultant for Danish Government Departments. Recently he joined the SHAPE Air Defense Technical Center, The

Hague, Holland, where he is mainly concerned with propagation measurements and reliability studies of radio communication systems.

Mr. Gudmandsen is a member of the Institution of Danish Civil Engineers.

❖

Kenneth C. Kelly (S'53–A'54) was born in New York, N. Y., on March 6, 1928. He received the B.S.E.E. degree in 1953 from the Polytechnic Institute of Brooklyn and is working on the M.S. degree at the University of California at Los Angeles.

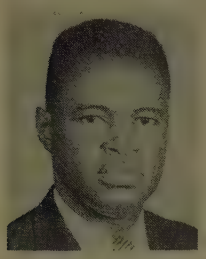

K. C. KELLY

During his military service from 1946 to 1949, Mr. Kelly was an electronics technician.

From 1950 to 1953, he was with the Polytechnic Research and Development Company, working on microwave instruments and components. In 1953, he joined the Antenna Department of Hughes Aircraft Co., Culver City, Calif., and has been engaged in research on antennas and phase shifters.

Mr. Kelly is a member of Eta Kappa Nu and Tau Beta Pi.

❖

Howard E. King (A'46, SM'55) was born in Seattle, Wash., on October 16, 1924. He received the B.S.E.E. degree in 1945 from the University of Washington and the M.S.E.E. degree in 1955 from the University of Illinois. From 1946 to 1952 he was a member of the broadcast section of the RCA Victor Division, designing fm and tv transmitting antennas, and took part in the development of the Empire State Building multiple tv antenna system. After a year with the Andrew Corporation, he was appointed as a research assistant of the Antenna Laboratory of the University of Illinois, until 1955. Since 1955 he has been a member of the technical staff of the Communications Division of the Ramo-Wooldridge Corporation.

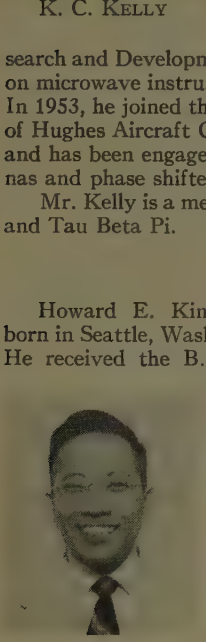

H. E. KING

❖

Ralph W. Klopfenstein (S'44–A'46–M'50–SM'54) was born on June 3, 1923, in Aberdeen, S. D. He received the B.S.E.E. degree from the University of Washington in 1944 and the M.S. and Ph.D. degrees in applied mathematics from Iowa State College in 1951 and 1954.

From 1945 to 1946, he was a radio matériel officer in the U. S. Naval Reserve. He became an instructor in the mathematics department of South Dakota School of Mines and Technology in 1946. In 1948, he joined RCA Victor in Camden, N. J., where he worked on the advanced development of television and fm transmitting antennas and filters. After three years as an instructor in mathematics at Iowa State, from 1950 to 1953, he returned to RCA Laboratories Division in Princeton, N. J., where he is now a member of the research staff.

R. KLOPFENSTEIN

Dr. Klopfenstein is a member of Sigma Xi, Phi Kappa Phi, the Mathematical Association of America, and SIAM.

❖

Bent Frantz Larsen (A'51–M'56) was born on June 30, 1923 in Copenhagen, Denmark. He received the M.S. degree in communication engineering in 1948 from the Royal Technical University of Denmark, Copenhagen. He was associated with the Microwave Laboratory of the Danish Academy of Technical Sciences from 1948 to 1951, working on the development of measuring devices, antennas, and equipment for propagation tests. During the university terms 1949 to 1950, he was on a leave of absence to study at the University of Paris on a scholarship granted by the French Government. He served in the Royal Danish Ordnance Corps at the Zealand Arsenal from 1951 to 1954, being engaged in supervision of overhaul and rebuilding of radar and fire control material and in planning of shop facilities and maintenance programs. In January, 1954, he returned to the Microwave Laboratory, the Danish Academy of Technical Sciences, where he now is working on statistical analyses of propagation data and the development of equipment for scatter propagation tests.

B. F. LARSEN

He is a member of the Society of Danish Engineers.

❖

Robert E. Miller (S'46–A'49–M'53–SM'55) was born on January 17, 1926 in St. Louis, Mo. He attended Iowa State College in the Navy V-12 program, and received the B.S.E.E. degree in March, 1946. After release from the Navy he returned to Iowa State College and continued studies under a teaching fellowship. He received the M.S.E.E. degree in 1948.

R. E. MILLER

In 1948 Mr. Miller became an associate engineer at the Applied Physics Laboratory, Johns Hopkins University, where he was in the missile guidance receiver group and was principally concerned with design of special test equipment for missile guidance receivers.

In 1951 he joined the staff of Stanford Electronics Laboratories, Stanford University, as a research associate, working on microwave tube applications for electronic countermeasures systems. Currently he is a group supervisor in the Systems Techniques Laboratory.

Mr. Miller is a member of Sigma Xi, Eta Kappa Nu, and Tau Beta Pi.

❖

Alan T. Waterman, Jr. (A'46–S'51–SM'57) was born on July 8, 1918, in North Hampton, Mass. He received the A.B. degree in physics from Princeton University and the B.S. degree in meteorology from California Institute of Technology in 1940. In 1949 and 1952 respectively, he received the M.A. and Ph.D. degrees in applied physics from Harvard University.

A. WATERMAN, JR.

Dr. Waterman worked as a meteorologist for American Airlines from 1940 to 1941 and was an instructor in meteorology at the University of Minnesota the following year. From 1942 to 1945 he did research in methods of weather forecasting for California Institute of Technology on contract for the Army Air Force. He also did research for the Wave Propagation Group of Columbia University in 1945. In 1945 and 1946, Dr. Waterman was chief meteorologist for the Electrical Engineering Research Laboratory of the University of Texas, and from 1946–1952, he was a graduate assistant at Harvard University. Since 1952, he has been doing research in radio wave propagation and countermeasures at Stanford University.

Dr. Waterman is a member of the American Physical Society, the American Meteorological Society, the American Association for the Advancement of Science, and Sigma Xi.

❖

Oakley M. Woodward, Jr., (S'38–A'40–SM'54) was born on January 13, 1915, at Davis, Okla. He received the degree of Bachelor of Science in electrical engineering from the University of Oklahoma, Norman, Okla., in 1938.

O. WOODWARD, JR.

After graduation Mr. Woodward joined the Seismograph Service Corporation of Tulsa, Okla. During 1941, Mr. Woodward was a research engineer at the RCA Manufacturing Company, Camden, N. J. Since 1942 he has been with RCA Laboratories, Princeton, N. J.

He is a member of Sigma Xi.

INSTITUTIONAL LISTINGS

The IRE Professional Group on Antennas and Propagation is grateful for the assistance given by the firms listed below, and invites application for Institutional Listing from other firms interested in the field of Antennas and Propagation.

ANDREW CORPORATION, 363 E. 75th St., Chicago 19, Ill.
Antennas, Antenna Systems, Coaxial Transmission Lines, Design, Development, Production.

ANTLAB, 4950 North High St., Columbus 14, Ohio
Antenna Pattern Range Measuring Systems.

COLLINS RADIO COMPANY, Cedar Rapids, Iowa
Antenna Design and Propagation Research Related for Airborne and Ground Communication Systems.

DEVELOPMENTAL ENGINEERING CORP., 1001 Conn. Ave. N.W., Washington, D. C. and Leesburg, Va
Research, Development, Installation of Antennas and Antenna Equipment for Super Power Stations.

DORNE AND MARGOLIN, INC., 30 Sylvester Street, Westbury, L. I., N. Y.
Antenna Research and Development—Radiation Pattern Measuring Services.

THE GABRIEL LABORATORIES, Div. of the Gabriel Co., 135 Crescent Road, Needham Heights 94, Mass
Research and Development of Antenna Equipment for Government and Industry.

HUGHES AIRCRAFT COMPANY, Culver City, Calif.
Research, Development, Mfr.: Radar, Missiles, Antennas, Radomes, Tubes, Solid State Physics, Computers.

I-T-E CIRCUIT BREAKER CO., Special Products Div., 601 E. Erie Ave., Philadelphia 34, Pa.
Design, Development and Manufacture of Antennas, and Related Equipment.

JANSKY & BAILEY, INC., 1339 Wisconsin Ave. N.W., Washington 7, D. C.
Radio & Electronic Engineering; Antenna Research & Propagation Measurements; Systems Design & Evaluation

MARYLAND ELECTRONIC MANUFACTURING CORPORATION, College Park, Md.
Antenna and System Development and Production for Civil and Military Requirements.

THE RAMO-WOOLDRIDGE CORPORATION, Los Angeles 45, Calif.

TRANSCO PRODUCTS, INC., 12210 Nebraska Ave., Los Angeles 25, Calif.
Antenna Design and Production—Radiation Pattern Measuring Services.

WHEELER LABORATORIES, INC., 122 Cutter Mill Road, Great Neck, N. Y.
Consulting Services, Research and Development, Microwave Antennas and Waveguide Components.

The charge for an Institutional Listing is $25.00 per issue or $75.00 for four consecutive issues. Application may be made to the Technical Secretary, The Institute of Radio Engineers, 1 East 79th Street, New York 21, N.Y.